



Experimental simulation of Titan's aerosols formation

Thomas Gautier

► To cite this version:

Thomas Gautier. Experimental simulation of Titan's aerosols formation. Planétologie et astrophysique de la terre [astro-ph.EP]. Université de Versailles-Saint Quentin en Yvelines; Ruhr-Universität Bochum, 2013. Français. NNT : . tel-00878846

HAL Id: tel-00878846

<https://theses.hal.science/tel-00878846>

Submitted on 31 Oct 2013

HAL is a multi-disciplinary open access archive for the deposit and dissemination of scientific research documents, whether they are published or not. The documents may come from teaching and research institutions in France or abroad, or from public or private research centers.

L'archive ouverte pluridisciplinaire **HAL**, est destinée au dépôt et à la diffusion de documents scientifiques de niveau recherche, publiés ou non, émanant des établissements d'enseignement et de recherche français ou étrangers, des laboratoires publics ou privés.



Thèse présentée pour l'obtention du titre de Docteur de l'Université de Versailles St Quentin en Yvelines. Spécialité: Astronomie Astrophysique.

Dissertation zur Erlangung des Grades eines Doktors der Naturwissenschaften in der Fakultät für Physik und Astronomie der Ruhr Universität Bochum

Experimental simulation of Titan's aerosols formation

by Thomas Gautier

Soutenue le 20 Septembre 2013, devant un jury composé de:

Pr. Philippe Bousquet	Président
Pr. Hervé Cottin	Rapporteur
Pr. Pascal Rannou	Rapporteur
Pr. Emmanuel Lellouch	Examineur
Pr. Horst Fichtner	Examineur
Pr. Jörg Winter	Directeur
Dr. Nathalie Carrasco	Directrice

Contents

Résumé.....	
Chapter I : Titan - Observations and Experimental Simulations	1
I.1 Titan.....	1
I.1.1 Past and present exploration.....	1
I.1.2 Current knowledge on Titan's atmospheric aerosols.....	4
I.2 Titan in a can: Laboratory analogs of Titan's aerosols	9
I.2.1 Gas Phase	11
I.2.2 Tholins optical properties in the Infrared range	12
I.3 Conclusion.....	15
Chapter II Methods.....	17
II.1 Experimental devices.....	17
II.1.1 The PAMPRE experiment: Synthesis of Titan's aerosols analogues	17
II.1.2 Bochum setup.....	23
II.1.3 Photochemical experiment: the APSIS setup.....	26
II.2 Ex-situ Analytical methods	29
II.2.1 Cryogenic trapping and Gas-Chromatography coupled to mass spectrometry: gas products identification.	29
II.2.2 Infrared analyses of tholins by ATR (performed at LATMOS).....	30
II.2.3 Tholins infrared spectroscopy using Synchrotron radiation.	31
II.2.4 Ellipsometry: Determination of sample thickness.	32
II.2.5 High resolution mass spectrometry for tholins chemical analysis	32
II.3 Conclusion.....	34
Chapter III Gas phase reactivity leading to aerosols.....	39

III.1	Introduction	39
III.2	Volatile products in the PAMPRE experiment: in-situ look to the tholins nursery ..	39
III.2.1	Experimental protocol	40
III.2.2	The case of hydrogen: H and H ₂	43
III.2.3	Organic species production	46
III.2.4	Implication for tholins formation processes: the case of ammonia and Methanimine	49
III.2.5	Conclusion.....	53
III.3	Improving sensibility: Cold trap experiments	54
III.3.1	Experimental setup and protocol.....	54
III.3.2	Results	55
III.3.3	Discussion	63
III.3.4	Conclusion.....	71
III.4	Volatiles products in Bochum experiment: kinetics, products and quantification ...	73
III.4.1	Experimental parameters	73
III.4.2	Providing Carbon for tholins formation: the consumption of methane.....	74
III.4.3	Kinetics.....	76
III.4.4	Identification by mass spectrometry	78
III.4.5	Identification by infrared spectroscopy	82
III.4.6	Absolute quantification of HCN and NH ₃	86
III.5	Conclusion	89
Chapter IV	Tholins: What are they made of? How does it influence their properties?	91
IV.1	Introduction	91
IV.2	Insight into tholins chemical composition.....	92
IV.2.1	Time of Flight mass spectrometry: Global description of the sample	92
IV.2.2	Orbitrap	94

IV.2.3	Analysis of the residue by GC-MS	107
IV.2.4	Conclusion.....	115
IV.3	Optical infrared properties.....	116
IV.3.1	Introduction	116
IV.3.2	A first comparison of tholins produced in PAMPRE and Bochum: Attenuated Total Reflectance spectroscopy.	116
IV.3.3	Quantifying the tholins absorption and exploring their far-infrared absorbance properties.....	120
IV.4	Conclusion.....	133
Chapter V	Effect of photochemistry: the APSIS experiment	135
V.1	Introduction	135
V.2	Analytical techniques and data treatment.....	136
V.2.1	In-situ Mass Spectrometry	136
V.2.2	GC-MS	138
V.3	Results	138
V.3.1	Methane consumption	138
V.3.2	Kinetics.....	140
V.3.3	Products identification (GC-MS)	142
V.3.4	Pressure influence on mass spectra	143
V.3.5	Products identification (MS)	146
V.4	Discussion.....	147
V.5	Conclusion.....	149
	General conclusion	151
	List of publications related to this thesis	157
	Table of figures	159
	References	167

Remerciements

And not, when I came to die, discover that I had not lived...

Henry David Thoreau

Tout d'abord je remercie ma famille, en particulier ma grande sœur Alex, pour leur soutien et leur foi en moi.

Je tiens également à remercier tout le personnel du LATMOS que j'ai eu l'occasion de côtoyer pendant ces années, et en particulier tous les membres de mon équipe tant pour leur soutiens dans mon travail que pour l'ambiance conviviale qui l'a entouré (et c'est peu dire !). Un merci spécial pour Cyril Szopa pour ses conseils et les parties de ping-pong. Surtout un énorme merci à ma directrice de thèse Nathalie Carrasco, qui m'a offert sa confiance et l'opportunité de faire cette thèse. Merci pour son aide, son soutien et sa joie de vivre communicative.

Merci également à toutes les personnes d'autres laboratoires avec qui j'ai eu la chance de collaborer et sans qui cette thèse n'aurait pas été possible. En particulier, un énorme merci à Vass pour le soutien réciproque pendant nos rédactions...

Parce que une thèse c'est également des rencontres, merci à toute la team des thésards (et pour ne pas oublier les post-docs et stagiaires également) du labo : Constantino, Loic, Kristell, Jennyfer (Super Co-Bulloc !), Maud, Christophe, Gaëlle, Sarah, Emilie, Tanguy, Maëva, Benjamin (et beaucoup d'autres...). Merci pour ces petites pauses dans le boulot qui aident à garder le rythme.

A special thanks for all the people from EP II Bochum, especially would like to thank Pr. Jörg Winter for supervising my thesis and Ilija Stefanovic and Brankica Sikimic that help me not only in the lab but also in everyday life.

Je tiens également à remercier tous mes amis qui m'ont permis de garder le moral et le cap pendant ces trois ans, merci entre autre à Seb, Yo, Bibi, Pierrot et Cécé (pour son acceptation :)) pour les soirées call-of.

Merci enfin aux amis du para (trop nombreux pour être énumérés sans en manquer un, mais le cœur y est), pour tous ces bons moments passés à Maubeuge dans le Ciel ou par terre rue Mouffetard...

Merci à tous,

Thomas

*If Stars should appear but one night every thousand years, how would men
believe and adore, and preserve for many generations the remembrance of
the city of gods which had been shown.
Ralph Waldo Emerson*

Résumé

La problématique de cette thèse est à mettre en relation avec l'étude de la composition et des propriétés des aérosols de Titan. Pour ce faire, j'ai produit en laboratoire et analysé des équivalents d'aérosols de Titan, appelés tholins. En effet, même si la mission Cassini-Huygens a permis d'avancer dans notre connaissance des aérosols dans l'atmosphère de Titan, leur formation ainsi que leur composition reste assez peu connue. Une des méthodes possible pour étudier ce sujet est donc de produire et d'analyser en laboratoire des analogues d'aérosols.

Le chapitre I de cette thèse présente l'état de l'art actuel concernant les aérosols de Titan à partir des observations faites par la mission Cassini-Huygens. Cet état de l'art est ensuite mis en relation avec les différentes études déjà faites en laboratoire pour étudier ces aérosols.

Le chapitre II est quant à lui dédié à la présentation des méthodes expérimentales utilisées durant cette thèse, que cela soit les réacteurs utilisés pour produire des aérosols, ou bien les méthodes analytiques mises en place pour les analyser.

Les principaux buts de cette thèse sont de caractériser la chimie et les voies de formation possible menant à la formation d'aérosols, ainsi que de déterminer la composition et les propriétés de ces aérosols à l'aide de techniques de pointe en laboratoire. Pour ce faire j'ai utilisé deux approches complémentaires.

Tout d'abord, comme présenté dans le chapitre III, une approche 'bottom-up' qui consiste à étudier la composition et la réactivité de la phase gazeuse menant aux aérosols. Cette étude est principalement basée sur des mesures par spectrométrie de masse dans deux réacteurs à plasma différents.

La seconde approche est une approche 'top-bottom' et est présentée dans le chapitre IV. Il s'agit d'analyser les tholins, tant pour leurs propriétés d'absorption dans l'infrarouge lointain et moyen, que pour leurs composition chimique. L'étude de ces propriétés peut permettre de remonter à certains mécanismes de formation des tholins.

Bien que non directement lié aux deux parties précédentes, le chapitre V présente une étude sur l'impact de la source d'énergie (photons versus électrons) sur la réactivité de la phase gazeuse.

Trois montages expérimentaux ont été utilisés pour cette thèse. Les deux premiers sont le montage PAMPRE et l'expérience de Bochum. Ce sont des réacteurs plasma très similaires dans leur conception et disposant d'instruments complémentaires dans l'analyse de la phase gazeuse. APSIS, le troisième est un réacteur photochimique utilisant le rayonnement synchrotron dans le VUV comme source d'énergie. Une comparaison entre ces trois montages est proposée dans la Table 1.

Table 1: Comparaison des différents montages expérimentaux utilisés pour cette thèse

	PAMPRE	Réacteur Bochum	APSYS
Dépôt d'énergie	RF Plasma 30 W	RF Plasma 50 W	Photons VUV 220-60 nm
Mélange de gaz	N ₂ -CH ₄ 0 ≤ %CH ₄ ≤ 10	N ₂ -CH ₄ 90-10	N ₂ -CH ₄ 90-10 + He
Pression	0.9 – 1.7 mbar	0.5 mbar	~mbar + ~5mbar He
Température	Température amb.	Température amb.	Température amb.
Echantillons collectés	- Tholins en poudre - Couches minces de tholins - Gaz (piégeage cryogénique)	- Tholins en poudre	- Gaz (piégeage cryogénique)

	- Résidu du piège froid		
Diagnostics disponibles	- SMQ	- SMQ	- SMQ
	- IRTF (30 cm)	- IRTF multi passage (7m)	
	- SOE		

Dans toutes ces expériences, le principe est similaire. Il s'agit d'apporter de l'énergie (soit sous forme de photons pour APSIS soit sous forme d'électrons pour les montages plasma) à un mélange gazeux d'azote et de méthane, à une pression d'environ un millibar. Le mélange est fait dans des proportions similaires à celles trouvées dans l'atmosphère de Titan (de 1 à 10% de méthane dans l'azote).

L'azote et le méthane vont dans un premier temps être soit dissociés soit ionisés, pour ensuite engendrer une chimie organique complexe aboutissant d'une part à la formation de composés en phase gaz et d'autre part à la production d'aérosols organiques solides, les tholins.

Concernant l'étude de la phase gazeuse, l'étude de la phase stationnaire obtenue avec différentes proportions de méthane (de 1 à 10%) dans le mélange initial montre une corrélation entre l'enrichissement de la phase gazeuse (nombre d'espèces détectées et leur quantité) et le pourcentage de méthane.

L'ammoniac et la methanimine sont détectés en phase gaz, en accord avec leur détection dans l'ionosphère de Titan par l'instrument INMS. La production de ces composés hautement polymérisables pourrait être une première étape dans la formation des tholins. Deux effets opposés dans la formation et croissance des aérosols peuvent être déduits des mesures sur la phase gaz. D'une part, la croissance organique via la co-polymérisation d'imines, et d'autre part un processus inhibiteur dû à la présence d'hydrogène atomique. Cet effet inhibiteur est à mettre en relation avec des observations récentes montrant une fixation de l'hydrogène sur des aérosols de laboratoire, au dépend de la croissance organique de l'aérosol.

En phase gazeuse, il a été détecté une grande quantité de nitriles, parfois quatre fois plus importante que la quantité d'hydrocarbures (pour des mélanges à faible pourcentage de méthane). Le principal produit détecté en phase gaz est le cyanure d'hydrogène, également détecté en grandes quantités dans l'atmosphère de Titan. Malheureusement la chimie des nitriles est encore largement inconnue, et ceux-ci sont souvent ignorés dans les modèles de chimie atmosphérique de Titan.

De manière générale, la composition du gaz dans mes expériences (plus d'une trentaine d'espèces détectées) est en accord avec les connaissances actuelles sur la composition de l'atmosphère de Titan. Ceci tend à démontrer l'intérêt des expériences de laboratoire (tout du moins celles capables de dissocier l'azote) comme moyen d'étude complémentaire aux observations pour l'atmosphère de Titan.

En plus de la détection des composés présents, j'ai pu effectuer une quantification relative de certains de ces composés, les mono-nitriles saturés, présentée sur la

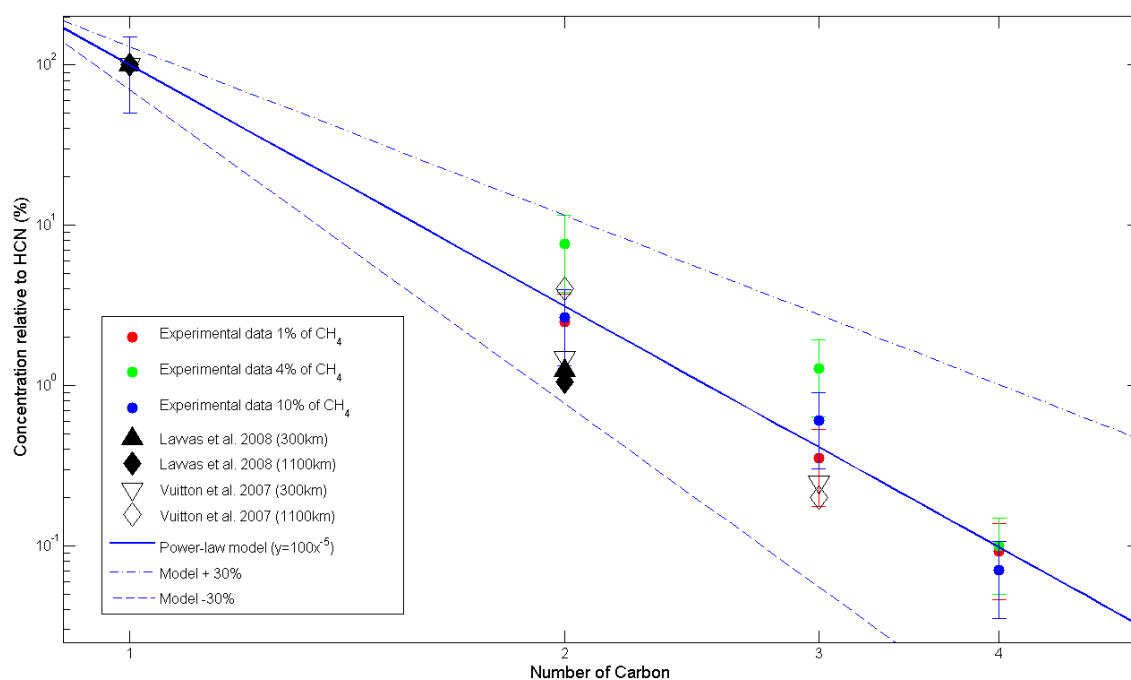


Figure 1: Quantification relative des mono-nitriles saturés. Les points de couleurs correspondent aux données expérimentales, les diamants et triangles vides aux observations d'INMS, et les triangles et diamants plein aux sortie de modèle photochimique de l'atmosphère de Titan.

Cette quantification m'a permis de proposer une modélisation en loi de puissance pour la concentration de ces composés qui est (avec HCN normalisé à 100) :

$$[C_xH_{2x-1}N] = 100x^{-5}$$

Où x est le nombre d'atomes de carbone dans la molécule. Cette loi empirique est en accord avec les observations de Cassini et les sorties de modèles photochimique de l'atmosphère de Titan et pourra permettre d'estimer la concentration de nitriles lourds en connaissant celle des légers. Le spectromètre infrarouge multi-passage présent sur l'expérience de Bochum m'a également permis de quantifier de manière absolue HCN et NH_3 (respectivement à 90 ppm et 15 ppm environ).

La seconde partie de ma thèse est dédiée à l'analyse des tholins. Les analyses chimiques nous donne un nouveau point de vue sur leur exact composition et révèle la grande complexité de ce matériau. Cette complexité a nécessité un traitement statistique des spectres de masse obtenus avec un spectromètre de masse à haute résolution (orbitrap).

En plus de l'analyse des tholins, un autre matériau a été analysé. Il s'agit d'un résidu de polymérisation des gaz neutres. Cette analyse a permis d'obtenir des informations sur les chemins de réactivité menant à la formation des tholins, en mettant en exergue les différences entre matériau produit simplement par la polymérisation des neutres (résidu) et un matériau produit dans un plasma réactif (tholins) par des processus impliquant à la fois des neutres, des ions et possiblement de la chimie hétérogène à la surface de l'aérosol.

Les principales molécules détectées dans les tholins contiennent une plus grande quantité d'azote que celles détectées dans le résidu. L'on peut supposer que la principale différence entre les tholins et le résidu est la chimie ionique ayant lieu lors de la formation des tholins mais pas du résidu. Cela pourrait signifier que la chimie ionique augmente l'inclusion d'azote dans les tholins, en comparaison avec la chimie des neutres qui va produire des molécules avec un ratio N/C plus faible.

Le spectre de masse des tholins montre des structures polymériques, qui sont confirmées par l'indentification de plusieurs familles de polymères dans le matériau. Cela renforce l'idée que les tholins seraient des co-polymères, probablement pas linéaires, mais plutôt des co-polymères hyperbranchés. Différentes hypothèses de croissance ont été testées pour

reconstruire le spectre de masse des tholins en supposant un co-polymère idéal de deux monomères. La Figure 2 propose une représentation schématique des différentes décompositions en bases proposés dans cette thèse.

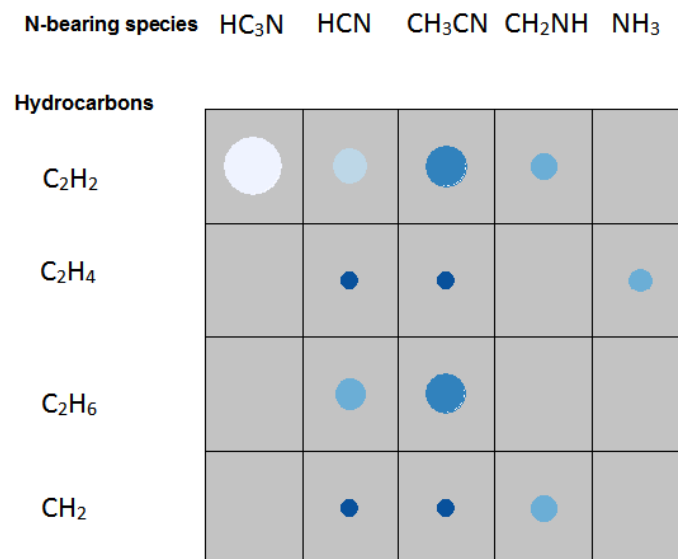


Figure 2: Représentation schématique des différentes reconstructions des spectres de masse. Une bonne concordance correspond à un cercle petit et sombre (voir le corps de la thèse pour de plus amples explications).

Malgré tout, une convergence des familles polymériques montre que, aux hautes masses ($m/z > 300$), le matériau peut être assimilé à un polymère moyen de formule $(CH_{1.5}N_{0.5})_n$.

J'ai également analysé les propriétés d'absorption dans l'infrarouge des tholins. Cette étude a permis de fournir pour la première la dépendance en fonction de la longueur d'onde du coefficient linéaire d'absorption des tholins, ϵ , du lointain au moyen infrarouge ($100\text{-}4000\text{ cm}^{-1}$). J'ai également étudié l'impact du pourcentage de méthane du mélange gazeux où sont formés les tholins sur leur spectre d'absorbance dans le moyen infrarouge. Cette influence est maximale sur les bandes amines (vers 3330 cm^{-1} et 3200 cm^{-1}) et est également très marquée sur les bandes attribuées aux carbones aliphatiques vers 2900 cm^{-1} comme présenté sur la Figure 3.

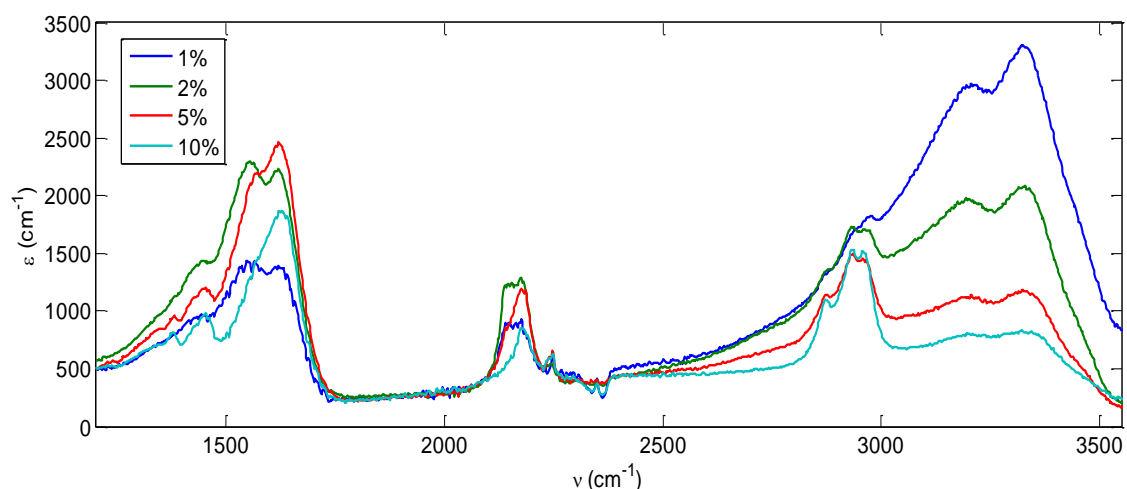


Figure 3: Comparaison des spectres IR de tholins produits avec différents pourcentage de méthane

Les spectres des tholins ont ensuite été comparés aux observations faites par les instruments CIRS et VIMS à bord de Cassini. Le massif à 2900 cm^{-1} montre une concordance entre les tholins et les observations de VIMS, supportant l'idée que les aérosols seraient les principaux contributeurs de la bande d'absorption observée par VIMS dans cette zone. En comparant les données de laboratoire dans le lointain infrarouge avec celles de CIRS, là aussi on obtient une bonne correspondance. Les deux spectres sont en accords sur de nombreuses bandes d'absorption, en particulier à 1450 cm^{-1} , 1380 cm^{-1} , 515 cm^{-1} et 325 cm^{-1} , renforçant la détection et l'attribution de ces bandes aux aérosols.

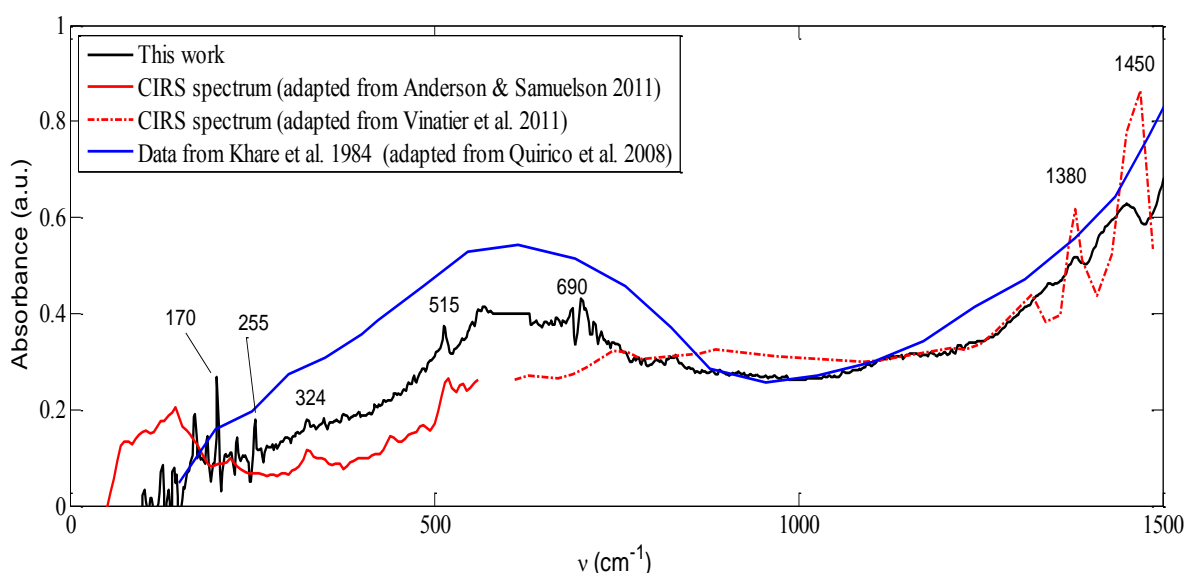


Figure 4: Comparaison des spectres de tholins (noir) et des observations de l'atmosphère de Titan par CIRS entre 50 et 1500 cm^{-1}

Ces comparaisons entre les données obtenues sur des tholins de laboratoire et des observations réelles des aérosols de Titan confirme que, même si ils ne sont pas parfaits, les tholins produits avec le réacteur PAMPRE sont de bons analogues d'aérosols de Titan, et que leur étude permet d'obtenir des indices sur les processus de formation et les propriétés des aérosols de Titan.

La dernière partie de cette thèse concerne des expériences faites avec le réacteur APSIS. Ce réacteur est un nouveau réacteur photochimique, utilisant un rayonnement synchrotron comme source d'énergie. Pour ces expériences, un mélange gazeux d'azote méthane est irradié par un spectre continu (60-350 nm) de photons VUV provenant de la ligne de lumière DISCO sur le synchrotron SOLEIL. Les produits neutres de la photochimie ont été suivis par spectrométrie de masse, montrant des constantes de temps de l'ordre de la quinzaine de minutes et une production d'espèces allant jusqu'à quatre ou cinq atomes lourds (carbone ou azote). Les hydrocarbures en C2 sont de loin les produits majoritaires dans ces expériences, mais des composés azotés tels que HCN, CH₃CN et C₂N₂ sont également détectés. Les résultats obtenus lors de ces expériences sont ensuite comparés aux expériences menées à l'aide de montage plasma tels que PAMPRE et aux mesures in-situ faites par INMS dans l'atmosphère de Titan.

Malgré des taux de production photochimique plus faibles et des conditions environnementales différentes, le réacteur APSIS semble plutôt bien simuler la composition des neutres dans la haute atmosphère de Titan. Cependant, avec comme but de former des particules solides pour pouvoir les étudier de la même manière que les tholins produits par plasma, l'efficacité de production du montage devra être améliorée dans le futur, par exemple en augmentant le temps de résidence des gaz dans le réacteur.

Les principaux résultats de cette thèse sont résumés dans la Table 2.

Table 2: Principaux résultats de cette thèse

	Gaz	Phase solide
Produits principaux	Contiennent de l'azote (principal produit = HCN)	Contiennent de l'azote
Diversité des produits	Grande (HCN <1% du carbone)	Grande (~15.000 espèces détectées)

	totale)	
Quantification	HCN ~ 90 ppm NH ₃ ~15 ppm	Coefficient d'absorption linéaire (ε) => impact de la variation du %CH ₄ sur le spectre IR des tholins <ul style="list-style-type: none"> - Diminution des bandes amines - Augmentation des bandes carbone aliphatique
Comparaison à Cassini	Loi de puissance pour la quantification relative des nitriles : [C _x H _{2x-1} N]=[HCN].x ⁻⁵	Spectres IR en accord : VIMS: 2900 cm ⁻¹ (carbone aliphatique) CIRS: 1480 – 1350 cm ⁻¹ (carbone aliphatique) 515 and 325 cm ⁻¹ (non identifiés)
Limites de la détection	Composés détectés les plus lourds : m/z ~130	Composés détectés les plus légers m/z ~60
Processus de formation	<ul style="list-style-type: none"> - La chimie ionique augmente l'incorporation d'azote dans les tholins - La transition gaz-solide à probablement lieu à quelques dizaine d'uma (m/z ~100) 	

Chapter I : Titan - Observations and Experimental Simulations

I.1 Titan

I.1.1 Past and present exploration

Titan has been first observed in 1655 by Christiaan Huygens and finally named by John Herschel in 1847. It is now known to be the largest satellite of Saturn among 62 detected, and the second biggest of the Solar System after Ganymede. It is also the only satellite of the Solar System that present a dense atmosphere, first suspected in 1908 by Comas i Sola who observed the darkening of Titan's limb.

The possibility of the existence of Titan's atmosphere was then justified by James Jeans who first studied the escape of planetary atmospheres and demonstrated that assuming cold temperature on Titan (below 100 K) volatiles compounds, with exception of Hydrogen and Helium could have been kept by Titan (Jeans 1931). The existence of this atmosphere was definitely proven in 1944 by Gerard Kuiper who detected the presence of methane (CH_4) around Titan with ground based spectroscopic measurements in the infrared wavelength range (Kuiper 1944). Ground based infrared spectroscopic observations performed in the 1970's detected four other hydrocarbons. Deuterated methane ($\text{CH}_3\text{-D}$), acetylene (C_2H_2), ethylene (C_2H_4) and ethane (C_2H_6) were thus added to the list of compounds present in Titan's atmosphere (Gillett 1975).

The next step on knowledge about Titan's atmosphere came from space exploration. Especially, the Voyager 1 and Voyager 2 space probes flew by Titan in the early 1980's and confirmed that brownish color of Titan was due to the presence of aerosols in the atmosphere, as suggested by Sagan based on laboratory experiments (Sagan 1971).

Voyager probes were able to observe Titan in the infrared thanks to the IRIS spectrometer (which performed absorption spectroscopy from 200 to 1400 cm^{-1}) and in the UV with the UVS instrument. Molecular Nitrogen (N_2) was determined as the major component of the atmosphere (Strobel and Shemansky 1982) and methane as the second most important compound, with a concentration of a few percent (Hanel et al. 1981). Numerous other

molecules have been quantified thanks to these observations, such as C_2H_2 , C_2H_4 , C_2H_6 and HCN (Maguire et al. 1981). Others were detected as traces such as C_4H_2 , HC_3N , C_2N_2 and CO_2 (Kunde et al. 1981; Letourneur and Coustenis 1993). Using limb observations and radio occultation it was also possible to deduce vertical temperature profile and vertical and latitudinal distribution of some compounds (Lellouch et al. 1989; Coustenis et al. 1991).

The previous space exploration mission only flew by Titan. The first (and up to now unique) mission to satellite within the Kronian system was the NASA/ESA Cassini-Huygens mission, launched in 1997 and which reached Saturn in 2004. In addition to study the whole system of Saturn, one of the objectives of this mission was to get deeper information about Titan (Coustenis et al. 2010). The objectives for the chemical study of Titan's atmosphere were:

- Determine the abundance of atmospheric constituents and their vertical and horizontal distribution.
- Detect new gaseous molecules.
- Determine the possible energy sources for the atmospheric chemistry and their relative contribution.
- Study the formation, composition and distribution of the aerosols
- Investigate the upper ionized atmosphere and determine its possible role on the neutral and ionized chemistry, and on the aerosols formation.

To do so, the mission carries twelve instruments, and the Huygens descent probe six. The instruments able to bring partial answers to the objective on the atmospheric chemistry were:

Onboard Cassini:

- CAPS (CAssini Plasma Spectrometer): dedicated to the study of charged particles in Saturn magnetosphere. Although it was not its first goal, this instrument has been able to detect heavy negatively charged ions in Titan's ionosphere (Young et al. 2004; Coates et al. 2007).
- INMS (Ion and Neutral Mass Spectrometer): in-situ monitoring of Titan's ionosphere. INMS measurements allowed identifying numerous gaseous species (and possibly aerosols precursors) and characterizing the chemistry in Titan's high atmosphere. (Waite et al. 2005; Vuitton et al. 2007).

- CIRS (Composite InfraRed Spectrometer): One of the infrared spectrometer of Cassini, originally built to characterize the thermal IR emission of Titan and thus the altitude and latitude profile of the atmosphere. CIRS can be used to detect and quantify gas compounds in Titan's low atmosphere (< 400 km). It has also detected some aerosols features in the far-IR (Flasar et al. 2005; Vinatier et al. 2010; Anderson and Samuelson 2011; Vinatier et al. 2012).
- VIMS (Visible and Infrared Mapping Spectrometer): It is the other IR spectrometer, in charge of characterizing the chemical composition of surfaces and atmospheres. VIMS also detected possible aerosol signature in the mid-IR. (Brown et al. 2004; Rannou et al. 2010).
- UVIS (UltraViolet Imaging Spectrograph): It is the only instrument on Cassini that can sample the mid-atmosphere (its altitude range goes from 250 km up to 1200 km), whereas IR spectrometer provide information on the low atmosphere and in-situ MS on the high atmosphere (Esposito et al. 2004).

Onboard Huygens:

- ACP-GCMS (Aerosol Collector and Pyrolyser – Gas Chromatograph and Mass Spectrometer): It collected aerosols and pyrolyzed them. Pyrolysis products were then introduced either directly in a MS or in a GC-MS. This experiment, probably the most interesting regarding the content of my thesis, did not worked nominally due to some technical problems. Nevertheless, it has been able to identify major aerosols pyrolysis product to be HCN and NH₃ (Israel et al. 2005; Coll et al. 2013).
- DISR (Descent Spectral Imager Radiometer): It was dedicated to imaging the surface of Titan. DISR performed spectroscopic measurements of the atmosphere (in both IR and visible), providing numerous information on the low atmosphere of Titan, as on the aerosols morphology (Tomasko and et al. 2005; Tomasko et al. 2008)
- HASI (Huygens Atmosphere Structure Instrument): It provided data on the physical properties of the atmosphere (Pressure, Temperature, Electrical Properties...) (Fulchignoni et al. 2005).

I.1.2 Current knowledge on Titan's atmospheric aerosols

Results from the Cassini mission and other observations allow drawing a first scheme of Titan's aerosols properties and formation processes. A complete overview of the problem can be found in Waite et al. 2010 and Tomasko and West 2010, the main results are reminded here.

I.1.2.a Formation processes

The INMS instrument which provided the neutral and ion mass spectra of Titan's high atmosphere around 1 000 km emphasized the presence of numerous different compounds, mainly hydrocarbons and nitriles (Waite et al. 2007; Vuitton et al. 2009) (see Figure 5).

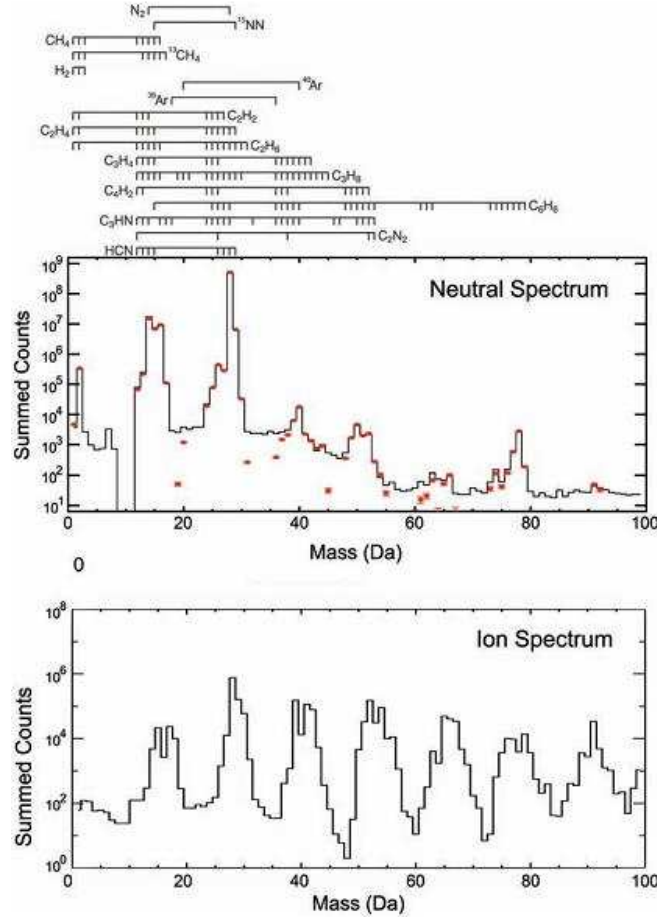


Figure 5: Composite mass spectra for neutrals (top) and ions (bottom) based on Cassini INMS data (black line) acquired during 17 flybys of Titan ~1000 km. Products signaled above the neutral spectrum are the one used for the mass deconvolution (red dots). From Waite et al. 2007.

These compounds could be the first step of the intense organic chemistry leading to aerosols production. Other measurements performed with the CAPS instrument showed the presence of heavy negatively charged ions around the same altitude (see Figure 6).

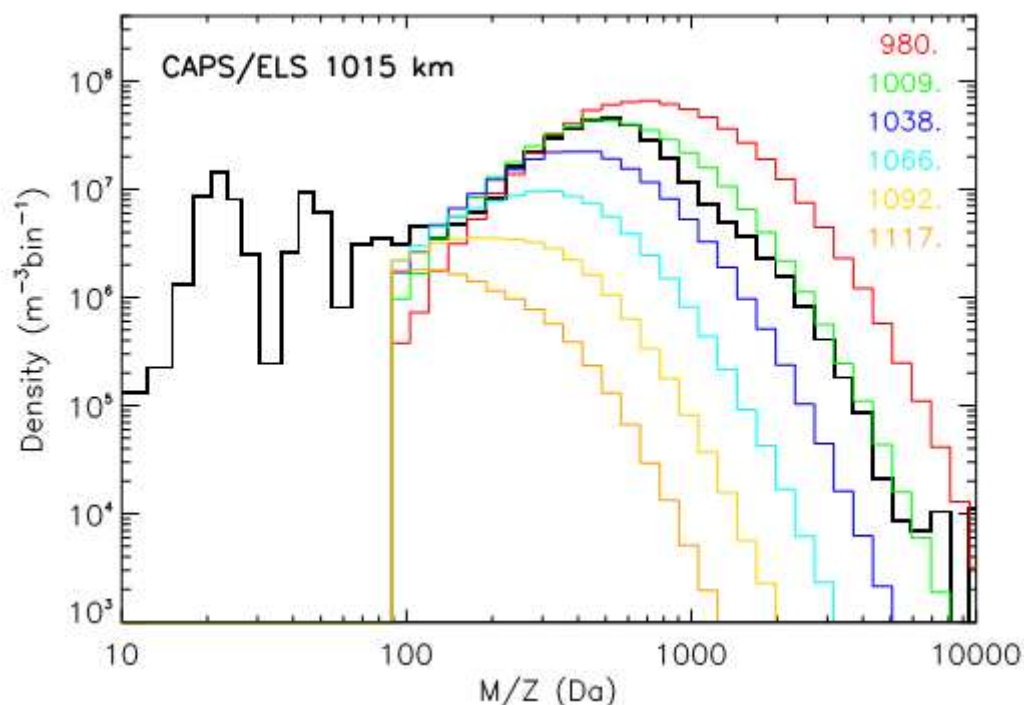


Figure 6: Masse/charge spectrum of negatively charged ions taken at 1015 km during flyby with the CAPS instrument (black line), and model outputs for different altitudes (color lines). From Lavvas et al. 2013

Models outputs from Lavvas et al. 2013 show that the heavy part of the distribution ($m/z > 100$) increases when altitude decrease, emphasizing a growth of these heavy negatively charged particles, when they sediment in Titan's high atmosphere. This result has been recently confirmed by measurements of the CAPS instrument that in addition found no evidence of these heavy particles above 1100 km (Wellbrock et al. 2012). These particles are probably aerosols that acquired charged in interaction with free electrons in Titan's ionosphere (Lavvas et al. 2013 and reference therein).

These observations led to a commonly proposed formation pattern presented in Figure 7. The first step of the chemistry leading to aerosols formation is the ionization and dissociation of nitrogen and methane. This activation can be done both by photochemistry with solar photons, or by collisions with electrically charged particles coming from Saturn's magnetosphere. Actually a study by Robertson et al. 2009 showed that, even if the concentration of species

detected by INMS is less during the night, when no photochemistry occurs, the species detected are similar to the one detected during the day. This would mean that both energy sources induce a similar chemistry in the atmosphere.

The second step of aerosols formation may be the formation of light volatiles such as HCN, C_2H_2 or NH_3 , actually detected in the atmosphere. These species could then themselves recombine to produce bigger ones such as aromatics molecules which then form bigger poly-aromatics hydrocarbons (PAH) complexes (which could be close to the heavy ions detected by CAPS) and then aerosols.

Nowadays, largely supported by laboratory experiments, it starts to be admitted that the chemistry does not exclusively pass through a hydrocarbon way involving PAH, but also probably includes a large amount of nitrogen and poly-heteroaromatics (PANH) compounds within aerosols (Imanaka et al. 2004; Vuitton et al. 2007; Imanaka and Smith 2010; Sciamma-O'Brien et al. 2010; Yelle et al. 2010; Gautier et al. 2011). This idea is supported by the results of the ACP instrument onboard Huygens which detected two nitrogenous compounds (HCN and NH_3) as main product of aerosols pyrolysis (Israel et al. 2005).

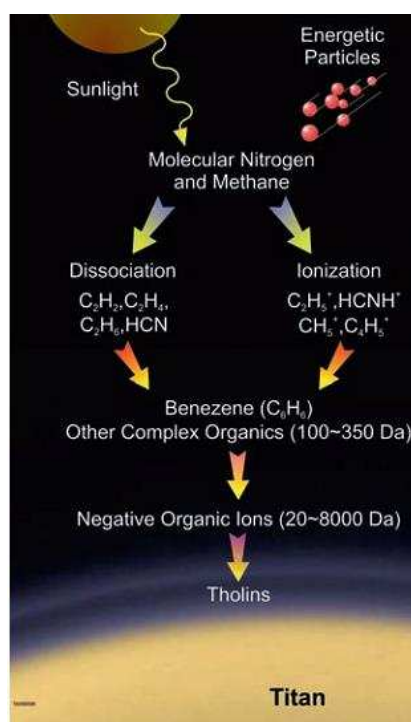


Figure 7: Proposed main step of aerosols formation in Titan's high atmosphere. From Waite et al. 2007

1.1.2.b *Physical and chemical properties of Titan's aerosols*

Polarimetric measurements done by the Voyager 2, Pioneer 11 (Tomasko and Smith 1982) and Huygens missions (Tomasko et al. 2008) showed an important backscattering of the linearly polarized light by the aerosols. This was interpreted as the consequence of light scattering by aggregated small particles, with radii of about 50 nm for the monomers. The best constraint on observation also requires using fractals particles instead of simple spherical aerosols (Cabane et al. 1993; Rannou et al. 1995; Rannou et al. 2003). Each aggregate seems to be composed by about ~3,000 monomers.

The main information available on Titan's aerosols composition comes from their signature in the infrared. The VIMS instrument measurements show a possible absorption band of the aerosols around 3.4 μm (2950 cm^{-1}) presented in Figure 8 (Bellucci et al. 2009; Rannou et al. 2010). This pattern could be due to aliphatic carbon $-\text{CH}_2$ and $-\text{CH}_3$ bonds within aerosols (see Chapter IV).

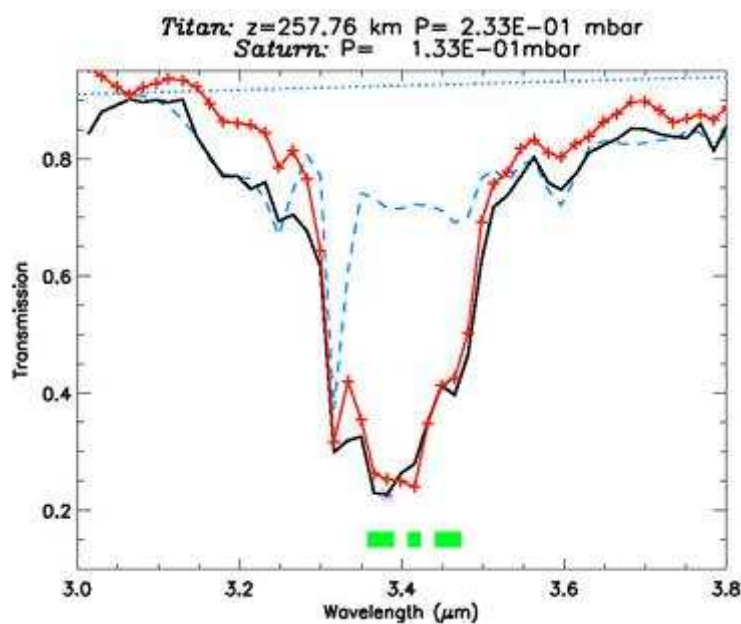


Figure 8: Observation of the 3.4 μm feature in Titan's (black) and Saturn's (red) atmospheres. The blue dashed line represents the CH_4 band at 3.3 μm modeled for 1.6% of CH_4 . From Bellucci et al. 09.

The CIRS instrument also provided aerosol signature in the far-Infrared below 1500 cm^{-1} as shown in Figure 9 (Vinatier et al. 2010; Anderson and Samuelson 2011; Vinatier et al. 2012).

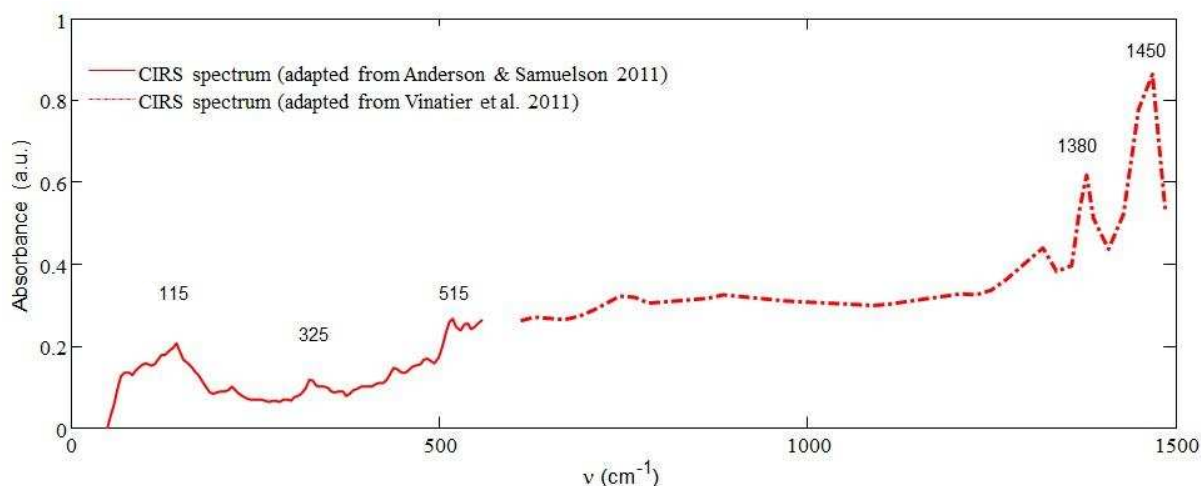


Figure 9: Titan's aerosols spectrum (15°S, ~80 km) in the far-IR. From Vinatier et al. 2010, Anderson & Samuelson 2011, Anderson, private communication.

The three bands at 1320, 1380 and 1450 cm^{-1} confirm the aliphatic carbon ($-\text{CH}_2$ and $-\text{CH}_3$) bonds in the aerosols. The other features in this spectrum are still unexplained. For more details on the IR spectroscopy of aerosols, refer to chapter IV of this thesis.

The ACP instruments onboard Huygens also provided a few information on the aerosols (Israel et al. 2005). Figure 10 shows the mass spectrum of the gas resulting from a pyrolysis of aerosols during Huygens descent. Red bars represent the signal from the sample and green one the signal during background measurements.

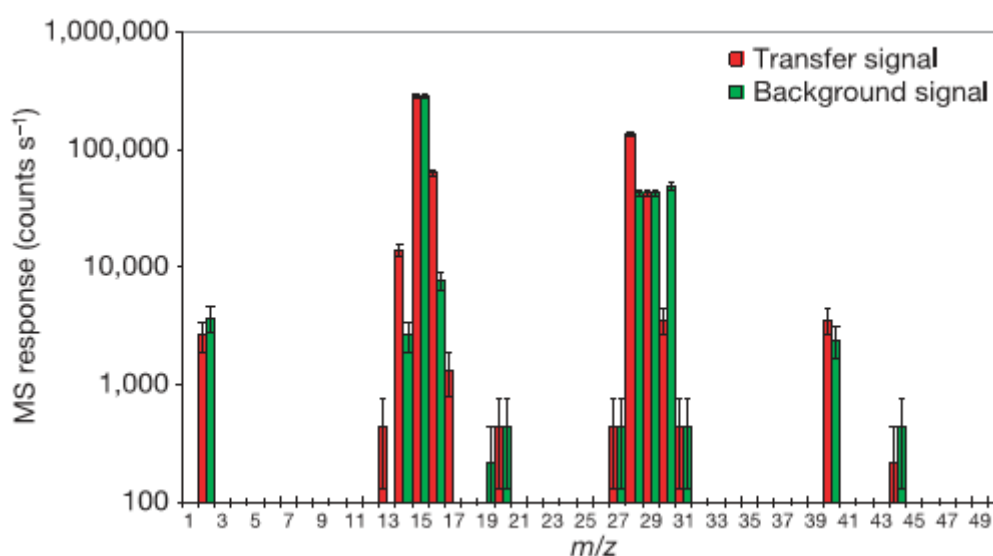


Figure 10: Mass spectrum of the gas resulting from pyrolysis of Titan's aerosols sample at 600°C. From Israel et al. 2005.

The main products detected by the ACP experiment are located at m/z 17 and m/z 27. These two peaks are respectively attributed to NH_3 and HCN . It has to be noticed that this products have been observed only when heating the sample up to 600°C . This indicates the refractory nature of Titan's aerosols and excludes the hypothesis that aerosols may be formed of pure hydrocarbons.

I.2 Titan in a can: Laboratory analogs of Titan's aerosols

Even though the Cassini-Huygens mission provided numerous information on Titan's aerosols, the knowledge of their formation processes and of their composition and properties is still fragmented.

To complete the scheme, the most accessible way is to perform laboratory experiments. All the existing laboratory simulation of Titan's atmosphere use basically the same principle: providing energy to a $\text{N}_2\text{-CH}_4$ (or close) gas mixture to induce first gas chemistry and then the formation of laboratory analogues of Titan's aerosols, so called tholins. Some of these simulations use photochemical irradiation, where photons provide energy to the mixture, whereas other experiments, such as PAMPRE, provide energy by electronic impact within a plasma. The problematic of comparing both energy source is not the main aim of this chapter, but has been discussed in the literature (Cable et al. 2011, Alcouffe 2010)

The three main parameters determined by Cassini-Huygens that should be taken into account for setting up an experiment simulating Titan's aerosols formation are the pressure, the temperature and the gas composition, i.e. the methane mixing ratio in nitrogen. The temperature profile determined by HASI is given in Figure 11. The pressure in the reactors I used during this thesis (see chapter II) was comprised between 0.5 mbar (Bochum reactor) and 8 mbar (APSIS reactor in certain conditions). In Titan atmosphere, this pressure corresponds roughly to the top of the stratosphere, i.e. 200-250 km. It should also be noticed that even if the temperature of 300 K used in my experiment is much higher than Titan's ground temperature (90 K), the temperature in Titan's atmosphere is maximum at the top of the stratosphere, with almost 190K at 250 km.

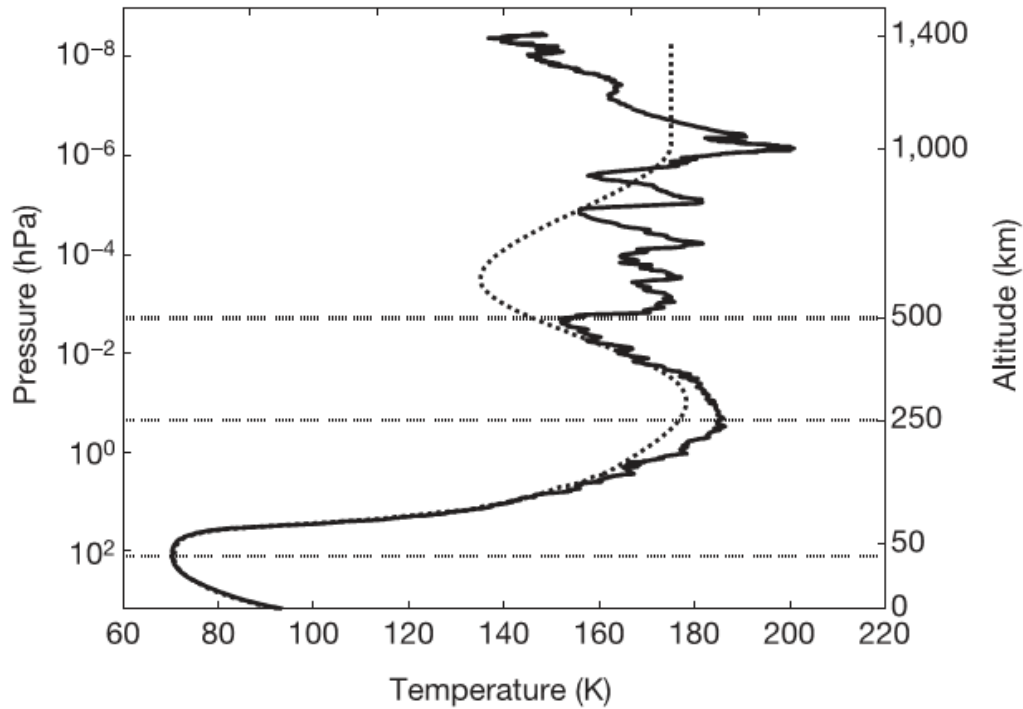


Figure 11: Titan's atmosphere temperature profile determined by HASI onboard Huygens. From Fulchignoni et al. 2005

The GC-MS instrument provided the CH_4 density profile in the low atmosphere, showing that CH_4 concentration is maximum at the ground, with a mole fraction of about 4.9% and decreases rapidly with altitude to reach 1.7% mixing ratio at 30 km before following an asymptotic behavior with a mixing ratio of 1.4% at 140 km (see Figure 12 and Niemann et al. 2005).

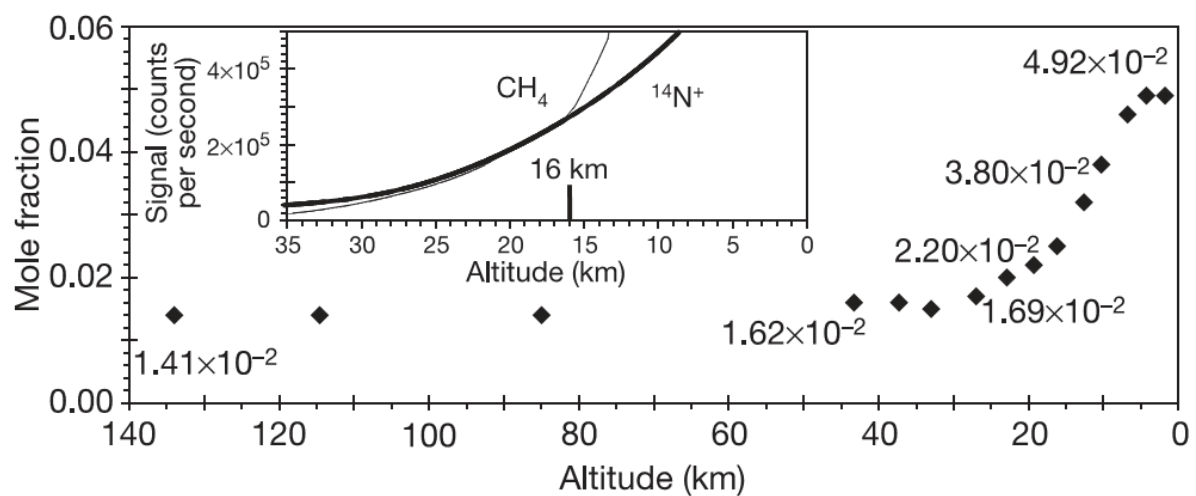


Figure 12: CH_4 mixing ratio in the low atmosphere from GC-MS measurements. From Niemann et al. 2005

Measurements performed with CIRS at and INMS confirmed a value of respectively 1.6 ± 0.5 % around 15 mbar and 2.2% around 1200 km (Flasar et al. 2005; Waite et al. 2005). These measurements confirmed that CH₄ is well mixed in the atmosphere above 30 km until at least the thermosphere.

To understand the formation of tholins, there are two different and complementary approaches. The first is bottom-up studies, where the work is focused on the study of the gas phase leading to tholins (both its composition and reactivity). The second is a top-bottom approach where tholins properties and composition are examined to infer their formation processes. I used these two different approaches for this thesis.

More than eighty references can be found in the literature on experimental simulations of Titan's atmosphere and tholins analysis. The properties and composition of both the gas phase and the aerosols produced are dependent on the experimental parameters. The main parameters varying from an experiment to another are the energy deposition method, the physical conditions (pressure, temperature), and of course the reactors design. However, two recent reviews papers (Cable et al. 2011; Coll et al. 2013) provided a quite complete overview of the experiments performed to study tholins formation.

I.2.1 Gas Phase

Several studies are dedicated to the gas phase in laboratory experiment, but, with exception of Ruiz Bermejo 2009 and Imanaka and Smith 2010, were performed before the Cassini Era. All these study were thus dedicated to the identification of compounds present in gas phase, for extrapolation on Titan's atmospheric composition.

Looking at the gas phase products in Titan's atmospheric experiments depicted in the literature, it appears clearly that these products are mainly hydrocarbons and nitrogen-bearing species (De Vanssay E and Raulin 1995; Coll et al. 1999; Ramírez et al. 2005; Imanaka and Smith 2010). Nitrogen bearing species are mainly nitriles with a few amines and imines. Most molecules detected are light species (less than 10 carbon or nitrogen atoms) with many unsaturated molecules. It has to be underlined that experiments using cold plasma produce an amount of nitrogen-bearing molecules much higher than photochemical irradiation simulations. A probable explanation is that the energy distribution function of the electron within a plasma is slightly wider (especially the tail of the distribution at high energies) than

the energy distribution of solar photons. These energetic electrons are the one able to dissociate and ionize N_2 (Szopa et al. 2006; Alcouffe et al. 2010).

However, the literature on the gas phase in Titan's atmospheric experiment is limited to providing an exhaustive list of compounds detected in the experiment, but is not focused on the transition between the gas phase and aerosols. Several questions remain thus on the gas phase and I will focus my work on the following two points:

- First, what are the mechanisms involved in the gas phase chemistry, and what is the reactivity of products detected in the frame of Titan's atmospheric chemistry?
- Second, what are the species "used" as precursors for aerosols formation?

1.2.2 Tholins optical properties in the Infrared range

Looking at the aerosols themselves, the main data available for comparing laboratory tholins with Titan's aerosols are their optical properties. Especially the infrared signature of Titan's aerosols provides numerous comparison points with their laboratory analogues. The first study analyzing tholins properties in the IR was Khare et al. 1984 which provided the optical constants of tholins from soft X-rays to Microwave frequencies. Due to its wide expertise area, this paper has been used as a reference for many studies and comparison with observations of Titan's atmosphere. However the tholins spectrum in the IR presents major discrepancies with actual observations of Titan (Anderson and Samuelson 2011). Recently, few studies started to investigate the absorption properties of tholins in the mid-infrared. Imanaka et al. 2004 reported the main function visible in the IR spectrum and the influence of the experimental pressure on the infrared signature of tholins (Figure 13).

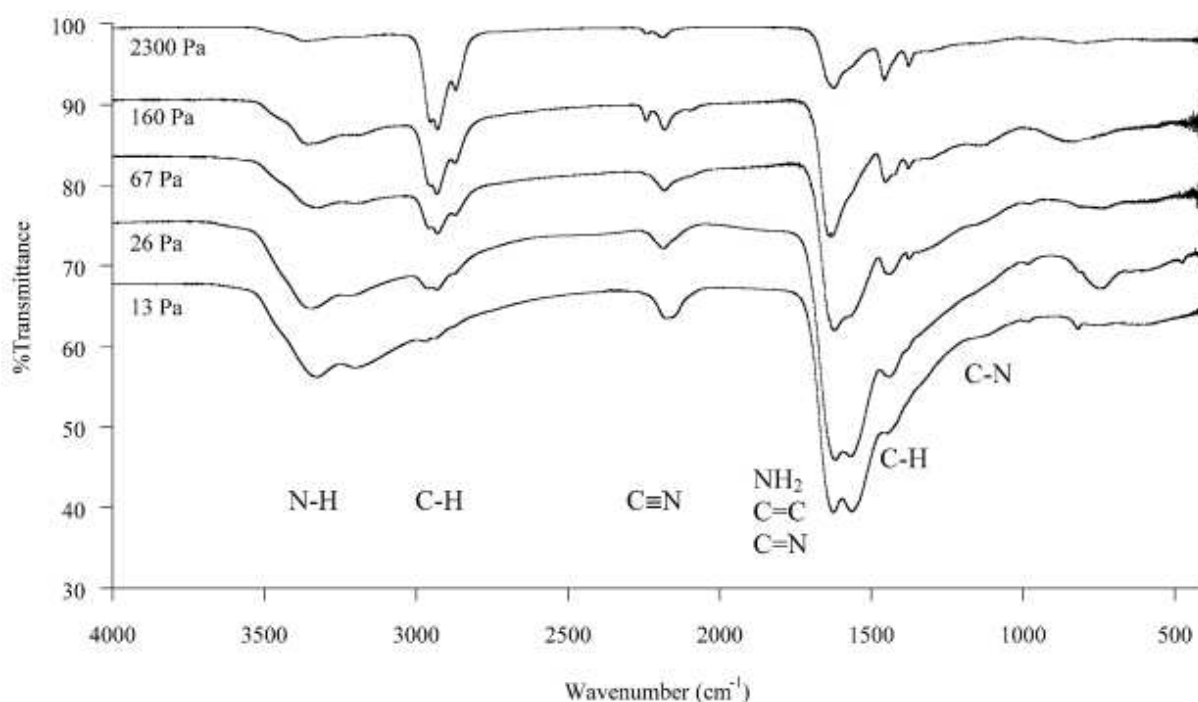


Figure 13: Comparison of IR spectra produced by plasma discharge in CH_4/N_2 90/10 gas mixture at different pressures. From Imanaka et al. 2004. The main bonding absorption area are reported on the spectra.

Authors also proposed a Gaussian deconvolution of the CN bonding pattern at 2200 cm^{-1} , emphasizing that this pattern can be fitted using 6 different Gaussians (and thus representing six different configurations for the CN bonds within tholins). The main observation of this study is the influence of pressure on the aliphatic carbon pattern around 2900 cm^{-1} . The higher the pressure, the more this pattern is visible. Bernard et al. 2006 also reported variability of this pattern and of the one at 2200 cm^{-1} between two samples harvested in two different area of the same experiments (and thus supposed to have two different compositions). Quirico et al. 2008 provided a comparison of the spectra in the mid-IR ($4000 - 500\text{ cm}^{-1}$) range of tholins produced in the PAMPRE setup with different methane percentage. Once again, the aliphatic carbon pattern appears to be highly variable with methane percentage, whereas the global structure of tholins spectra is similar. Quirico et al. 2008 also compared tholins spectra with the spectrum of a poly-HCN polymer. Even if the spectra present similarities, it is clear that such polymeric material is not able to properly reproduce the spectrum of tholins. Although I did not focused on the optical constants (n and k index) of tholins during my thesis, it has to be noticed that two papers have been published recently on this problem in the visible wavelength (Imanaka et al. 2012; Sciamma-O'Brien et al. 2012) providing comparison

with data on Titan's aerosols. The influence of methane percentage on these index have been investigated during my thesis by the PAMPRE team (Mahjoub et al. 2012).

All these studies provided numerous information on tholins optical properties in the mid-IR and on the chemical functions present in the samples. However, it has to point out two main lacks in the literature:

- With exception of the old Khare et al. 1984 data, there is no study providing the aerosols absorption properties in the far-Infrared (below 500 cm^{-1}), whereas, as seen above, the CIRS instrument onboard Cassini detected Titan's aerosols signatures in this domain.
- The experimental data available in the literature on tholins infrared absorption properties are usually not compared with actual observations on Titan's aerosols, either from the VIMS or from the CIRS instruments, respectively in the mid- and far-infrared.

In addition to comparing tholins with Titan's aerosols, studies can be performed on tholins using advanced experimental analyses. Indeed, a bottom up approach can be used by investigating on the chemical composition of laboratory tholins to infer the composition and thus the formation processes of Titan's aerosols.

Previous studies have been performed on tholinomics, the field defined in Pernot et al. (2010) as the chemical analysis of tholins. Elemental analysis provided a first chemical information on the C/N/H ratios in tholins (Imanaka et al. 2004; Sciamma-O'Brien et al. 2010; Cable et al. 2011). But it is not sufficient to determine their exact molecular composition. This is the reason why other types of chemical analyses have been used for tholinomics, such as infrared spectroscopy, X-ray photoelectron spectroscopy (Tran et al. 2003; Ruiz-Bermejo et al. 2008; Ruiz-Bermejo et al. 2009), chromatographic techniques such as gas chromatography-mass spectrometry (GC-MS); pyrolysis-GC-MS; high performance liquid chromatography (HPLC) (Ruiz-Bermejo et al. 2008; Coll et al. 2013), Nuclear Magnetic Resonance Spectroscopy (Derenne et al. 2012; He et al. 2012a; He et al. 2012b) or high resolution mass spectrometry (Hörst et al. 2012, Imanaka and Smith 2010; Pernot et al. 2010; Somogyi et al. 2012). All these analyses confirmed that tholins are probably based on organics polymer like structures,

not only made of hydrocarbons but also including a large amount of nitrogen which contributes to chemical functional groups of interest for astrobiology, such as amines or nitriles.

The remaining questions on tholins composition that I will try to answer in this thesis are:

- What are the predominant molecules in tholins, and what is their role in tholins formation?
- What are the chemical structures present in tholins and how do they differ in different tholins samples?

I.3 Conclusion

One of the most striking points about Titan is the huge amount of organic aerosols present in the atmosphere. The aerosol formation is not a minor phenomenon but actually a major aspect of Titan's atmosphere. Actually the amount of aerosols produce is so large that the surface of the satellite cannot be seen from space in the visible wavelengths. Such quantity of aerosols (totally opaque in the visible, much less in the infrared) is of high impact on Titan's atmospheric dynamic and radiative balance (Tomasko and West 2010).

In addition to its interest for planetary science, the study of Titan's aerosols, particularly their composition, is of high interest for astrobiology. Indeed, this material is among the most complex organic material known in the Solar System with exception of Earth. Based on laboratory experiment, it appears that Titan's aerosols are probably formed of H, C and N based complex molecules up to several hundreds of atomic mass units (amu). Some laboratory studies performed on Titan's aerosols analogs pointed out the formation of pre-biotic molecules such as amino-acids or purine bases when these materials are submitted to hydrolysis or produced in oxidative environment (Neish et al. 2009; Neish et al. 2010; Hörst et al. 2012).

The aim of this thesis is to answer some of the questions still running on Titan's aerosols through the study of tholins. All the measurements performed on laboratory tholins will, as much as possible, compared to the fragmentary data available on Titan's aerosols.

The main questions will be to characterize the chemistry and possible pathways leading to tholins formation. The second point assessed by this thesis will be to characterize with cutting

edge analytical techniques the properties and composition of tholins. To answer these questions, my work can be split up in two approaches.

The first one, presented in chapter III, is a bottom-up approach, by characterizing the reactivity and composition of the gas phase leading to tholins formation. This study is mainly based on mass spectrometric measurement in two N_2/CH_4 plasma reactors.

The second part of my work, presented in chapter IV, uses a top-bottom approach. This part is dedicated to the analysis of tholins using several techniques. The first one is the characterization of tholins mid- and far-infrared absorption properties. The second is the study by high resolution mass spectrometry (orbitrap) of tholins to investigate their chemical composition and get some clues on their formation pathways.

Although it is not directly linked to the first two parts, chapter V presents a study on the impact of the energy source used (plasma or photo-irradiation) on the gas phase reactivity.

Chapter II Methods

In this chapter, we are going to see the different reactors used for this thesis, and present all the analytical techniques I used to characterize samples produced in these setups.

II.1 Experimental devices

II.1.1 The PAMPRE experiment: Synthesis of Titan's aerosols analogues

II.1.1.a Setup

The PAMPRE (Production d'Aérosols en Microgravité par Plasma REactif) setup, developed in LATMOS since 2002 (Szopa et al. 2006), is a radio frequency capacitively coupled plasma used to simulate the chemistry occurring in Titan's atmosphere and leading to the formation of solid aerosols. The PAMPRE experiment has been developed on the basis of a previously existing reactor developed in GREMI laboratory (Boufendi and Bouchoule 1994) used for dusty plasma studies in argon-silane discharges.

The stainless steel reactor is cylindrical; 30 cm in diameter by 40 cm height. A scheme of the PAMPRE setup is given in Figure 14. Optical windows are displaced around the reactor to allow spectroscopic diagnosis, UV-Visible emission spectroscopy and Infrared absorption spectroscopy. At the bottom of the reactor, a capillary tube connects the reactor to a quadrupole mass spectrometer.

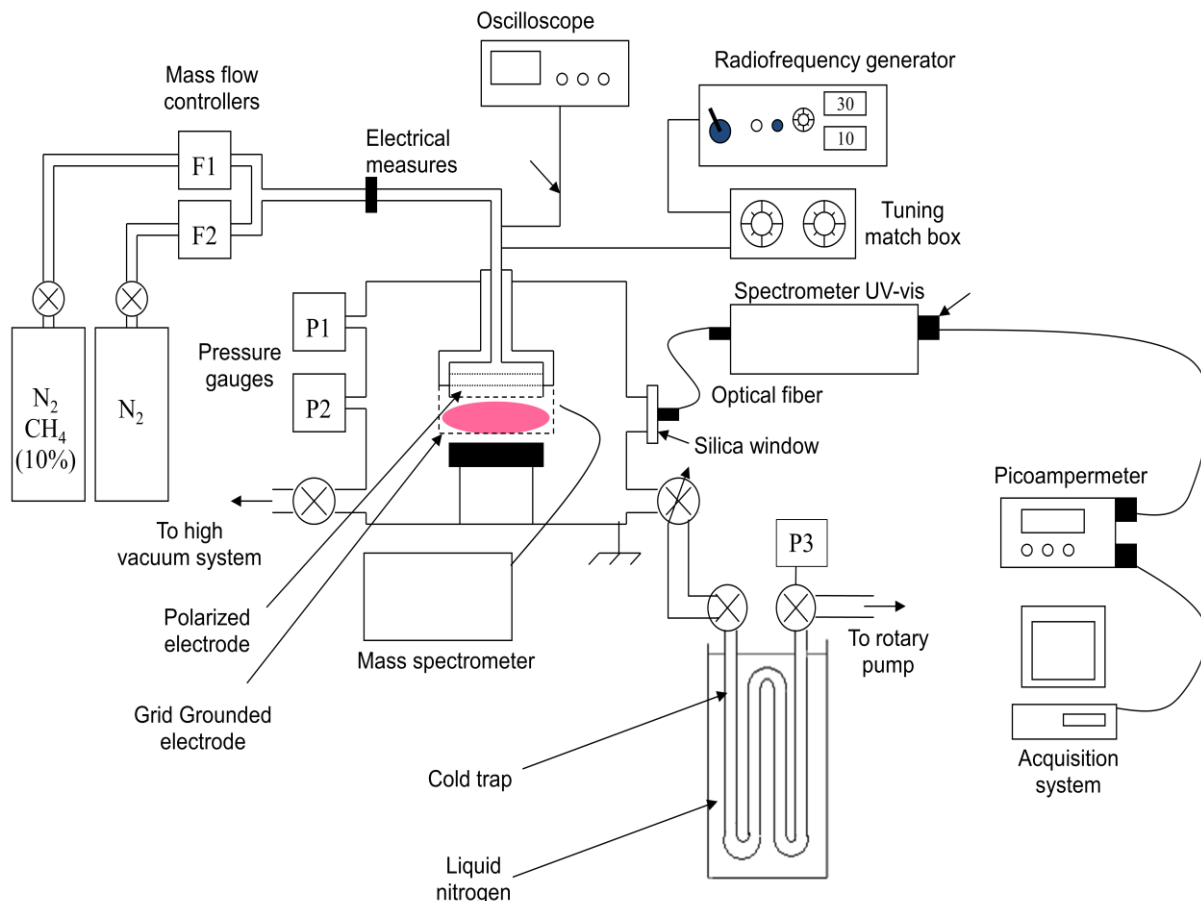


Figure 14: PAMPRE experimental setup and diagnoses

All the experiments performed with PAMPRE in this thesis were done with an injected power of 30 W and in continuous current mode. The upper electrode is driven by a RF voltage at 13.56 MHz, and a grounded cylindrical grid confine the plasma in a controlled volume. This grid allows optical emission spectroscopy in the UV-Visible range. For IR measurements the cage is then withdrawn and a metallic plate in front of the polarized electrode ensures the role of the grounded electrode. The cold trap visible in this figure is described in detail in the ex-situ diagnoses part.

The gas mixture can be adjusted from 0% to 10% of methane in nitrogen using two bottles (100% N₂ and N₂:CH₄ 90:10). A third bottle containing pure argon can also be used for actinometric measurements. The gas is introduced in the reactor using mass flow controllers (MKS 247C) through the cathode using a showerhead design to ensure the uniformity of the gas within the discharge. The gas is then pumped out by a primary vane pump that allows to

vacuum the chamber down to 10^{-2} mbar. A turbo molecular pump (Alcatel ACT 200T) is used to pump the reactor down to 10^{-6} mbar for cleaning purposes.

Gas pressure is monitored by two pressure gauges, one baratron (MKS PR 4000) for working conditions pressures between 10^{-2} and 100 mbar, and a Penning gauge (Edwards Penning 505) for the 10^{-2} - 10^{-6} mbar pressure range, to check the ultimate vacuum for cleaning procedures

Pressure can be controlled either by adjusting the incoming gas flow rate, or by using a diaphragm valve to limit pumping efficiency. Standard gas flow used for the experiments is of 55 standard cubic centimeter per minute (sccm) and the total pressure in the reactor is of 0.90 ± 0.05 mbar (with exception of experiment performed with a cold trap, see below).

Once plasma is triggered on, nitrogen and methane molecules are ionized and dissociated to initiate a complex organic chemistry leading to the formation of volatile compounds and of solid material. The solid material, so called tholins, can then be seen as an analogue of Titan's aerosols. The principal advantage of the PAMPRE design is that the aerosols are electrically charged. This means that, in addition to their weight, the ions drag force, the neutral drag force and a thermophoresis induced force, they are submitted to an electrostatic force. This allows particles to remain in levitation in the electric field as long as the forces compensate. Particles can then grow in volume (i.e. without any wall interaction, as in a free atmosphere) until they are too big to be maintained in the plasma. Once they reach this point, particles fall down through the confining grid at the bottom of the plasma and can be collected in the glass vessel surrounding the reactive area.

II.1.1.b In situ diagnoses

On the PAMPRE experiment, several diagnoses allow monitoring in-situ the plasma, neutral gases and dust in the reactor.

a. Quadrupole mass spectrometer: monitoring neutral gas

The first available diagnosis is a quadrupole mass spectrometer (QME 200, Pfeiffer). This spectrometer has a resolution of $m/\Delta m = 100$ at m/z 100 and covers the mass range from 0 to 100 amu. Gas sampling is done through a capillary tube (0.8 mm in diameter), with a sampling orifice located 1 cm outside the reactive plasma. The capillary is long enough to reduce the gas flow rate between the reactor chamber and the QMS and keep operating

pressure in the MS below 10^{-5} mbar. This QMS allows detecting only stable neutral species. The QMS operates in electron impact mode at the standard 70eV electron energy. The QME 200 can be operated in two different methods. The first one, so called "scan analog" method provides the mass spectrum of a selected mass range, i.e. intensity of a peak versus the m/z ratio of this peak. This mode is especially used for detection and identification of species in the reactive mixture.

The second method, Multiple Ion Detection (MID), provides the temporal evolution of one (or several) selected peak, with a time resolution down to 0.2 s (depending of the concentration of the species, in order to get enough signal in the selected time dwell). This mode allows monitoring species of interest and their kinetics.

b. Optical Emission Spectroscopy (OES): plasma characterization

The second diagnosis on the PAMPRE experiment is a visible and ultra-violet spectrometer that can monitor the optical emission spectrum of the plasma. This can for example provide information on neutral temperature, nitrogen or cyanide bands intensity (Alcouffe et al. 2010). The light emitted by the plasma discharge passes through a silica window and then enters an optical fiber. The fiber exit is located at the entrance slit of the 60 cm focal length monochromator (Jobin-Yvon HRS). The maximal resolution of the spectrometer is 25 000, but in order to increase the signal to noise ratio, a split aperture providing a resolution of 5 000 is used on this spectrometer. A photomultiplier is displaced on the exit slit of the monochromator to collect signal, the current is measured by a Pico ammeter.

During my thesis, I mainly used this diagnosis to perform actinometric measurements of atomic hydrogen, which cannot be detected with the QME 200 mass spectrometer available on PAMPRE. I thus used actinometry to determine the atomic hydrogen content in the gas mixture. Actinometry is a diagnosis commonly used for the study of plasma discharges, which, among others, allows determining the H concentration. Hydrogen atoms are produced from the CH_4 dissociation and are excited by electronic collision to radiative levels. These levels are then depopulated by radiative emission. In optical emission spectroscopy, the intensity of an H line is then proportional to the electron density in the plasma n_e , to the rate coefficient for the population of the radiative level, k_{e-H} , function of the electron temperature T_e and to $[\text{H}]$, the atomic hydrogen density.

$$I(H) = A(H) \times k_{e-H}(Te)[H] \quad (1)$$

Equation (1) shows that the intensity of the hydrogen lines depends on the hydrogen density, but also on some plasma parameters. In order to get free from this problem, it is possible to use argon as an actinometer gas. In PAMPRE experimental conditions, argon follows the same population/depopulation processes than hydrogen. The intensity of an argon line can then be established as:

$$I(Ar) = A(Ar) \times k_{e-Ar}(Te)[Ar] \quad (2)$$

The A parameter is a constant in the equation (1) but differs for argon and hydrogen. A depends on the volume of the plasma observed by OES, the spectral calibration factor of the optical device at a given wavelength, the photon energy and the Einstein coefficient for the observed line.

It is possible to combine equation (1) and equation (2) to get the H atoms density as follows:

$$[H] = B \times \frac{I(H) \times k_{e-Ar}(Te)}{I(Ar) \times k_{e-H}(Te)} [Ar] \quad (3)$$

Since the amount of argon is constant, [H] is proportional to the ratio between the intensities of the H and Ar lines, a constant B, and the ratio of the electronic rate coefficients.

To use this equation, we need to assume that the ratio of the electronic rate coefficients is constant. Alcouffe et al. 2010 showed that the electron temperature in the PAMPRE plasma varies when solid dusts are present in the plasma. However, Gicquel et al. 1998 calculated that the ratio of the electronic rate coefficients increase only about 10% when increasing electron temperature from 1 eV to 5 eV. Since electron energy remains on the order of few eV in PAMPRE experiment, we can consider, in a first approach, that the ratio is constant.

Spectra are recorded in the visible to the near-IR (475-825 nm) using a colored glass filter to eliminate overlapping of second order lines in the red and near-IR range. A spectrum of the discharge in the full wave range is given in Figure 15.

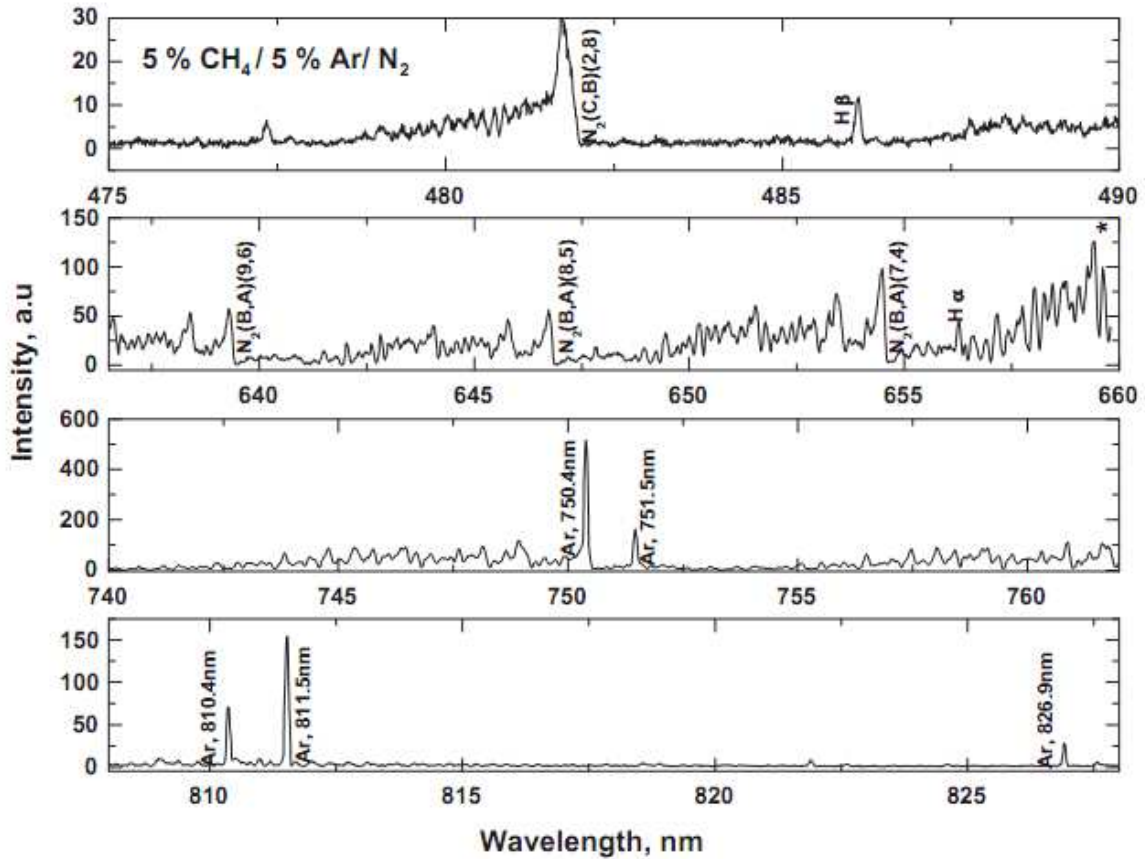


Figure 15: Emission spectrum obtained from 475 to 828 nm for a 95:5 N_2/CH_4 plasma discharge with 5% Ar as actinometer.

The spectrum is dominated by nitrogen molecular emission bands of the second positive system (SPS) $N_2(C \rightarrow B)$ and first positive system (FPS) $N_2(B \rightarrow A)$, hydrogen emission of $H\alpha$ (656.3 nm) and $H\beta$ (486.1 nm) and atomic Ar lines. In order to have limited variations of the electronic rate constants, one should use lines with excitation energies of the same order of magnitude and with similar cross sections for electron collisions excitation (Gicquel et al. 1998). As the excitation energies for Ar (811.5 nm) and $H\beta$ are similar (13.07 eV and 12.74 eV respectively) and as the lines are well isolated, these two lines were chosen for actinometric measurements in our case.

c. Fourier transform infrared spectroscopy: gas and aerosols IR signature

The third diagnosis available on the PAMPRE setup is the Fourier Transform InfraRed spectrometer (FTIR, from Thermo Scientific). It is the only diagnosis able to study dust directly in the reactor and not ex-situ. This spectrometer covers a spectral range from 550 cm^{-1}

up to 4000 cm^{-1} , with an achievable resolving power of 0.1 cm^{-1} , although this resolution is not needed in the case of dust absorption (most often I used a resolution of 2 cm^{-1} or 4 cm^{-1}). A sketch of the IR setup seen from above is given in Figure 16.

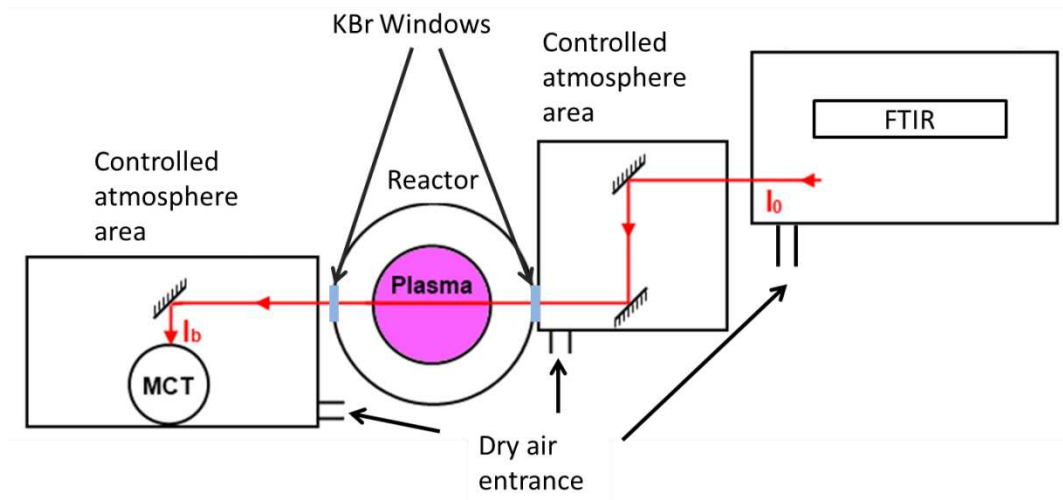


Figure 16: Sketch of FTIR setup on the PAMPRE reactor, seen from above

The infrared beam is emitted by the FTIR and then focalized by two gold mirrors to reach maximum focalization point within the plasma. The beam is then collected by a Mercury Cadmium Telluride detector cooled down with liquid nitrogen to avoid thermal noise. In this set-up, the beam passes through the plasma. This allows getting the absorption spectra of the mixture in the reactor. Some gases presenting high absorption in the infrared (such as CH_4 , C_2H_2 or HCN for example) can then be detected easily. Since the beam passes through the plasma only once (no multi reflection, pass length of $\sim 30\text{cm}$), the spectral signature of the dust is still low.

II.1.2 Bochum setup

The second reactor used during my thesis is a plasma reactor developed at the Ruhr University Bochum, in the Institute for Experimental Physics II. This reactor has been designed for the study of dusty plasma and producing astroanalog dusts (Kovacevic et al. 2003; Kovačević et al. 2005; Stefanović et al. 2005). I used this reactor as a complementary setup of the PAMPRE reactor. Both reactors have slight differences, which induce differences in the experimental parameters, but they have complementary diagnoses. In particular the Bochum reactor host a multi-pass FTIR, whose pass length through the plasma is much higher than the one on the PAMPRE experiment.

II.1.2.a Reactor

The reactor is a capacitively coupled radiofrequency plasma working at 13.56 MHz. A general scheme of the setup (top-view) is given in Figure 17. The chamber has a diameter of 55 cm and a height of 30 cm. Polarized electrodes are two parallel stainless steel plates, 30 cm in diameter and separated by 8 cm, and the reactor walls are grounded. The RF power applied to the plasma during this thesis was typically of 60 W for experiments at 0.5 mbar. As for the PAMPRE setup, the experiments presented in this thesis were performed in continuous working conditions.

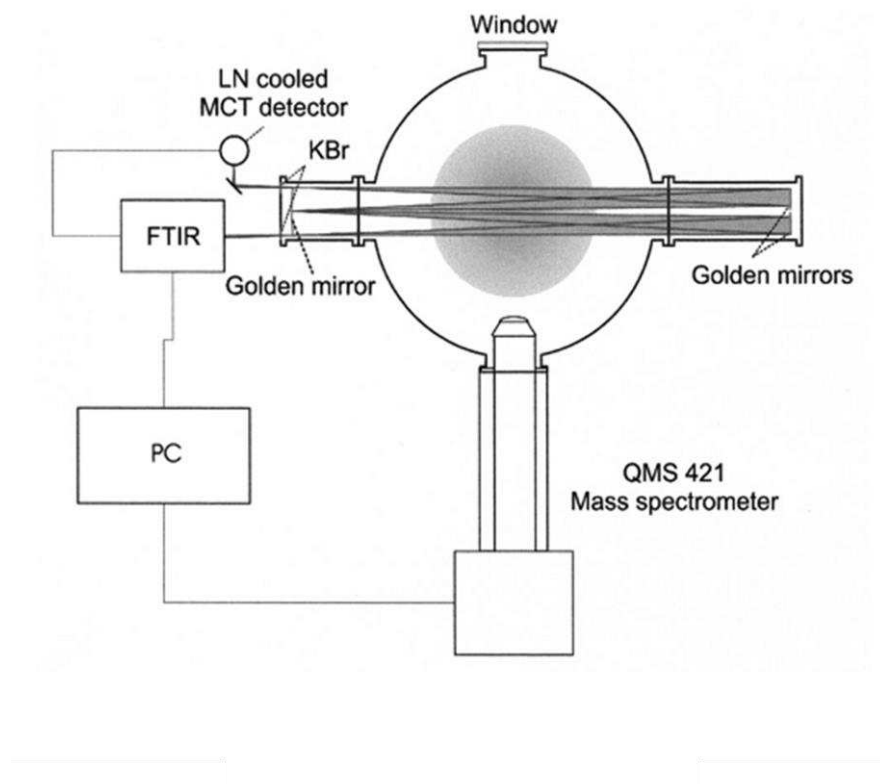


Figure 17: Scheme of the Bochum plasma reactor, seen from above

The reactor is directly pumped by a turbo molecular pump (Pfeiffer TPU 261 C). This configuration limits the pressure range achievable in the reactor to a few 10^{-1} mbar. Gas flow is controlled by mass flow controllers (MKS 247C) and settled at 15 sccm total flow. I used a gas mixture of $N_2:CH_4$ with 90% of nitrogen and 10% of methane at a pressure of 0.5 mbar. In order to avoid film deposition on windows, the Nitrogen flux is built in a way that it flushes

the optical parts when introduced in the experiment. To clean the chamber between each experiment, oxygen plasma is used to eliminate dust and film deposited on the electrodes.

II.1.2.b In-situ Diagnoses

a. Fourier Transform infrared spectroscopy: Gas phase quantification

The infrared spectrometer installed on this reactor uses the same principle of Fourier Transform Infrared Spectroscopy (FTIR) as described for the PAMPRE reactor. The main difference between the two setups is that the spectrometer used for the Bochum reactor (Bruker Equinox 55) has a multi-pass analysis mode. Once emitted by the spectrometer, the infrared beam passes through KBr windows to enter the plasma chamber. The beam is then reflected several times by gold mirrors on both sides of the plasma (see Figure 17). This increases the effective pass length of the beam in the reactive medium, and thus the sensibility of the detection. The beam has a radius of 1 cm, but because of the multi reflections of the beam, the final monitored area has a size of 2 cm height by 5 cm wide. The pass length through the plasma can be adjusted from 0.6 m (two passes) up to 7.2 m (24 passes). After multi-passing the plasma, the beam is focused on a liquid nitrogen cooled MCT detector. The influence of atmospheric water and CO₂ is minimized by enclosing the detection system and flushing it with desiccated and CO₂ purified air.

b. Quadrupole mass spectrometry: Products and kinetics monitoring

The quadrupole mass spectrometer (Plasma Process Monitor 422, Pfeiffer) uses also similar principles as the one on the PAMPRE reactor. The resolution of the spectrometer is about $m/\Delta m = 100$ at m/z 100, and the spectrometer extraction hood is directly located within the reactor chamber to enable ions detection. However the lower pressure in Bochum setup induces a higher detection limit of the MS.

c. Tholins harvest: Thermophoretic technique

The solid aerosols produced in a RF plasma are electrically charged, and thus submitted to five different forces (Bouchoule 1999; Berndt et al. 2009):

-The electrostatic force \mathbf{F}_e

-The Gravity \mathbf{F}_g

- The ion drag force \mathbf{F}_i
- The neutral drag force \mathbf{F}_n
- The thermophoretic force \mathbf{F}_{th}

As long as the dusts are maintained in the plasma, these forces counterbalance such as their resultant (\mathbf{F}_r) equals zero:

$$\mathbf{F}_r = \mathbf{F}_e + \mathbf{F}_i + \mathbf{F}_n + \mathbf{F}_g + \mathbf{F}_{th} \quad (4)$$

Any modification of the forces cited above would then induce a movement of the particles and possibly its ejection from the plasma. This happens for example when dust get bigger, which improve both their surface and weight, and thus affect (principally) both neutral drag force and gravity, implying the ejection of the dust from the plasma (case of PAMPRE reactor).

On Bochum reactor, the dust is collected using a modification of the thermophoretic force. The general principle is described in Godde et al. 2011. The thermophoretic force is proportional to the square of the particle radius (r_p) and of the neutral gas temperature (T_n) gradient:

$$F_{th} \propto r_p^2 \times \nabla T_n \quad (5)$$

A metallic plate (usually copper or stainless steel) is introduced within the plasma. The plate is then cooled down using liquid nitrogen, inducing a gradient in the neutral gas temperature within the reactor. The gradient will increase the strength of the thermophoretic force and thus modify the global balance of forces applied to the dust. The dust will then be shifted toward the cold spot, in our case the metallic plate were dust accumulate. This plate is then removed from the plasma, with dust forming a thin layer on its surface.

II.1.3 Photochemical experiment: the APSIS setup

Even if plasma simulations are the most efficient for production of Titan's aerosols analogues, it is important to note that Titan's atmospheric chemistry is mainly driven by photochemical processes (Robertson et al. 2009). To address the issue of the sensitivity of the global chemistry to the energy source, the LATMOS team designed a new photochemical

reactor, APSIS, for Atmospheric Photochemistry Simulated by Synchrotron. Photon sources covering the VUV spectrum needed to dissociate molecular nitrogen may be found on synchrotron radiation facilities (see Figure 18 and Imanaka and Smith 2007). The APSIS reactor is coupled with a VUV photon source. In the work presented here, the photon source was DISCO, a VUV bending magnet based beam line at the SOLEIL synchrotron radiation facility (Giuliani et al. 2009; Giuliani et al. 2011). The DISCO beam line has three end-stations including the APEX (Atmospheric Pressure Experiment) one, used for the APSIS reactor. The APEX station is fitted with a differential pumping system which allows delivering VUV photons from 220 nm down to 60 nm, up to a pressure of 1 bar.

The photon flux of DISCO is given in Figure 18, with the solar photon flux at the top of Titan's atmosphere, as the activation cross sections of N_2 and CH_4 . As visible in this figure, the spectrum of DISCO is 10^4 - 10^6 times more intense than the solar one, which ensure achievable time scales for experiments, but much more uniform on the 60 – 170 nm range. Contrary to the solar spectrum, the DISCO spectrum does not present peak at Lyman α at 121.6 nm.

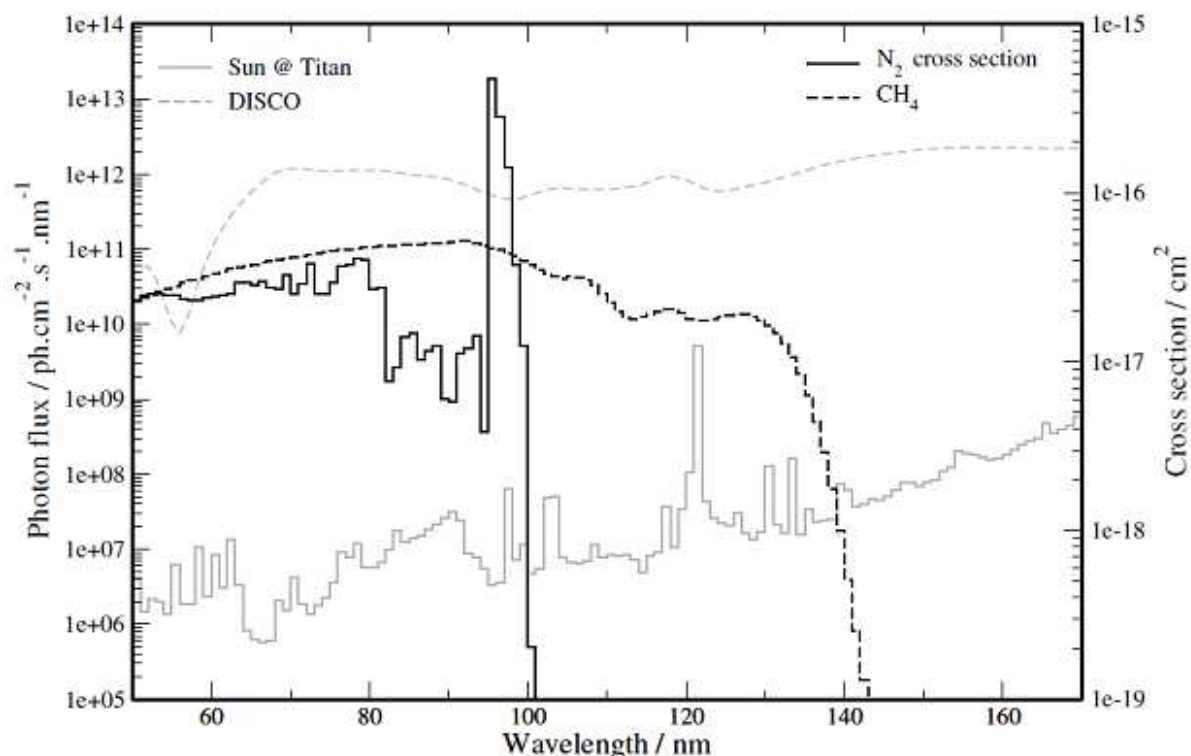


Figure 18: Energy spectra of APSIS and solar spectrum at the top of Titan's atmosphere. From Peng et al. 2013

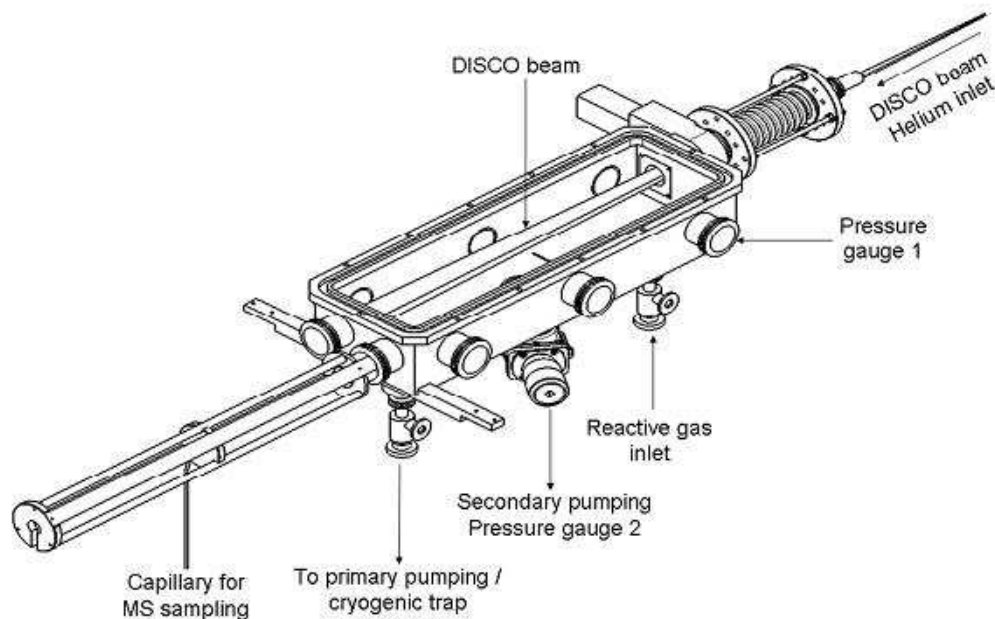


Figure 19: Scheme of the APSIS reactor

The reactor (presented in Figure 19) is a stainless-steel parallelepiped box with inner dimensions of 500 mm x 114 mm x 92 mm. The geometry of the reactor is elongated to accommodate the optical depth of CH_4 in the running experimental conditions. The reactive gas mixture consists in 10 % of methane in molecular nitrogen (purity >99.999%, Air Liquide). The gas flow can be adjusted from 0 to 10 sccm with a MKS mass flow controller. The out flowing of the gas is ensured by a primary pumping. The pressure in the reactor is measured with an absolute capacitance gauge (Ceravac, Oerlikron). The partial pressure of the reactive mixture reaches a few millibars and residence time of the gas is a few minutes. The reactor can be pumped down to 10^{-5} mbar with a turbo molecular pump before each experiment for cleaning purpose. A Helium flow is introduced upstream the reactor (see Figure 19) to confine reactive mixture inside the reactor without using any windows.

The diagnosis available on the APSIS reactor is the quadrupole mass spectrometer of the PAMPRE reactor, which can be relocated on the APSIS setup. It is also possible to adapt the cryogenic trapping (see below) of the PAMPRE reactor on APSIS.

II.2 Ex-situ Analytical methods

Despite the fact that in-situ diagnoses can provide numerous information on the samples, it can be needed to use ex-situ methods to perform deeper analyses. In this section, we are going to see the one used during my thesis to get deeper in the knowledge of tholins and gas phase compositions.

II.2.1 Cryogenic trapping and Gas-Chromatography coupled to mass spectrometry: gas products identification.

These analyzes were performed at the Laboratoire Génie et Procédé des Matériaux (LGPM), Ecole Centrale Paris, in collaboration with Arnaud Buch.

A cryogenic trap can be settled on the outlet of the experiment to condense gases (Figure 14). Even if it is not directly considered as an in-situ measurement since trapped gases are analyzed ex-situ by Gas Chromatography coupled to Mass Spectrometry (GC-MS), this setting provides information on the gases produced in the reactor. The trap is a cylindrical glass coil, with a diameter of 1.3 cm, 1 m length and a total volume of 133 cm³, which is immersed in liquid nitrogen. The gas pumped from the reactor flows through this trap where products coming from the reactive gas mixture can condense depending on the pressure and the temperature. Since the trap is cooled by liquid nitrogen, the gas temperature is ~77K. The presence of the trap reduces the efficiency of pumping and thus a rise of the pressure in the reactor with a constant inlet of 55 sccm of gas. With the cold trap, the pressure in the reactor rises from 0.90 mbar up to 1.7 mbar. The pumping induces a pressure gradient from the reactor ($P=1.7$ mbar) to the pump such that the pressure in the cold trap is lower than 1.7 mbar. This setup allows the trapping of all the species condensable in these temperature and pressure conditions. A Bourdon pressure gauge measures the pressure in the trap in the range from 0 to 1000 mbar with a resolution of ± 10 mbar.

The trap is heated and then pumped with a turbo pump before each experiment in order to remove water vapor adsorbed on the trap walls. At the end of an experiment, the trap can be isolated from the reactor with a gas valve and connected to a GC-MS for the analysis of the gas phase.

The Gas Chromatography coupled to Mass Spectrometry (GC-MS) is an analytic technique that allows separating and identifying chemical species (in gas or liquid phase). A complex

mixture can be introduced in the chromatograph. First, the species are separated depending on their elution time on the chromatographic column. The column exit is connected to a mass spectrometer which then allows identifying the different species.

The GC-MS used for analysis of the gases condensed in the cold trap is a ThermoScientific GC-Trace coupled to a ThermoScientific DSQ II Mass Spectrometer operated in a quadrupole detection mode.

For the analyses of the gas phase using the cold trap (both on PAMPRE, presented in part III.3.2.b and on APSIS, presented in part V.3.3 of this thesis) the chromatographic column used for the gas separation was a MXT-QPlot (Restek) 30 m long, 0.25 mm internal diameter and 10 μm stationary phase thickness designed to easily separate volatile compounds up to five carbons. The column temperature was set with a temperature isotherm at 30°C during 5 minutes, then a gradient of 5°C/min from 30°C to 190°C and a second isotherm at 190°C for 5 minutes. Helium was used as a carrier gas at a constant 1 mL.min⁻¹ flow rate. The injector used is an Optic 3 thermal desorber working either in split (1/10) or in splitless mode. The gas phase can be trapped in split mode at low temperature (-80°C) in the injector's liner filled with a mixture of Tenax and Carboseive®. This step allows concentrating the target species. In order to inject them in the GC, the injector liner was then quickly heated (with a rate of 16°C.min⁻¹) at 250°C. It operated in splitless mode. The temperature of the detector was set to 200°C.

I also used GC-MS to analyze the solid residue formed in the cold trap as presented in part IV.2.3. The column used for this analysis is a CP-Chirasil-Dex CB(Varian), L=30m, ID=0.25 mm, df=0.53 μm . The injector temperature is 270°C, Helium flows at 1mL/min as a carrier gas, split is 1/20. Temperature ramp used is: 34°C during 5 min then 5°C/min up to 190°C and then isotherm at 190°C for 5 minutes.

II.2.2 Infrared analyses of tholins by ATR (performed at LATMOS)

Attenuated Total Reflection (ATR) is a diagnosis used for studying a solid sample in the mid-infrared. I used this technique to analyze tholins produced both in the PAMPRE reactor and in Bochum reactor. The dust is displaced on the surface of a prism with a high refraction index (ATR crystal). The infrared radiation entering the prism is totally reflected inside it and an evanescent wave can escape the crystal through the upper face, and passes then through the

sample. The wave is then attenuated in the area where the sample absorbs in the infrared, depending on the chemical functions present in the sample.

This technique is very useful due to the simplicity of the use of the spectrometer in this mode, and allows the identification of the main absorption bands in a sample. However it is not a quantitative analysis, and only provides the absorbance spectrum of the sample. The spectrum is also dependent on the quantity of dust displaced on the crystal and on the pressure applied to the sample to maintain it on the crystal.

II.2.3 Tholins infrared spectroscopy using Synchrotron radiation.

For the infrared analysis of tholins with quantitative information, I also used an infrared microscope installed on the SMIS (Spectroscopy and Microscopy in the Infrared using Synchrotron) beam line at the SOLEIL synchrotron facility (Dumas et al. 2006). This diagnosis allows to get the spectrum of tholins from the mid- to the far-infrared (4000 – 50 cm^{-1}). A NicPlan microscope was used coupled to a Nicolet Magna System 560 Fourier Transformed Infrared (FTIR) spectrometer. The IR sources utilized for the present work were the synchrotron radiation for mid-IR and the internal Globar source for the far-IR. The detectors were either the Mercury-Cadmium-Telluride (MCT) detector of the microscope (mid-IR), or a silicon doped bolometer from Infrared Laboratories, cooled down to 4.2 K with liquid helium (far-IR). Analyses were performed in double transmission mode. This means that the infrared beam passes through the sample, is reflected by a mirror and passes again through the sample. With this configuration it is possible to analyze tholins thin films and apply the Beer-Lambert law to get the linear absorption coefficient of the sample. Samples were deposited as thin film on two different kind of substrates for measurements in mid- and far-infrared. Silicon wafers were used for the far-infrared and low emissivity MirrIR[®] substrates were used for the mid-infrared analyses. To ensure the repeatability of the measurements in the far-IR, thin film analyses were performed on the three samples, three times each, i.e. 9 sample spectra were taken in the far-IR range. I also collected three points of references on two tholins-free silicon wafers to be used as substrate reference spectra. In the mid-IR, 6 spectra were collected on the thin film deposited on MirrIRTM substrates and blanks were performed on a tholins free substrate. Spectra were recorded at a spectral resolution of 4 cm^{-1} after co-adding 512 scans at a Michelson mirror velocity of 1.26 cm.s^{-1} .

II.2.4 Ellipsometry: Determination of sample thickness.

These measurements were performed at LISV, Université de Versailles St Quentin, mainly by Ahmed Mahjoub from the PAMPRE team.

In order to apply the Beer-Lambert law it was necessary to determine the thickness of the samples. Ellipsometry allows measuring this thickness. Ellipsometry technique is based on the measurement of the change of the light polarization upon light reflection on a sample (Fujiwara 2007). The reflected light from the sample surface is elliptically polarized. ρ , the ratio between the complex reflection coefficients r_p and r_s , respectively for the light polarized perpendicularly and parallel to the incident plan is related to ψ and Δ parameters defined as:

$$\rho = \frac{r_p}{r_s} = \tan(\psi)e^{i\Delta} \quad (6)$$

The ellipsometry parameters, ψ and Δ , are related to the complex refractive indices of the substrate and of the different layers and to the thickness of the sample. A model taking into account the optical properties and thickness of the different layers must be established in order to deduce both the optical constants and the layer thickness. The method is described in details in Sciamma-O'Brien et al. 2012 and Mahjoub et al. 2012.

We used an M-2000V spectroscopic ellipsometer from J.A. Woollam Co. The M-2000V is a rotating compensator ellipsometer with a CCD detector that measures all wavelengths simultaneously across the spectral range 370 nm to 1000 nm.

The layer modeling was performed by Ahmed Mahjoub, using the Complete-EASETM software (Complete EASETM Data Analysis Manual By J.A Woollam Co Inc. June 15, 2008). Uncertainties on each sample are due to film non uniformities calculated by the Complete-EASETM software.

II.2.5 High resolution mass spectrometry for tholins chemical analysis

These analyses were performed at the Institut de Chimie des Substances Naturelles (CNRS Gif sur Yvette) in collaboration with Isabelle Schmitz-Afonso and David Touboul.

II.2.5.a LTQ-Orbitrap

To get chemical information on tholins composition, I used orbitrap high resolution mass spectrometry. The spectrometer used was a LTQ-Orbitrap from ThermoScientific. The

principle of Orbitrap technology (Makarov 2000) is to inject ions into a cylindrical trap composed of two co-axial electrodes, as presented in Figure 20.

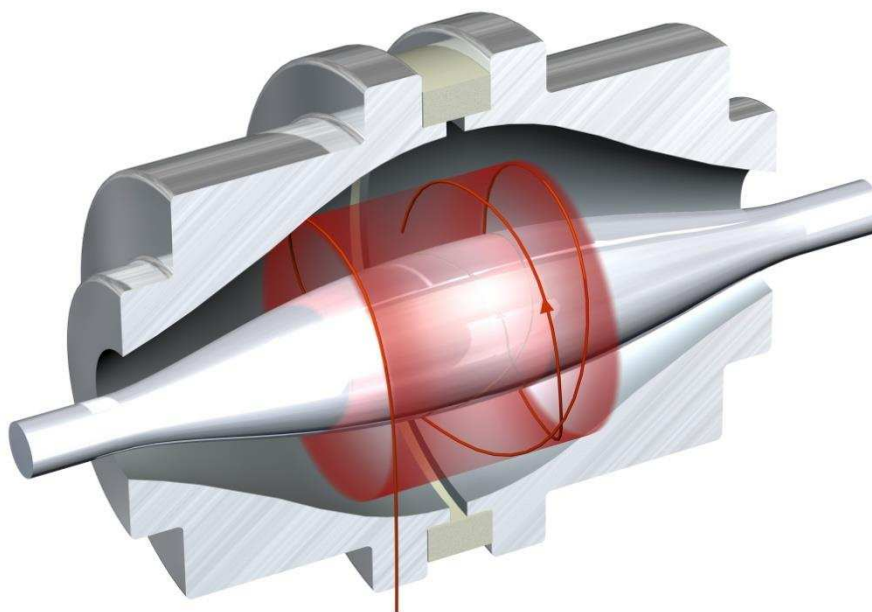


Figure 20: Scheme of principle of the orbitrap electrodes. The two electrodes are the cylindrical part in the center of the chamber and the one surrounding the chamber. Scheme from ThermoScientific LTQ-Orbitrap documentation.

Ions are collected in the linear ion trap and axially ejected and collected in a C-shaped ion-trap to be finally injected in the Fourier transform Orbitrap (Makarov et al. 2006). Once in the Orbitrap chamber, ions assume a circular orbit around the central electrode and their axial oscillations produce a periodic signal on the outer electrodes which can be converted to a mass spectrum using a Fourier transform algorithm.

For this thesis, mass spectra were acquired with a hybrid linear trap/Orbitrap mass spectrometer (LTQ Orbitrap). The samples are solubilized in methanol before injection in the spectrometer.

Acquisition parameters of the spectrometer were: needle voltage 4.5kV; capillary temperature 275°C; tube lens voltage 65V. The mass spectrometer was externally calibrated using caffeine, MRFA peptide and ultramark. Data were acquired from 50 u to 800 amu and integrated on several hundred scans (usually between 350 and 400). Data were acquired with a resolution chosen at $m/\Delta m = 100\,000$ at m/z 400. The experimental mass accuracy was found to be inferior to 1 ppm at m/z 150. Data were processed using XCalibur 2.0 software

and its peak attribution function. Attribution parameters were: maximum authorized deviation: 5 ppm; maximum carbon atoms: 60; maximum nitrogen atoms: 60; maximum hydrogen atoms: 100; maximum oxygen atoms: 2. Nitrogen rule was used and charge was set to +1 (-1 for analysis in negative mode).

II.2.5.b Time of flight analyzer

I also analyzed tholins with a LCT-TOF mass spectrometer. The Time Of Flight analyzer principle is to determine the m/z ratio of ions using a time measurement. Ions are accelerated in an electric field. Ions of the same charge will then have the same energy, and the time of flight between entrance in the field and the detector (related the speed of the ions) depends on the m/z ratio. This technology allows getting the mass spectrum of tholins with a wide intensity dynamical range.

Samples were analyzed using a LCT-Premier ESI-TOF (Waters Technology) in W mode (double-reflectron). Spectra were acquired from 80 to 1500 amu and for this work, the resolution at m/z 500 was measured to be $m/\Delta m = 9000$ in positive ionization mode and 13 000 for negative ionization mode. Injection was made in direct infusion at 6 $\mu\text{L}/\text{min}$. For positive ionization mode, analytical parameters were: Capillary: 3000V; Sample Cone: 40V; Desolvation temperature: 350°C; Source temperature: 120°C and desolvation gas flow: 500 L/hr. For the negative mode analysis, parameters were: Capillary: 2300V; Sample Cone: 40V; Desolvation temperature: 350°C; Source temperature: 120°C; Desolvation gas flow: 500 L/hr and aperture Voltage: 5V.

II.3 Conclusion

The samples I analyzed during my thesis can be grouped in 4 different categories. The first one is the gas phase, analyzed either in-situ in the reactors or ex-situ using cryogenic trapping. The second one is bulk tholins, i.e. tholins produced and harvested in nominal conditions in the PAMPRE reactor. Roughly, bulk tholins can be considered as (more or less) spherical dust grains grown in levitation within the plasma (Hadamcik et al. 2009; Alcouffe et al. 2010). Figure 21 presents the aspect of tholins samples produced with different methane concentrations in the reactive plasma. It shows that the color of tholins changes with the content of methane in the gaseous phase, resulting from a modification of the chemical and physical properties of the tholins.

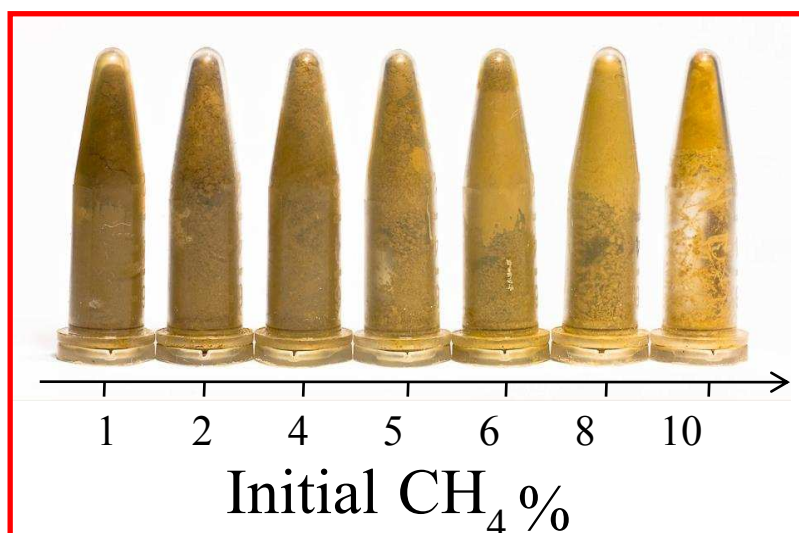


Figure 21: Picture of tholins produced in the PAMPRE experiment with different methane concentration in percentage of CH₄ in N₂. (Credits: Pascal Pernot)

Tholins can also be produced as thin film. In this case, a dielectric substrate is placed on an electrode within the plasma. An organic film made of tholins is then deposited on the substrate. This kind of tholins thin film is particularly useful for optical analyses. The last category of sample I analyzed is a so called "residue". This residue is an organic solid material that forms within the cold trap when gases trapped in it are warmed up to room temperature. Figure 22 shows the apparition of the residue in the cold trap when warmed up to the room temperature. Residue formation is time depending and time constant is approximately 10 minutes; no major visible evolution is seen after a while.

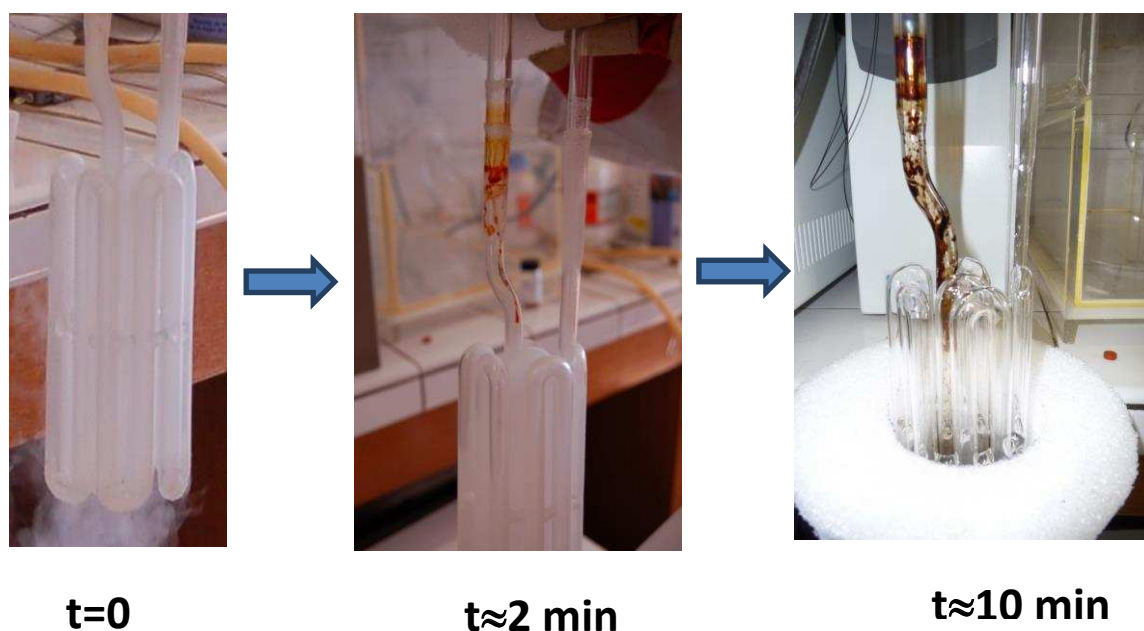


Figure 22: Residue polymerization when the cold trap is warmed up from liquid nitrogen temperature to the room temperature

The advantages and inconvenient of each experimental device I used during my thesis can be summarized in Table 3.

Table 3: Advantages and disadvantages of the diagnoses used for this thesis

Diagnosis	In-situ / Ex-situ	Advantage	Inconvenient	Sample analyzed
QMS	in-situ	<ul style="list-style-type: none"> Access to the whole neutral gas from 1 to 100 amu 	<ul style="list-style-type: none"> Only stable neutrals Low resolution Not quantification for product 	Gas
OES	in-situ	<ul style="list-style-type: none"> Access to some radical and ionic species Relative quantification 	<ul style="list-style-type: none"> Information only on species that emit in the UV-Visible 	Gas (neutral and ions)
FTIR	in-situ	<ul style="list-style-type: none"> Only in-situ diagnosis on dust Detection and quantification of the gas 	<ul style="list-style-type: none"> Low sensibility without multi-passing Can detect only gas with infrared 	Gas and bulk tholins

CHAPTER II - METHODS

			signature	
Cold trap/ GC-MS	ex-situ	<ul style="list-style-type: none"> • Improve the sensibility of detection on minor species • Relative concentration of species 	<ul style="list-style-type: none"> • No absolute quantification • Possible chemistry occurring in the trap? • Species detected depend on the column chosen 	Gas
ATR	ex-situ	<ul style="list-style-type: none"> • Easy to use • Quick access to tholins IR spectrum 	<ul style="list-style-type: none"> • Not quantitative • Highly variable to external parameters 	Bulk tholins
Synchrotron based FTIR	ex-situ	<ul style="list-style-type: none"> • Quantitative (combined with ellipsometry) • Provides spectrum of tholins in the far-infrared 	<ul style="list-style-type: none"> • Difficult to implement / use (need of Synchrotron beam time) 	Tholins thin films
Orbitrap	ex-situ	<ul style="list-style-type: none"> • Ultra High resolution on tholins MS => enable peak attribution 	<ul style="list-style-type: none"> • Access only to the soluble fraction of the sample • Tricky data treatment (>15 000 peaks in one spectrum) • Nonlinear behavior for low intensity peaks in complex mixtures 	Bulk tholins and Residue
TOF	ex-situ	<ul style="list-style-type: none"> • Wide dynamical range • Global aspect of tholins MS 	<ul style="list-style-type: none"> • Access only to the soluble fraction of the sample • Resolution lower than orbitrap 	Bulk tholins

A summary of the three different experimental setups used during this thesis is given in Table 4.

Table 4: Comparison of the experimental setup used for this thesis

	PAMPRE	Bochum reactor	APSIS
Energy deposition	RF Plasma 30 W	RF Plasma 50 W	VUV photons 220-60 nm
Gas mixture	N ₂ -CH ₄ 0≤%CH ₄ ≤10	N ₂ -CH ₄ 90-10	N ₂ -CH ₄ + He
Pressure	0.9 – 1.7 mbar	0.5 mbar	~mbar + ~5mbar He
Temperature	Room temp.	Room temp.	Room temp.
Samples collected	- Bulk tholins - Tholins thin films - Gas (cryogenic trapping) - Cold trap Residue	- Bulk tholins	- Gas (cryogenic trapping)
Available diagnoses	- QMS - FTIR (30 cm) - OES	- QMS - Multipass FTIR (7m)	- QMS

Chapter III Gas phase reactivity leading to aerosols

III.1 Introduction

In order to understand the processes leading to the formation of tholins, it is needed to study the medium where tholins are created, i.e. the gas phase where tholins come from. As said previously, tholins are formed in a reactive gas mixture of N_2 and CH_4 . Ionization and/or dissociation of these two species lead to the formation of heavier gas compounds that will themselves be able to react and lead to heavier compounds, and so on until the formation of a solid phase, tholins.

The aim of this chapter is to study the gaseous compounds produced by the chemistry in the initial nitrogen and methane mixture. This study is focused on two different aspects of this chemistry. The first is being as thorough as possible in the identification of the products, and the characterization of the gas phase. The second aspect is to get some clues on the reactivity kinetic of the gas phase, especially looking at the dissociation of methane.

In a first step, we are going to see the identification and characterization of the gas phase *in-situ* in the PAMPRE reactor. In a second part we will see a study performed to enhance the detection of minor species in PAMPRE using a cryogenic trapping. The third part will be dedicated to the study of the gas phase in the reactor of Bochum.

III.2 Volatile products in the PAMPRE experiment: *in-situ* look to the tholins nursery

A previous study performed using mass spectrometry (Sciamma-O'Brien et al. 2010) showed the influence of the methane initial concentration on the aerosol mass production efficiency. A maximum has been found for the intermediate initial concentrations of methane (~5% of CH_4 in N_2). This result highlights a competition between a polymerization growth process correlated with the methane concentration, and an inhibition process anti-correlated with the methane concentration. Several hypotheses were proposed to explain this inhibition process in the aerosol production, all of them involving the increase of the global hydrogen content in the gas phase coming from methane dissociation: either by saturation of the growing solid

grains with hydrogen (molecular or atomic), or by production in the gas phase of saturated volatiles.

The composition of the gas products as a function of the initial methane concentration was thus studied to find some clues on the sensitivity of aerosol production with initial methane amount in the gas mixture (Carrasco et al. 2012). Stable neutrals were analyzed using in-situ quadrupole mass spectrometry. A relative quantification of atomic hydrogen was also performed using optical emission spectroscopy (OES). The detected products can be compared with the one detected by cryogenic trapping (see part III.3 and Gautier et al. 2011) and in other laboratory experiments (Coll et al. 1999; Ramírez et al. 2001; Bernard et al. 2003; Ramírez et al. 2005; Tran et al. 2005). Results presented in this part have been published in Carrasco, Gautier et al. 2012.

III.2.1 Experimental protocol

The experiments presented here the total gas flow rate ($\text{N}_2 + \text{CH}_4$) is fixed at 55 sccm and the pressure in the reactor is 0.9 mbar. A constant Argon flow rate corresponding to an amount of 5% (2.75 sccm) is added to the gas mixture for actinometrical measurements. Since Argon is a noble gas, it does not participate in the gas phase chemistry, and it has been checked that a small amount (<10%) does not modify the plasma discharge properties.

Before each experiment, the chamber is cleaned with ethanol and pumped down to 2×10^{-6} mbar using a turbo molecular pump. While pumping, the reactor and the mass spectrometer are heated up to 110°C for several hours in order to desorb impurities from the chambers walls. Once the reactor is cooled down, a 30 minutes argon plasma ensures the outgassing of the metallic confining box. Initial gas mixtures studied contained 1%, 2%, 5% and 10% of methane in nitrogen, covering the range studied in Sciamma-O'Brien et al. 2010 for comparison.

Despite all these precautions, a weak signature of air (N_2 , O_2 , CO_2 , Ar) can be seen in the blank mass spectra, with contributions at m/z 14, 16, 28, 32, 40 and 44, as presented in Figure 23. The blank (black curve) corresponds to the mass spectrum of the isolated mass spectrometer at a vacuum limit of 3×10^{-8} mbar.

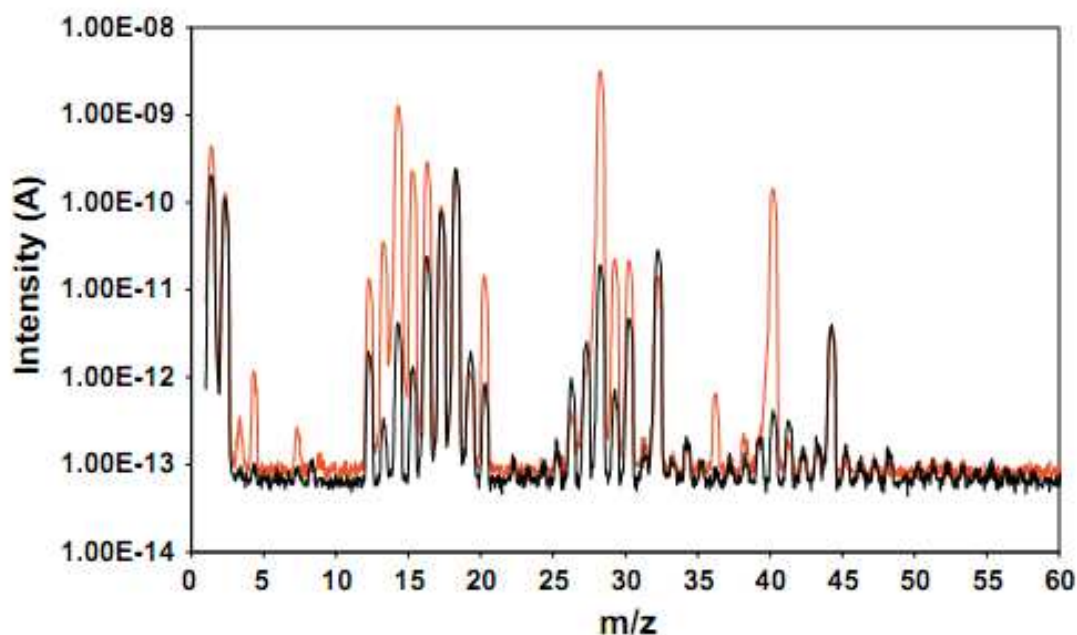


Figure 23: Black: Blank mass spectrum of the mass spectrometer only (no connection to PAMPRE). Red: Initial mass spectrum (plasma off) obtained with a $\text{N}_2\text{-CH}_4$ gas mixture with 5% of methane.

The water signal, with a main peak at m/z 18, is quite important but stable. Figure 23 also presents the spectrum of a $\text{N}_2\text{:CH}_4$ 95:5 gas mixture in the PAMPRE reactor with plasma turned off. The intensity threshold for recording signal has been chosen at 10^{-13} A. For studying the stationary state, long time scales acquisition is possible. Thus the dwell time for each mass is 2s. The mass spectrometer used can analyze gas phase up to m/z 100, but no significant detection was found above m/z 60 for this study. All spectra are thus limited to the m/z 1 to 60 range.

Before studying the reactive plasma, some general comments can be made on the reference gas mixture mass spectra before plasma ignition (see Figure 24).

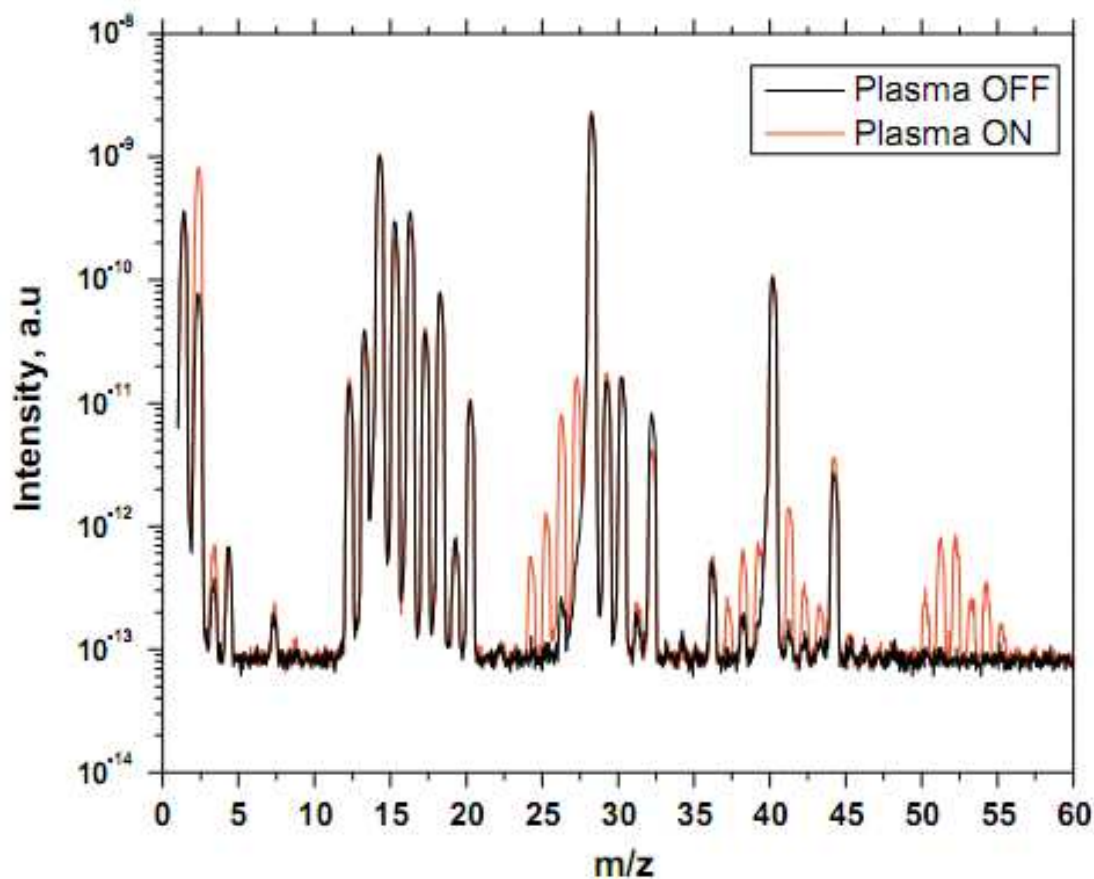


Figure 24: Mass spectrum of a $\text{CH}_4\text{-N}_2$ 10-90% gas mixture plasma off (black) and on (red)

The initial mixture is mainly composed by molecular nitrogen and methane, which can be identified on the mass spectrum with their following fragments. Molecular nitrogen involves fragments at m/z 7 (N^{2+}), 14 (N^+), 15 ($^{15}\text{N}^+$), 28 (N_2^+), 29 ($^{15}\text{N}^{14}\text{N}^+$) and 30 ($^{15}\text{N}^{15}\text{N}^+$). Methane exhibits fragments at m/z 12, 13, 14, 15 and 16, respectively C^+ ; CH^+ ; CH_2^+ ; CH_3^+ and CH_4^+ . In order to avoid possible effect of water at m/z 16, the peak chosen for the study of methane is the m/z 15 peak, almost as intense.

Additional argon is introduced for complementary optical emission spectroscopy measurements, leading to large contributions at m/z 20, 36 and 40. As the absolute intensity measured by the mass spectrometer is not faithfully reproducible, mainly due to the progressive clogging of the filament in the ionization chamber and a slow drift of the amplification factor of the channeltron, we chose to work with relative intensities among the products. For each experiment series, mass spectra are recorded before the plasma discharge. The initial state is hereafter called initial condition and labeled with the subscript 0. When the

plasma is on, mass spectra are recorded after the transient regime when the discharge is at the stationary state (Sciamma-O'Brien et al., 2010). This stationary state is labeled with the subscript SS. The spectra are therefore normalized with a peculiar correction factor $[N_2]_0/I_0(28)$ where $I_0(28)$ is the intensity current (A) of the mass peak m/z 28 and $[N_2]_0$ the nitrogen concentrations in the initial gas mixture (plasma off). When normalized, spectra are expressed in arbitrary units (AU).

III.2.2 The case of hydrogen: H and H₂

Optical emission spectroscopy measurements have been done for plasma conditions with initial amount of CH₄ from 1% to 10% in nitrogen. The argon amount was always the same (5%). Figure 25 shows the intensity of H β (486.1 nm) and Ar (811.5 nm) lines as a function of the CH₄ percentage.

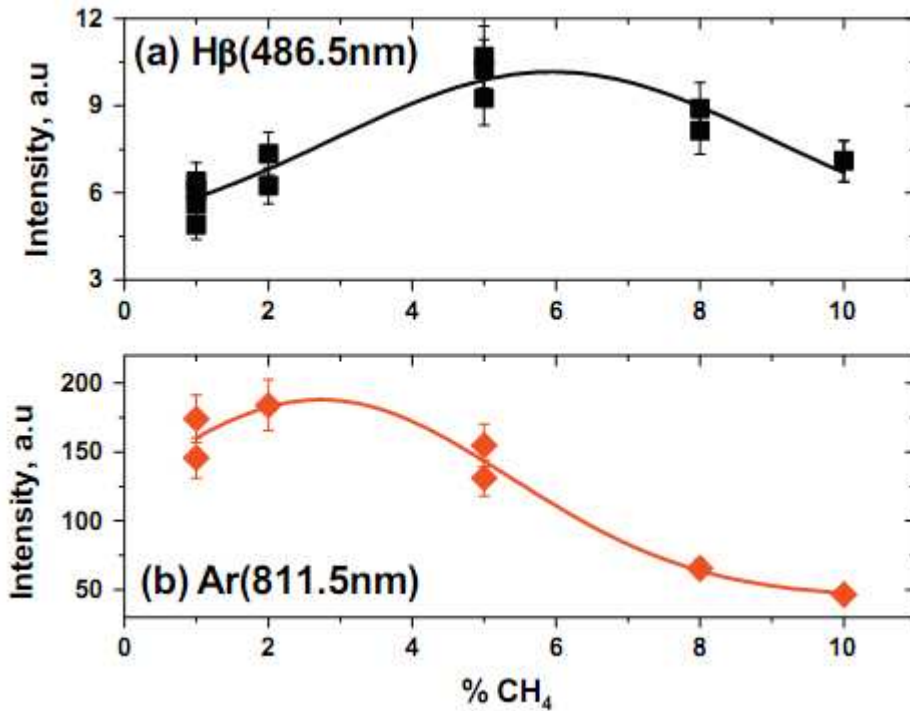


Figure 25: Evolution of H β and Ar (811.5 nm) lines intensities with the percentage of methane in nitrogen.

The H β emission reaches a maximum for about 5% of CH₄. Whereas the argon density is constant, Ar line varies with the CH₄ amount. As shown in Eq. (2), this variation is related to the electron density and temperature. In order to remove the influence of electron density, the ratio H β /Ar, proportional to the atomic hydrogen density, is calculated and presented in Figure 26.

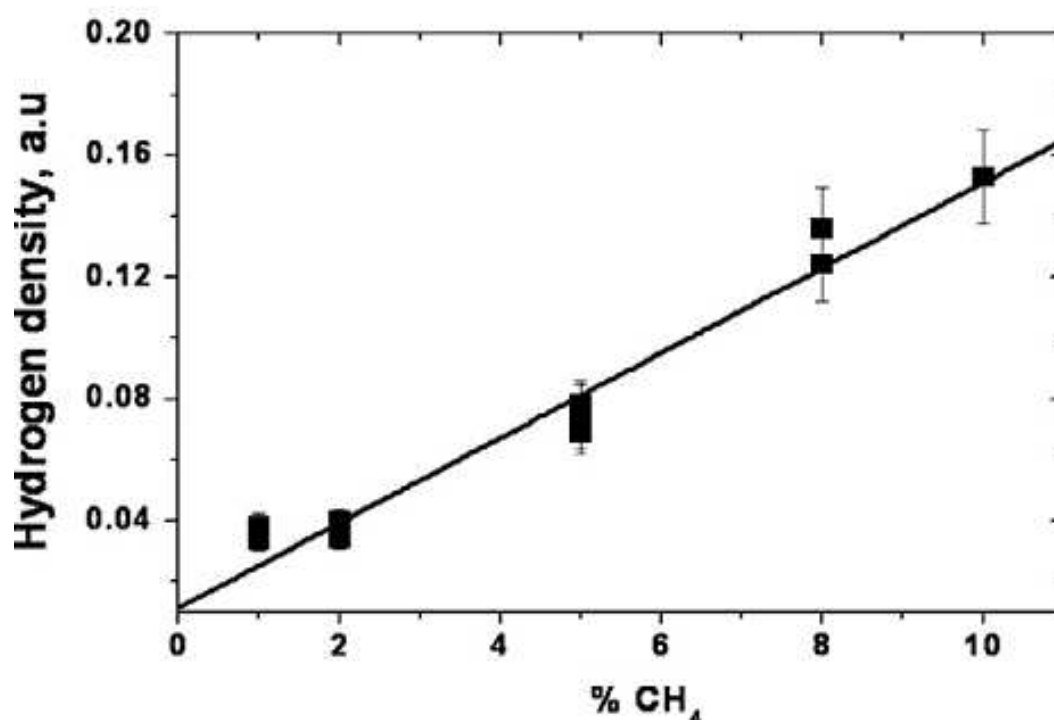


Figure 26: Evolution of atomic hydrogen density with % CH₄

From Figure 26, it can be deduced that [H] increases linearly with the injected amount of CH₄. This positive linear increase with [CH₄]₀ is anti-correlated with the decrease of the gas-to-solid conversion efficiency measured in Sciamma-O'Brien et al. 2010. As a consequence, atomic hydrogen provides a possible important clue to understand inhibition of the aerosol production observed when the amount of methane increases.

Information of molecular hydrogen production is contained in the m/z 2 intensity production $I_{ss}(2) - I_0(2)$, difference between stationary state and initial mass spectra. Indeed this indicator informs us about the global hydrogen content in the reactive plasma, summing the major contribution of molecular hydrogen, but also of atomic hydrogen efficiently recombined on the metallic sampling line before the ionization chamber of the mass spectrometer. Secondary contributions from hydrocarbon products fragmentation are negligible. Indeed, as shown on Figure 24, the m/z 2 signal increases from 8×10^{-11} A to 1×10^{-9} A. A similar production of a few 10^{-9} A can be observed for the peak at m/z 28. It corresponds to the ethane C₂H₄ signature, which has no significant contribution at m/z 2 in its fragmentation pattern (NIST and Pfeiffer databases). All the other products peaks are at the most of the order of 1×10^{-11} A.

The fragments of these products can therefore not contribute significantly to the m/z 2 signal. The contribution of atomic hydrogen can also be considered as negligible if we compare with the concentrations of H_2 and H predicted by Pintassilgo and Loureiro 2010 for a N_2 - CH_4 afterglow plasma model, corresponding to ten times less H atoms than H_2 molecules. As a consequence, $I_{ss}(2)-I_0(2)$ can at first order be assimilated to molecular hydrogen signature. Figure 27 reports the molecular hydrogen production (difference between the stationary $I_{ss}(2)$ and the initial $I_0(2)$ intensities of the mass peak at m/z 2), as a function on the initial methane concentration (upper panel), or as a function of the consumed methane (lower panel). Error bars are calculated as $\pm 2 \sigma$ on the statistical among several recorded spectra for each condition. The uncertainty is larger for the $[CH_4]_0 = 8\%$ conditions because of an unusual drift of the signal during this specific experiment.

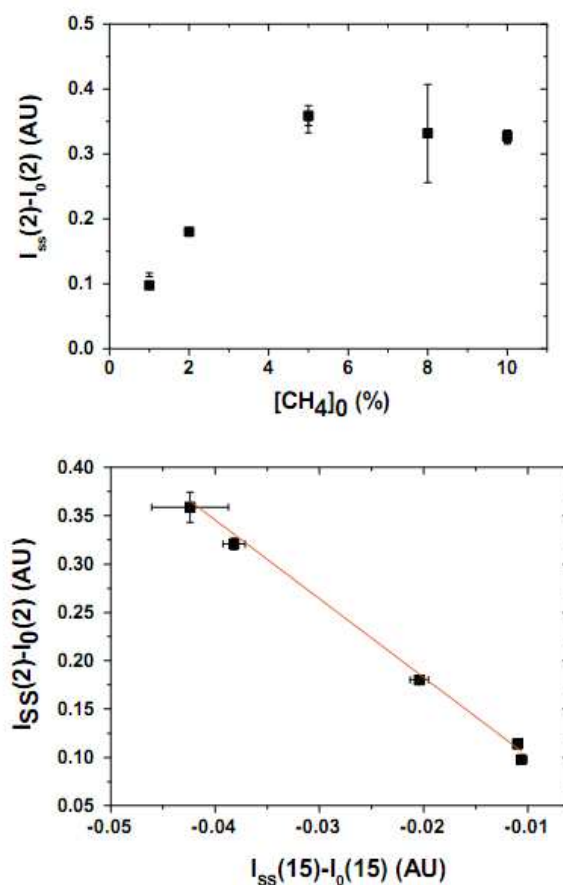


Figure 27: (Top) Hydrogen production (corresponding to the difference between the stationary and the initial intensities of the $m/z=2$ peak) according to the initial methane percentage. (Bottom) according to the methane consumption (difference between stationary and initial intensities of the peak at $m/z=15$)

We observe on Figure 27 (upper panel) that $I_{ss}(2)-I_0(2)$ increases globally with the initial methane content, but reaches an asymptote for initial concentrations higher than 5% of methane. This can be related to the same asymptote observed in Sciamma-O'Brien et al. (2010) for methane consumption $I_{ss}(15)-I_0(15)$. Both parameters are strongly correlated as can be seen on the lower panel of Figure 27. This H_2 enrichment with the initial concentration of methane is consistent with the time-dependent measurement carried out by Majumdar et al. 2005 with a 2:1 $CH_4:N_2$ gas mixture. Moreover, this result shows that molecular hydrogen concentration is dominated by the methane dissociation processes more than by all the secondary reactions producing H_2 and occurring in the plasma (neutral-neutral, ion-molecule and ion dissociative recombination reactions).

On the contrary, H concentration increases linearly with initial methane concentrations (Figure 26). No asymptote is observed for initial methane concentrations higher than 5% as for molecular hydrogen. This suggests that atomic hydrogen production is more independent from methane direct dissociation than molecular hydrogen. Atomic hydrogen is probably more linked with other reactions as for example dissociative recombination of positive ions (Plessis et al. 2010) and inhibition of aerosols formation.

III.2.3 Organic species production

Figure 24 illustrates the rich product formation in the stationary plasma for an initial methane concentration of 10%: a production of species can be observed in the ranges m/z [24–29], m/z [36–44] and m/z [50–55]. These mass ranges correspond respectively to elemental formula of $C_xH_yN_z$, $x + z = 2$, $C_xH_yN_z$, $x + z = 3$, $C_xH_yN_z$, $x + z = 4$. Those will be named C2, C3 and C4 blocks in the following. Ionization of a complex mixture of neutrals by electronic impacts with electrons at energy of 70 eV leads to overlapping cracking patterns in the mass spectra, which are commonly reported as difficult to interpret and set up a recurring issue for spectra analysis. Only the main univocal mass peaks are often treated (Deschenaux et al. 1999; Majumdar et al. 2005).

For this reason, we first analyzed the evolution of the mass intensities according to the methane amount, without any tentative identification. Results are plotted in a semi log scale on Figure 28, with 2σ uncertainties on the measurements calculated by a four times repetition of each spectrum measurement. Globally, we observe an important effect of the initial amount

of methane in the gas mixture, with more and more gaseous species, also with larger intensities, detected when the initial methane concentration increases. Less products peaks are observed in the mass spectrum for the 1% methane condition, in comparison with the 10% methane one. This result is in agreement with the previous study of Sciamma-O'Brien et al. 2010 on the gas-to-solid conversion efficiency. It was shown that this efficiency decreases drastically with the initial methane concentration, meaning that for similar methane consumption, the gas mixture becomes more and more favorable to gaseous products in the detriment of solid products when methane increases.

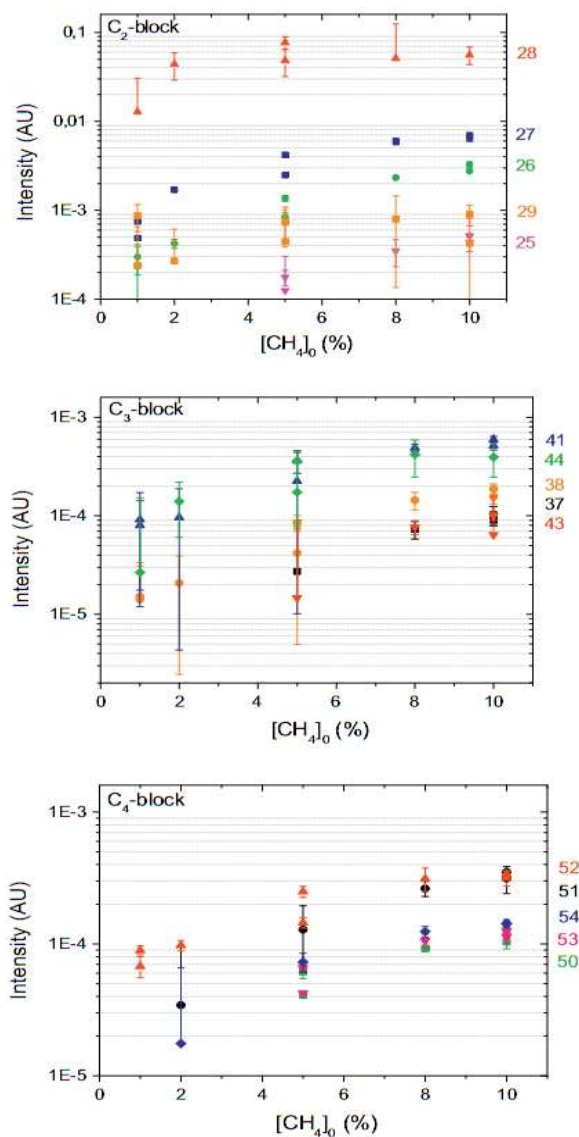


Figure 28: Evolution of significant peaks detected, according to the initial methane amount. Reported uncertainties are 2 σ calculated on four repetitions of each spectrum and two experiments per methane condition.

Differential mass spectra for all the detected peaks ($I_{ss}(X)-I_0(X)$) have been measured for $[CH_4]_0 = 1-10\%$. Results obtained at 1%, 5% and 10% of methane in the initial gas mixture are plotted in Figure 29.

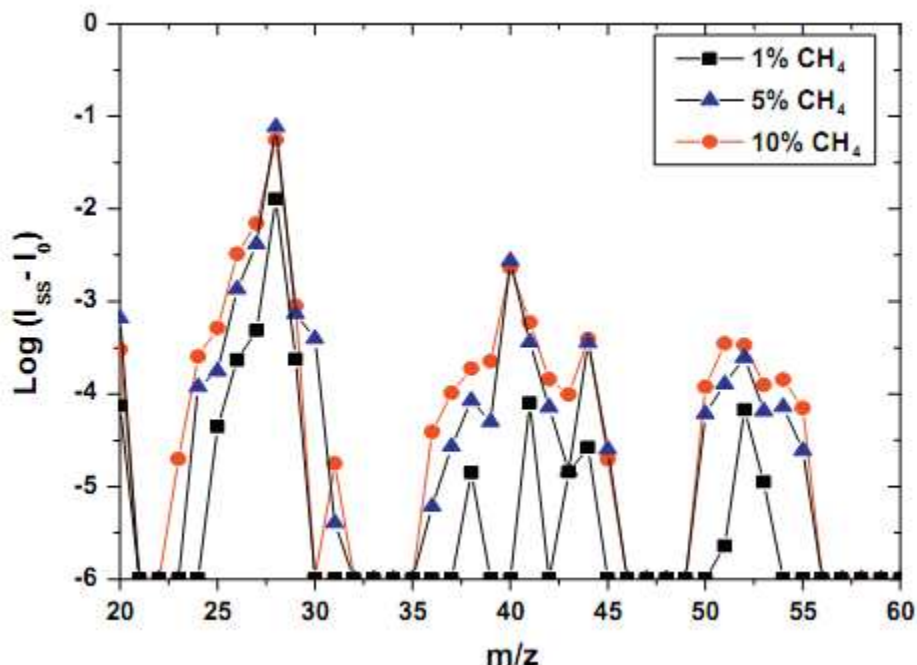


Figure 29: Differential mass spectra (stationary state - initial spectrum) for initial gas mixtures of 1% (black), 5% (blue) and 10% (red) of methane in the initial gas mixture

We observe that for 1% initial methane concentration, fewer molecules are produced in the plasma. The identification is less ambiguous and the spectra can be treated in details. Mass peaks can be singly attributed as follows. The heaviest detected block, of C₄ compounds is dominated by the peak at m/z 52 and is attributed to C₂N₂, which has only one other fragment in the NIST database at m/z 26 (5% of the m/z 52 intensity). C₄H₄ is not possible because its fragments at 50 and 51 amu, which are important in the NIST database (50% of the main m/z 52 peak) are in disagreement with the observed mass spectrum. C₂N₂ comes from the recombination of two CN radicals. C₂N₂ has previously been observed in Titan's atmosphere (Vuitton et al. 2007; Cui et al. 2009; Robertson et al. 2009) and in N₂-CH₄ plasma experiments (Bernard et al. 2003; Majumdar et al. 2005; Ramírez et al. 2005) CN radicals have moreover been detected by optical emission spectroscopy in N₂-CH₄ plasmas (Alcouffe et al. 2010; Horvath et al. 2011).

The C3 block includes 4 main peaks at mass m/z 44, 43, 41 and 38. Propane (C_3H_8) is the most probable product at m/z 44. The odd masses at m/z 41 and 43 can be attributed to nitrogen-bearing species. Acetonitrile (CH_3CN) is unambiguously attributed to m/z 41, and has been cross-confirmed as a major product in the experiment by the GCMS analysis (see part 3 of this chapter). The mass peak at m/z 43 is the signature of ethanimine $CH_3-CH=NH$ (and/or amino-ethene with the unsaturation carried by the $C=C$ bond: $CH_2=CH-NH_2$), which is cross-confirmed by the ion detection of Mutsukura 2001. Ethanamine has been shown to be produced by the reaction between $N(^2D)$ and C_2H_4 (Balucani et al. 2010). However, it is not to exclude that this mass peak may also be the result of a fragmentation pattern of amino-methanimine ($H_2N-CH=NH$), its fragmentation pattern being unknown. However, the ion study of Mutsukura 2001 does not show the signature of amino-methanimine.

The m/z 38 mass peak is observed in all the reactive N_2-CH_4 studies made by mass spectrometry (Majumdar et al. 2005; Imanaka and Smith 2010), but there is not clear evidence to attribute this fragment yet. A C_2N^+ fragment from the C_2N_2 neutral can be suspected.

The C2 block shows significant peak intensities for m/z 25, 26, 27, 28 and 29. They are in agreement with the similar N_2-CH_4 plasma studies performed by Majumdar et al. 2005. Three main points can be extracted from these C2 block data, largely complicated by the overlapping of several hydrocarbon and nitrogenous containing fragments.

The HCN formation (main peak at m/z 27), is cross identified as the major gaseous products in the cold-trap analysis (see part 3 of this chapter).

An important intensity of the m/z 28 peak, corresponds mainly to ethylene C_2H_4 . Indeed, as we analyze the differential spectrum between final and initial states, the increase of the m/z 28 peak cannot be due to a production of N_2 .

The production of acetylene C_2H_2 at m/z 26 is possible but its main fragment at m/z 26 is mixed with the contributions of the CN^+ fragments of all abundant nitriles.

III.2.4 Implication for tholins formation processes: the case of ammonia and Methanimine

Ammonia, NH_3 , is of great interest concerning prebiotic chemistry, providing reactive nitrogen-containing species to Titan's atmosphere. It has been detected and quantified by the INMS instrument onboard Cassini (Yelle et al. 2010).

In mass spectrometry, the ammonia production signature at m/z 17 is partially hidden by the contribution of the water signal of the mass spectrometer. In order to extract this information from the data, we precisely quantified the I_{17}/I_{18} ratio given by the only water signature in our QMS, using all the spectra recorded without plasma, so in absence of ammonia. Thirty-eight spectra have been recorded and a statistical fluctuation of I_{17}/I_{18} can be deduced. A maximum error bar of $\pm 2\sigma$ is calculated and plotted for each experimental condition in Figure 30. The I_{17}/I_{18} measurement outside this statistical water range corresponds thus to a significant difference compared with the water ratio. A larger value of I_{17}/I_{18} is consequently significant for the production of ammonia when the plasma is on and contributing to I_{17} .

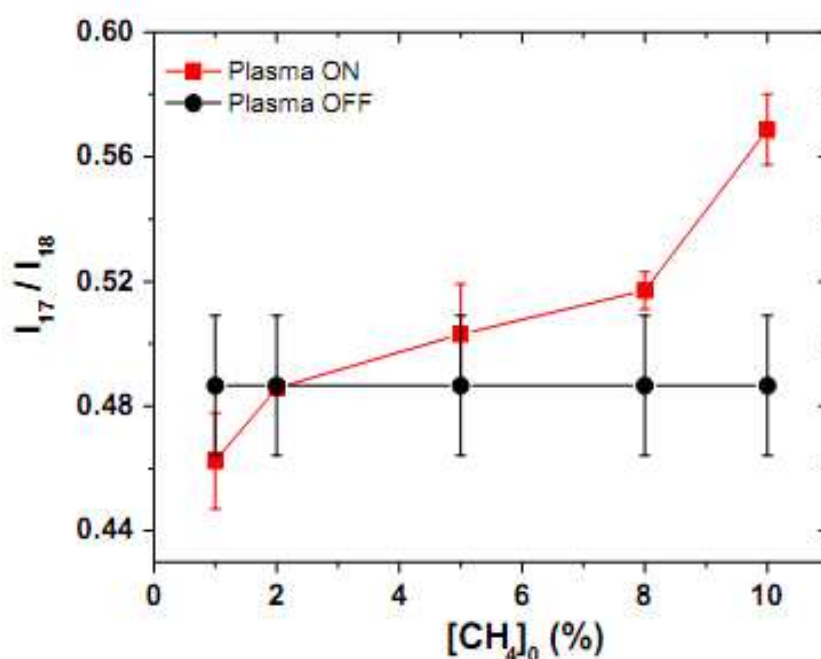


Figure 30: Ratio I_{17}/I_{18} as a function of %CH₄, plasma on (red) and plasma off (black)

An increase of the ammonia production with the initial amount of methane can actually be observed on Figure 30, and becomes significant for methane concentrations higher than 5%. An ammonia production is not discarded for methane concentration below 5% but it is not important enough to be distinguished from the experimental uncertainty of the I_{17}/I_{18} water ratio.

Ammonia formation in CH₄-N₂ plasmas is an important issue which has not been definitely solved yet (Uyama and Matsumoto 1989; Mutsukura 2001; Horvath et al. 2011). In any case

the key is the production of NH radicals, which react with molecular hydrogen to produce ammonia through the reaction:



This reaction explains that ammonia production is promoted by a hydrogen-rich gas mixture, and thus increases with methane percentage.

The NH radical is suggested in the literature to be both produced by gas phase mechanism, involving ion chemistry:



and radical chemistry:



Some studies suggests that the radical pathway can in some conditions be catalyzed on the surface of the reactor (Touville et al. 1987). However, in PAMPRE the ratio volume/reactor surface is actually larger in our case than in the setup of Touville et al. 1987. We can thus assume that reactions are mainly in the plasma volume and that this wall effect can be neglected.

In addition to the identified and well-known mechanisms listed above, dissociative recombination with electron of protonated amines may also provide plausible pathways in the plasma towards ammonia, as the one suggested by Yelle et al. 2010 for Titan's atmospheric chemistry from protonated methanimine dissociative recombination.

In PAMPRE, a firm detection of methanimine, $\text{CH}_2=\text{NH}$ at m/z 29 can be given for $[\text{CH}_4]_0 = 1\%$. Actually an additional contribution at m/z 29 can be given by the propane fragmentation 44 (50%) 29 (100%) pattern (from database of the Pfeiffer QMS 200). The ratio of these two peaks in the differential spectra is therefore plotted in Fig. 27 as a function of initial percentage of methane.

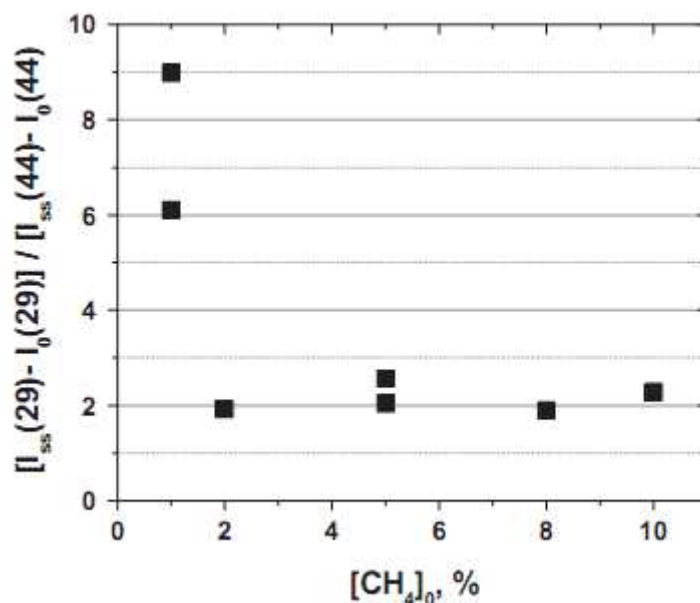


Figure 31: Evolution of the ratio between the increases of m/z 44 and m/z 29 when the plasma is ON. The stable value of about 2 for $\text{CH}_4[0]$ concentration larger than 2% is in agreement with a co-evolution of fragments intensities for propane. However, the larger value of this ratio for 1% initial methane concentration indicated the additional contribution of methanimine at m/z 29.

For $[\text{CH}_4]_0$ larger than 2%, the ratio is constant and consistent with the propane pattern, showing that this compound becomes the main contributor to the m/z 29 peak for these methane amounts. On the other hand, the ratio is much larger for $[\text{CH}_4]_0 = 1\%$, and becomes inconsistent with propane. It confirms the important contribution of methanimine at m/z 29 in these experimental conditions. Methanimine was previously detected in a $\text{N}_2\text{-CH}_4$ micro-wave plasma discharge by Fujii and Norihisa 1999; Kareev et al. 2000; Fujii and Kareev 2001.

However, micro-wave discharges are well-known to be very warm and to be compared with combustion processes. Its detection in the PAMPRE gas mixture confirms thus the methanimine production in much cooler experimental conditions, more representative of the cold Titan's atmospheric chemistry. The detection of this compounds is of high importance for the understanding of tholins formation. Indeed, methanimine (which is mainly produced by the reaction between $\text{N}(^2\text{D})$ and methane (Balucani et al. 2009)) has been detected and quantified by the INMS instrument onboard Cassini (Yelle et al. 2010) and is suspected to be one of the precursors of Titan's aerosols.

III.2.5 Conclusion

The study of the stationary gas phase composition obtained with various initial methane concentrations from 1% to 10%, confirms the enrichment of the gas phase – number of species detected and global quantity – with the input of methane. A specific case is found at 1%, which almost only produces nitrogenous species and few hydrocarbons. Atomic hydrogen is quantified and an anti-correlation is found between the abundance of atomic hydrogen and the aerosol production efficiency. This result is in agreement with the inhibiting heterogeneous effect suggested in Sciamma-O'Brien et al. 2010. A modeling of nitrogen–methane RF plasma, similar to the study of Pintassilgo et al. 1999 but which was dedicated to a N_2 - CH_4 glow discharge, would be an essential complementary tool enabling to interpret the correlations found here between volatiles and aerosol production.

Moreover ammonia and methanimine are detected in the plasma in agreement with the detection by INMS in Titan's ionosphere (Yelle et al. 2010). The production in the gas phase of such highly polymerizable species provides promising clues to understand the production of tholins.

In the frame of Titan's upper atmosphere, this study confirms two main antagonist effects on aerosol production and growth. The first effect supports the organic growth process suggested by Balucani et al. 2009; 2010 and involving a co-polymerization with imine species. The second one is an inhibiting effect of atomic hydrogen on the aerosol production. This effect is related to the observation of Sekine et al. 2008a; 2008b, showing an efficient fixation of atomic hydrogen on aerosols. Here we show that the efficient hydrogen fixation is made at the expense of the aerosol organic growth itself and has to be considered as a competition with the aerosol organic growth process.

III.3 Improving sensibility: Cold trap experiments

As seen in part 2 of this chapter, the in-situ mass spectrometry is a powerful tool to analyze the gas mixture in the PAMPRE reactor. However this technique has two main issues that prevent an exhaustive analysis of the gas phase. First the sensibility of the MS itself only enables detection of the major species in the gas phase. Second, the ionization method used for QMS (electronic impact at 70 eV) induces a cracking pattern of the molecules detected. Since the patterns overlap, it can be quite tricky to identify clearly the original molecule, and if so, to quantify it. Even though for doing such quantification, it is possible to do a single value decomposition treatment. This has been applied for example for the treatment of the Cassini –INMS spectra (Cui et al. 2009), but the non-unique decomposition results are highly dependent of the chosen database (Carrasco et al. 2012).

In order to go further in the identification and the quantification of species in the PAMPRE reactor I therefore used a cryogenic trapping that allows concentrating minor species. Once species are trapped, I used a Gas Chromatograph coupled to a Mass Spectrometer (GC-MS) to analyze the mixture. In GC-MS species are first separated in chromatographic column before injection in the mass spectrometer. Since species enter the spectrometer separately, their cracking patterns do not overlap anymore, and it is much easier to identify it.

In this part is presented the first study of the gas products in PAMPRE, both on their detection and their relative quantification. This study will help to understand the chemistry in the gas phase, highlighting key organic species responsible for the resulting in tholins formation. Results presented in this part have been published in Gautier et al. 2011.

III.3.1 Experimental setup and protocol

In the study presented here, the trap is heated and then pumped with a turbo pump before each experiment in order to remove water vapor adsorbed on the trap walls. Experiments are 3h long and repeated at least two times in order to ensure the repeatability of the measurement.

At the end of an experiment, the trap is isolated from the reactor with a gas valve. The pressure inside it while it is still immersed in liquid nitrogen was below the limit of detection of the Bourdon gauge. When the trap is warmed up to room temperature, the light species trapped sublime back to the gas phase and a solid residue is formed when the trap returns to

room temperature. In the present section, only the gas phase present in the cold trap is analyzed. The analysis of the solid residue can be found in chapter IV.

The absence of condensation of both N_2 and CH_4 in the trap is checked with non-reactive experiments (plasma off), where a 55 sccm flux of N_2 - CH_4 90:10 is injected in the reactor in the same pressure conditions. After a 3 hour run the trap is taken out of liquid nitrogen and left at room temperature to warm up. As no pressure increase is observed, neither nitrogen nor methane get trapped.

The gas trapped is analyzed by Gas Chromatography coupled to Mass Spectrometry (GC-MS). The cold trap is connected to a GC-MS device through a six port gas valve to perform direct injection of the trapped gas.

Before each injection, a blank experiment is performed under the same analytical conditions without any sample injected. This blank injection allows to clearly identify potential contaminant species, and discriminates them from chemical species evolving from the sample. No specific contamination was detected in the blank except usual column releases.

III.3.2 Results

III.3.2.a Evolution of the gas phase pressure with methane percentage

When the trap is warmed up, the gas pressure inside the cold trap increases, showing the presence of gas products accumulated during the experiment and condensed in the trap. For the different experiments carried out, this pressure is shown to depend on the methane concentration of the gas mixture injected in the reactor. This indicates that the total amount of condensable species produced changes with the amount of methane introduced in the reactor. The evolution of the total gas pressure measured in the cold trap after warming up to room temperature is given in Figure 32 as a function of the CH_4 concentration. The evolution of the carbon gas to solid conversion yield obtained from a previous study (Sciamma-O'Brien et al. 2010) is also plotted in this figure. This yield is defined as the ratio between the mass of solid carbon incorporated in the tholins and the mass of reactive gaseous carbon coming from the CH_4 consumption in PAMPRE. It reflects the efficiency of the reactive gas mixture to produce solid aerosols, relatively to the carbon element transfer from reactants (CH_4) to products.

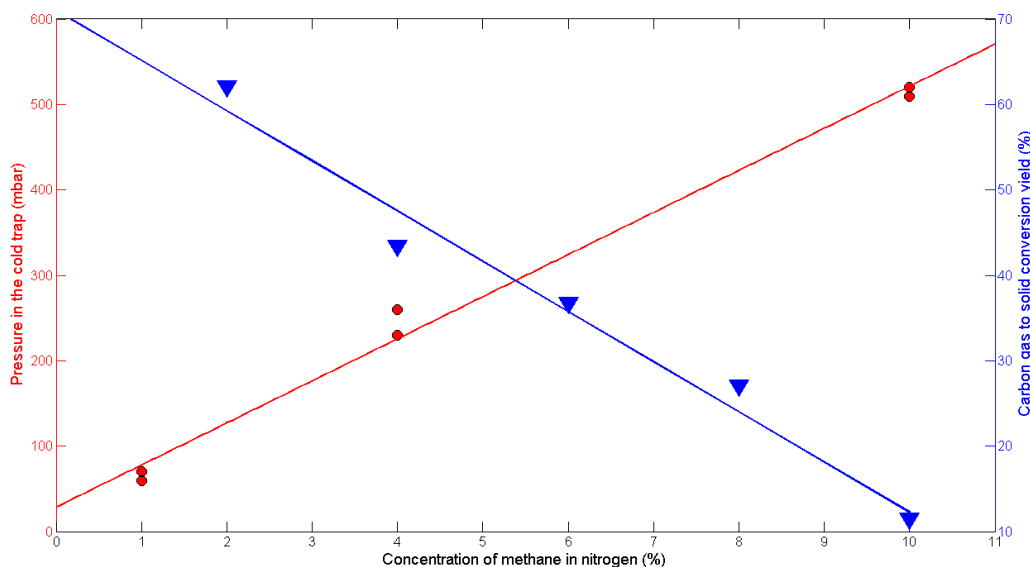


Figure 32: Evolution of the total gas pressure in the cold trap after warming up to room temperature (red dots) and of the carbon gas to solid conversion yield (blue triangles, adapted from Sciamma-O'Brien et al. 2010) as a function of CH_4 concentration.

Figure 32 shows that the highest pressure difference measured between two similar experiments is of 14%, ensuring a satisfying reproducibility of the measurements. Moreover, this pressure linearly increases with the CH_4 concentration. The pressure in the cold trap rises from 60 mbar after an experiment with 1% of CH_4 in the gas mixture up to 500 mbar of gas in the cold trap after an experiment with 10% of CH_4 in the gas mixture. On the other hand, the carbon gas to solid conversion yield linearly decreases with the increasing concentration of methane in nitrogen. For 2% of CH_4 in the experiment, the carbon gas to solid conversion yield is 62% while for 10% of CH_4 in the gas mixture the yield plummets to 12% (Sciamma-O'Brien et al. 2010).

The opposite evolution of the two parameters with the CH_4 concentration in the reactive gas mixture is consistent with the product formation trend in the PAMPRE reactor. At low CH_4 concentrations, gaseous products are essentially converted into solid phase (tholins); the amount of gas remaining is thus low. Inversely, for high CH_4 concentrations, the gas products are not consumed much to create tholins, and stay in the gas phase; the total gas pressure in the trap is then higher.

III.3.2.b GC-MS results

The three chromatograms given in Figure 33, Figure 34 and Figure 35 correspond to three experiments respectively at 1%, 4% and 10 % of CH_4 in N_2 . All the peaks have been identified using their elution order and their mass spectra. The peaks of highest intensity seen in these chromatograms can be attributed to nitriles. The main peak is due to hydrogen cyanide (HCN), the second peak in intensity is acetonitrile (CH_3CN) while the two other predominant peaks are attributed to propanenitrile ($\text{CH}_3\text{CH}_2\text{CN}$) and propenenitrile (CH_2CHCN). Peak labels correspond to their identification in Table 2.

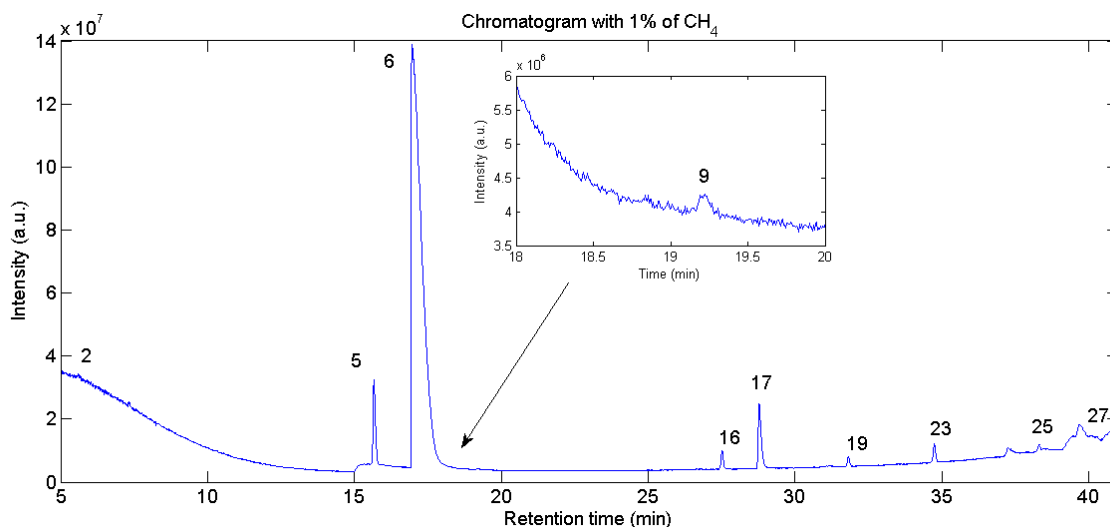


Figure 33: Chromatogram of the cold trap content for an experiment performed with 1% of CH_4

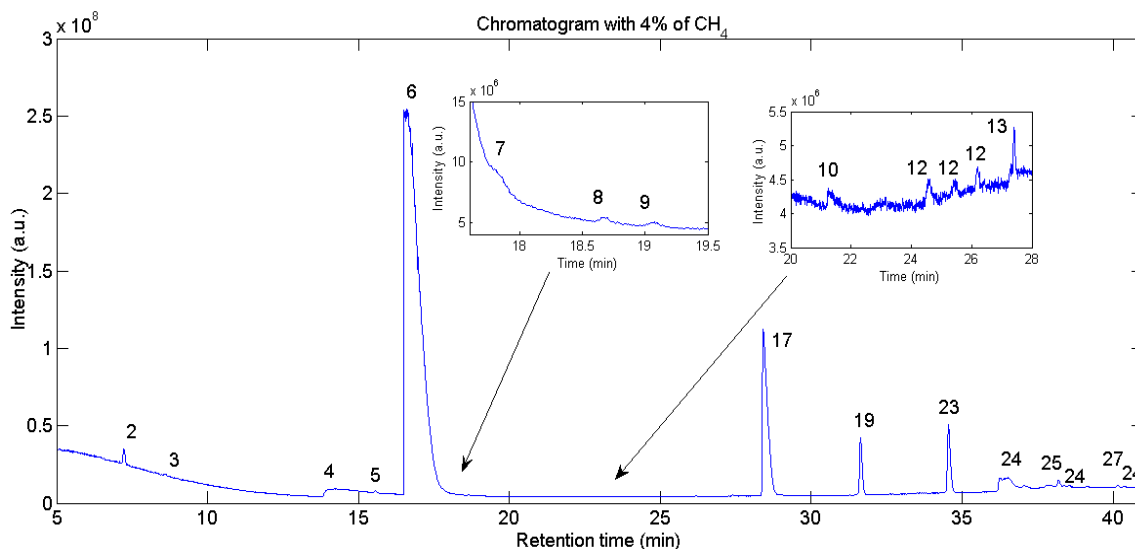


Figure 34: Chromatogram of the cold trap content for an experiment performed with 4% of CH_4

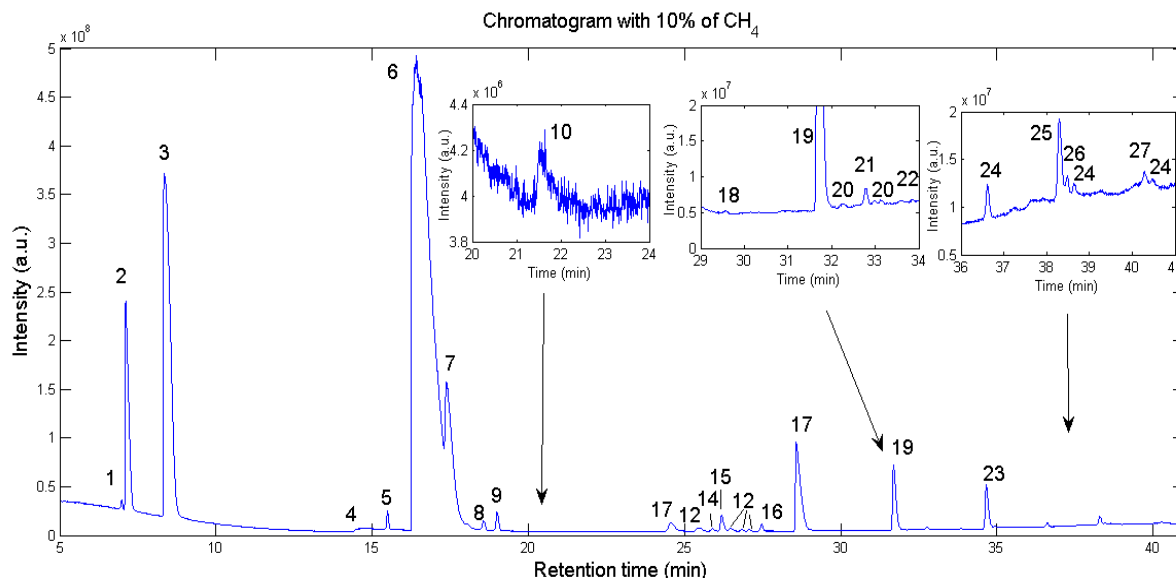


Figure 35: Chromatogram of the cold trap content for an experiment performed with 10% of CH₄

From the analysis of all the chromatograms obtained, whatever the methane concentration, more than 30 species have been detected (cf. Table 5) among which a large amount of nitriles, many hydrocarbons, and a few aromatics, mainly heteroaromatic compounds.

Considering that the MS response is similar for all the detected compounds, whatever the methane concentration in the reactor is, nitrile peaks are always the overriding peaks in the chromatograms, meaning that nitriles are the main species in the gas phase.

For samples produced with 1% and 4% of CH₄ in the experiment, the chromatograms look similar, with just a small increase of the existing peaks. However, for the sample produced with 10% of CH₄, new peaks can be observed on the chromatogram. From their retention time and their mass spectra, these peaks can be identified as hydrocarbons. Hydrocarbons containing two carbon atoms (C₂) are eluted at Tr=5.3 minutes (Ethylene), Tr=7.2 minutes (Acetylene) and Tr=8.6 minutes (Ethane). C₃ hydrocarbons are identified at Tr=17.2 minutes (propene), Tr=17.4 minutes (propane) and Tr=18.9 minutes (propyne), while C₄ hydrocarbons are eluted in the range of Tr=25 to 27 minutes. Thanks to pre-concentrated injections performed on a sample coming from an experiment with 10% CH₄ in the reactor, a small signal due to heavier compounds (C₅H₁₂, C₅H₁₀, C₅H₈, C₆H₆) can also be detected for retention time higher than 35 minutes.

The list of all the gaseous compounds detected is given in Table 5.

Table 5: List of gaseous compounds detected in our experiment, in Titan's atmosphere and in other laboratory experiments. a: Cui et al., 2009; Robertson et al., 2009; Vuitton et al., 2007 ; b : Bernard et al., 2003; c : Ramírez et al., 2001; Ramírez et al., 2005; d : Tran et al., 2005

Compounds detected in PAMPRE	Formul a	Peak identification in chromatogram of fig.31	Detected in Titan atmosphere	Detected in other Laboratories experiments
Nitrogenous compounds				
Hydrogen cyanide	HCN	6	a	b,c
Ammonia	NH ₃	4	a	b
Ethanedinitrile	C ₂ N ₂	5	a	b,c
Methyl isocyanide	C ₂ H ₅ N	13	a	
Acetonitrile	C ₂ H ₃ N	17	a	b,c,d
Propiolonitrile	HC ₃ N	16	a	b,d
2-Propenenitrile	C ₃ H ₃ N	19	a	c
Propanenitrile	C ₃ H ₅ N	23	a	c
2-methylpropanenitrile	C ₄ H ₇ N	25		c
Butanenitrile	C ₄ H ₇ N	27		c
C ₄ H ₅ N isomer	C ₄ H ₅ N	24	a	
C ₅ H ₇ N isomer	C ₅ H ₇ N			
Pentanenitrile	C ₅ H ₉ N			
Pentanedinitrile	C ₅ H ₆ N ₂			
Butanedinitrile	C ₄ H ₄ N ₂			
Butanenitrile,3-dimethyl	C ₅ H ₉ N			
Hydrocarbons				
Acetylene	C ₂ H ₂	2	a	b,c,d
Ethylene	C ₂ H ₄	1	a	b,c,d
Ethane	C ₂ H ₆	3	a	b,c,d
Allene	C ₃ H ₄	8		b,c
Propyne	C ₃ H ₄	9	a	b,c,d
Propene	C ₃ H ₆		a	c,d
Propane	C ₃ H ₈	7	a	b,c,d
1-Buten-3-yne	C ₄ H ₄	14		c
C ₄ H ₆ isomer	C ₄ H ₆	18	a	c,d
C ₄ H ₈ isomer	C ₄ H ₈	12		c,d
n-Butane	C ₄ H ₁₀	15		c,d
i-Butane	C ₄ H ₁₀	11		c,d
C ₅ H ₈ isomer	C ₅ H ₈	22		c
C ₅ H ₁₀ isomer	C ₅ H ₁₀	20		c,d
n-Pentane	C ₅ H ₁₂	21		c,d

Aromatic species			
Tetrazolo[1,5-b]pyridazine	$C_4H_3N_5$	26	
Triazine	$C_3H_3N_3$		
Benzene	C_6H_6	a	c,d
Pyrrole	C_4H_5N		
Other species			
Methanol	CH_3OH	10	
Ethanol	C_2H_5O		
Acetone	C_2H_6O		

III.3.2.c Comparison to Titan

The list of compounds detected in the cold trap with GC-MS and presented in Table 5 is consistent with the currently known list of Titan's atmospheric compounds (Vuitton et al. 2007; Waite et al. 2007; Lavvas et al. 2008; Cui et al. 2009; Robertson et al. 2009). In addition, it was also possible to detect some heavy nitriles not detected on Titan, such as butanenitrile ($CH_3-(CH_2)_2-CN$) and pentanenitrile ($CH_3-(CH_2)_3-CN$). The non-detection of these molecules on Titan could be explained by the fact that these molecules are expected to be at very low concentrations, far below the current limit of detection of the instruments onboard Cassini/Huygens. In this case, we suggest some minor species to be present in Titan's atmosphere.

III.3.2.d Comparison to other laboratory studies

It is possible to compare these results with other experimental works containing gas phase analysis. This comparison has been mainly done with experiments closed to PAMPRE experiment, i.e. able to dissociate molecular nitrogen. This criterion limits comparison with plasma experiments (Ramírez et al. 2001; Bernard et al. 2003; Ramírez et al. 2005). A comparison with the work of Tran et al. (2005), a photochemical experiment, where nitrogenous compounds (such as HCN) were introduced to provide nitrogen to the reactive mixture is also included.

As shown in Table 5, most of the species detected in my experiments are also consistent with the compounds detected in other lab experiments with the same light species detected and with a longer list of heavy nitriles (Ramírez et al. 2001; Bernard et al. 2003; Ramírez et al. 2005).

However, a few differences are observed between the experimental setups. There are two possible explanations for these differences. First, for experiments capable of dissociating

molecular nitrogen, differences observed probably come from the detection methods used. The molecules detected are indeed at very low concentrations and could remain unseen if the separation and detection methods were not optimized to detect them. For example, Tran et al. 2005 detected more heavy compounds than in this work due to their GC column whose stationary phase is optimized for light aromatics detection (Restek RTX-502.2 capillary column). Second, the lack of nitrogenous compounds in some photochemical irradiation experiments (Bar-Nun et al. 2008) can totally be explained by the fact that molecular nitrogen is not dissociated. Indeed, the bond energy for N_2 is 9.7eV which means that this molecule needs a radiation with a wavelength lower than 128 nm to be photo-dissociated and to release a nitrogen atom that could be involved in further reactions. Since silica cuts off radiation around 200 nm, if an experimental setup uses silica windows, molecular nitrogen will not be dissociated nor will it be used to form nitrogen-bearing species.

Finally, it is interesting to note that ammonia was detected by GC-MS in much lower concentrations than expected (Bernard et al. 2003). One possible explanation for this lack of NH_3 is the use of stainless steel for transfer and injection in the GC-MS, since ammonia is known to adsorb onto it. The ammonia concentration detected in the GC-MS chromatograms might therefore not be representative of the ammonia present in the cold trap. A solution for ammonia detection might be to perform a Siltek® treatment of the stainless steel parts (see part 2 and 5 of this chapter for further discussions on ammonia).

III.3.2.e Oxygen containing compounds

A few oxygen-bearing compounds have also been detected (cf. Table 5) in our experiments: three compounds with low peaks areas (less than 0.1% of the HCN peak area). Those can be explained by the presence of remaining micro-leaks due to the use of a low pressure experiment. They have been measured to be lower than 10^{-3} sccm, four orders of magnitude lower than the 55 sccm injected gas flow rate. The oxygen contamination can thus be considered as negligible in this work.

III.3.2.f Aromatic species

As shown in Table 5, aromatic compounds have also been detected in the cold trap. These aromatic compounds are however less numerous than reported in other laboratory experiments (Ramírez et al. 2001). This could be due to the GC column I used for this work,

which was optimized for the detection of light molecules containing approximately up to 6 carbon or nitrogen atoms.

Moreover, the detected aromatic compounds are mainly heteroaromatics, containing at least one nitrogen atom. The main aromatic species detected is tetrazolo[1,5-b]pyridazine which seems to be the bountiful aromatic compound in the gas mixture. The topological formulas of this compound and its experimental mass spectrum compared to theoretical mass spectra from NIST database are shown in Figure 36.

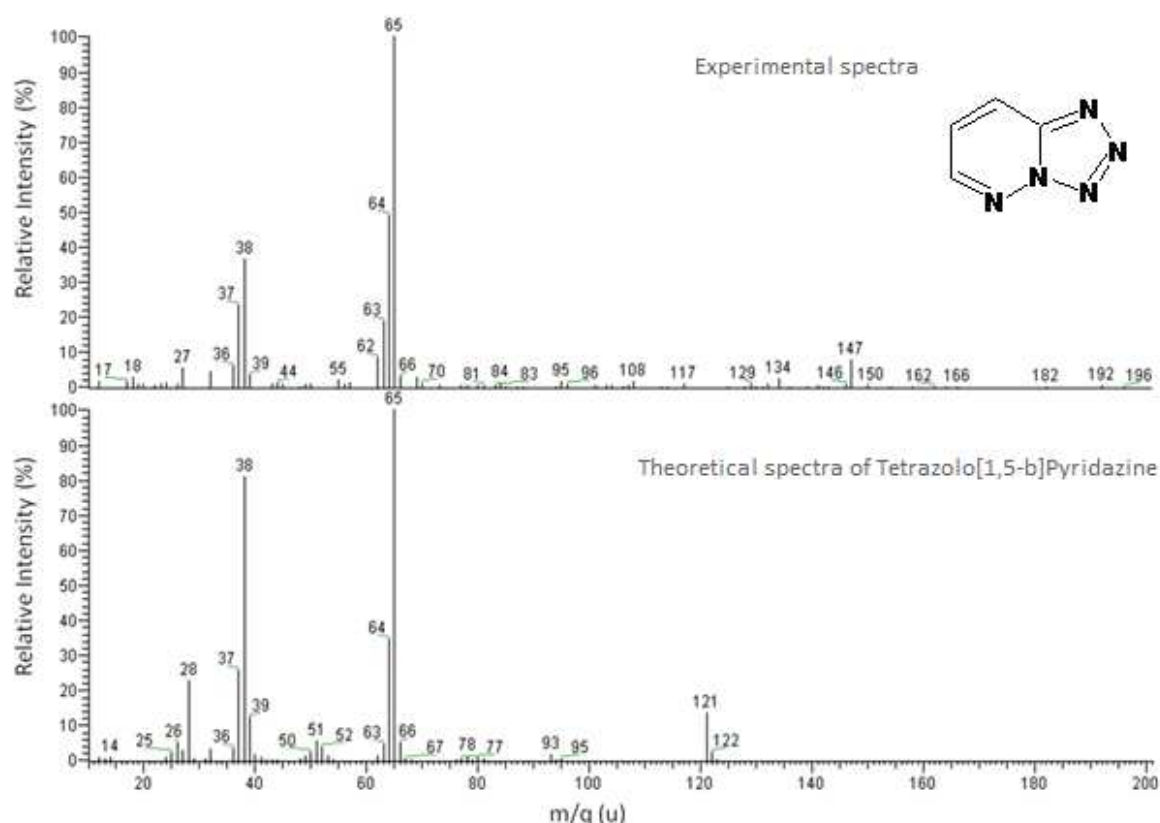


Figure 36: Experimental (up) and theoretical (down) spectra of tetrazolo[1,5-b]pyridazine. The topological scheme of this compound is given in the upper spectrum

The formation of Tetrazolo[1,5-b]pyridazine is not well explained yet. A possible hypothesis could be the addition of Propenenitrile (C_3H_3N), one of the most abundant molecules detected in the cold trap, with tetrazole (CH_2N_4). Tetrazole is basically formed by a reaction between hydrogen cyanide (HCN) and N_3^+ . N_3^+ is known to be present in nitrogen plasmas (de Petris et al. 2006).

III.3.3 Discussion

III.3.3.a The Predominance of nitriles

In order to characterize the evolution of the nature of the chemical species detected in the sample as a function of the injected methane concentration, a qualitative ratio ρ has been defined as $\rho = n_N/n_{CH}$. Where n_N is the number of N-bearing compounds and n_{CH} is the number of hydrocarbons. Even if this ratio characterizes only the number of detected species and does not take into account the relative area of the peaks in the chromatograms, ρ provides a good first-level indicator of the nitrile to hydrocarbon ratio which allows the relative comparison of the results obtained with the three methane concentration chromatograms. The evolution of ρ with the CH_4 concentration is given in Table 6.

Table 6: Evolution of ρ , the ratio of nitrogen bearing compounds versus hydrocarbon compounds detected in our experiment as a function of methane concentration of the gas mixture injected in the plasma reactor

CH₄ concentration	1%	1%	4%	10%	10%
n_N	7	11	19	12	16
n_{CH}	2	3	6	15	17
ρ	3.5	3.7	3.2	0.8	0.9

As we can see, the value of this ratio shows significant differences between low methane concentrations (1 and 4%) and high methane concentrations (10%). At low CH_4 concentrations the number of nitrile compounds is at least 3 times higher than the number of hydrocarbons, while at high CH_4 concentrations there are more hydrocarbons than nitriles. This suggests a change in the gas chemistry for the 10% of methane condition, compatible with the gas to solid conversion efficiency studied in Sciamma-O'Brien et al. 2010.

III.3.3.b Discussion on the possible predominance of N-Bearing compounds in Titan's aerosols

Even for experiments with low ρ values (experiments with 10% of methane in the initial mixture), if considering the area of peaks, nitriles are by far the major chemical products in

the gas phase. Therefore they are suspected to largely contribute to the chemistry leading to the formation of aerosols in our experiment.

For a long time, Titan's aerosols were considered to be formed by the aggregation of poly-aromatic hydrocarbons (PAH) (Waite et al. 2007). However, for the last few years, several publications have considered that nitrogenous compounds contribute significantly to the aerosol formation process.

This hypothesis is based on several clues. First, the observational data from the Cassini-Huygens mission have shown that there is a large amount of nitrogenous molecules such as nitriles or imines in Titan's atmosphere (Vuitton et al. 2007; Waite et al. 2007; Vuitton et al. 2009; Yelle et al. 2010). Second, atmospheric chemistry models have also inferred that quite a large amount of nitriles should be present in Titan's atmosphere, even more than hydrocarbons for a given number of atoms (Lebonnois et al. 2001; Hébrard et al. 2006; Lavvas et al. 2008). On the other hand, some observational data analyses have implied that the concentration of nitriles is slightly smaller than the hydrocarbon concentration (Vinatier et al. 2010). Models have also started to formulate hypotheses on the presence of a chemical pathway producing poly aromatic nitrogenous hetero-cycles (PANH), instead of a commonly admitted full PAH pathway in Titan's atmospheric chemistry (Vuitton et al. 2007). This tends to be confirmed by the detection of nitrogen-bearing aromatics in analogues of Titan's aerosols produced in laboratory experiments such as the PAMPRE tholins (Pernot et al. 2010).

III.3.3.c Nitrile reactivity

The laboratory experiments which are capable of dissociating N_2 are known to generate a complex chemistry producing both hydrocarbons and nitrogenous compounds (Bernard et al. 2003; Imanaka et al. 2004; Tran et al. 2005). Moreover, structural and chemical analyses performed on tholins produced with different laboratory experiments have confirmed that they contain large amounts of nitrogen (Imanaka et al. 2004; Carrasco et al. 2009; Pernot et al. 2010; Sciamma-O'Brien et al. 2010), in agreement with the ACP-Huygens results (Israel et al. 2005).

Despite the detection and the apparent importance of nitrogenous compounds in the formation of tholins (Khare et al. 2002; Hudson and Moore 2004; Imanaka et al. 2004), the gas

chemistry and reactive schemes of nitriles are still largely unknown and largely underestimated in atmospheric models of Titan (Hébrard et al. 2006; Lavvas et al. 2008). The only part of the nitrile chemistry that is taken into account in some models, deals with reactions between CN radicals or the lightest nitriles and hydrocarbons (Hébrard et al. 2006; Cui et al. 2009).

Even if the agreement between models and observations is not perfect (Hébrard et al. 2007), HCN production is the most understood pathway (Yung 1987) leading to nitriles in Titan's atmosphere. Several mechanisms have been proposed to produce nitrogen-bearing tholins by polymerization of HCN, CN or CH₃CN (Wilson and Atreya 2003; Krasnopolsky 2009), either on a hydrocarbon, to produce a nitrile, or on another nitrile, to produce a dinitrile (Lavvas et al. 2008).

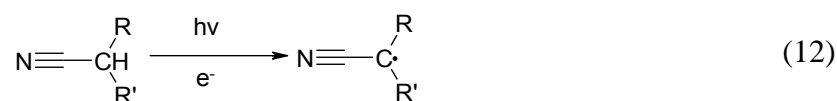
However, it is important to note that even the production of a simple molecule like acetonitrile is still an open question and deserves a particular attention in order to better explain the large densities observed in different regions of Titan's atmosphere. All the recent post-Cassini models use the rate constant from Sato et al. 1999 to describe the kinetics of the reaction between N(²D) and C₂H₄; but the branching ratios of the reactions have not been quantified yet and can lead to several scenarios implemented in photochemical models. In all cases, this reaction is treated as either the only pathway or at least one of the most important enabling the production of acetonitrile. Wilson and Atreya 2003, Hébrard 2006 and Lavvas et al. 2008 implemented a 100% acetonitrile production pathway, whereas Krasnopolsky 2009 used only a 20% acetonitrile pathway (and 80% for NH+C₂H₃). However, the RRKM calculations of Takayanagi et al. 1998 and the molecular crossed-beam experiments of Balucani et al. 2000 predict 2H-azirine and ketene-imine as the major products at low temperature, with a very minor direct production of acetonitrile. It would be useful to do experiments at the temperature range of Titan's atmosphere to try and confirm/quantify if the isomerization of these two major products towards acetonitrile could explain an efficient production of acetonitrile from the reaction N(²D)+C₂H₄ as suggested by Balucani et al. 2000.

Reactions with CN radical have been widely studied in the last twenty years. Butterfield et al. 1993 have shown that the reactions of CN with allene, butadiene, propylene and propenenitrile can take place in the gas phase. Carty et al. 2001 have confirmed the reaction

of CN with allene and they have also added the reaction of CN with methylacetylene. Yang et al. 1992 have studied the reactivity of CN with alkanes (C_2H_6 , C_3H_8 , C_4H_{10} , C_5H_{12} and C_8H_{18}), while Seki et al. 1996 have studied its reactivity with acetylene and ethanedinitrile. A study of the addition of CN to CH_4 , C_2H_6 , C_2H_4 , C_2H_2 and C_3H_6 can be found in Sims et al. 1993 and the reaction $CN+CH_3CN$ is given in Zabarnick 1989. In addition, Monks et al. 1993 have considered some of the previous reactions in an oxygenated medium, and Hoobler and Leone 1997 have studied the reactions of C_2H with HCN or CH_3CN .

However, due to the lack of knowledge on the nitrile's reactivity, few studies propose other pathways than $CN + \text{hydrocarbon}$ to form heavy nitriles. And yet Recent CIRS observations compared the nitrile lifetimes at 300 km of altitude predicted by the photochemical model of Wilson and Atreya 2003 with the observed nitrile enrichment in the North polar latitudes of Titan. They have shown an unsuspected specific reactivity of nitriles on Titan (Teanby et al. 2010). Therefore, it is of high priority to study the underestimated reactivity of nitriles, which are known to be very efficient polymerization products in plasma physics (Yu et al. 1988; Lefohn et al. 1998; Bhat and Upadhyay 2003; Jampala et al. 2008).

Nitriles are rarely considered as reactive molecules. However, knowing how labile the hydrogen in alpha position of a nitrile molecule is (Carey and Sundberg 2007), it is reasonable to consider that they can be involved in the chemical pathways leading to the production of aerosols in Titan's atmosphere. The energy coming from the solar radiation and/or the Saturn magnetosphere electron bombardment or a chemical reaction with a sufficiently reactive radical could free the alpha hydrogen of a nitrile molecule, as shown in the following scheme. A much more reactive radical would result from these processes, and could play a role in Titan's complex atmospheric chemistry.



In addition, nitriles could also provide reactive species to form pre-biotic molecules at the surface of Titan or cometary dusts. Particularly, if tholins deposited on Titan's surface could get in contact with liquid water, a hydrolysis reaction would occur, leading to the formation of

amino compounds (Khare et al. 1986; Hudson and Moore 2004; Neish et al. 2010; Ramírez et al. 2010). This contact between tholins and liquid water would be possible since frozen water is abundant at Titan's surface (Tobie et al. 2005). One could expect ice melting from impacts (or cryovolcanism) which may lead to episodic presence of liquid water with a lifetime from 10^2 to 10^4 years (O'Brien et al. 2005).

III.3.3.d Nitrile quantification

a. Criteria of relative quantification

In my experiments, a direct quantification of compounds was not possible due to the fact that absolute intensities differed from a chromatogram to another (even for two experiments with the same methane concentration). A quantitative analysis in gas chromatography requires the addition of an internal or external standard in the solute, which was not possible with the configuration of the experimental system. However, by considering each experiment individually, a relative quantification of the nitrile concentrations can be done.

In order to look for possible growth mechanisms, the area of chromatographic peaks corresponding to nitrile compounds are measured. Only mono-nitriles with a saturated alkyl chain were studied for quantification. Dinitriles are excluded because of the two step process they require to be produced. Nitriles with unsaturated radicals are not taken into account either because their formation requires the addition of a CN radical on a pre-existing unsaturated molecule. For example, the formation of propiolonitrile (HC_3N), detected both in Titan's atmosphere and in my experiment, is formed by the addition of CN on acetylene (Seki et al. 1996). In this work I look for new patterns different from the usual CN + hydrocarbons pathway.

Five nitriles correspond to these criteria in my data: hydrogen cyanide (H-CN), acetonitrile ($\text{CH}_3\text{-CN}$), propanenitrile ($\text{CH}_3\text{-CH}_2\text{-CN}$), butanenitrile ($\text{CH}_3\text{-CH}_2\text{-CH}_2\text{-CN}$) and isobutyronitrile ($(\text{CH}_3)_2\text{CHCN}$).

The chromatographic peak areas of these species are plotted as a function of the number of carbon atoms present in the molecule. As both butanenitrile and isobutyronitrile contain four carbon atoms, their respective areas are added.

b. Calibration of the peak areas

As the samples were analyzed through a gas chromatograph coupled with a mass spectrometer, the data collected correspond to peak areas and not directly to the concentration of compounds. To infer the relative concentrations of the nitriles from their area I had to use the ionization cross section of nitriles.

The mass spectrometer ionizes the molecules by electron impact accelerated at 70eV. Unfortunately, at this energy, the nitrile ionization cross sections are still unknown. It is however possible to estimate these cross sections using the theoretical calculations developed by Fitch and Sauter 1983.

Using their semi-empirical formula the ionization cross section, Q ($\times 10^{-16}$ cm²), of a molecule can be calculated based on its atomic composition and on the available experimental ionization cross sections. This formula is given in Equation (13):

$$Q = 0.082 + \sum_{i=1}^8 \alpha_i n_i \quad (13)$$

where α_i is a coefficient which depends on the type of atom and n_i is the number of atoms for each element. The formula is valid for molecules containing H, C, N, O, F, Cl, Br and I. Coefficients for hydrogen, carbon and nitrogen are respectively 0.73×10^{-16} cm², 1.43×10^{-16} cm² and 1.20×10^{-16} cm².

Using equation (13) I calculated the ionization cross section for the five nitriles chosen for the study presented here. They are given in Table 7.

Table 7: Calculated ionization cross section of the nitriles. The calculation is performed using the formula proposed in Fitch and Sauter (1983)

Compounds	Formula	$Q \text{ (} \times 10^{-16} \text{ cm}^2 \text{)}$	$\frac{Q_{HCN}}{Q_{RCN}}$
Hydrogen Cyanide	HCN	3.442	1
Acetonitrile	C ₂ H ₃ N	6.332	0.544
Propanenitrile	C ₃ H ₅ N	9.222	0.373
Butanenitrile	C ₄ H ₇ N	12.112	0.284
Isobutyronitrile	C ₄ H ₇ N	12.112	0.284

The electron impact ionization cross sections have an influence on the area of the chromatographic peaks. As a first approximation we can consider that the area A of a species s , is directly dependent on the species concentration and on its cross section:

$$A_s \propto C_s Q_s \quad (14)$$

As I am looking for the relative concentrations, the peak area of a hydrocarbon i has to be multiplied by the factor corresponding to the ratio Q_{HCN}/Q_{RCN} . For example, as the cross section of butanenitrile is approximately four times higher than the one of hydrogen cyanide, the area of the butanenitrile peak has to be divided by four to be compared to the area of the hydrogen cyanide peak.

c. The nitrile concentration decrease law

After applying this cross section correction to the areas of the chosen nitrile peaks, the relative nitrile concentrations (HCN area normalized) as a function of the number of carbon atoms in the molecules were plotted.

Figure 37 shows the relative concentration of the five chosen nitriles seen in Table 7 after correcting their relative concentrations using their respective ionization cross sections.

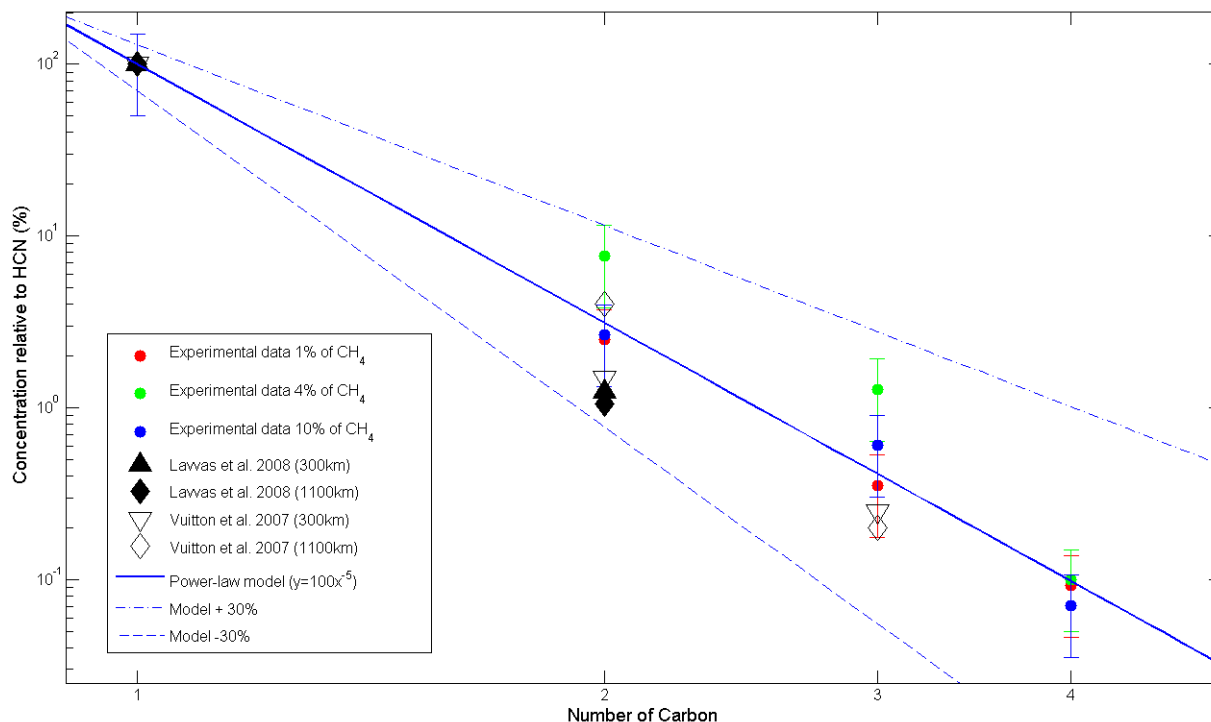


Figure 37: Relative concentration of the nitriles as a function of carbon in the molecules. The red, green and blue dots represent the experimental data from this work, for experiments with 1%, 4% and 10% of methane in the reactor, respectively. The blue line is the empirical power law model ($y=ax^b$) associated to these experimental data. The dot-dashed line represents the model value plus 30% ($a'=a+30\%$; $b'=b-30\%$) while the dashed line is the model value minus 30% ($a''=a-30\%$; $b''=b+30\%$). The empty black diamonds and triangles are observational data (Vuitton et al. 2007 and reference herein), at 1100 and 300km from Titan's ground, respectively. The full diamonds and triangles are data from computer modeling (Lavvas et al. 2008) at 1100 and 300 km from Titan's ground, respectively.

The first trend observed on this figure is the decrease of nitrile concentrations when the number of carbon inside the molecules increases. The shape of this decrease can be modeled with a mathematical power law. The empirical model linked to my data, plotted in Figure 37, is in good agreement with the experimental data within error bars. Those are estimated at up to 50%, including uncertainties on ionization cross-sections, GC-MS peak areas, reproducibility of the injection protocol in the GC-MS, the production process and trapping in the PAMPRE experiment.

This power-law decrease shows interdependence between the concentrations of the different nitriles, i.e. the concentration of a $C_xH_{2x-1}CN$ ($x \in \mathbb{N}^*$) nitrile is first order dependent on the concentration of the $C_{x-1}H_{2x-3}CN$ nitrile.

One can see in Figure 37 that there are no significant differences between the data sets, whatever the percentage of methane in the experiment. As a consequence a general power law can be extracted from all the experimental data. Equation (15) gives this power-law decrease when HCN is normalized to 100%:

$$[C_xH_{2x-1}N] = 100x^{-5} \quad (15)$$

x is the number of carbon atoms in a nitrile with saturated carbonaceous radical; ($x \in \mathbb{N}^*$). Equation (15) assumes that HCN is normalized to 100%. Using this power law model, it is then possible to estimate the concentration of heavy mono-nitriles with carbonaceous saturated radicals if the concentration of light nitriles is known. As shown in Figure 37, the experimental data and the associated power-law empirical model are also totally consistent with Titan's observational data from INMS (Vuitton et al. 2007) as well as with the results from photochemical models (Lavvas et al. 2008). Equation (15) can therefore determine the expected concentration of heavy nitriles, not yet detected, in Titan's atmosphere.

Dobrijevic and Dutour 2006 proposed a power-law equation to model the concentration decrease of molecules whose growth comes from the regular addition of a unique monomer. In the same way, we can consider that the power-law model I used is also linked to a polymerization scheme of the molecules.

In that case, to go from a $C_{x-1}H_{2x-1}CN$ nitrile to a $C_xH_{2x+1}CN$ nitrile, the required monomer would have to bring one carbon atom and two hydrogen atoms within a linear formula. The intuitive candidate is the methyl fragment, CH_3 , which could react with a pre-existing nitrile that lost a hydrogen atom.

Overall, my results highlight that nitriles are reactive compounds, in agreement with the recent CIRS observation by Teanby et al. 2010 and seem to be less inert than implemented in models, where they are mostly considered as chemical reaction sink (Lebonnois et al. 2001; Wilson and Atreya 2003; Hébrard et al. 2006; Lavvas et al. 2008).

III.3.4 Conclusion

A large amount of nitriles in the trapped gas mixture has been found, as high as four times the amount of hydrocarbons for a gas mixture with low methane concentration. The main product detected is hydrogen cyanide which has also been detected in large amounts in Titan's

atmosphere (Teanby et al. 2007; Vinatier et al. 2010). This detection by GC-MS is in agreement with the in-situ analysis of the gas phase presented in part 2 of this chapter. I have also detected heavier nitriles such as ethanenitrile, propanenitrile and propenenitrile. These heavier nitriles, also detected in Titan's atmosphere, are assumed to be the major compounds in the PAMPRE reactive medium. An increase in the ratio between nitriles and hydrocarbons with the decrease of methane concentration in the reactor is also observed.

The results of the PAMPRE experiment are consistent qualitatively with Titan's atmospheric composition, this tends to demonstrate that laboratory experiments, at least those allowing nitrogen dissociation, can be used complementarily to observational data in order to predict both the presence and possible concentrations of compounds which are not yet detected.

On a larger scale, I have detected more than thirty compounds, which, for some of them, had never been detected in experimental simulations before but were expected since they had been observed in Titan atmosphere. Heteroaromatic compounds have also been detected, supporting the hypothesis of PANH pathways for the growth of Titan's aerosols.

The results presented here show the possible importance of nitrogenous compounds in Titan's atmospheric chemistry. This study brings more clues to the previously proposed chemical route for aerosol formation in Titan's atmosphere which would predominantly use nitrogen-bearing compounds instead of PAHs (Vuitton et al. 2007; Pernot et al. 2010).

Unfortunately, the nitrile gas chemistry is still mostly unknown, and nitriles are often underrepresented in Titan atmospheric models even though we know, both from observations and from computational models, that they are present in large amounts on Titan (Teanby et al. 2007; Lavvas et al. 2008; Vuitton et al. 2009; Teanby et al. 2010; Vinatier et al. 2010).

In addition, in the study presented here, I have been able to relatively quantify some of the unsaturated mono-nitriles present in the gas phase. Using this relative quantification I proposed a power-law model for the concentration of radically saturated mono-nitriles, which is (with HCN normalized to 100%) $[C_xH_{2x-1}N] = 100x^{-5}$ where x is the number of carbon atoms in the molecule. With this law, it is possible to estimate the concentration of heavy nitriles due to chemical production (no transport and no loss) knowing the concentration of the lighter nitriles.

It will be important in the future to go further and study the possible role of nitriles in Titan's atmospheric chemistry. Indeed, this study suggests that these compounds could have a key role in the formation of organic aerosols in the high atmosphere of Titan, and more generally in the organic chemistry which takes place on Titan. These molecules including nitrogen are interesting in astrobiology as well since they are known for their reactivity and as precursor of amino acids.

III.4 Volatiles products in Bochum experiment: kinetics, products and quantification

As said in chapter II, the reactor in Bochum and the PAMPRE reactor can be complementary used. Even if some small differences in the reactors design induce small changes in the operating parameter, their similarity allows conducting complementary experiments.

Especially in this part I study the gas phase chemistry through in-situ mass spectrometry and FTIR. The MS results allow to study the kinetic of the gas phase chemistry whereas in this case FTIR is useful to identify unambiguously some products and provide an absolute quantification of the products.

III.4.1 Experimental parameters

Since the configuration of the reactor is slightly different from the PAMPRE reactor configuration, it is impossible to work in the exact same conditions. The main difference induced is that the nominal working pressure in the reactor of Bochum is of 0.1 mbar. By decreasing the pumping efficiency and increasing the gas flow it is possible to increase the total pressure in the reactor.

However, the pressure range is upper limited by the plasma ignition. In particular, to trigger on and maintain the plasma, the electrons free path should be long enough. Indeed the longer the time is between two collisions, the more electrons can be accelerated in the electric field, and thus acquire a kinetic energy high enough to ionize neutrals during the next collision. But increasing the pressure in the reactor decreases the electron free path length. In fact, with Bochum reactor configuration, it is impossible to maintain the plasma above 0.7 mbar in a N₂-CH₄ gas mixture. However, even at 0.7 mbar, plasma needs a quite high injected power (compared to the PAMPRE setup) of 50 - 60 W to maintain. All experiments presented in this part are thus performed at 0.6 mbar and 50 W.

In order to enhance the chemistry of the volatile phase and the production of dust, it is also necessary to increase the residence time of the gas in the reactor. To do so, in addition of decreasing the pumping efficiency, I also decreased the total gas flow in the reactor compared to PAMPRE. For the experiments presented here the total gas flow was of 15 sccm.

Since one of the goals of working with this experiment was the use of the powerful FTIR diagnosis available on it, I also optimized the gas composition in order to get the maximal signature of dust in infrared (see chapter IV). The gas mixture used for all experiments is therefore a mixture of N₂/CH₄ 90/10 which is the mixture where the dusts are the most visible with the FTIR on this setup.

III.4.2 Providing Carbon for tholins formation: the consumption of methane

When looking to the chemistry occurring in the reactor, before looking for kinetic effects, the first step is to look at the reactants and products of this chemistry.

The methane dissociated and ionized in the discharge provides the total amount of both carbon and hydrogen content in tholins. Looking to its consumption thus provides a clue on how much material is available for tholins formation. The estimation of methane consumption can be done using in-situ mass spectrometry in the MID mode.

Figure 38 presents the MID-MS of the methane peaks normalized to nitrogen peak (I_{15}/I_{28} and I_{16}/I_{28} ratios).

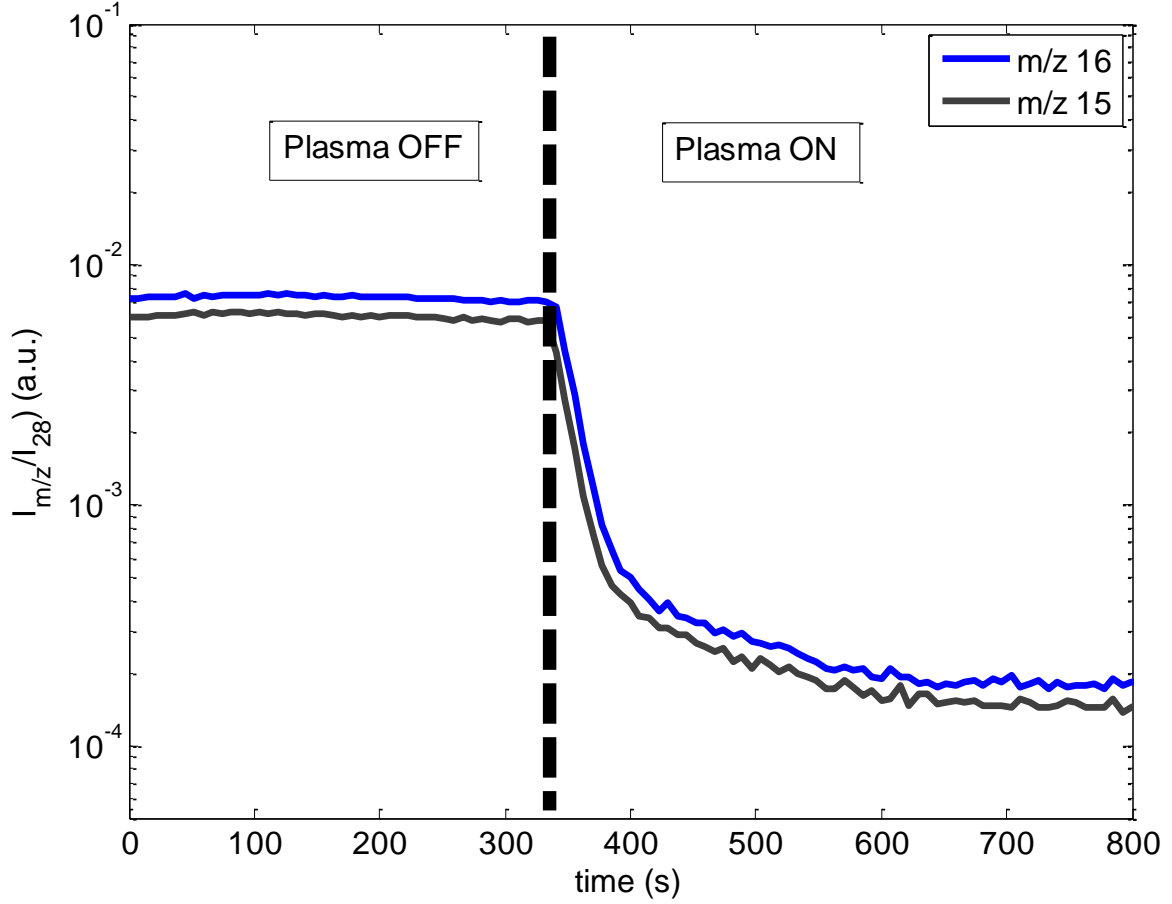


Figure 38: Methane (I_{15}/I_{28} and I_{16}/I_{28}) consumption when triggering on the plasma seen by MID MS. The dashed line is the instant time of plasma ignition.

The consumption of methane when triggering on the plasma is clearly visible in this figure. To quantify the consumption efficiency, e_{CH_4} , I used the same method as described in Sciamma-O'Brien et al. 2010:

$$e_{CH_4} = \frac{I_{0(CH_4)} - I_{ss(CH_4)}}{I_{0(CH_4)}} \quad (16)$$

Where $I_{0(CH_4)}$ is the initial intensity of the CH_4 peak before plasma ignition and $I_{ss(CH_4)}$ is the intensity when the steady state is reached when plasma is on. To avoid the influence of pressure in the MS on the signal intensities, all intensities are normalized relatively to m/z 28 (N_2) before calculation.

The methane consumption efficiency calculated for the Bochum reactor is around 96% (for both m/z 15 and m/z 16 peaks). At steady state, the concentration of methane is an equilibrium between incoming gas flux in the right hand and consumption of methane (both by

dissociation and ionization processes) and outgoing gas flux in the other hand. For comparison, the methane consumption efficiency in the PAMPRE reactor is about 50% for such gas mixture (Sciamma-O'Brien et al. 2010).

This difference may come from different factors. First, the injected power in Bochum experiments is higher than the 30W injected in PAMPRE. The total pressure in the reactor can also impact the electron density in the plasma (Alcouffe et al. 2010) and thus the dissociation of methane (proportional to n_e). Finally, the total gas flow in Bochum's reactor is much smaller (15 sccm) than in PAMPRE reactor (55 sccm). This means that the source term in the methane concentration equilibrium is much lower and thus cannot counterbalance the methane consumption by the discharge.

III.4.3 Kinetics

The temporal evolution of several species when plasma is triggered on is given in Figure 39.

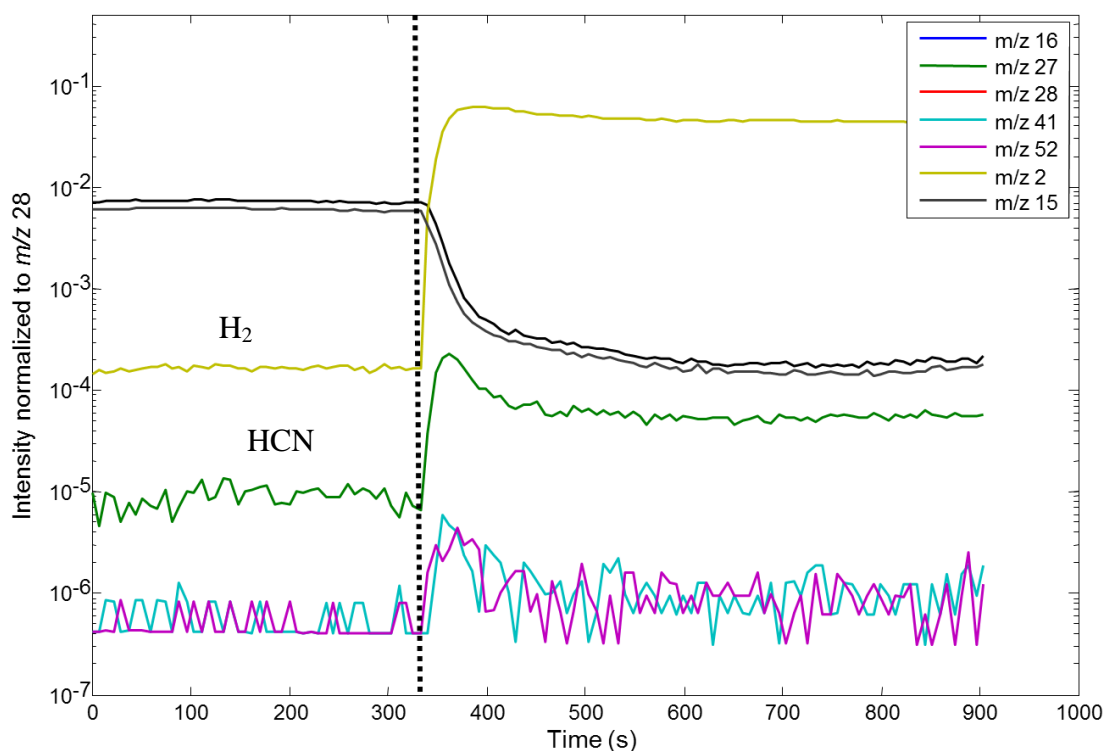


Figure 39: Time dependence of the MS signal normalized to m/Z 28 for different species. The vertical dashed line represent the instant when plasma is triggered on.

Blue and black curves represent methane (respectively at m/z 16 and 15) which is consumed when the plasma is on. Green and yellow curves represent the two main products observed

respectively HCN and H₂. Their concentration increases when plasma is initiated, then reach a maximum after a few tens of seconds before stabilization at a steady state value. The last two curves are for m/z 41 and 52 which represent the detection of heavier products.

The decrease of methane peaks follows an exponential law that can be fitted in order to get the characteristic time of this decrease. On first order the intensity of signal follows the law:

$$I = I_0 \times e^{-t/\tau} \quad (17)$$

Where I_0 is the original intensity and τ is the time constant of the decrease and is equal to the inverse of the exponent parameter obtained by fitting the curve. The exponential fit of the m/z 16 peak is given in Figure 40.

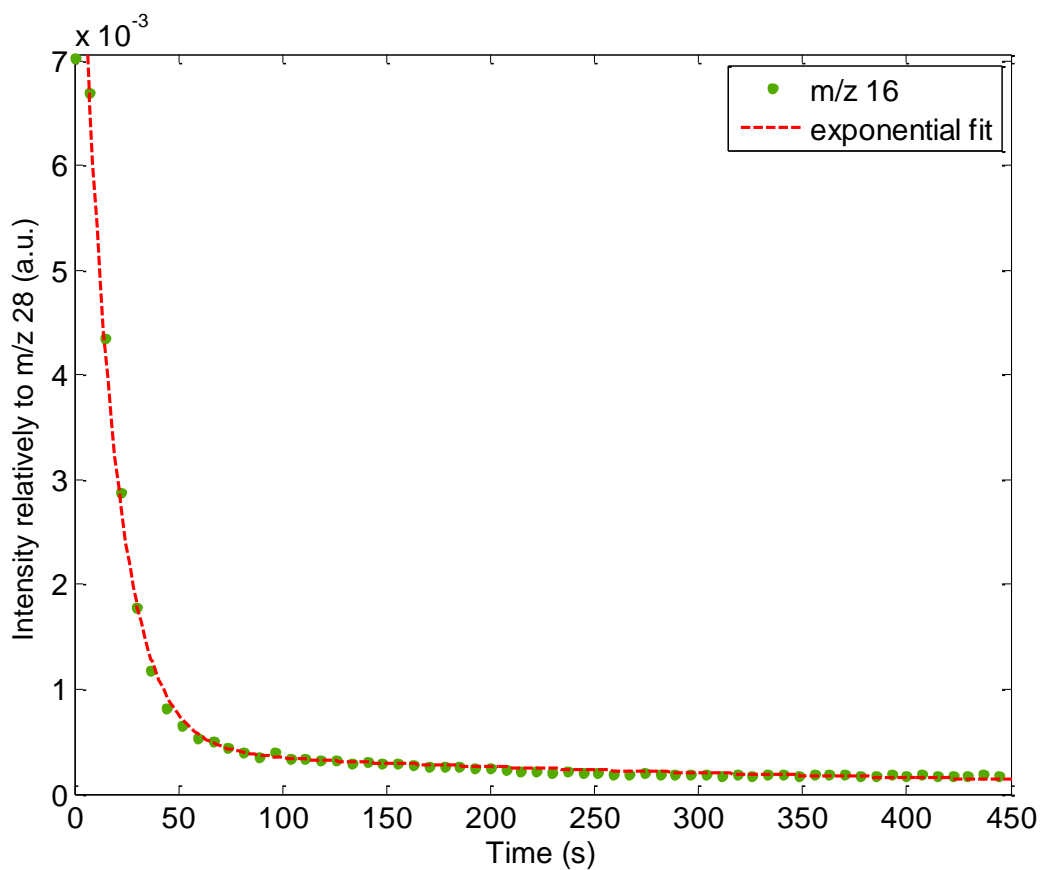


Figure 40: Measurement (green dots) and exponential fit (red dashed curve) of the decrease of methane peak when plasma is triggered on. Time is set to 0 for the plasma ignition.

The time constant found for methane consumption in this experiment is of 18 ± 3 s, which is the same order of magnitude as the time constant of methane consumption in PAMPRE which

is about 35s in a N_2/CH_4 plasma (Fleury et al. In preparation). This similarity was not expected and should be stressed out since the two setups are different as are the running parameters. This might mean that the methane consumption processes do not differ so much from an experiment to another. It also has to be noted that this decay is quite slow compared to processes usually induced by electronic collision (a few μs) and to residency time of the gas in the reactor (a few seconds), indicating that these processes may not be the only ones for the consumption of methane in the reactor. A possible process slowing down the methane consumption might be recombination on the walls and electrodes of the experiment

III.4.4 Identification by mass spectrometry

The first method I used for detecting products in the reactor is in-situ MS. Figure 41 presents the analog neutral mass spectrum of a N_2-CH_4 90-10 plasma in the Bochum reactor in the m/z [1-45] range. Above m/z 45, no products can be detected due to the low sensitivity of the spectrometer.

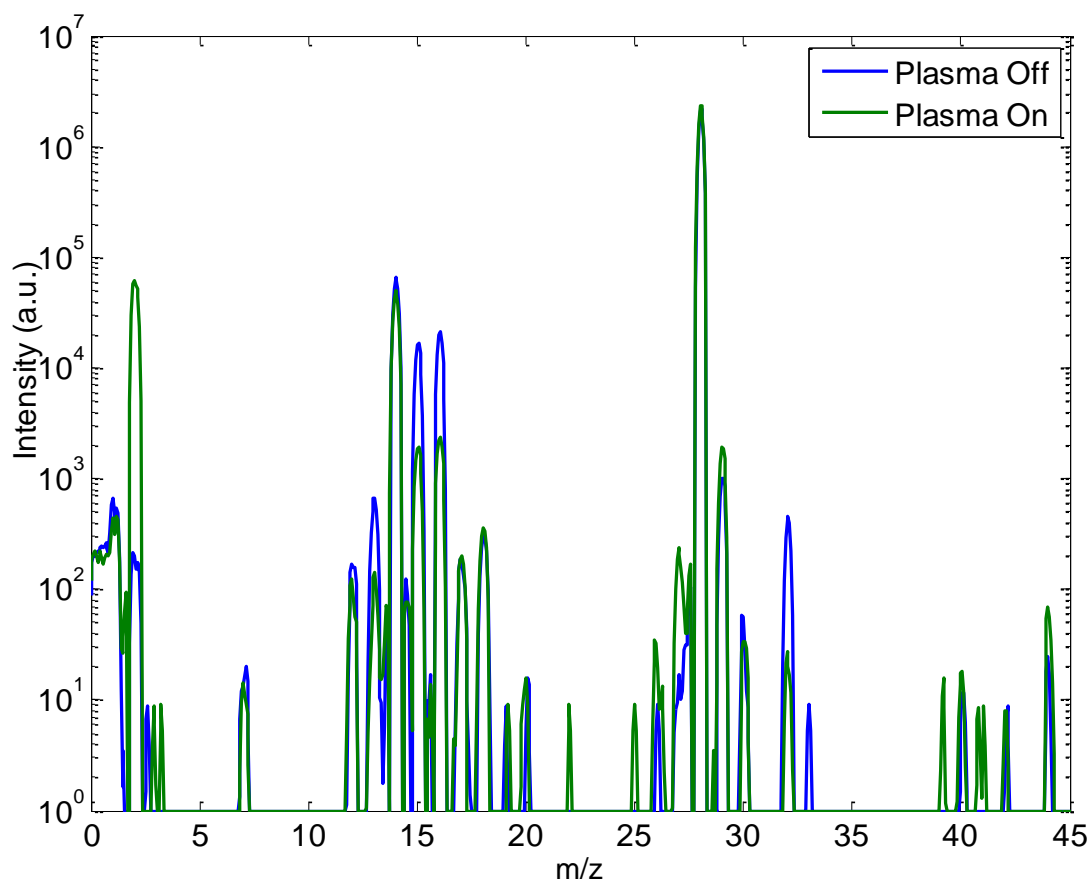


Figure 41: Neutral Mass spectrum of a N_2-CH_4 90-10 plasma in the Bochum reactor, plasma off (blue) and on (green)

With exception of the decrease of methane peaks (m/z 16, 15, 13, 12) and of the increase of some major peaks such as m/z 2 and 27 (H_2 and HCN) it is not obvious to detect other variations.

In order to enhance the visibility of the other products, as in part 2 of this chapter, I used the relative mass spectrum (i.e. spectrum plasma on divide by spectrum plasma off). To get proper spectra, it is better to calculate this relative mass spectrum on the bargraph (i.e. one peak at each m/z and not a continuum spectrum).

The bargraph intensity of a peak at a given m/z i is obtained by integrating the signal on the m/z range $[i-0.5; i+0.5]$.

The bargraph relative mass spectrum of the experiment presented in Figure 41 is given in Figure 42.

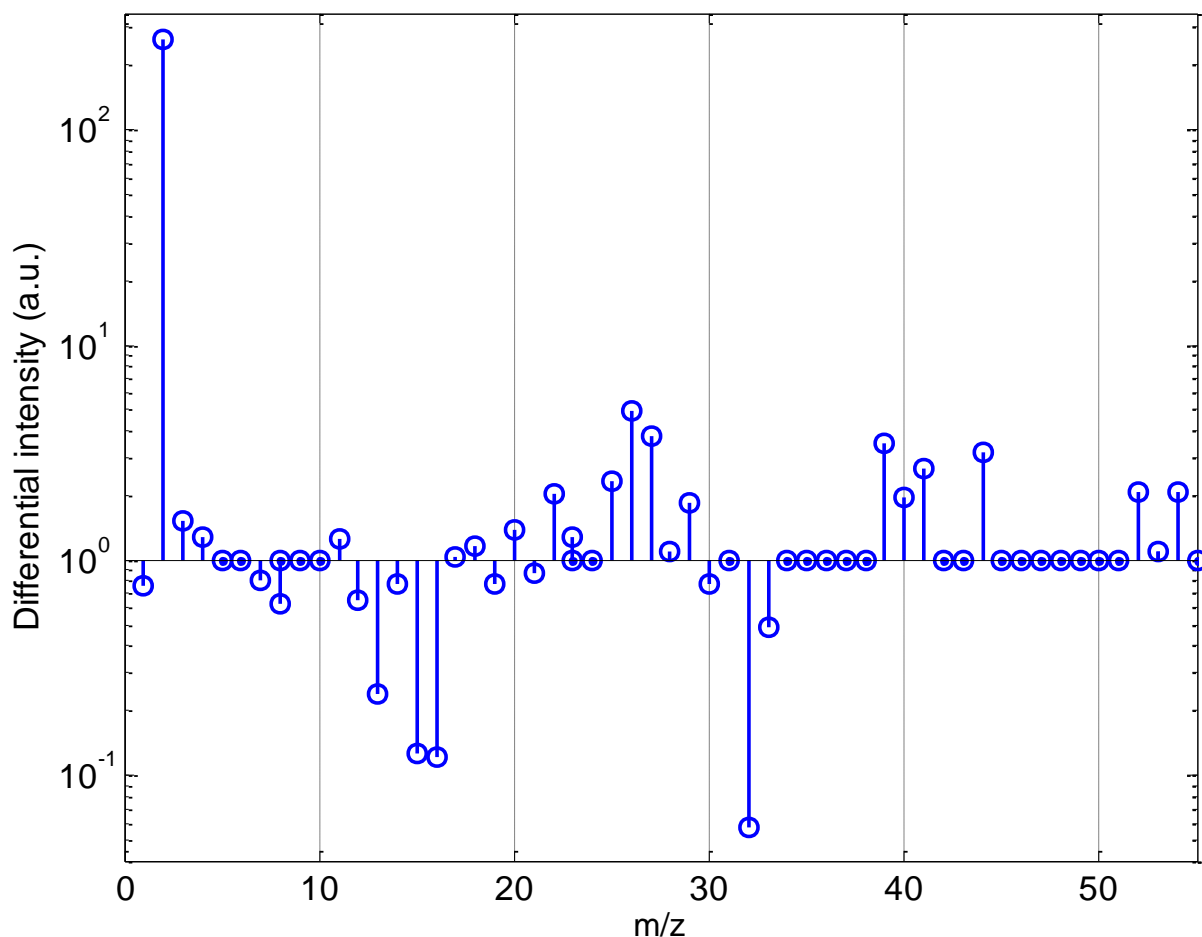


Figure 42: Bargraph relative mass spectrum (I/I_{blank}) of a 10% methane experiment

On this figure, the species consumed by the plasma ignition appear below the 10^0 line and the species produced during the experiment above. The main consumed species visible on this plot is methane at m/z 16 (CH_4^+), 15 (CH_3^+), 13 (CH^+) and 12 (C^+). The lower decrease of the peak at m/z 14 indicates that in opposition of the consumption of methane, another species with a peak at m/z 14 (or a double ionization of its peak at m/z 28) is produced.

The strong decrease of the peak m/z 32 comes from the highly effective dissociation of the residual oxygen in the experiment.

The main product visible in Figure 42 is at m/z 2. This peak corresponds to molecular hydrogen, H_2 , but also contains the contribution of atomic hydrogen recombined in the MS and the fragmentation pattern of all heavier hydrocarbon compounds produced.

Looking at the C2 pattern, main products are at m/z 27, 26, 25 and 29. The peak observed at m/z 22 is the results of the double ionization of the peak visible at m/z 44. These peaks cannot be unambiguously attributed but are certainly due to C2 hydrocarbon, nitrile or amine species (see Table 8 for tentative attribution). Main peaks in the C3 pattern are located at m/z 39, 40, 41 and 44 and C4 pattern presents peaks at m/z 52, 54 and a really slight peak at m/z 53. The list of peaks detected and their tentative attribution is summarized in Table 8 (NIST Mass Spec Data Center 2010a).

Table 8: List of the main peaks detected in the relative mass spectrum and their possible attribution. Possible attribution is not exhaustive but corresponds to the main products expected according to the analysis of the gas phase in PAMPRE both by MS and cryogenic trapping plus GC-MS.

m/z	Possible attribution	($I_{ss}-I_0$)/I_{28}
2	H_2^+	$2.6e^{-2}$
25	C_2H^+ (fragment of C_2H_2)	$3e^{-6}$ (upper limit)
26	$C_2H_2^+$, CN^+ (fragment of HCN)	$1.0e^{-5}$
27	HCN^+ , $C_2H_3^+$ (fragment of C_2H_4)	$9.7e^{-5}$
29	CH_2NH^+	$3.7e^{-4}$
39	$C_3H_3^+$ (fragment of C_3H_4), $HCCN^+$ (fragment of CH_3CN)	$6e^{-6}$
40	$C_3H_4^+$, $C_2H_2N^+$ (fragment of CH_3CN)	$3e^{-6}$
41	CH_3CN^+	$4e^{-6}$
44	$C_3H_8^+$	$1.9 e^{-5}$
52	$C_3H_2N^+$, $C_4H_4^+$	$3e^{-6}$ (upper limit)
53	$C_3H_3N^+$	$3e^{-6}$ (upper limit)
54	$C_4H_6^+$, $C_2H_2N_2^+$	$3e^{-6}$ (upper limit)

III.4.5 Identification by infrared spectroscopy

In order to unveil the ambiguity on species identification it is possible to use Fourier Transform Infrared Spectroscopy. Figure 43 presents the infrared transmittance spectrum of a plasma experiment with 10% of methane in nitrogen. This spectrum is the sum of 5000 spectra taken with a spectral resolution of 1 cm^{-1} in order to optimize the gas phase detection.

Since the reference spectrum is taken with the reactants gases in the reactor (plasma off), the species consumed by plasma ignition appear in negative (i.e. below the baseline around $A=0$) and species produced in the plasma in positive. The continuum of the spectra is not perfectly flat around $A=0$ but presents some broad bands around 1600 cm^{-1} , 2200 cm^{-1} and 3300 cm^{-1} . These bands do not come from the gas phase. Such broad bands cannot come from a gaseous compound, but are the infrared absorption signature of a solid phase. Actually from the cross comparison with tholins spectra (see Chapter IV), we can say that these three bands are the infrared signature of the dust in suspension in the plasma.

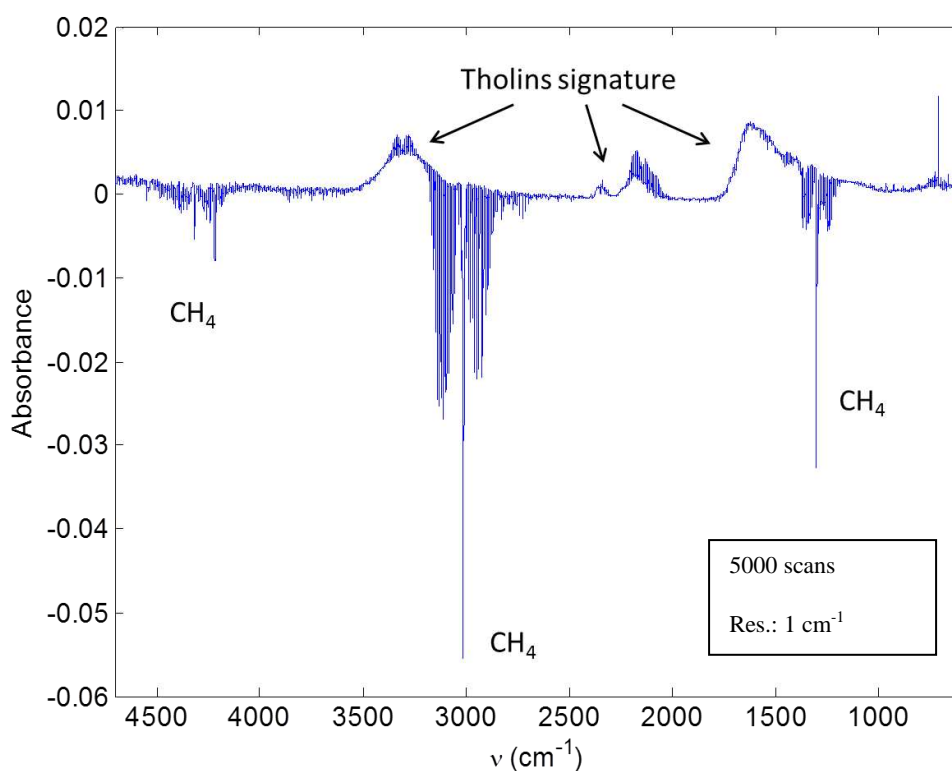


Figure 43: in-situ Infrared spectrum of a 90/10 N_2/CH_4 experiment. The reference spectrum is taken with gases in the reactor before plasma ignition. Species consumed appear in negative and products in positive compared to the $A=0$ line.

The only species consumed visible on this spectrum is methane (nitrogen does not have signature in the IR) with four main features at 1305 cm^{-1} , 2730 cm^{-1} , 3015 cm^{-1} and 4350 cm^{-1} (see Figure 44 for methane reference spectrum).

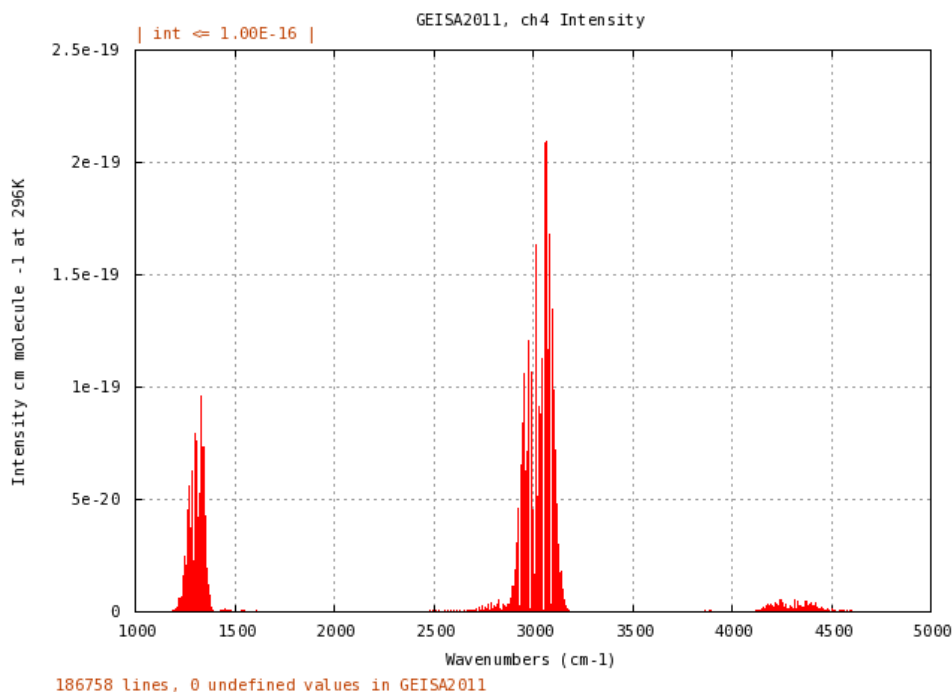


Figure 44: Reference spectrum of CH_4 in gas phase in the $1000\text{-}5000\text{ cm}^{-1}$ wavenumber range measured at room temperature (from the GEISA database)

Four products with a strong IR signature were identified using the NIST and GEISA databases (NIST Mass Spec Data Center 2010b; Jacquinet-Husson et al. 2011): Hydrogen Cyanide (HCN), Acetylene (C_2H_2), Propyne (C_3H_4) and Ammonia (NH_3). Figure 45, Figure 46 and Figure 47 present a close up of the spectrum in the area where these gases are detected.

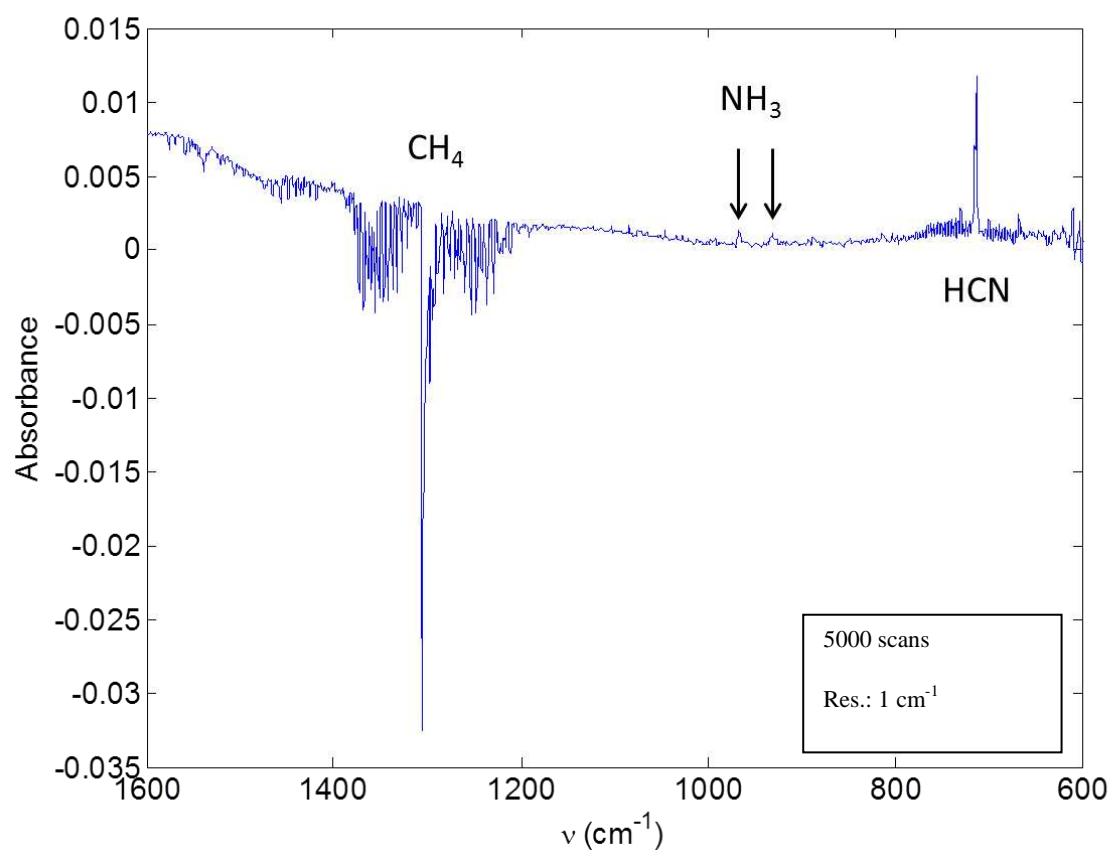


Figure 45: Close up of Fig.29 in the 600 - 1600 cm⁻¹ wavenumber range

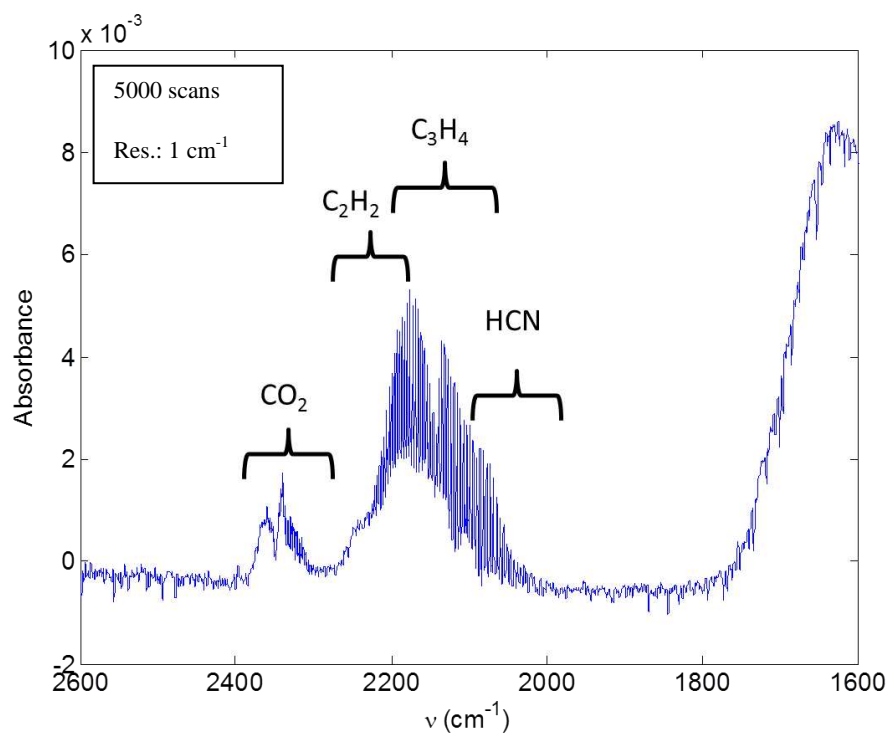
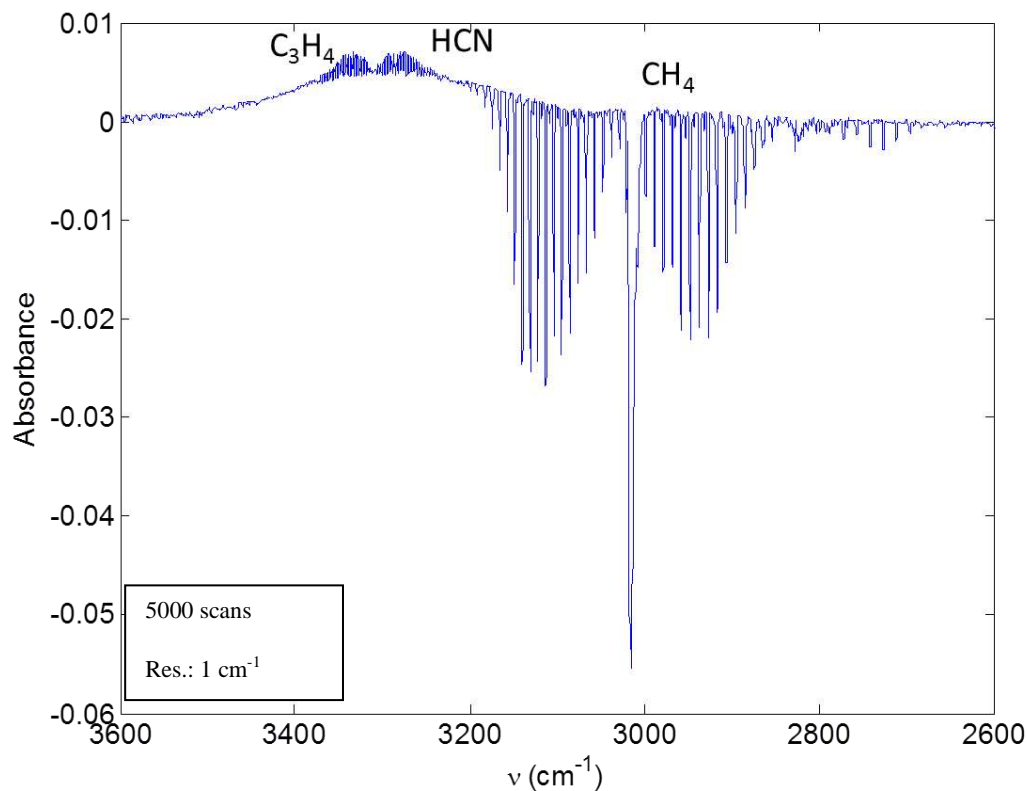


Figure 46: Close up of Fig.29 in the 1600 - 2600 cm^{-1} wavenumber range**Figure 47:** Close up of Fig.29 in the 2600 - 3600 cm^{-1} wavenumber range

As seen in Figure 45, HCN is detected totally unambiguously with its peak at 713 cm^{-1} . For Ammonia, even if the bands have weak intensities compared to the noise (S/N ratio ~ 3), the detection is robust thanks to the presence of the doublet at 930 cm^{-1} and 960 cm^{-1} which is characteristic of NH_3 and that appears in all 5000 spectra.

HCN is also visible in Figure 46 around 2150 cm^{-1} , but the bands is over imposed with bands of C_2H_2 and C_3H_4 . A small variation of the baseline at 2350 cm^{-1} is attributed to CO_2 . As said previously, the optical pathway of the IR beam is under the flow of dry purified air, but the absorption coefficient of CO_2 is so strong that even a small variation of the CO_2 concentration induces a detectable variation of the infrared spectrum.

The absorption band visible in Figure 47 around 3300 cm^{-1} is also mainly due to HCN absorption, with a minor contribution of propyne on the right wing of the pattern ($\sim 3380\text{ cm}^{-1}$).

III.4.6 Absolute quantification of HCN and NH_3

Since HCN and NH_3 have bands without over imposition of other species (respectively at 713 cm^{-1} and $930\text{-}960\text{ cm}^{-1}$) it is possible to estimate their concentration using the Beer-Lambert law:

$$I(\lambda) = I_0(\lambda) \times \exp(-\varepsilon(\lambda) \times l \times [C]) \quad (18)$$

Where $I(\lambda)$ is the intensity of the beam after passing through the gas, $I_0(\lambda)$ is the original intensity of the beam, l is the pass length of the beam through the gas, $[C]$ the concentration of absorbing molecules and $\varepsilon(\lambda)$ the absorption cross section of the molecule at a given wavelength.

Absorbance, A , is defined as:

$$A(\lambda) = -\ln\left(\frac{I(\lambda)}{I_0(\lambda)}\right) \quad (19)$$

So

$$A(\lambda) = \varepsilon(\lambda) \times l \times [C] \quad (20)$$

Knowing $\varepsilon(\lambda)$ it is then possible to calculate the concentration of a given gas:

$$[C] = \frac{A(\lambda)}{\varepsilon(\lambda) \times l} \quad (21)$$

The absorption cross sections I used for the calculation of the concentration of NH_3 and HCN comes from the GEISA database (Jacquinet-Husson et al. 2011). In order to overcome the resolution difference between laboratory data and the database, the calculation is performed on the peak area for both observed intensities and absorption cross sections. For HCN the integration is done in the $710\text{-}720\text{ cm}^{-1}$ range. For the two NH_3 bands, the integration are performed respectively in the $928\text{-}935\text{ cm}^{-1}$ and $963\text{-}970\text{ cm}^{-1}$ ranges.

Concentrations for HCN and NH_3 are summarized in Table 9.

Table 9: Calculation of absolute concentration for HCN and NH₃

	HCN	NH ₃	
ν (cm ⁻¹)	[710-720]	[928-935]	[963-970]
$\epsilon(\lambda)$; (cm ⁻¹)	$4.70 \pm 0.01 \times 10^{-18}$	$2.88 \pm 0.01 \times 10^{-18}$	$4.03 \pm 0.02 \times 10^{-18}$
A (sum of 5,000 spectra; a.u.)	$1.78 \pm 0.03 \times 10^{-1}$	$1.9 \pm 0.2 \times 10^{-2}$	$2.3 \pm 0.1 \times 10^{-2}$
[C] (molc.cm ⁻³)	$1.05 \pm 0.02 \times 10^{12}$	$1.8 \pm 0.2 \times 10^{11}$	$1.6 \pm 0.1 \times 10^{11}$
[C] ppmv	87.6 \pm 1.5	15.0 \pm 1.8	13.7 \pm 0.7

The calculation performed on the two bands of ammonia is consistent within their error bars and give an ammonia absolute concentration of about 14 ppm. Such concentration of NH₃ explains the high difficulty of detecting it through mass spectrometry.

The concentration of hydrogen cyanide measured by FTIR of about 88 ppm is in agreement with the in-situ mass spectrometry measurement (see Figure 41) where the intensity of the peak at m/z 27 (HCN) is four orders of magnitude below the peak at m/z 28 (see Table 8).

Once the concentration of HCN is known, we can use the law established for the relative concentrations of nitriles found in part 3 of this chapter (Gautier et al. 2011) in order to calculate the concentration of heavier nitriles.

In order to validate the law for the Bochum reactor, it was first checked on the CH₃CN measurement. The value measured by MS of 4 ppm for CH₃CN is in agreement with the 2.8 ppm found for CH₃CN when applying the law with HCN concentration measured by FTIR.

This justify the application of this law in order to estimate the concentration of CH₃CN and CH₃CH₂CN from the IR measurement of HCN concentration.

 Table 10: Measured (from FTIR) and inferred (from MS + calculation) concentrations of HCN, CH₃CN and CH₃CH₂CN

	HCN	CH ₃ CN	CH ₃ CH ₂ CN
MS value	72	4	Not detected
(I_{ss}-I₀)/I₂₈ (ppm)			
Concentration measured by FTIR (ppmv)	87.6	Not detected	Not detected
Concentration Calculated (ppmv)	87.6	2.8	0.4

Using this calculation method, we can estimate the absolute concentration of CH₃CN and CH₃CH₂CN to be about 2.8 ppm and 0.4 ppm respectively. Such a concentration of CH₃CN induces absorption for its strongest peak around 1400 cm⁻¹ of about 7 x10⁻⁴, slightly above the noise level . However this peak cannot be detected unambiguously since it is located in the wing of an intense methane band. The second strongest peak of acetonitrile is around 3000 cm⁻¹ but should have an intensity of 2 x10⁻⁴ in my spectrum, which is not sufficient to enhance clear detection.

It is also possible to estimate the gas-gas carbon conversion yield (Y_{HCN}) from methane toward the major gas product, hydrogen cyanide. CH₄ and HCN have both one carbon atom, HCN is detected at a concentration of 87.6 ppm, and methane (injected at 10% concentration) is dissociated at a rate R_d of 96%. The production yield of HCN can thus be expressed as:

$$Y_{HCN} = \frac{HCN}{[CH_4]_0 \times R_d} \quad (22)$$

$$Y_{HCN} = \frac{87.6 \text{ } e^{-6}}{0.1 \times 0.96} = 9.1 \text{ } e^{-4} \quad (23)$$

This conversion yield can be compared to the one obtained on the PAMPRE setup. Sciamma-O'Brien et al. 2010 estimated the carbon gas to solid conversion yield (Y_c) to be about 2.5% for a CH₄:N₂ 10:90 gas mixture at 0.9 mbar.

As a first order the gas-gas conversion yield for carbon can be estimated as $1-Y_C$ (the carbon produced from CH_4 dissociation is either integrated to the solid phase, either in gas compounds). More than 95% of the carbon is thus converted in gas (where HCN is the major product) in the PAMPRE reactor for such gas mixture.

The HCN production yield in Bochum is thus surprisingly low compared to the carbon gas to the one estimated in PAMPRE (at least a few tens of percent for HCN). This underlines the low amount of gas products in Bochum reactor in comparison with PAMPRE. The fate of carbon in Bochum reactor is still unknown since it is impossible to estimate the carbon gas to solid conversion yield in this experiment. A possible explanation could be that the carbon conversion from gas to solid is much more efficient in Bochum reactor, carbon being thus mainly incorporated in the dust. Another possible explanation is that at least a part of the carbon is not taken into account in the balance presented above. Especially this carbon could be present in gas species not quantified in my experiments such as C_2H_2 .

III.5 Conclusion

Results obtained on the Bochum experiment are useful for the study of the influence of the experimental setup on the tholins production. For the gas phase, it seems that even with different setups working at slightly different conditions, it is possible to get similar results.

While the FTIR sensibility in this setup also enables the absolute quantification of species, looking at the mass spectrometry measurement we can see that the species produced are similar and their kinetics is also on the same order of magnitude.

In a more general way, the studies presented in this chapter on the gas phase are of high importance for the understanding of the tholins formation processes. Comparison of these results with the actual chemistry occurring in Titan's atmosphere is also a strong bridge between experimental simulations and observations, and understanding tholins formation in laboratory will definitely help to understand aerosols formation on Titan.

The gas phase reactivity is the first key step toward tholins. By comparing results on two different setups, it appears that that different configuration does not influence drastically the resulting chemistry.

The second main aspect is the predominance of nitrogenous compounds (nitriles, amines or imines) within products detected. This tends to confirm the probable importance of such compounds for the formation of tholins, which is now a wide point of discussion in the literature.

Another striking point coming from the gas phase analysis is that all molecules detected are light species, below 150 Daltons. Of course, this can be due to experimental techniques (heavier compounds are also expected to have smaller concentrations, possibly below the limit of detection of the instruments), but if present, these compounds are clearly not among the main products in the gas phase. Analysis of the solid phase could therefore provide information on such molecules.

There is also one question that remains opened, with no specific answer in this thesis, and that should be kept in mind. It is to know if the molecules detected in the gas phase are the one used for the tholins growth, or if; on the contrary, the molecules visible in the gas phase after tholins formation are the ones not, or partially, used for the formation of solid.

Chapter IV Tholins: What are they made of? How does it influence their properties?

IV.1 Introduction

In chapter III of this thesis we have seen a bottom-up approach on the study of tholins formation, by first analyzing the gas phase chemistry leading to tholins. In this chapter I am going to use a top-bottom approach, by studying the composition and properties of tholins to infer their possible formation processes.

The samples analyzed in this part are tholins produced in the PAMPRE and Bochum reactors. The chemical composition of a residue produced in the cold trap plugged on PAMPRE (see chapter III.3) is also studied. This residue comes from polymerization of the gases trapped and its formation does not involve ionized chemistry. This residue might also be similar to a possible organic material formed on the surface of aerosols in the low atmosphere of Titan. Indeed, at low altitude, some reactive gases such as HCN or CH₃CN can condensate on the surface of aerosols. This could thus induce chemistry in the condensed phase at the surface of aerosols. Reasonably, we can make the assumption that this chemistry would lead to the formation of an organic material possibly similar to the residue I analyze here. A list of the samples analyzed and the analytical techniques used is given in Chapter II.

In the first part of this chapter I study the chemical composition of these materials using several analytical devices such as Gas-chromatography coupled to Mass spectrometry (GC-MS), Orbitrap high resolution mass spectrometry (O-HRMS) and Time of Flight (ToF) mass spectrometry. All these analyses provide information on the exact composition of tholins and on the molecules that compose them.

The second part of this chapter will be dedicated to the study of the optical properties of tholins in the infrared region. These properties are directly linked to the chemical composition of tholins and therefore provide some information on it. The infrared analyses are presented in

two parts, one is the study of tholins using ATR spectroscopy, the other one is a quantitative analysis of tholins absorption spectra in the mid- and far-infrared using Synchrotron radiation.

IV.2 Insight into tholins chemical composition

This part is focused on the chemical analysis of tholins using several analytical techniques based on mass spectrometry. Results presented in this part have been partially submitted for publication in Gautier et al. 2013a

IV.2.1 Time of Flight mass spectrometry: Global description of the sample

In order to get information on the whole polymeric structure of tholins, I analyzed it using Time of Flight mass spectrometry. This analytical technique has a wide dynamical range and allows relative quantification between peaks, which cannot be easily done with Orbitrap (Olsen et al. 2005; Scigelova and Makarov 2006).

Results

The spectrum obtained is given in Figure 48 and presents a polymer-kind shape organized in regularly spaced clusters separated by 13.5 amu. This 13.5 amu spacing has already been reported in previous study on tholins mass spectra (Pernot et al. 2010). This intercluster transition pattern corresponds to an average transition, which means that several transition patterns (such as for example CH₂, m/z 14 and HCN, m/z 27) can in fact be found in the material. The global distribution of the peaks can be fitted by a log-normal law, centered on 254 amu, with a width of 312 amu and asymmetric coefficient of 0.75.

CHAPTER IV – THOLINS: WHAT ARE THEY MADE OF? HOW DOES IT INFLUENCE THEIR PROPERTIES?

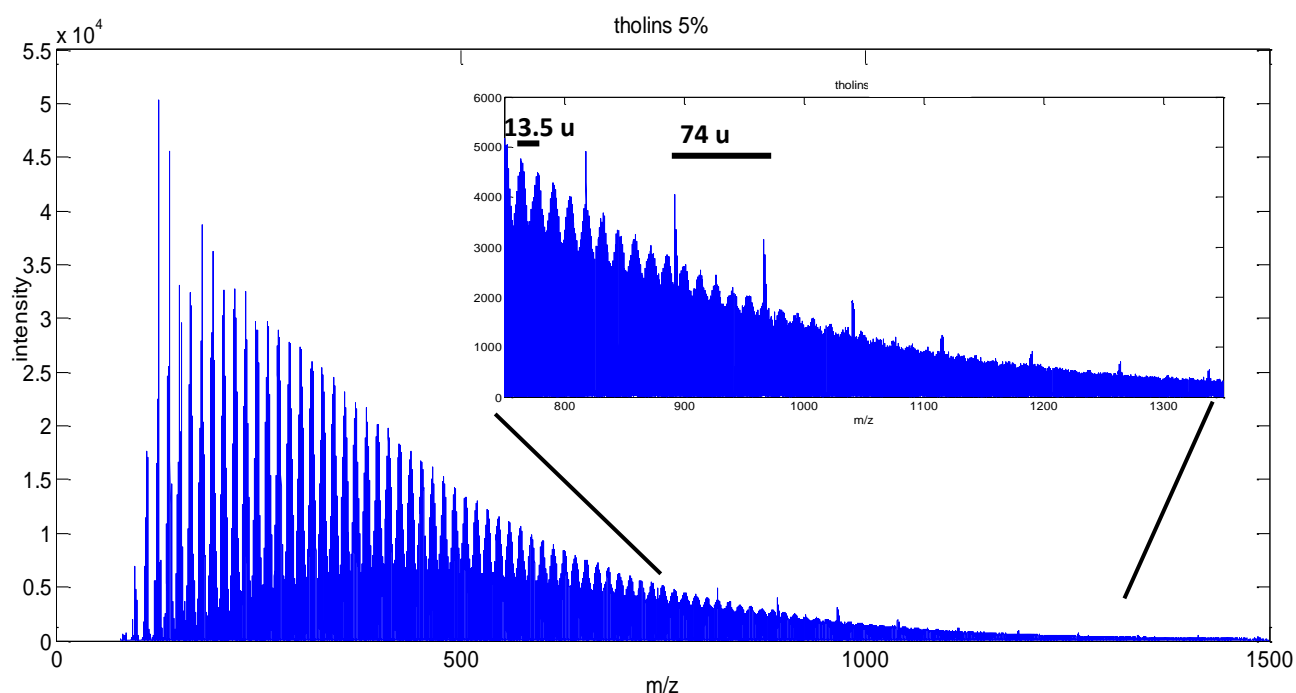


Figure 48: Tholins 5% mass spectrum acquired with LCT-Premier ESI-TOF mass spectrometer. Close up shows the inter-clusters spacing of 13.5u and 74u in the 750-1350 mass range

At masses higher than m/z 750 appears a second system of cluster spaced by a delta of m/z 74. Unfortunately, the mass resolution of the mass spectrometer is too low to resolve this pattern, which could be due for instance to aminoguanidine (m/z 74.0851, CH_6N_4), Ethanediamine,N-methyl (m/z 74.1249, $\text{C}_3\text{H}_{10}\text{N}_2$) or Propanediamine (m/z 74.1249, $\text{C}_3\text{H}_{10}\text{N}_2$), compound.

It is also visible on Figure 48 that the two major compounds in tholins 5% are respectively at m/z 127 and m/z 141. Thanks to cross comparison with Orbitrap spectra (see below), these peaks have been respectively attributed to melamine (127.0725, $\text{C}_3\text{H}_6\text{N}_6$) and Hexamethylenetetramine (HMT) (141.1133, $\text{C}_6\text{H}_{12}\text{N}_4$). This last compounds is in agreement with recent NMR studies that identified HMT as a major components in tholins produced in a different reactor (He et al. 2012a). HMT is also of high interest for astrobiology due to its polymerization properties and is suspected to be present in cometary ices thanks to laboratory experiments (Cottin et al. 2002; Vinogradoff et al. 2011).

IV.2.2 Orbitrap

In this part I present a further investigation on the chemical patterns in tholins molecular structure, investigated by high resolution mass spectrometry. The high complexity of materials such as tholins or organic matter in carbonaceous meteorites has been revealed by previous analyzes (Pernot et al. 2010; Callahan et al. 2011). This complexity enforces the need for a statistical approach to treat this kind of complex high resolution mass spectra.

The statistical approach is based on the methods proposed for tholinomics in Pernot et al. 2010. In this article, authors proposed an analytical method that allows decomposing the mass spectrum of tholins into several 'chemical families' according to their position in a three dimensions Van Krevelen diagram. They also proposed a possible reconstruction of tholins spectrum assuming a polymeric growth pattern based on two possible monomers. Following the same process, I investigate here several other possible growth patterns, compatible with the known chemistry occurring in Titan's atmosphere.

IV.2.2.a *Experimental set-up and protocol*

All the experiments performed for this work are performed with two N₂/CH₄ mixtures containing 1 and 5% of methane respectively. The pressure in the reactor is 0.90 ± 0.05 mbar and the gas temperature in the reactor is close to room temperature. Dust samples are accumulated during two hours in a glass vessel surrounding the reactive plasma and then collected into vials as presented in Figure 21. In this part I also propose a reanalysis of data acquired for a previous study Pernot et al. 2010 on tholins produced under the same experimental conditions with 2% and 10% of methane in nitrogen respectively.

a. Samples treatment for mass spectrometric analyzes

For mass spectrometric analyzes, tholins are first dissolved in methanol (HPLC grade, Baker) at a concentration of 1 mg.mL⁻¹, then mixed thoroughly and the resulting solution is filtered through a PTFE 0.2 μm membrane. The choice of methanol as the solvent is consistent with a previous study on tholins solubility (Carrasco et al. 2009).

Residue is also dissolved in methanol for analysis. It can be noticed that tholins are poorly soluble in methanol (~30% solubility) whereas the residue is totally soluble. This implies that

CHAPTER IV – THOLINS: WHAT ARE THEY MADE OF? HOW DOES IT INFLUENCE THEIR PROPERTIES?

a mass spectrum of the residue is more representative of the sample than a mass spectrum of tholins.

The samples are then infused in an Electrospray Ionization (ESI) Source in MeOH/Water (50/50 in volume) at a rate of $10 \mu\text{L}\cdot\text{min}^{-1}$. As a first approach for data treatment, I only considered the main ion sources, protonation (positive ion mode) and deprotonation (negative ion mode). In the positive ionization mode detected ions are $[\text{M}+\text{H}]^+$ species, with M the analyzed molecule. In the negative ionization mode, ions detected correspond to the deprotonated species, $[\text{M}-\text{H}]^-$.

All materials (e.g. bulk tholins and residue) are then analyzed using a high resolution LTQ-Orbitrap (Thermo Scientific) mass spectrometer equipped with an ESI source.

Acquisition parameters in positive ion mode are: needle voltage 4.5kV; capillary temperature 275°C ; capillary voltage 25V; tube lens voltage 65V; sheath gas flow rate 12. In negative ion mode, parameters are: capillary temperature 275°C ; capillary voltage -15V; tube lens voltage -45V; sheath gas flow rate 12.

The mass spectrometer is externally calibrated using caffeine, MRFA peptide and ultramark. Data are acquired between m/z 50 and m/z 800 and integrated on several hundred scans (usually between 350 and 400). Data are acquired with a resolution fixed at 100 000 for an ion at m/z 450. The experimental resolution $m/\Delta m$ is determined to be $\sim 200\,000$ at m/z 150. Data are processed using XCalibur 2.0 software and its peak attribution function. Attribution parameters are: maximum authorized deviation: 5 ppm to ensure possible attribution for species of low masses ($m/z < 120$); maximum carbon atoms number: 60; maximum nitrogen atoms number: 60; maximum hydrogen atoms number: 100; the last three parameters are set to be sure to possibly attribute all existing peaks in the sample. Nitrogen rule is used and charge was set to +1 (and -1 for analysis in negative ion mode). In order to take into account possible oxygen contamination (in the reactor due to residual gases after pumping or when sample is exposed to air), two oxygen atoms are also allowed in the peak attribution. Oxygen contamination is found to be negligible at first order, and all oxygenated peaks are removed from spectra before statistical analysis.

IV.2.2.b Results

a. Methane percentage influence on tholins mass spectra

Figure 49 presents the Orbitrap mass spectra of four different tholins samples produced with 1%, 2%, 5% and 10% of methane in the gas mixture. Two kinds of structures are visible on these spectra: first, intense and isolated peaks (mainly at $m/z < 150$); second, regularly spaced clusters generally obtained when analyzing a polymeric material.

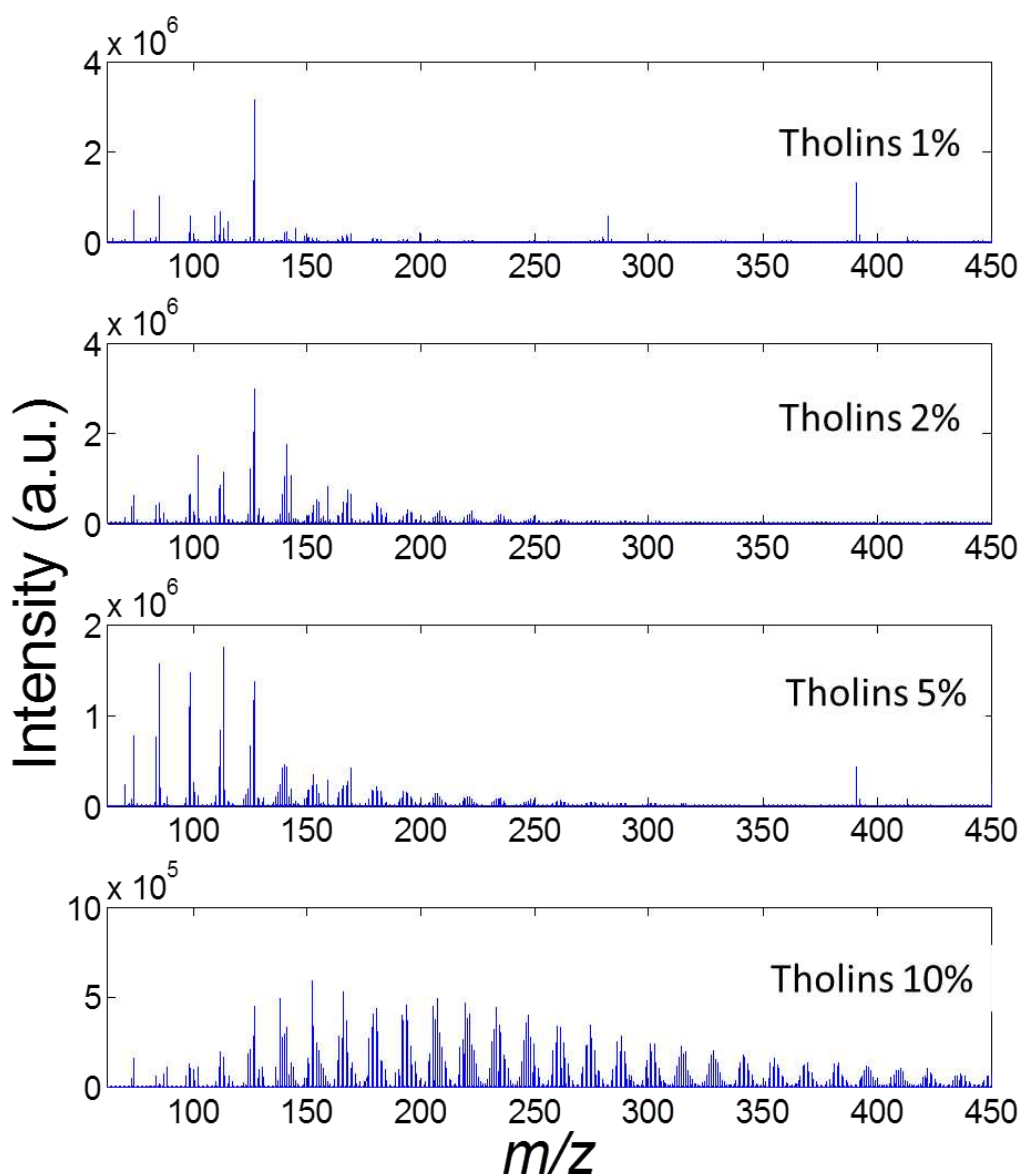


Figure 49: Orbitrap mass spectra in positive ion mode of tholins samples produced with 1%, 2%, 5% and 10% of methane. Spectra at 2% and 10% are adapted from Pernot et al. 2010.

The cluster structure is representative of almost all the material at high methane percentage, whereas the first structure is highly predominant in spectra of tholins produced with 1, 2 or 5 percent of methane, but it is minor in samples produced with 10 % of CH₄.

These light species are mainly located in the right wing of the Van Krevelen diagram (cf. Figure 51), which means compounds containing a large amount of nitrogen (N/C ratio higher than 1.5). These light but nitrogen-rich species are therefore less incorporated in samples produced at 10% of methane. The decrease of nitrogen content in tholins with increase of methane percentage, has also been observed on tholins at a global scale, by elemental analysis (Sciamma-O'Brien et al. 2010) and by infrared spectroscopy, studying the evolution of aliphatic carbon/amines bands ratio (see infrared analyses in this chapter and Gautier et al. 2012).

Figure 50 presents a close up of Figure 49 centered on the peaks detected around m/z 127. At this m/z value, two major ion peaks are detected at m/z 127.0725 ($\Delta m = -1.31$ ppm) and m/z 127.0977 ($\Delta m = -1.30$ ppm), respectively attributed to C₃H₆N₆ (possibly melamine) and C₅H₁₀N₄.

As shown in Figure 50, there is an inversion in the relative intensity of these two peaks when increasing the methane percentage. C₃H₆N₆ is more predominant for tholins produced with 1, 2 and 5 methane percentage whereas for 10% C₅H₁₀N₄ is the major compound. At an intermediate percentage (5%), both peaks have similar intensities. Here is given the case of peaks at m/z 127 but this phenomenon can be observed in all predominant clusters.

The chemical formula indicates that molecules which contain more nitrogen are predominant for low methane concentration tholins. This is consistent with the increase of global nitrogen content in tholins when methane percentage decreases as observed in the elemental analyses (Sciamma-O'Brien et al. 2010).

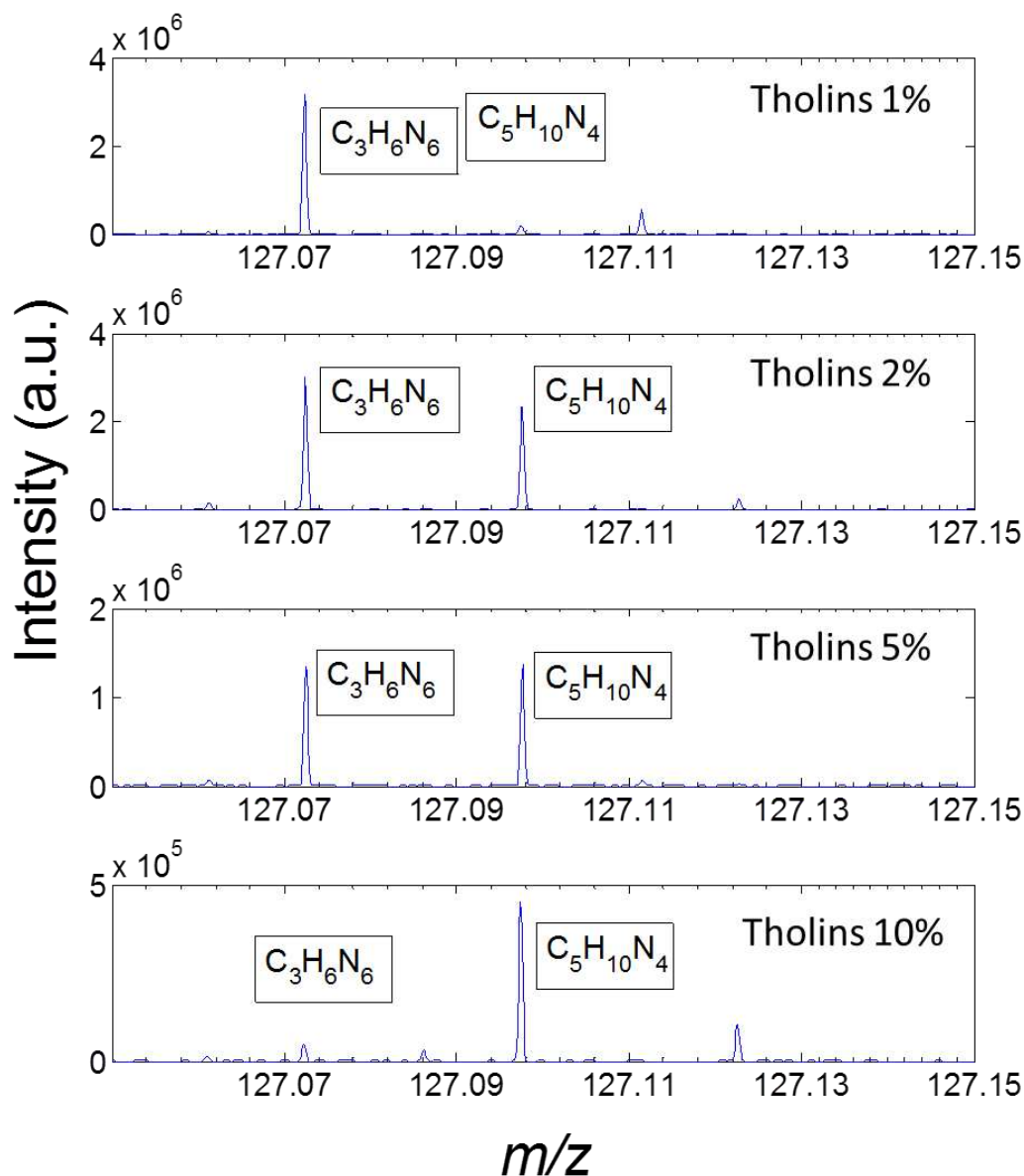


Figure 50: Close up of Fig. 5 on the peaks around m/z 127 for each tholins sample

In order to compare the samples, Van-Krevelen diagrams adapted for nitrogen bearing molecules (Imanaka and Smith 2007; Pernot et al. 2010; Somogyi et al. 2012) can be plotted. This diagram consists in scatter plotting the H/C ratio as a function of N/C ratio in the detected molecules, as shown in Figure 51.

In this figure, several phenomena are enlightened. First, a decrease of the number of nitrogen bearing species in tholins is observed when methane percentage increases. This is visible by the depletion of the right "wing" (i.e. $N/C > 1$) of the diagram when increasing the methane

percentage, correlated with an increase of the density of the detected compounds with low N/C and H/C ratios ($N/C < 0.5$ and $H/C < 2$). The latter may be linked to an increase of unsaturated hydrocarbons content in tholins, observed recently by NMR on tholins (Derenne et al. 2012). Finally, one can see a convergence of the several branches (alignments of points in the VK diagram) toward convergence points at some specific values: one is located at $H/C=1.5$ and $N/C=0.5$ and the other at $H/C=1$ and $N/C=1$. These ratios correspond respectively to a $(CN_{0.5}H_{1.5})_n$ and $(CNH)_n$ average composition. Convergence points at $H/C=1$ and $N/C=1$, $H/C=1.5$ and $N/C=0.5$ and $H/C=0.5$ and $N/C=0.5$ were also found in studies performed on tholins produced in other plasma experiments (Imanaka and Smith 2010; Somogyi et al. 2012). It might then be possible that this kind of convergence occurs in Titan's aerosols.

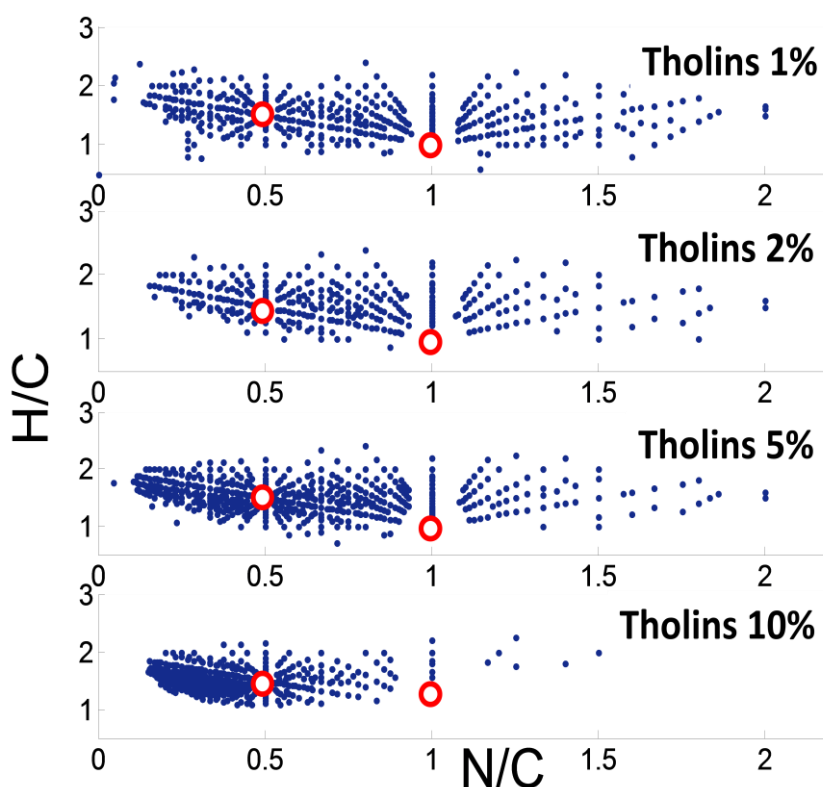


Figure 51: Van Krevelen representation of tholins 1%, tholins 2%, tholins 5% and tholins 10% samples. Convergence areas are emphasized by red circles.

This convergence towards one point is clearly visible if we represent samples in a 3D Van-Krevelen diagram (Pernot et al. 2010). The third dimension introduced is the logarithm of m/z

of each ion peak. Such a 3D diagram is given in Figure 52 for tholins produced with 5% of methane.

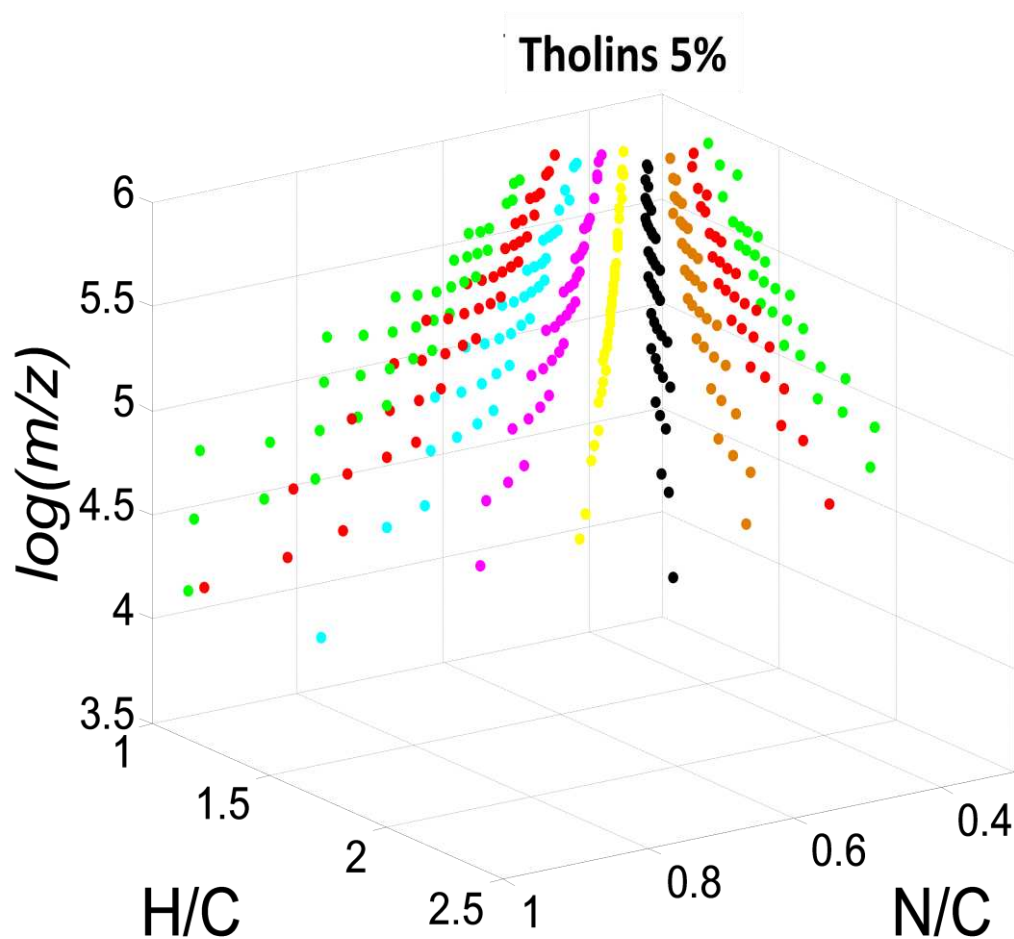


Figure 52: 3D Van Krevelen diagram of tholins 5%. Colors represent families identified within the HCN/CH₂ monomers basis (cf. part 5)

From Figure 52, it is clear that the convergence occurs for high mass ions. This would mean that after enough polymerization steps, the material composition tends toward average ratios of H/C=1.5 and N/C=0.5, i.e. an ideal co-polymer with a mean formula of (C₂H₃N)_n. Since residue presents similar Van Krevelen diagram than tholins (molecules detected are similar, see part c.), the 3D Van Krevelen diagram of residue also presents this convergence at high masses toward H/C=1.5 and N/C=0.5 point.

b. Comparison of tholins mass spectra obtained in the positive and negative ionization modes

Recent work on tholins chemical analyzes showed the interest of using the negative ionization mode for tholins characterization by mass spectrometry (Somogyi et al. 2012). The comparison between positive and negative ionization modes of tholins produced in PAMPRE with 5% of methane is given in Figure 53. The negative mode produces less chemical species than the positive mode. However the number of species detected is not negligible.

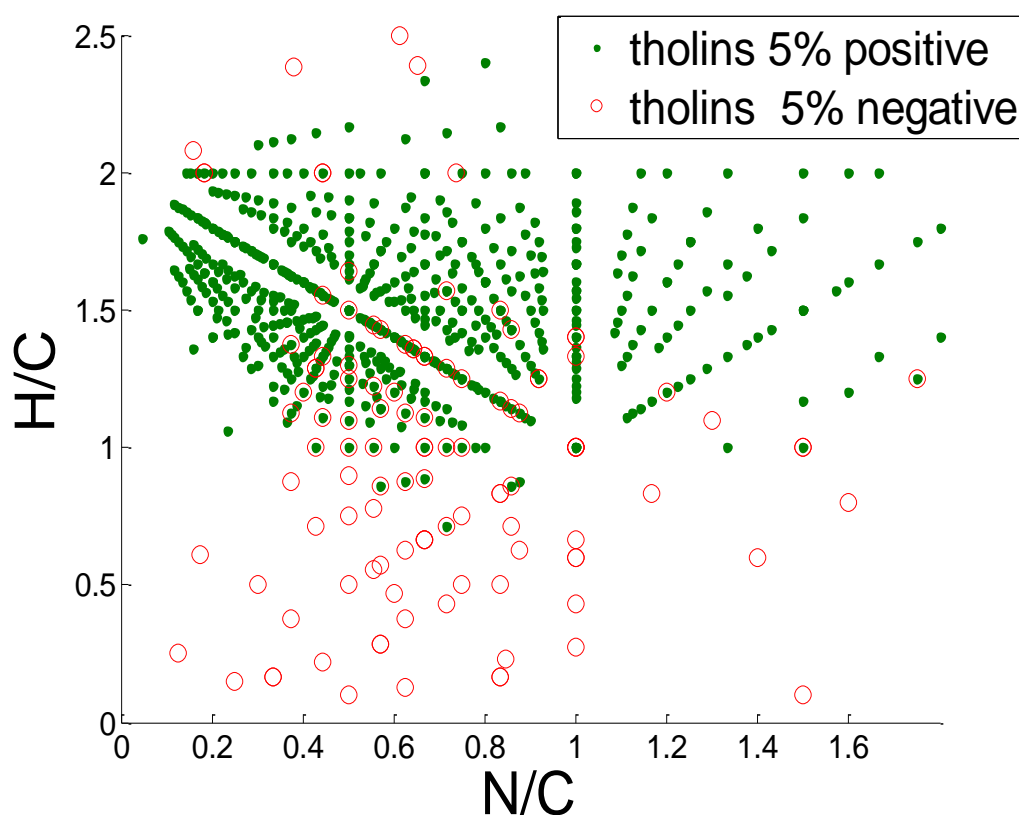


Figure 53: Van Krevelen diagram of tholins 5% analyzed in positive (green dots) and negative (red dots) ionization modes.

The molecules detected in the negative ion mode are not the same as the molecules detected in the positive ion mode, and generally present a lower H/C ratio. This clearly illustrates the utility of both measurements. Indeed, positive ionization seems to emphasize the detection of hydrogen rich nitrogenous compounds such as amines, whereas negative ionization mode allows detecting compounds, possibly nitriles or cyclic compounds, poorer in hydrogen. Both amines and nitriles functions have been detected unambiguously in tholins by infrared

spectroscopy (Imanaka et al. 2004; Quirico et al. 2008; Gautier et al. 2012). The detection of fewer compounds in the negative ion mode may be connected with the infrared analyses where amines bands are much more predominant in tholins spectrum than nitriles bands. This is consistent with an important amine contents in tholins.

c. Comparison of the composition of tholins versus residue

The mass spectrum of the residue 5% is shown in Figure 54 with the spectrum of tholins 5% as a reference point. Figure 55 presents a close up of Figure 54. As revealed by Figure 54, both spectra are relatively similar, with a little bit more intense peaks at low m/z values for the residue. But looking at Figure 55 it is clear that the distribution of peaks inside clusters is totally different between the two materials. The distribution of peaks in a cluster is systematically shifted toward low masses for the residue compared with tholins. This observation is enlightened in Figure 55 for the m/z 120-130 range, but it is observed for the entire spectrum.

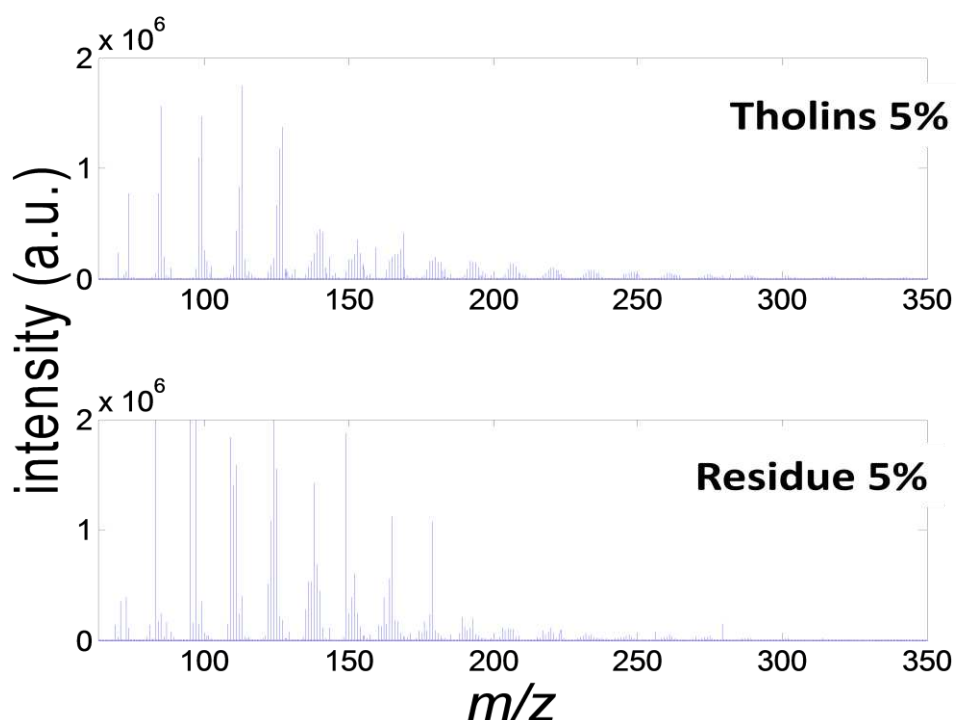


Figure 54: Orbitrap mass spectra of tholins 5% (up) and residue 5% (down)

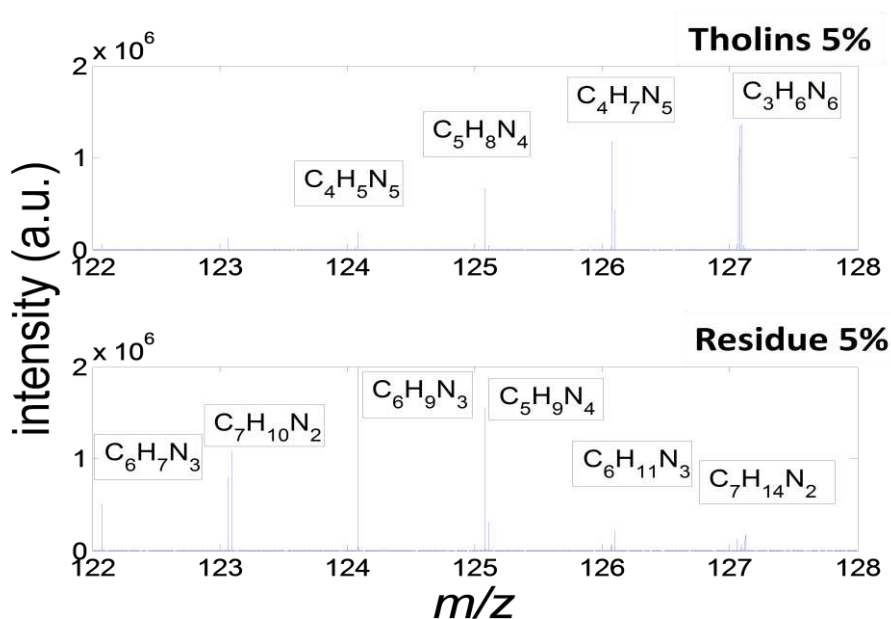


Figure 55: Close up of Figure 54 on the 120-130 m/z range. Textbox indicate formula attribution for the predominant present in the detected clusters.

It must be noted that all the peaks observed in tholins are systematically present in the residue too. This means that Van Krevelen diagrams are exactly the same for residue and tholins since this representation does not include information on the peak intensities. However, the dominant peaks in tholins are not the dominant ones in the residue. Indeed, the shift of peaks toward low masses (in the same cluster) observed in the residue (see Figure 55) seems to be due to a larger incorporation of carbon compared to nitrogen in the residue. This means that the ion chemistry plays a more important role in the formation of tholins, whereas the chemistry generating the residue seems to mainly induce polymerization of carbon rich molecules. It can also be noticed that a heterogeneous chemistry probably occurs in the two formation processes. In the PAMPRE reactor, this chemistry could occur on the surface of tholins growing in the gas phase (solid-gas process), whereas in the cold trap, the residue is formed during the melting of condensed icy species, potentially leading to a solid (residue)-liquid chemical process.

IV.2.2.c Discussion

I briefly remind here the main steps for chemical families identification (Pernot et al. 2010). All detected molecules C_xH_yN_z can be represented in a hypothetical basic base formed of two

CHAPTER IV – THOLINS: WHAT ARE THEY MADE OF? HOW DOES IT INFLUENCE THEIR
PROPERTIES?

molecules, for example CH_2 and HCN . Then, each molecule detected in the mass spectrum can be defined as $\text{C}_\alpha\text{-(CH}_2\text{)}_m\text{-(HCN)}_n$ where:

- n is the number of N atoms, systematically attributed to HCN units;
- $m = (\text{H}-\text{N})/2$ considering that all H atoms but in $(\text{HCN})_n$ belongs to CH_2 . H and N are respectively the number of Hydrogen atoms and Nitrogen atoms detected in a molecule
- α is the number of carbon atoms completing the pure copolymer, thus $\alpha = \text{C} - (\text{H} + \text{N})/2$. It is used to discriminate between families of compounds

The formulae for n , m and α depend on the base chosen for the representation. Here I test several alternative bases to determine which one provides the best representation of the material. Two bases, HCN/CH_2 and $\text{HC}_3\text{N}/\text{C}_2\text{H}_2$ are used to validate the process proposed in Pernot et al. 2010. I also studied the following bases: $\text{HCN}/\text{C}_2\text{H}_2$; $\text{HCN}/\text{C}_2\text{H}_4$; $\text{HCN}/\text{C}_2\text{H}_6$; $\text{CH}_3\text{CN}/\text{CH}_2$; $\text{CH}_3\text{CN}/\text{C}_2\text{H}_2$; $\text{CH}_3\text{CN}/\text{C}_2\text{H}_4$; $\text{CH}_3\text{CN}/\text{C}_2\text{H}_6$; $\text{CH}_2\text{NH}/\text{CH}_2$; $\text{CH}_2\text{NH}/\text{C}_2\text{H}_2$ and $\text{NH}_3/\text{C}_2\text{H}_4$.

The distribution of the families, i.e. the number of families used to describe the whole material and the global intensity of the family (equal to the normalized sum of all peaks belonging to the family) is studied for each base. An example of the distribution for three different bases ($\text{HC}_3\text{N}/\text{C}_2\text{H}_2$; $\text{HCN}/\text{C}_2\text{H}_2$; $\text{CH}_3\text{CN}/\text{C}_2\text{H}_4$) is given in Table 11.

CHAPTER IV – THOLINS: WHAT ARE THEY MADE OF? HOW DOES IT INFLUENCE THEIR
PROPERTIES?

Table 11: Family representation for different bases

Base	m	α	Nber family	Distrib. maximum	Graphic Representation
$(\text{HC}_3\text{N})_n$ $(\text{C}_2\text{H}_2)_m$	$(\text{H}-\text{N})/2$	$\text{C}-\text{H}-2\text{N}$	26	-13	
$(\text{HCN})_n$ $(\text{C}_2\text{H}_2)_m$	$(\text{H}-\text{N})/2$	$\text{C}-(\text{N}+\text{H})/2$	16	-5	
$(\text{CH}_3\text{CN})_n$ $(\text{C}_2\text{H}_4)_m$	$(\text{H}-3\text{N})/4$	$\text{C}-(\text{H}+\text{N})/2$	8	-1	

The whole set of distributions represented by blue dots is summarized in Table 12. The size of the dot is proportional to the number of families used to describe the polymer, and the color of the dot is linked to the position of the distribution relatively to the $\alpha=0$ family.

CHAPTER IV – THOLINS: WHAT ARE THEY MADE OF? HOW DOES IT INFLUENCE THEIR
PROPERTIES?

Table 12: Schematic representation of bases. The radii of the dots represent the size of the distribution (i.e. number of families needed to describe the polymer). The colors of the dots are linked to the eccentricity of the distribution: the darkest dots are, the most centered on 0 the distribution is.

N-bearing species	HC ₃ N	HCN	CH ₃ CN	CH ₂ NH	NH ₃
Hydrocarbons					
C ₂ H ₂					
C ₂ H ₄					
C ₂ H ₆					
CH ₂					

In a general way, we can consider that the narrowest (corresponding to the minimum of statistical entropy) the distribution is; the best it represents the sample, in the sense that it provides the most parsimonious description of the sample. For two distributions of the same width, the one the most centered on $\alpha=0$ (i.e. which requires the less carbon compensation) is considered as the best.

Different effects are noticeable in Table 12. For the hydrocarbons patterns, it seems that CH₂ and C₂H₄ present systematically better polymer reconstruction than C₂H₂ and C₂H₆ when used with nitriles as nitrogenous compounds. This could mean that hydrocarbon needed for tholins initiation should not be highly unsaturated. According to the fact that C₂H₄ has been actually detected in Titan's atmosphere, and that it is a stable neutral species, it is probably a more accurate candidate pattern for the polymerization than CH₂.

On the choice of the nitrogen bearing pattern, nitriles, and especially CH₃CN and HCN seem more accurate than ammonia, which is a better polymeric base than imines. Looking at distributions, and considering stable neutral species, the best possible bases are HCN/C₂H₄ and CH₃CN/C₂H₄. This is fully in agreement with the main chemical species identified in the atmosphere of Titan. Although it was not considered as an exclusion criteria, it is interesting

to remind here that the convergence point observed in the Van Krevelen diagram corresponds to a C:H:N ratio of 1:1.5:0.5, which is also the ratio found considering $2 \text{ HCN} + \text{C}_2\text{H}_4$.

IV.2.2.d Conclusion

In addition to tholins analyses, a residue of neutral gases polymerization was also analyzed. This provided some information on the reactive pathways to tholins formation, emphasizing minor differences between a material produced by polymerization of neutral gases (residue) and a material (tholins) produced in the reactive plasma by processes including ionized and/or heterogeneous chemistry. The predominant molecules detected in tholins contain more nitrogen than the one detected in residue. We can assume that the main difference between both materials is the ion chemistry, involved in tholins formation but not in residue formation. This could mean that this ion chemistry enforces nitrogen incorporation into tholins, compared to neutral chemistry that leads to molecules with lower N/C ratio.

Tholins spectra display polymeric structures which are confirmed by the identification of several polymer families in the material. This enhances the fact that tholins are co-polymer like materials, probably not linear co-polymer but hyper branched co-polymer (Klee 2005). Nevertheless, at high masses ($m/z > 300$), material can be assimilated to an average ideal $(\text{CH}_{1.5}\text{N}_{0.5})_n$ polymer as shown by the convergence of all the polymer families.

A further step for tholinomics would be to extend the statistical analysis presented here at masses higher than m/z 500 to study the convergence point of the families.

IV.2.3 Analysis of the residue by GC-MS

Even if the orbitrap provides a deep insight in tholins and residue compositions, it gives the m/z ratio of the molecules detected, but not their structure. Indeed for each $\text{C}_x\text{H}_y\text{N}_z$ formula, there are several possible isomers, each of them having different chemical properties. In order to unveil the ambiguity on the m/z ratio, it is possible to use chromatographic techniques. This has been done analyzing the residue with Gas Chromatography Coupled to Mass spectrometry and is presented in this part.

IV.2.3.a Direct analysis

GC-MS allows a first analysis of the residue. The residue analyzed here was produced with 4% of methane in the reactor. The simplest analysis possible using GC-MS on solid material is dissolving it and then injecting it into the chromatographer. For this analysis, the samples were dissolved in dichloromethane (Cl_2CH_2). The method used for these analyses are given in part II.2.1 of this thesis.

The chromatograms obtained are given in Figure 56 and Figure 57 with the peaks identified. As seen in these figures, many peaks in the chromatograms cannot be identified. This is mainly due to the nature of compounds present in tholins-kind (both tholins and residue) materials (mainly nitriles here), which are underrepresented in the databases available for product identification.

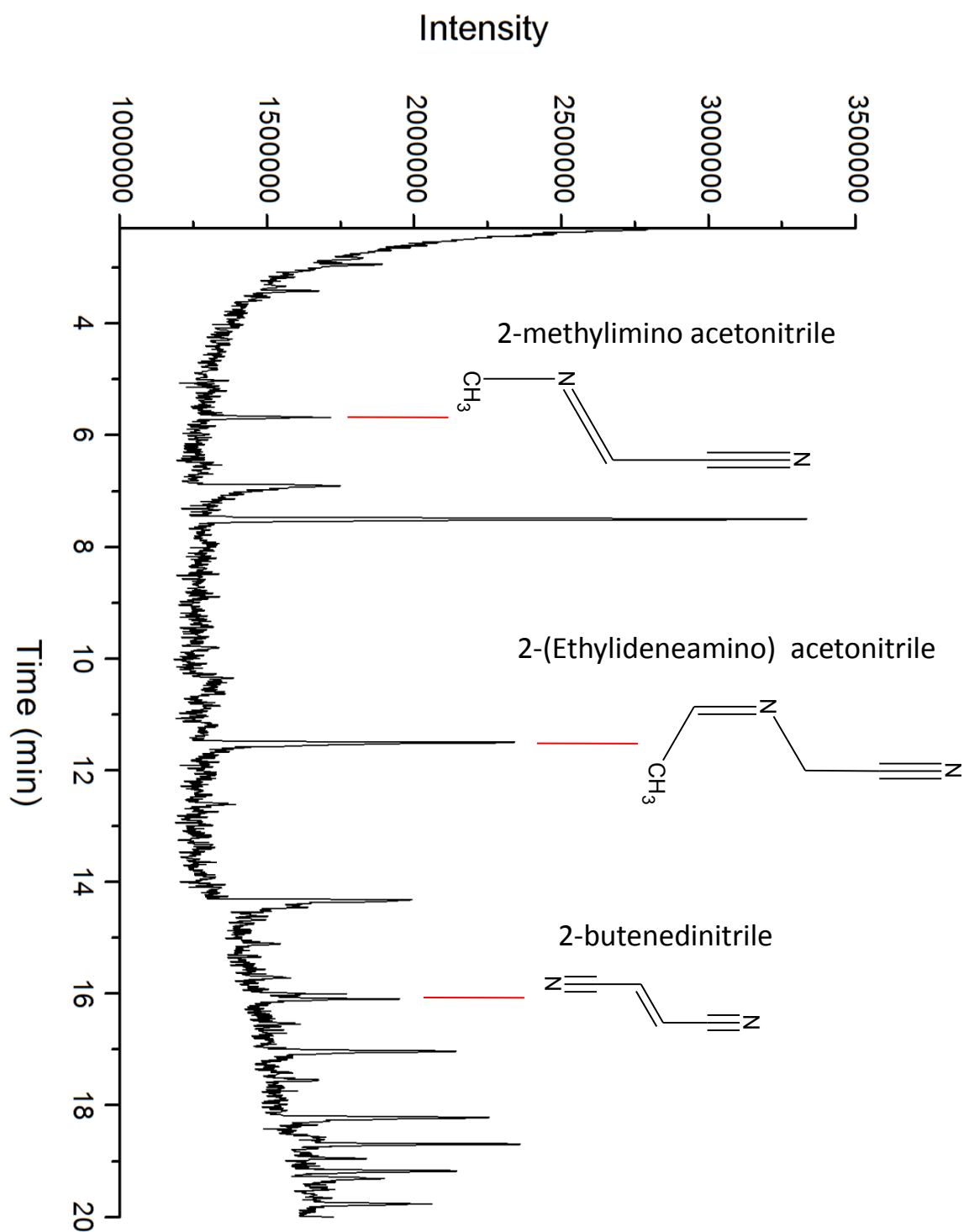


Figure 56: Chromatogram of direct analysis of residue (4%) dissolved in Cl_2CH_2 in the 2-20 min retention time range. Identified peaks are labelled.

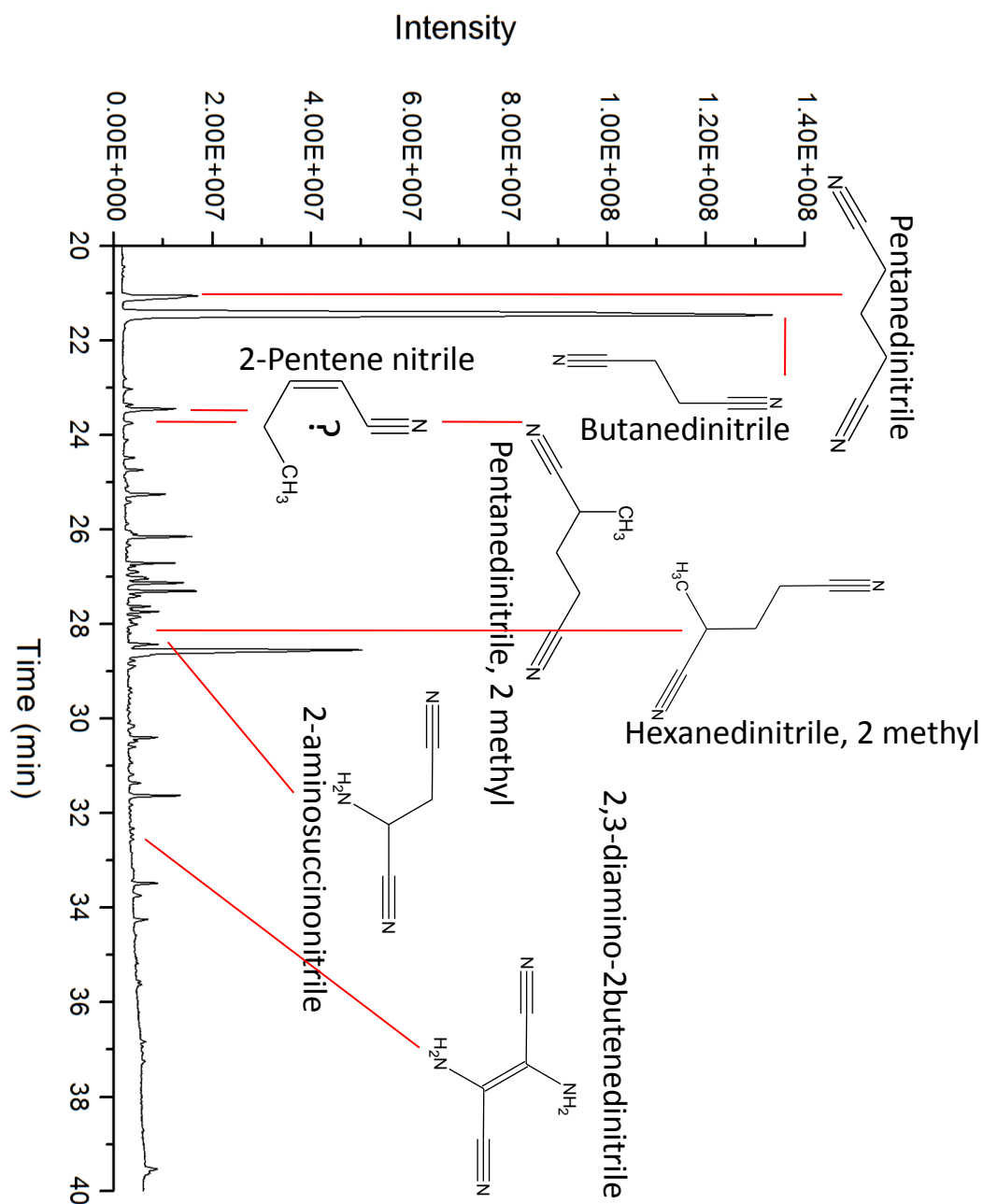


Figure 57: Chromatogram of direct analysis of residue (4%) dissolved in Cl₂CH₂ in the 20-40 min retention time range. Identified peaks are labeled.

CHAPTER IV – THOLINS: WHAT ARE THEY MADE OF? HOW DOES IT INFLUENCE THEIR
PROPERTIES?

Table 13: List of molecules detected using direct injection and their formula

Molecule name	Formula
2-methylimino acetonitrile	CH_3NCHCN
2-(Ethylideneamino) acetonitrile	$\text{CH}_3\text{CHNCH}_2\text{CN}$
2-butenedinitrile	NCHCCHCN
Pentanedinitrile	$\text{NCCH}_2\text{CH}_2\text{CH}_2\text{CN}$
Butanedinitrile	$\text{NCCH}_2\text{CH}_2\text{CN}$
2-Pentenitrile	$\text{CH}_3\text{CH}_2\text{CHCHCN}$
Pentanedinitrile, 2-methyl	$\text{NCCH}(\text{CH}_3)\text{CH}_2\text{CH}_2\text{CN}$
Toluene	$\text{C}_6\text{H}_5\text{CH}_3$
Hexanedinitrile, 2-methyl	$\text{NCCH}(\text{CH}_3)\text{CH}_2\text{CH}_2\text{CH}_2\text{CN}$
2-aminosuccinonitrile	$\text{NCCH}_2\text{CH}(\text{NH}_2)\text{CN}$
2,3-diamino-2-butenedinitrile	$\text{NCC}(\text{NH}_2)\text{C}(\text{NH}_2)\text{CN}$

This technique allowed identifying a tens of molecules within the residue (see Table 13), all of them being nitrogenized (either bearing amine functions or nitrile functions or both). However such direct analysis detects only the volatile compounds present in the mixture. In order to go further in the identification and detect some of the refractory molecules, it could be useful to use derivatization techniques.

IV.2.3.b Derivatization

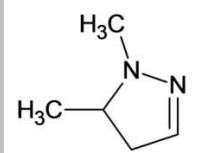
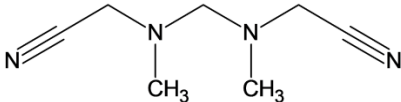
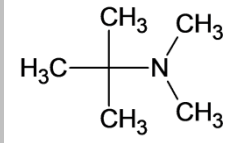
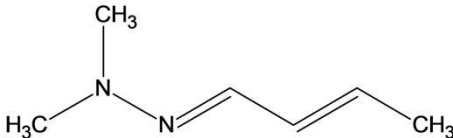
The aim of derivatization is to get refractory compounds volatiles. To do so, it is possible to make these compounds react with a derivatization agent in order to attach a highly volatile function to the original molecule.

CHAPTER IV – THOLINS: WHAT ARE THEY MADE OF? HOW DOES IT INFLUENCE THEIR
PROPERTIES?

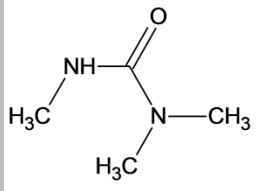
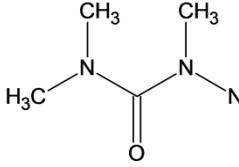
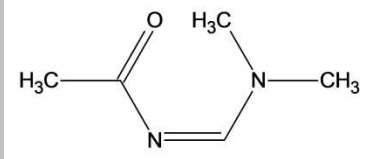
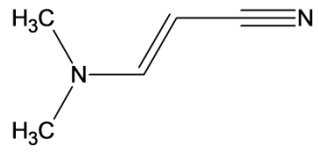
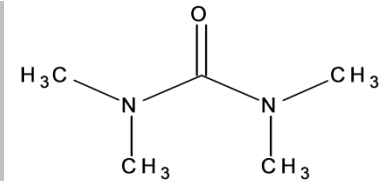
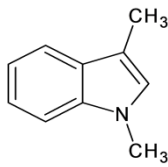
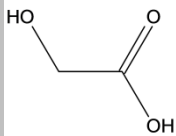
For derivatization the dry residue is treated (high temperature for a few minutes) with a derivatization agent. The two derivatization agents used for this work are DMF-DMA (N,N-dimethylformamide dimethylacetal) and MTBSTFA (N-(t-butyldimethylsilyl)-N-methyltrifluoroacetamide). DMF-DMA is an alkylation agent generally used for derivatization of amines (primary and secondary) and carboxylic acids (Meierhenrich et al. 2001; Freissinet et al. 2010). MTBSTFA is a silylation (adjunction of $-\text{Si}(\text{CH}_3)_2-\text{C}(\text{CH}_3)_3$ fragment) agent commonly used for amino acid derivatization (Buch et al. 2009).

The molecules detected using these derivatization techniques are summarized in Table 14.

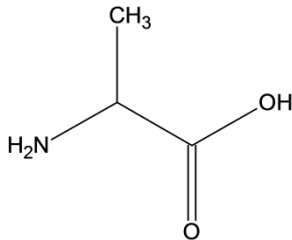
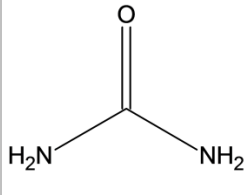
Table 14: List of detected molecules in residue derivatized

Name	Derivatization	Retention time (min)	Formula
1,5-dimethyl 2-pyrazoline	DMF-DMA	2.41	
1,5-dicyano-2,4-dimethyl- 2,4-diazapentane	DMF-DMA	4.2	
2-propanamine,N,N-2- trimethyl	DMF-DMA	5.5	
2-butenal, dimethylhydrazone	DMF-DMA	6.3 and 7.4	

CHAPTER IV – THOLINS: WHAT ARE THEY MADE OF? HOW DOES IT INFLUENCE THEIR PROPERTIES?

N,N,N'-trimethylurea	DMF-DMA	8.7	
N-nitrosotrimethylurea	DMF-DMA	9.9	
Acetamide, N-[(dimethylamino)methylene]	DMF-DMA	11.7	
3-dimethylaminoacrylonitrile	DMF-DMA	13.0	
Tetramethyl-urea	DMF-DMA	17.1	
1H-indols, 1,3-dimethyl	DMF-DMA	23.8	
1-ol-acetic acid	MTBSTFA	21.3	

CHAPTER IV – THOLINS: WHAT ARE THEY MADE OF? HOW DOES IT INFLUENCE THEIR
PROPERTIES?

Alanine	MTBSTFA	24.8	
Urea	MTBSTFA	28.3	

As for direct analyses, the main difficulty for interpreting these data comes from the lack of reference in the databases for such N-rich organic compounds. For the few peaks identified, as for direct analysis, most of them are highly nitrogenized compounds, mainly nitrile or amines.

The presence of oxygenated species (whereas no oxygen is introduced in PAMPRE), including amino acid such as Alanine, also has to be noticed. These oxygenated compounds may be formed by oxidation of the material, either when it is harvested and exposed to air, or when dissolved in methanol before derivatization.

Even if these compounds are clearly not formed in the gas phase in the PAMPRE reactor, their presence is still interesting for the astrobiological aspect of tholins science. Indeed, even if unwanted, the formation of these compounds did not imply specific manipulations. It could then be possible that such a process occurs naturally on Titan's. Some studies in literature show similar behavior for tholins in water-ammonia solutions (Neish et al. 2010).

Finally the GC-MS analyses I performed during my thesis were only performed on the residual material from the cold trap. A similar analysis is performed by Jing He at LGPM (Ecole Centrale Paris) but on bulk tholins harvested from the PAMPRE experiment.

IV.2.4 Conclusion

All these chemical analyses unveiled the high chemical complexity of tholins. More than 15 000 different species have been detected in the material from m/z 50 to m/z 500. With such a large distribution of molecules it has been possible to perform statistical analyses on the mass spectra. This enhanced the co-polymeric structure of tholins, with several possible pathways families for the chemical growth of the polymer.

It has also been possible to propose some key molecules, such as HMT or Melamine, detected in residue and tholins, which seem to have specific importance either because they are the most intense detected molecules, or because of they are good candidates for basis of the polymeric growth.

The next step in the chemical investigation on tholins is clearly to identify these molecules as it has been done on the residue. I currently run experiments in this objective to identify the most predominant molecules in tholins. These experiments are based on analyses of tholins and standard compounds using Liquid Chromatography coupled to Orbitrap Mass spectrometry.

IV.3 Optical infrared properties

IV.3.1 Introduction

Titan's aerosols have a major impact on several parameters of Titan's atmosphere, such as the greenhouse effect (McKay et al. 1991), or condensation (Lavvas et al. 2011). The properties of the produced tholins allow a better analysis and understanding of observational data of the atmosphere of Titan.

In this part we provide new optical data on tholins produced on two different setups. Tholins are analyzed both by ATR and using Synchrotron facility. Tholins spectra is given from the far-IR ranges down to 100 cm^{-1} , a spectra region that was not studied since the Khare et al. (1984) work, to the mid-IR up to 4000 cm^{-1} . The tholins spectra are then compared with those of Titan's aerosols recently acquired by the CIRS and VIMS instruments. Results presented in this part have been partially published in Gautier et al. 2012 and Mahjoub et al. 2012.

IV.3.2 A first comparison of tholins produced in PAMPRE and Bochum: Attenuated Total Reflectance spectroscopy.

A first spectral analysis of tholins in the infrared can be easily performed using Attenuated Total Reflectance (ATR) spectroscopy. Before each measurement, the cell is cleaned with ethanol. A blank is then performed before the deposition of a few amounts (around 0.1 mg) of tholins on the diamond cell.

Spectrum is then recorded at a spectral resolution of 4 cm^{-1} . The final spectrum is the sum of 400 measurements. The automatic correction for air signature and ATR measurement of the OMNIC[®] operation software is then applied. Since ATR is not a quantitative measurement and for the purpose of comparing different samples, all spectra are then normalized.

The samples analyzed in this part are bulk tholins produced with a gas mixture of $\text{N}_2:\text{CH}_4$ 90:10 in the PAMPRE (Pressure 0.8 mbar, Flow 55 sccm) and Bochum (Pressure 0.6 mbar, Flow 15 sccm) reactors.

Figure 58 presents the comparative ATR spectra of tholins produced with 10% of methane in nitrogen in the PAMPRE reactor (red) and in Bochum reactor (blue). In order to enable

comparison, baselines were subtracted using the Fityk software and both spectra were normalized on the 1550 cm^{-1} band.

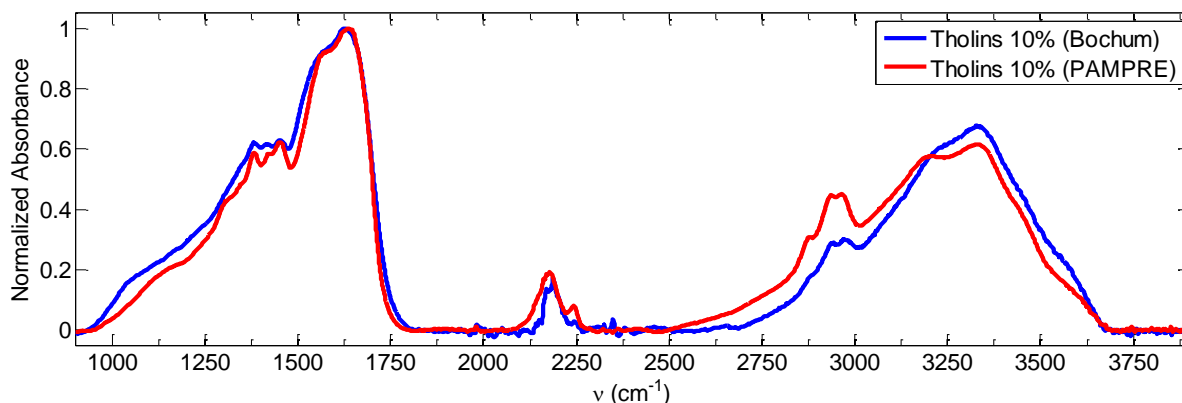


Figure 58: Comparative ATR spectra of tholins produced in PAMPRE (red) and in Bochum reactor (blue). Both spectra were normalized.

As visible in Figure 58, both spectra are very similar. The absorption bands, representing the chemical function in tholins, are the same. Amines ($-\text{NH}$ and $-\text{NH}_2$) present large strong absorption bands at 3300-3500 cm^{-1} , aliphatic carbons ($-\text{CH}_2$, $-\text{CH}_3$) are detected around 2900 cm^{-1} and the band at 2200 cm^{-1} . The large intense pattern around 1500 cm^{-1} is due to all the double bonds ($\text{C}=\text{C}$, $\text{C}=\text{N}$) present in the tholins, with also a contribution of aliphatic carbon and aromatic bonding.

A specific comparison between samples can be done focusing on the aliphatic carbon bands around 3000 cm^{-1} . Indeed, It is possible to model this 2800-2900 cm^{-1} pattern using a combination of Gaussian curves. In this area, there are up to five possible stretching modes for C-H bonds, corresponding to $-\text{CH}_3$ asymmetric ($\sim 2970 \text{ cm}^{-1}$); $-\text{CH}_2$ asymmetric ($\sim 2930 \text{ cm}^{-1}$); $-\text{CH}$ ($\sim 2900 \text{ cm}^{-1}$); $-\text{CH}_3$ symmetric ($\sim 2910 \text{ cm}^{-1}$) and $-\text{CH}_2$ symmetric ($\sim 2870 \text{ cm}^{-1}$) (Imanaka et al. 2004,).

On the next figures, the contribution of the amine bands around 3200 cm^{-1} has been removed. This means that the pattern visible in these figures is only due to the contribution of aliphatic carbons ($-\text{CH}_2$ and $-\text{CH}_3$) bands. The Gaussian deconvolution of tholins produced in PAMPRE with 10% of methane is given in Figure 59 and the one of tholins produced in the same conditions in the Bochum reactor is presented in Figure 60.

CHAPTER IV – THOLINS: WHAT ARE THEY MADE OF? HOW DOES IT INFLUENCE THEIR PROPERTIES?

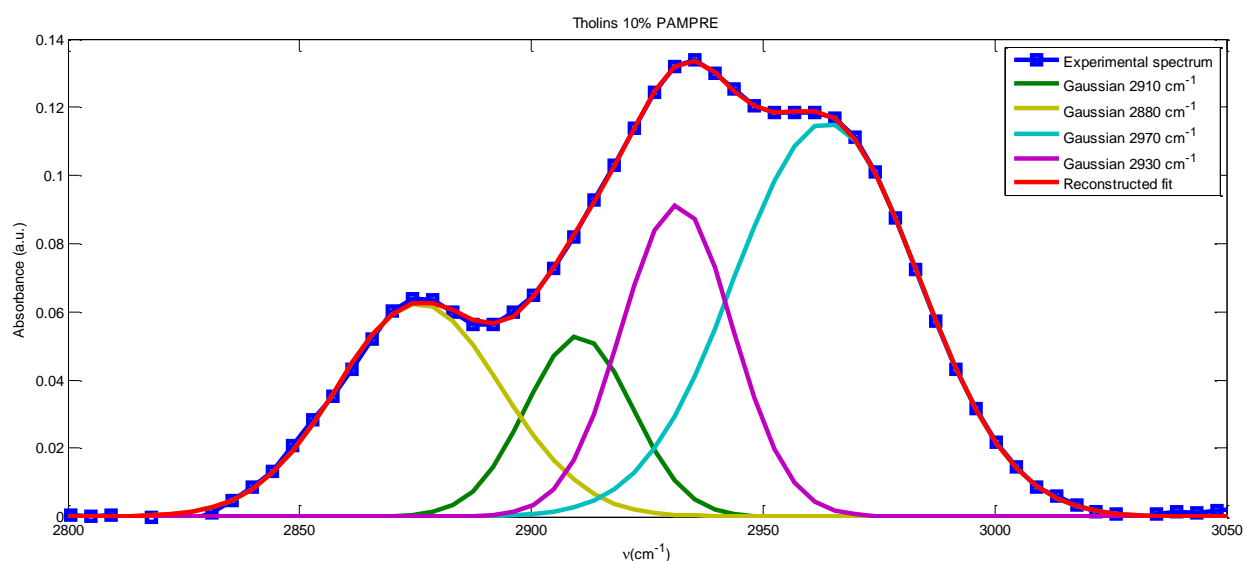


Figure 59: Gaussian deconvolution of aliphatic carbon bands of tholins produced in PAMPRE with 10% of methane.

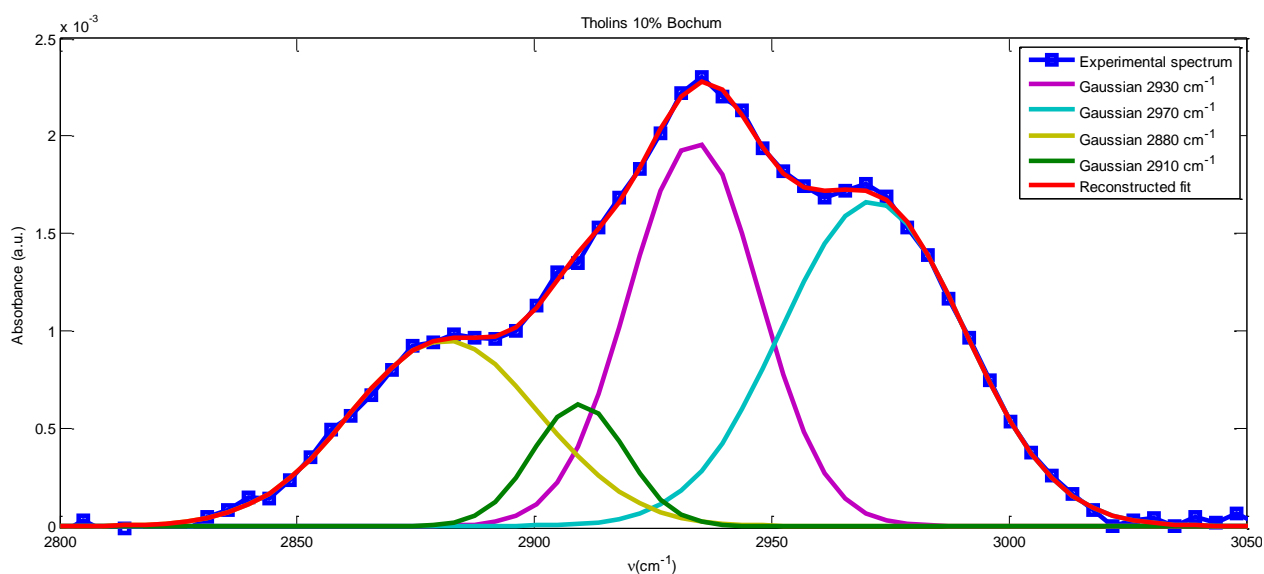


Figure 60: Gaussian deconvolution of aliphatic carbon bands of tholins produced in Bochum reactor with 10% of methane.

In order to get this Gaussian deconvolution, I first initialized the fitting process with five Gaussians located at the wavenumber cited above for the five $-\text{CH}_x$ bonding. As visible in Figure 59 and Figure 60, in the case of tholins, the $-\text{CH}$ band at 2900 cm^{-1} is not necessary at all to fit the spectrum. If present, these CH bonds should be of minor importance in tholins compared to CH_2 and CH_3 .

CHAPTER IV – THOLINS: WHAT ARE THEY MADE OF? HOW DOES IT INFLUENCE THEIR PROPERTIES?

Secondly, even if the patterns present in tholins produced in PAMPRE and in Bochum are highly similar, there are still few differences. Especially looking at the ratio between $-\text{CH}_3$ and $-\text{CH}_2$ bonding, it appears that tholins produced in PAMPRE have more $-\text{CH}_3$ bonds (bands at 2970 cm^{-1} and 2910 cm^{-1}) relatively to $-\text{CH}_2$ (bands at 2930 cm^{-1} and 2880 cm^{-1}) bonds than tholins produced in Bochum, as presented in Table 15.

Table 15: Ratios between CH_3 and CH_2 bands in IR spectra of tholins produced in PAMPRE and Bochum reactor

Bands ratio (CH_3/CH_2)	PAMPRE	Bochum
2970/2930 (asymmetric stretching)	1.25	0.85
2910/2880 (symmetric stretching)	0.85	0.63

This means that tholins produced in this reactor are slightly different than the one produced in PAMPRE. In details, in Bochum tholins the carbon is probably linked to longer and less branched aliphatic chains, which induce more $-\text{CH}_2$ and less $-\text{CH}_3$ in the structure, than the carbon in PAMPRE tholins. This can be due to the residence time of dust in the plasma, which is higher in Bochum reactor (due to smaller gas flow). This induces a longer processing time for aerosols and reticulation of the polymer (Yasuda 1976; Chan et al. 1996).

IV.3.3 Quantifying the tholins absorption and exploring their far-infrared absorbance properties.

IV.3.3.a Experimental setup and protocol

a. Sample production

The production of tholins is performed in the PAMPRE reactor with a continuous 55 standard cubic centimeter (sccm) gas flow rate. In this part, are prepared with various N₂:CH₄ gas mixtures including: 1%, 2%, 5% and 10% of methane. For the production of tholins, the power injected in the reactor was 30 W and the gas pressure 100 Pa. Substrates for thin film deposition are placed on the grounded electrode.

Two types of substrates are used for tholins thin film deposition, MirrIRTM and silicon wafers. Tholins on MirrIRTM substrates (Low-e microscope slides from Kevley Technologies, dim. 25mm x 75mm x 2mm) are used for acquiring data in the mid-IR frequency region, from 700 cm⁻¹ up to 4000 cm⁻¹ (14.2 μm to 2.5 μm). For the far-IR analyses, the thin films are deposited onto circular silicon wafers (1 cm diameter, 0.5 mm thickness). Thin films on silicon substrates allow for obtaining the spectra from 700 cm⁻¹ down to 100 cm⁻¹ (14.2 μm to 100 μm).

Deposition of thin films on MirrIRTM substrates is achieved after 2 hour long experiments. Since the absorption of tholins is weak in the far-IR, productions of thin film on silicon are three hours long in order to increase the thickness of the sample.

Three Si substrates are used in order to ensure of film properties in the far-IR. For Mid-IR, only one MirrIRTM substrate is used, but as the substrate is large enough, three different areas are studied.

b. Far- and Mid-Infrared spectroscopy

Spectra are recorded at the SMIS (Spectroscopy and Microscopy in the Infrared using Synchrotron) beam line of SOLEIL synchrotron radiation facility in France (Dumas et al. 2006). A NicPlan microscope is used coupled to a Nicolet Magna System 560 Fourier Transformed Infrared (FTIR) spectrometer. The IR sources utilized for the present work are the synchrotron radiation for mid-IR and the internal Globar source for the far-IR. The

detectors are either the Mercury-Cadmium-Telluride (MCT) detector of the microscope (mid-IR), or a silicon doped bolometer from Infrared Laboratories, cooled down to 4.2 K with liquid helium (far-IR). Analyses are performed in transmission mode.

To ensure the repeatability of the measurements in the far-IR, thin film analyses are performed on the three samples, three times each, i.e. 9 sample spectra are taken in the far-IR range. I also collected three points of references on two tholins-free silicon wafers to be used as the substrate reference spectra. In the mid-IR, 6 spectra are collected on the thin film deposited on MirrIRTM substrates and blanks are performed on a tholins free substrate. Spectra are recorded at a spectral resolution of 4 cm⁻¹ after co-adding 512 scans at a Michelson mirror velocity of 1.26 cm.s⁻¹.

IV.3.3.b Results

All the spectra presented hereafter correspond to average spectra. Error bars are the standard deviations of measurements performed on samples produced in the same conditions.

a. Thickness calibration and linear absorption coefficient determination

Figure 61 presents an absorbance not calibrated spectrum of tholins (produced with 5% of methane) from 100 cm⁻¹ to 3500 cm⁻¹. The spectrum is made of two parts:

- 1) below 700 cm⁻¹ corresponding to the measurement of tholins film deposited onto silicon
- 2) above 700 cm⁻¹ corresponding to the measurement of film deposited on MirrIRTM substrates.

The non-continuity of the spectrum at 700 cm⁻¹ is due to the difference of thickness of the two samples.

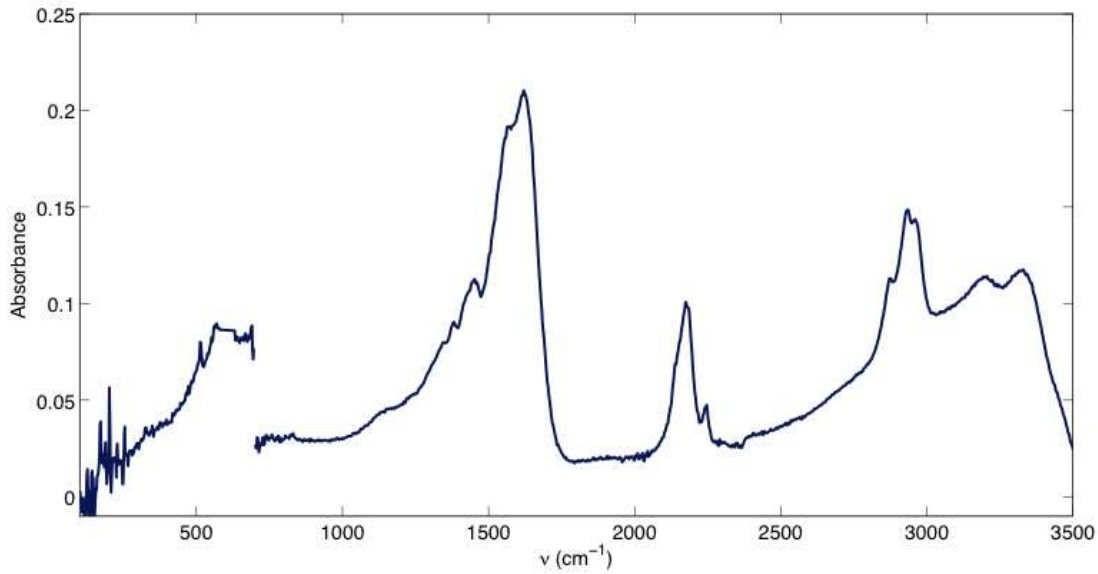


Figure 61: Reconstructed experimental spectrum of tholins produced in PAMPRE with 5% of methane before calibration of the sample thickness.

In order to consider the effect of the film thickness, the linear absorption coefficient, ε , should be used. The calculation of this coefficient requires the sample thickness, d .

The reflected signal is measured and found negligible compared to the transmitted contribution. The linear absorption coefficient, ε (cm^{-1}), can thus be defined using the Beer-Lambert law:

$$I_t = I_0 \times \exp(-\varepsilon \times d) \quad (24)$$

where d is the sample thickness, I_t is the intensity of the transmitted signal, I_0 the incident intensity.

Note that the absorption coefficient ε is a function of the absorption cross-section, σ , and the density of absorbent molecules, $[n]$, not measurable here:

$$\varepsilon = \sigma \times [n] \quad (25)$$

Absorbance, A , being defined as:

$$A = 1 - I_t/I_0 = 1 - \exp(-\varepsilon \times d) \quad (26)$$

The average thickness of thin films on silicon wafers is measured by ellipsometry to be 1300 ± 45 nm. The multilayer structure of MirrIRTM substrates does not allow ellipsometric measurements. The thickness of the film is thus estimated by fitting both parts of the spectrum depicted in Fig.1 in order to get continuity of ε on the whole spectral range. Using this method, the estimated thickness of the tholins films on MirrIRTM substrates is 580 ± 50 nm. In order to validate this thickness estimation, tholins films have been deposited on CaF₂ substrates of the same thickness that MirrIRTM substrates and during the same duration. Measurement on the film deposited on pure CaF₂ gives a thickness of 550 ± 25 nm. This value is in agreement with the thickness estimated by fitting the spectra. I thus consider that the thicknesses of films on pure CaF₂ provides a good estimation of the thickness of the film on MirrIRTM substrates, and used this method to infer the thickness of other films deposited on MirrIRTM as shown in Table 16.

Table 16: Experimental conditions and thickness of the different studied samples

Sample	Injected % CH ₄	Deposit duration	Thickness (nm)
Si n°1	5%	3h	1250 ± 40
Si n°2			1340 ± 40
Si n°3			1300 ± 40
CaF ₂	1%	2h	550 ± 25
CaF ₂			420 ± 10
CaF ₂			490 ± 15
CaF ₂	10%		580 ± 25

The difference of thickness between films on silicon and on CaF₂ comes from both their respective production times and the dielectric properties of the substrates, as discussed in Mahjoub et al. 2012. Note that since both Si and MirrIRTM substrates are reflective mirrors, the optical path length during the absorption is equal to two times the film thickness.

b. Band assignment

In the following, absorption spectra are measured from tholins produced with 5% CH₄ in N₂ as the gas mixture. It has been shown that in the PAMPRE experiment, 5% of methane injected corresponds to approximately 2% in steady state conditions (Sciamma-O'Brien et al. 2010). The wavenumber dependence of the linear absorption coefficient ϵ is shown in Figure 62.

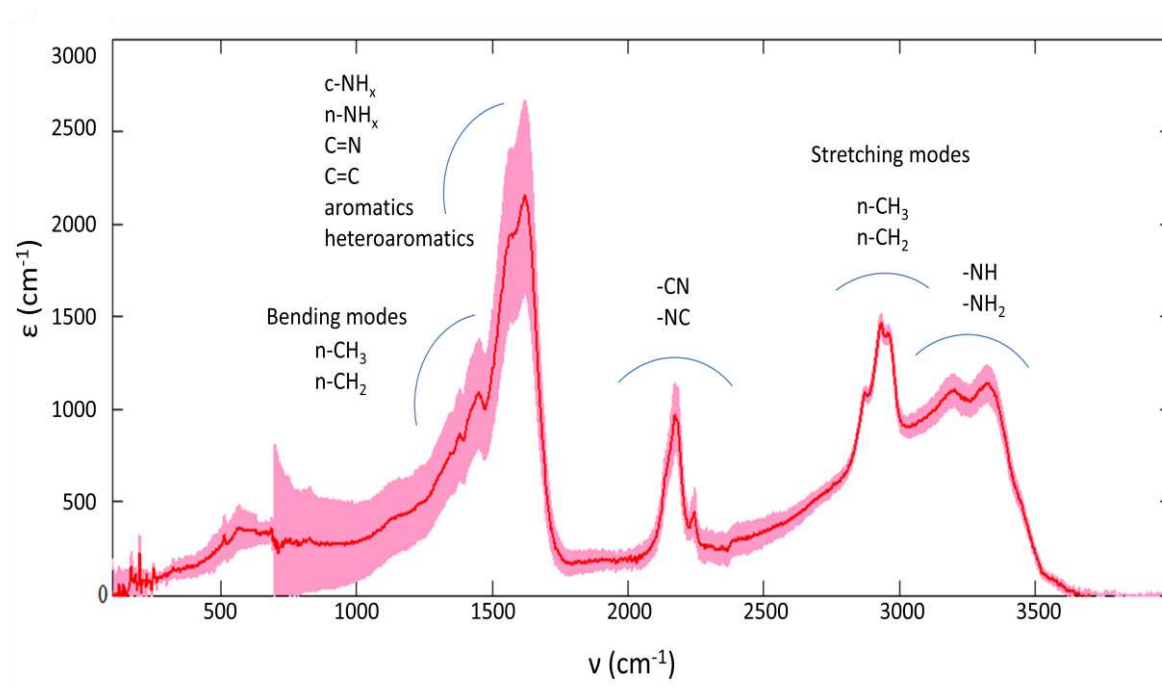


Figure 62: Evolution of ϵ from the far- to the mid-Infrared for tholins produced in PAMPRE with 5% of methane. Average spectrum is given by the red curve. Pink envelopes indicate this standard deviation (1σ) of the spectra, representing the variation of the spectrum from one measure to another on the same sample. Possible attributions are given for major bands of the spectrum. n-X and c-X mean that the functional group X is attached to respectively an aliphatic or an aromatic skeleton.

The red curve corresponds to the average spectrum, and the pink envelope includes both the film thickness uncertainty and the statistical 1σ standard deviation errors from the different measurements.

The larger uncertainty observed at shorter wavenumbers (around 700 cm^{-1}) is due to both the limitations of the MirrIRTM substrates and the detection efficiency of the MCT detector.

Silicon has a strong absorption band in the 590 cm^{-1} - 620 cm^{-1} range which prevents the determination of the linear absorption coefficient in this range when the spectra is divided by blank spectra. The spectrum is therefore interpolated between 590 and 620 cm^{-1} .

The spectrum shown in Figure 55 depicts common tholins absorption features in the mid-IR, described for example in Coll et al. 1999; Imanaka et al. 2004; Quirico et al. 2008 or Imanaka et al. 2012. Broad and intense bands at 3200 cm^{-1} ($3.13\text{ }\mu\text{m}$) and 3330 cm^{-1} ($3.00\text{ }\mu\text{m}$) are due to primary -NH and secondary amines -NH₂. The 2880 cm^{-1} ($3.47\text{ }\mu\text{m}$) band is attributed to -CH₃ symmetric stretching. The 2930 cm^{-1} ($3.41\text{ }\mu\text{m}$) and the 2960 cm^{-1} ($3.38\text{ }\mu\text{m}$) bands are attributed to -CH₂ asymmetric stretching and -CH₃ asymmetric stretching.

The three bands observed at 2140 cm^{-1} ($4.67\text{ }\mu\text{m}$), 2175 cm^{-1} ($4.60\text{ }\mu\text{m}$) and 2250 cm^{-1} ($4.44\text{ }\mu\text{m}$) can be attributed to nitriles -C≡N, isocyanides -N≡C or carbodiimide -N=C=N- stretching modes.

The 1560 cm^{-1} and 1630 cm^{-1} bands cannot be assigned unambiguously. They can correspond to several possible functional groups, such as aromatic or aliphatic -NH₂, C=N double bonds, C=C double bonds, aromatics or heteroaromatics (bearing nitrogen). This precludes a precise assignment of these bands.

At lower wavenumbers, we observe two bands at 1380 cm^{-1} ($7.2\text{ }\mu\text{m}$) and 1450 cm^{-1} ($6.9\text{ }\mu\text{m}$). As suggested in Vinatier et al. 2012, the 1450 cm^{-1} band is probably a contribution of asymmetric C-H bending of CH₃ and scissor in plane bending of C-H in CH₂, and the 1380 cm^{-1} band the symmetric bending of C-H in CH₃.

Several absorption features are also visible in the far-IR frequency range, as shown in Figure 55. First a broad feature extends from 400 to 600 cm^{-1} , which might be due to amorphous carbon nitride (Rodil et al. 2001; Quirico et al. 2008). But as said in Quirico et al. (2008) "it cannot be simply interpreted in terms of wagging or skeletal modes of simple molecules, but rather as lattice vibrations within the covalent solids". Thus, this band is left unassigned.

The band observed at 690 cm^{-1} ($14.49\text{ }\mu\text{m}$), could possibly be attributed to C-H bending out of plane in carbon-carbon double bonds (usually 665 to 730 cm^{-1}) or to ring out of plane deformation vibration in aromatics (usually 670 - 720 cm^{-1}). Absorption due to aromatic rings

deformations are known to be more intense than absorption due to C-H out of plane bending mode. Further analysis on the aliphatic and aromatic content in tholins could confirm a preferential assignement of theses bands to aromatics ring deformations.

Bands are also visible at 515 cm^{-1} ($19.42\text{ }\mu\text{m}$), 324 cm^{-1} ($30.86\text{ }\mu\text{m}$), 255 cm^{-1} ($39.22\text{ }\mu\text{m}$) and 170 cm^{-1} ($58.82\text{ }\mu\text{m}$). However, their assignments are not obvious because of a lack of litterature data for these weak bands.

c. Impact of the percentage of methane on tholins spectra

I studied the influence of the methane concentration of the reactive gas mixture in the PAMPRE experiment on tholins spectra. Figure 63 presents ε as a function of the wavenumber for tholins produced with 1%, 2%, 5% and 10% of methane in the gas mixture injected. Sciamma-O'Brien et al. 2010 have shown that these injected ratios respectively correspond to $\sim 0.2\%$, $\sim 0.5\%$, $\sim 2\%$, $\sim 5\%$ of methane in the steady state conditions of the reactive plasma.

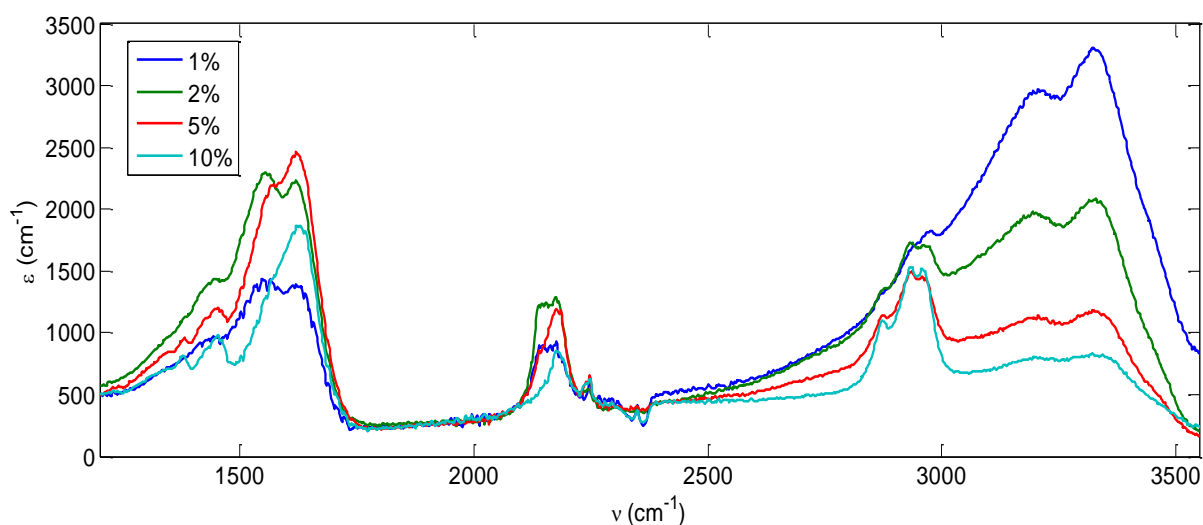


Figure 63: Absorption spectra of tholins in the mid-Infrared with different initial CH_4 concentrations in the gas mixture (1% in blue, 2% in green, 5% in red and 10% in cyan).

When comparing the spectra presented in Figure 63, the most striking point is a growth in intensity of the amine bands at 3200 cm^{-1} and 3330 cm^{-1} when the concentration of methane decreases in the initial gas mixture. These bands are obvious when 1% of methane is injected, whereas they are quite low in the spectrum when 10% of methane is used. This is consistent with the elemental analysis presented in Sciamma-O'Brien et al. 2010, showing an increase of

the nitrogen content in tholins for the lower methane concentrations. Nevertheless, in spite amines were recently confirmed to be functional groups present in PAMPRE tholins with solid nuclear magnetic resonance (Derenne et al. 2012), their predominance was not expected considering the unsaturation supported by nitrogen reported in previous studies performed both on the gas phase (Coll et al. 1999; Gautier et al. 2011) and on tholins (Somogyi et al. 2005; Carrasco et al. 2009; Pernot et al. 2010).

This increase of the amine bands is correlated to the decrease of the intensity of the 2900 cm^{-1} pattern, attributed to aliphatic methyl. For the lowest methane concentration (1%) the 2900 cm^{-1} pattern is very weak, whereas for the highest methane concentration studied (10%) it is one of the strongest absorption bands in the spectra. The increase in the strength of these bands suggests that the amount of aliphatic methyl increases in tholins when they are produced with a higher methane percentage.

Another variation observed on the spectra presented in Figure 63 is the progressive vanishing of the band at 2140 cm^{-1} compared to the 2175 cm^{-1} band. As said in section previously, these bands and the one at 2250 cm^{-1} are due to stretching modes of several kinds of carbon-nitrogen triple bonds. Their exact attribution is still unclear, but the 2140 cm^{-1} band decreases with respect to the 2175 cm^{-1} band when the methane percentage increases. This is consistent with the increase of the saturated aliphatic carbons, also observed on the 2900 cm^{-1} pattern. The 2140 cm^{-1} and the 2175 cm^{-1} bands could respectively be attributed to unsaturated and saturated nitriles.

Another visible effect visible in Figure 63 is the plummeting of the band at 1560 cm^{-1} respective to the 1630 cm^{-1} band. Indeed for low methane concentrations, the 1560 cm^{-1} band is as intense as the one at 1630 cm^{-1} , whereas it is almost undetectable in the spectra of tholins produced with 10% methane. This band is not clearly identified, but may involve nitrogen, such as cyclic or aliphatic amines (c- NH_x or n- NH_x), C=N or heteroaromatics, since this band intensity decreases with the decrease of the N_2 concentration in the gas mixture introduced in the experiment.

Finally, the relative increase of the absorption bands at 1450 cm^{-1} and 1380 cm^{-1} with increasing CH_4 percentage is also noticeable, as is the growth of broad low intensity bands

centered at 1230 cm^{-1} and 1140 cm^{-1} . These bands are possibly due to carbon-carbon or carbon-hydrogen bonds.

All these band variations enforce the notion that the amount of molecules with hydrocarbon skeleton in tholins increases with the methane concentration in the reactive gas mixture, whereas tholins produced with low methane concentrations seem to be based on amine rich polymers.

d. Comparison with Cassini CIRS and VIMS observations

Figure 64 shows tholins absorption spectra in the far- and mid-IR spectral range (black curve). Also plotted in this figure is the tholins spectrum of Khare et al. 1984, in blue. The CIRS and VIMS spectra of Titan's aerosols in the mid- and far-IR are plotted in red (Bellucci et al. 2009; Anderson and Samuelson 2011; Kim et al. 2011; Vinatier et al. 2012).

In order to compare the tholins absorption spectra obtained with different conditions, a normalization coefficient is applied to the spectra. The Khare et al. 1984 spectrum is normalized to the maximum intensity of the entire tholins spectrum (i.e. the 1560 cm^{-1} band). VIMS and CIRS spectra are normalized to the maximum of our spectrum (i.e. the CIRS spectrum is normalized at the 1450 cm^{-1} band, and the VIMS spectrum at the 2930 cm^{-1} band).

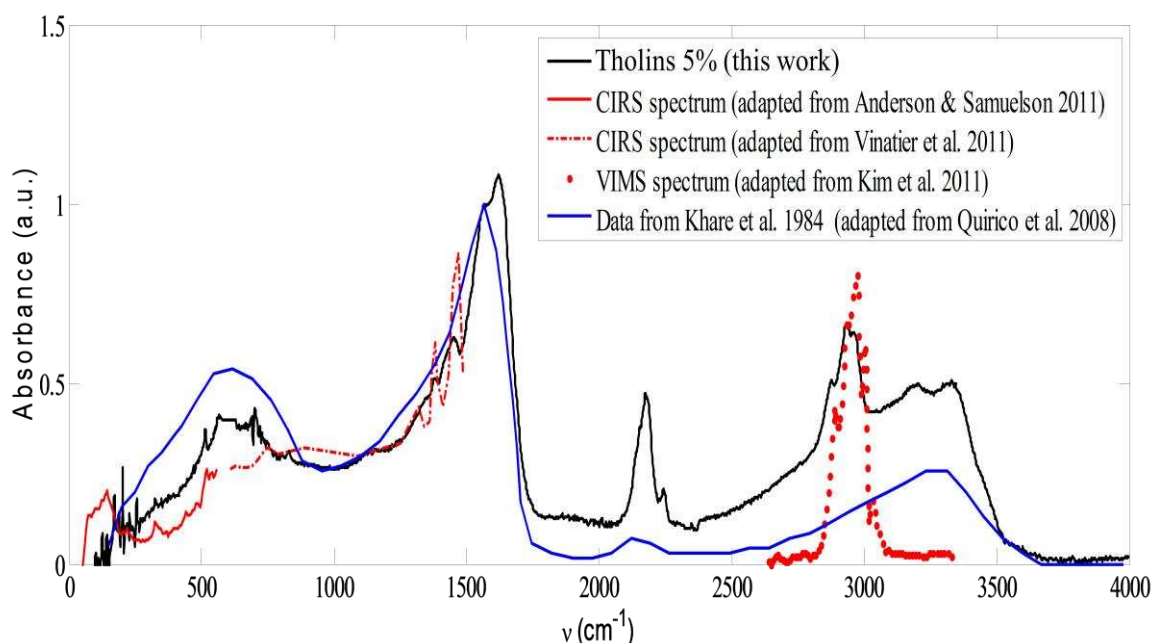


Figure 64 : Absorbance spectrum from far-IR to mid-IR of PAMPRE tholins made with 5% of CH₄ (black curve) compared to Quirico et al. 2008 tholins spectra (extracted from Khare et al. 1984 tholins, blue), Cassini-CIRS observations (red line, from Anderson and Samuelson 2011 and Vinatier et al. 2011) and Cassini-VIMS spectra (red dots, from Kim et al. 2011).

The analysis of Figure 64 is discussed in the mid- and far-IR spectral regimes:

i. Mid-Infrared

The 2900 cm⁻¹ (3.4μm) pattern, emphasized in Figure 65, is in general agreements with the feature observed by VIMS (Bellucci et al. 2009; Rannou et al. 2010). This pattern is not present in the spectrum presented by Khare et al. 1984, produced with a 10% initial methane concentration. But in PAMPRE setup, the intensities of these bands are maximum with 10% methane introduced in the experiment (cf. Figure 63), and almost as intense as the feature at 1500 cm⁻¹.

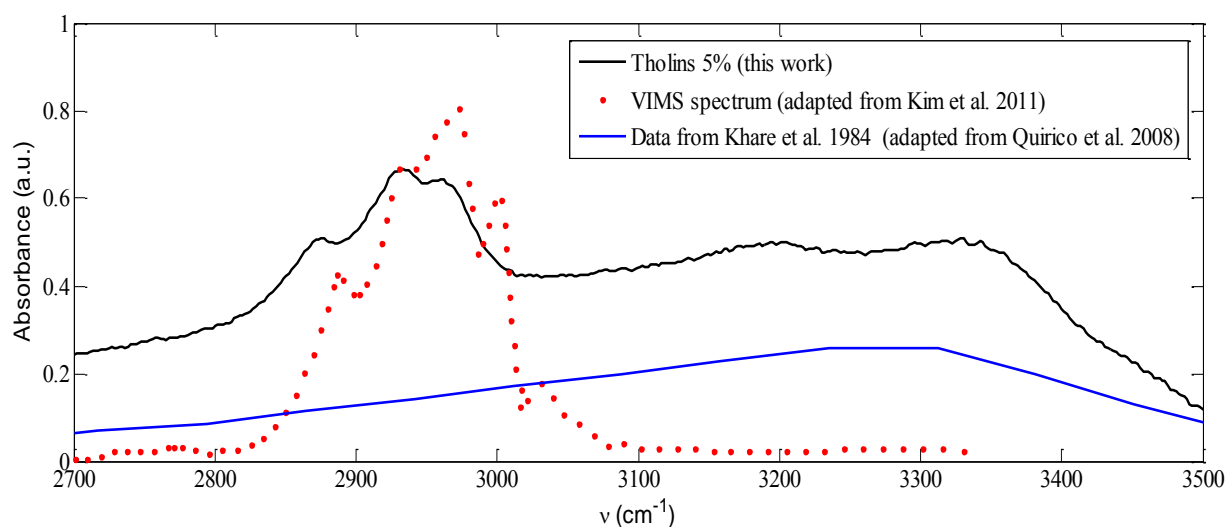


Figure 65: Close up of Fig. 57 on the 2900 cm^{-1} pattern. Black line represents our tholins 5% spectrum. Red dots are the spectrum derived from observations with Cassini-VIMS attributed to Titan's aerosols (extracted from Kim et al. 2011). The blue line represent tholins spectra reconstituted from Khare et al. 1984 data (from Quirico et al. 2008).

A possible explanation is as follows. Despite the same initial methane concentration between this work and Khare et al. 1984, the effective consumption of methane might be different. Indeed, the residual methane concentration in a steady state in the plasma is quite different than from the initial one as shown in Sciamma-O'Brien et al. 2010. And yet, as shown previously the intensity of the 2900 cm^{-1} pattern is highly correlated with the methane concentration. However, it must be underlined that other plasma parameters can influence the chemical composition of tholins in addition to the injected amount of CH_4 , such as the working pressure as seen in the ATR measurement above and shown in Imanaka et al. 2012.

Figure 65 compares the shape of the 2900 cm^{-1} feature between tholins spectrum and the derived aerosol spectrum from VIMS observations (extracted from Kim et al. 2011).

Among the five main bands observed in the VIMS data (2885 cm^{-1} , 2930 cm^{-1} , 2965 cm^{-1} , 3000 cm^{-1} and 3030 cm^{-1}) two are not found in PAMPRE tholins spectrum: the 3000 cm^{-1} band, attributed to CH_3CN ice by Kim et al. 2011, and the weak 3030 cm^{-1} band. The spectral position of the 2930 cm^{-1} band (attributed to n-CH_2 assymetric stretching) in my data corresponds exactly to one of the absorption bands detected with VIMS in Titan's atmosphere. For the 2885 cm^{-1} and 2965 cm^{-1} bands, I assume they are actually the same as the bands detected in tholins respectively at 2880 cm^{-1} and 2960 cm^{-1} and attributed to CH_3 stretching

modes. Indeed infrared spectra of solids can present slight frequency shifts due to the chemical environment for the functional group generating the absorption band (see Figure 66) ("Infrared Spectra" by NIST Mass Spec Data Center, S.E. Stein, director). Particularly, a shift of a few wavenumbers toward higher wavenumbers may arise from the influence of aromatics on the methyl vibration. In the same way, the chemical environment of the methyl group responsible for this pattern has a major impact on the presence of the bands shown in Figure 66. In this figure the impact of the insertion of an heteroatom in the cycle of toluene on the 2900 cm^{-1} pattern is observed.

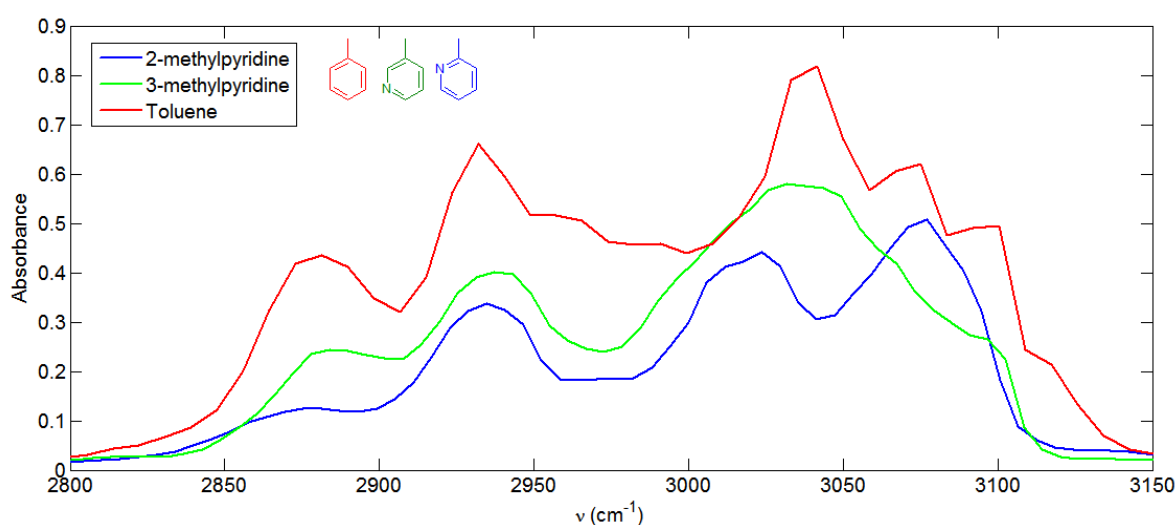


Figure 66: Infrared spectra of toluene (red), 2-methylpyridine (blue) and 3-methylpyridine (green) extracted from the NIST database.

The red line represents the spectrum of a methyl group bonded to a pure carbon aromatic ring (toluene), whereas green and blue lines are spectra with the methyl group bonded to an heteroaromatic ring (here pyridine) in two different positions. It is clear from Figure 66 that the composition of the chemical environment of the methyl group (and even the position of the nitrogen in the cycle comparing blue and green spectra) has a major influence on the shape of the spectra, and it can induce both band intensity changing and band position shifting.

The fact that PAMPRE tholins bands do not perfectly fit the bands seen with VIMS still does not imply that these bands in Titan's atmosphere cannot come from aerosols absorption. But

this might suggest that the chemical environment of the methyl functional groups in Titan's aerosols are, even slightly, different from the observed features in our tholins.

In Kim et al. 2011, the authors proposed that the 2900 cm^{-1} absorption pattern observed by VIMS could be due to ices. As shown in this work, tholins present an intense absorption at this wavenumber. We can thus suggest that aerosol absorption can explain the VIMS observations better than ices, and this is in agreement with Rannou et al. 2010 and Bellucci et al. 2009. Moreover, the presence of ices seems unlikely at the altitude of the observation since Fulchignoni et al. 2005 measured a temperature of about 180 K at 300 km.

ii. Far Infrared

A close up of Fig. 4 in the $100\text{ cm}^{-1} - 1500\text{ cm}^{-1}$ wavenumber range ($100\text{ }\mu\text{m} - 6.6\text{ }\mu\text{m}$ wavelength range) is given in Figure 67. In this range, tholins spectrum is compared with the absorption spectra attributed to Titan's aerosols derived from CIRS observations (Vinatier et al. 2010; Anderson and Samuelson 2011; Vinatier et al. 2012).

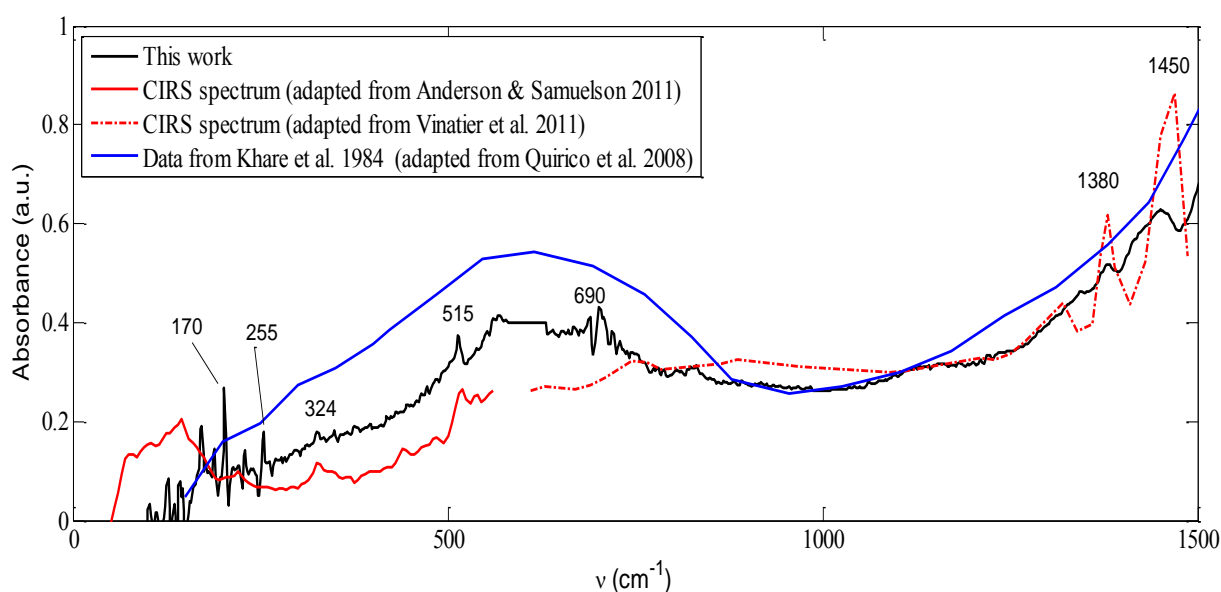


Figure 67: Close up of Fig.57 in the far-IR range. Black line represents our tholins 5% spectrum. Titan's aerosols spectra derived from observations with Cassini CIRS (Anderson and Samuelson 2011; Vinatier et al. 2011) are plotted in red. The blue line represents tholins spectra reconstituted from Khare et al. 1984 data (from Quirico et al. 2008).

In this frequency range, two absorption bands are clearly present in both the CIRS and the tholins spectrum, the band at 1380 cm^{-1} ($7.2\text{ }\mu\text{m}$) and the band at 1450 cm^{-1} ($6.9\text{ }\mu\text{m}$). A third

band is visible around 1320 cm^{-1} ($7.6\text{ }\mu\text{m}$) in the CIRS spectrum but not in PAMPRE tholins spectrum (or really weak) and may be due to an overtone of the C-H bending in $\equiv\text{C-H}$ group signature observed at 630 cm^{-1} from CIRS. This absence could mean that tholins produced with PAMPRE contain less alcyne than the Titan aerosols.

Furthermore, as illustrated in Figure 67, the broad band visible around 600 cm^{-1} in my spectrum is also present in other laboratory tholins spectra (e.g. Imanaka et al. 2012; Imanaka et al. 2004; Quirico et al. 2008), but is not present in Cassini-CIRS spectra.

This feature is speculated to arise from the lattice vibration in solids (Rodil et al. 2001). This would mean that this band could only originate from large scale solid material such as laboratory tholins film, whereas this band could not be observed on suspended single particles (free and not assembled), such as aerosols in Titan's atmosphere.

Finally, spectra of tholins exhibit a few features in the far-IR below 700 cm^{-1} , ($14.3\text{ }\mu\text{m}$). Some of these features, especially the bands at 325 cm^{-1} ($30.77\text{ }\mu\text{m}$) and 513 cm^{-1} ($19.49\text{ }\mu\text{m}$) are also visible in CIRS spectra (Anderson and Samuelson 2011). Up to now these bands are attributed to noise in CIRS spectrum.

The fact that these two bands are also present in tholins spectrum could tend to confirm that these weak absorption bands visible in CIRS spectrum are not noise but are due to aerosols. Further investigation on this spectral range of observations of Titan's atmosphere could confirm such hypothesis.

IV.4 Conclusion

In this chapter I presented several studies on tholins composition, based on both mass spectrometry investigations (GC-MS, Orbitrap, TOF) and infrared spectroscopy techniques (ATR, Synchrotron based FTIR). These studies confirmed the high complexity of tholins, as presented previously in the literature, and allowed to get deeper in the knowledge of tholins composition. First, the detection of a few tens of molecules with a probable high interest for tholinomics such as HMT or Melamine has been done. Then, high resolution mass spectrometry allowed obtaining the exact formula of literally thousands of molecules present in tholins, most of them being nitrogenized. These mass spectrometric measurements also

showed that tholins have a co-polymeric structure that can be studied using a statistical approach on the high resolution mass spectra.

The large inclusion of nitrogenous species in tholins has also been confirmed by the optical measurement in the IR range where tholins show an important signature of amines functions. The IR measurements done here also provide the wavenumber dependence of the linear absorption coefficient ε , from the far-IR (100 cm^{-1}) to the mid-IR (4000 cm^{-1}) range. The impact of methane percentage in the experiment on the mid-IR spectra of tholins is also studied. Comparisons are performed between different tholins material and data derived from Cassini CIRS and VIMS observations, enhancing the similarities between laboratory tholins and Titan's aerosols. Furthermore, the mid- and far-IR data provided in this work could also be used for comparison to other astronomical environment where tholins material is supposed to be relevant, such as cometary ices, Triton and TNO surfaces or diffuse interstellar medium (Gradie and Veverka 1980; Pendleton and Allamandola 2002; Dotto et al. 2003).

Chapter V Effect of photochemistry: the APSIS experiment

V.1 Introduction

As said in chapter I, there are two main kinds of experiments used to simulate Titan's atmospheric reactivity based either on photochemical reactors or on plasma reactors. In chapter III and IV, I presented results obtained on a plasma-based experiment. Plasma discharges are more efficient for the production of aerosols, but one should keep in mind that Titan's chemistry is mainly driven by photochemical processes (Robertson et al. 2009). In order to study the influence of the energy source on the chemistry, we designed a new photochemical reactor, APSIS, described in details in chapter I. In order to provide VUV photons, APSIS is coupled with the DISCO beam line at SOLEIL synchrotron facility. Indeed ionization and dissociation of molecular nitrogen requires photon wavelengths below 100 nm. Typical leak-tight windows made of LiF, CaF₂ or MgF₂ are capable of handling the pressure difference between the ultra-high vacuum of the beam line and the pressure of the reactor, but are opaque below ~110 nm (11.3 eV), preventing the activation of molecular nitrogen. Although it is relatively easy to irradiate any media with UV photons through windows, it is much more difficult to deliver to a gas sample VUV photons with energy above the transparency limit of the windows.

Therefore, the APSIS chamber is coupled windowless to the DISCO beam line, using a differential pumping system. A non-reactive carrier gas, helium, is continuously injected between the beam line and the APSIS chamber in order to prevent the reactive mixture to be pumped out of the reactor into the differential pumping system. The spectrum of the DISCO beam line is generally $10^4 - 10^6$ times more intense than the solar spectrum at Titan but much more uniform and has no peak at Ly- α , 121.6 nm. This experiment differs significantly from the single previous synchrotron study of Titan's atmosphere (Imanaka and Smith 2007, 2010), working at 0.066 or 0.13 mbar and using a narrowband synchrotron radiation source.

Since we want to study the effect of the energy source only, the experiments presented here were done in the same experimental conditions (temperature and pressure) as in the PAMPRE plasma reactor in order to compare the chemistries generated with photons and electrons. All the experiment of this section were performed with a $\text{N}_2:\text{CH}_4$ 90:10 gas mixture. Table 17 resumes the experiments performed with this setup. The work presented in this part has been published in Gautier et al. 2013b and Peng et al. 2013 and was done in a large collaboration group. My main contribution was to run the experiment during Synchrotron shifts (24h a day, a few days per semester).

Table 17: List of experiments performed on APSIS

Reactive (N_2+CH_4) gas flow (sccm)	Partial pressure (N_2+CH_4) (mbar)	Total pressure with Helium (mbar)	Approximate residence time of the gas mixture (min)
0.6	1.3	2.1	11
2	1.5	2.5	4
7	4.5	7.0	3
10	6.5	8.7	3

V.2 Analytical techniques and data treatment

V.2.1 *In-situ* Mass Spectrometry

The analytical treatment of the MS data acquired on APSIS was mainly performed by Z. Peng from the Laboratoire de Chimie Physique. For a better understanding of the data, I briefly remind here the main step of data treatment.

The DISCO photon flux, (a few 10^{11} ph.s^{-1} for 0.1 nm bandwidth) leads to a nitrogen dissociation ratio of less than 10^{-4} . The signal at m/z 28 of N_2 should therefore be constant enough throughout the experiments to be considered as a fixed reference. A slight electronic

drift is often observed during the experiments lasting several hours. It affects proportionally all the ion signals, confirmed by a similar drift of the total pressure measurement in the ion source of the mass spectrometer. The intensity of the mass peak at m/z 28 is therefore used to normalize the mass spectra.

We made two types of experiments in order (i) to monitor the time-dependent evolution of a series of mass peaks during the irradiation (MID measurements), and (ii) to characterize the stationary states before (DISCO OFF) and after (DISCO ON) irradiation on a continuous mass range (scan analogs). Studying the stationary state allows to increase the signal to noise ratio by long acquisition time-scales: a 10 seconds dwell time is chosen for each mass between m/z 2 to 80.

We monitored the temporal evolution of the gas mixture composition recording the intensity of the maximum of mass peaks of interest in Multiple Ion Detection (MID) mode: m/z 15, 26, 27, 28, 38, 39, 41, and 52. The signal at each of these masses was accumulated during 1 s, leading to a total time-resolution of 15 s. As described in Sciamma-O'Brien et al. 2010, the peak at m/z 15 is representative of methane. A possible contribution of $^{15}\text{N}^+$ also occurs for $\text{N}_2\text{-CH}_4$ gas mixtures, but for a gas mixture with 10% of methane, this contribution is found to be negligible. Except for m/z 28 dominated by N_2 signature, the ion masses chosen in the MID method correspond to product formation in mass regions C2, C3 and C4, with 2, 3 or 4 heavy (C or N) atoms bearing species respectively.

In order to determine the intensity of each peak, the signal is integrated for each m/z . The baseline is calculated by averaging the signal above m/z 70 (no peaks detected at such high m/z) and subtracted to all peaks, assuming a constant baseline in the spectrum. The shift of the peak center to the integer m/z value (each peak is slightly shifted of about 0.25 amu to the right) also has to be taken into account. The intensity value for a given, i , corresponds then to the integration of the signal on the interval $[i-0.25, i+0.75]$. After determining the intensity of each peak, the intensities are normalized relatively to nitrogen (m/z 28) in order to get relative intensities. To get an estimation of the product relative concentrations, the difference spectrum (DISCO on –DISCO off) is then calculated.

V.2.2 GC-MS

The cold trap used on APSIS is the same than the one used for the study presented in part 3 of this chapter. Since the timescale of the experiment is larger and the amount of species produced is lower, the trap is settled for longer period, i.e. 8 hours.

After the experiment, the trap is isolated and heated up to room temperature to release species into the gas phase. The GC-MS and the column used for this work are the same than in Part 3. The analytical parameters are given in paragraph II.2.1 of this thesis.

A temperature programming was used for the analysis, starting with an isotherm at 30 °C for five minutes, followed by a gradient of 5 °C.min⁻¹ from 30 °C to 190 °C, and ending with a second isotherm at 190 °C for 5 min. The carrier gas is helium (99.999%) with a constant flow rate of 1 mL.min⁻¹. Helium flow is injected through the trap in order to ensure a better introduction of products into the GC. Injector is heated up to 250 °C and operates in the splitless mode. Temperature of the ion source is set at 200 °C. A blank run is performed before each injection, to ensure that there is no contamination from the previous run.

V.3 Results

V.3.1 Methane consumption

Figure 68 provides the time evolution of the methane and acetylene amount relatively to nitrogen in the experiment for an experiment performed with 0.6 sccm total gas flow. The methane concentration is evaluated through the I_{15}/I_{28} ratio of the MID signals.

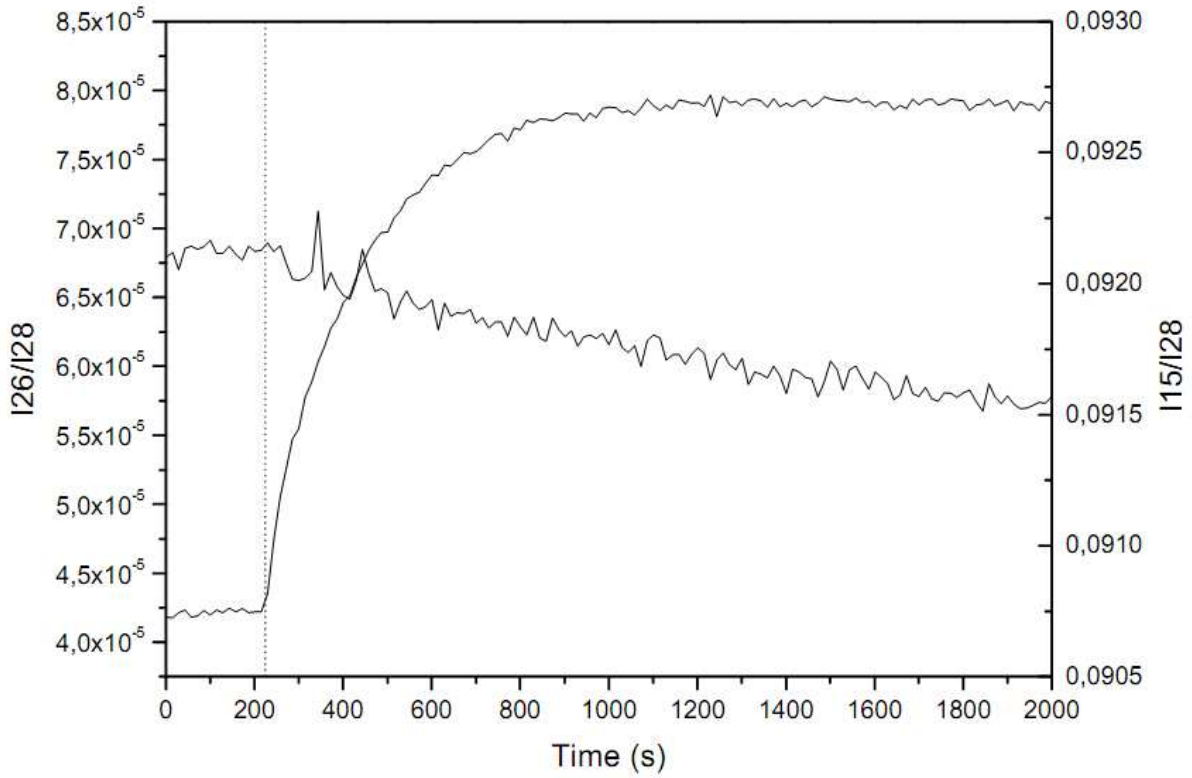


Figure 68: Evolution of I_{15}/I_{28} (methane/nitrogen) and I_{26}/I_{28} (acetylene/nitrogen) ratios in an experiment performed with 0.6 sccm total gas flow. The dashed line represent the starting time of the photo-irradiation

The starting time of the photo-irradiation by VUV photons can be easily located by the instantaneous increase of acetylene detected at m/z 26.

The consumption of methane relatively to nitrogen can be calculated as:

$$\Delta CH_4 = \frac{(\frac{I_{15}}{I_{28}})_0 - (\frac{I_{15}}{I_{28}})_{SS}}{(\frac{I_{15}}{I_{28}})_0} \quad (27)$$

The subscript 0 refers to the initial conditions (before the irradiation by the synchrotron beam) and the subscript SS refers to the steady state conditions when MS signal reaches an asymptotic value.

This ratio has been calculated for several gas flow conditions and is presented in Table 18.

Table 18: ΔCH_4 and their standard deviation calculated for several experimental conditions

Total gas flow (sccm)	ΔCH_4	$\sigma(\Delta CH_4)$
0.6	1.7e-2	0.3e-2
2	4.6e-3	1.0e-3
7	3.4e-3	0.6e-3
7	3.0e-3	0.6e-3
7	3.7e-3	1.7e-3
10	3.2e-3	0.2e-3

As visible in this table, the methane consumption relatively to nitrogen decreases when the total gas flow in the reactor increases from a few percent for 0.6 sccm down to a few per thousand for 10 sccm. This decrease of the consumption efficiency is probably due to the dilution effect of the photons. Indeed, if the penetration length of photons (in the wavelength range of methane absorption, 100-130 nm) in the reactor is about 15 cm at 0.6 sccm, it is only of 3 cm for a 10 sccm experiment.

V.3.2 Kinetics

From the evolution of the m/z 26 ion, it is possible to deduce the timescale τ of the experiments. Figure 68 shows that this species follows a simple exponential law:

$$I_{26}(t) = I_{26_{ss}} - (I_{26_{ss}} - I_{26_0}) \times e^{(-t/\tau)} \quad (28)$$

τ can be estimated by a linear fit of $\log(I_{26_{ss}} - I_{26(t)})$ (Figure 69).

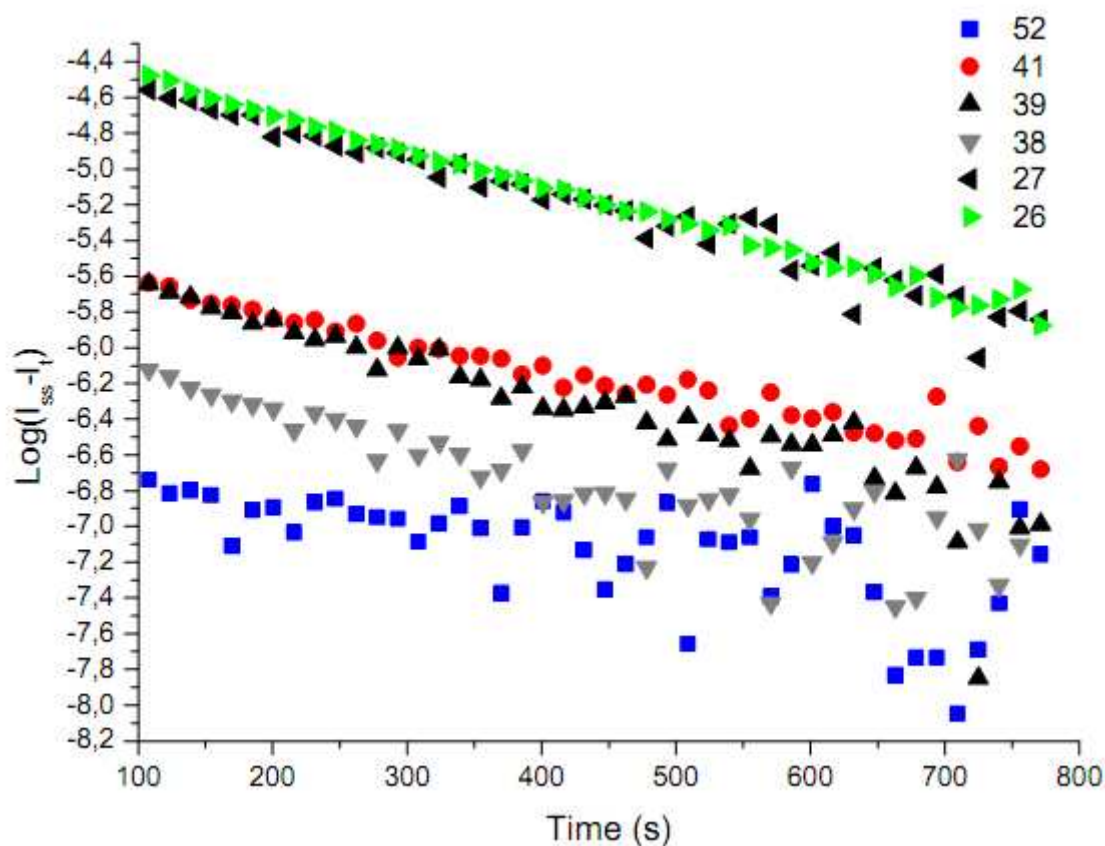


Figure 69: Temporal evolution of $\log(I_{ss} - I)$ for m/z 26, 27, 38, 39, 41 and 52. Experiment performed at 10 sccm.

As seen in chapter III, the MS peak intensities are not directly representative of the corresponding neutral concentrations. This is mainly due to the different ionization thresholds and fragmentation patterns of the products. Nevertheless, the ratio of the main peaks intensities versus the peak at m/z 28 still provides a rough estimation of the mole fraction of the products. The products mole fractions are about 10^{-5} for C2 compounds and about 10^{-6} for C3 and C4.

Figure 69 shows the exponential decay for the peaks at m/z 26, 27, 38, 39, 41 and 52. The timescale is of about 5 to 8 minutes for all the gas flow conditions studied, comparable to the residence time of the gas in the reactor (a few minutes).

Species with mass signatures at m/z 26, 27, 38, 39, 41 and 52 are produced simultaneously with methane consumption (see Figure 68), showing a production of C2, C3 and C4 species. The timescales calculated for the species mentioned are given in Table 19.

Table 19: Production time scales

m/z gas flow	26	27	38	39	41	52
10 sccm	500 ± 10 s	515 ± 30 s	645 ± 120 s	490 ± 60 s	705 ± 50 s	990 ± 360 s
0.6 sccm	320 ± 20 s					

An increase of the timescale with the mass of the products is observed, in agreement with a sequential growth process. However, the overlapping of the fragments in the MS (see part 2 of Chapter III) does not allow explicit identification of those products. In order to relieve this indetermination, we accumulated the products in a cryogenic trap and analyzed the content by GC-MS.

V.3.3 Products identification (GC-MS)

The GC-MS analysis of products accumulated during 8 running hours of a 7 sccm experiment is shown on Figure 70. The species detected (C2 and C3 species plus two C4 (2-butene and ethane dinitrile) are in agreement with the results of the MID analysis. The major species detected are the C2 compounds such as ethane (C_2H_6), ethylene (C_2H_4) and acetylene (C_2H_2). The major C3 compounds detected are acetonitrile (CH_3CN), propane (C_3H_8) and propene (C_3H_6). Even if the number of detected species using cold trap – GC-MS is lower in APSIS than in PAMPRE, it has to be stressed out that these compounds are in agreement with the product detected in the cold trap on the PAMPRE experiment. All compounds detected in APSIS are also detected in PAMPRE. Moreover the main compounds detected in APSIS are also the predominant species in PAMPRE with the exception of HCN, which is the main

product identified in PAMPRE. HCN cannot be unambiguously detected probably due to co-elution of HCN with water. However due to the detection of a species at m/z 27 in mass spectrometry, it is probable that HCN is indeed formed in the APSIS reactor.

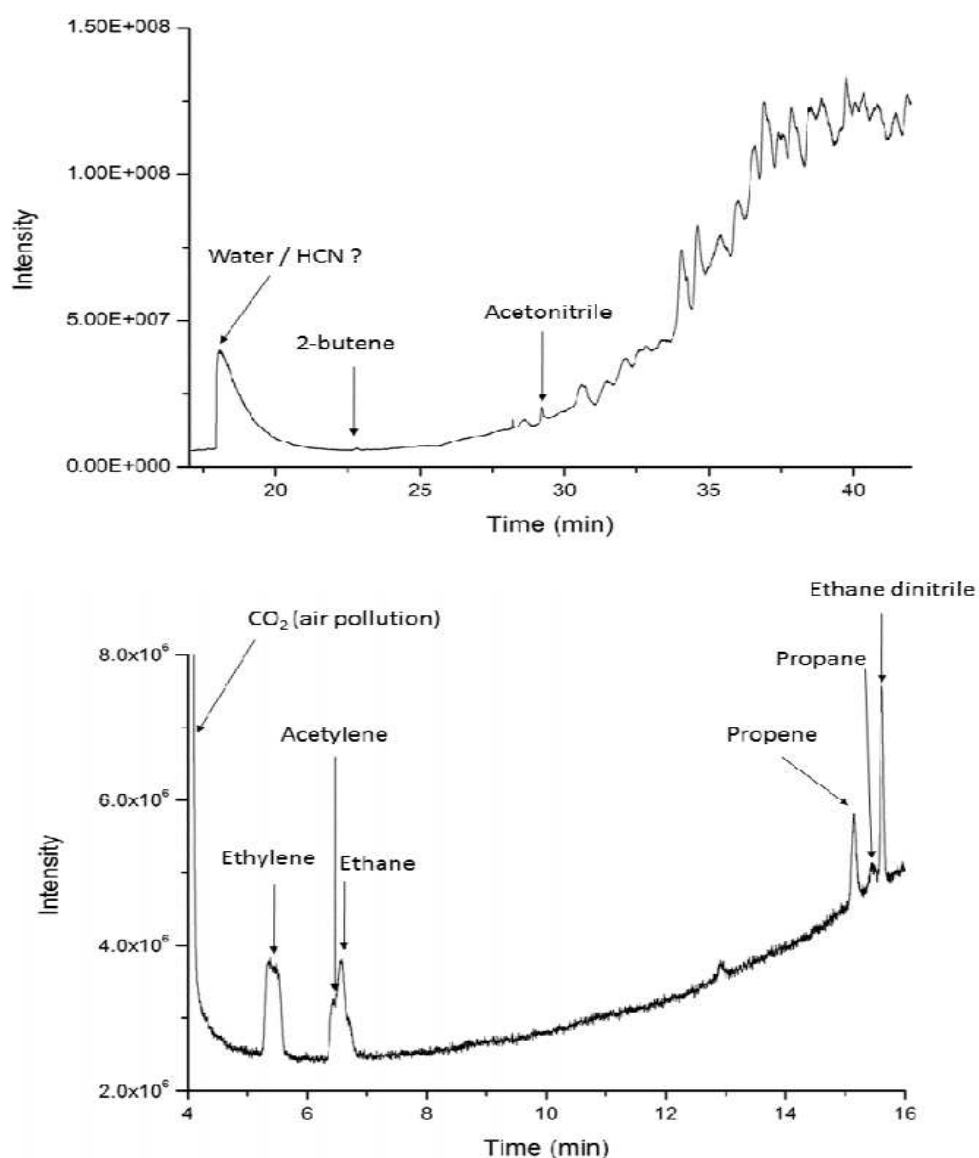


Figure 70: GC-MS of the content of the cold trap after an experiment with 7sccm gas flow

V.3.4 Pressure influence on mass spectra

As seen previously, the detection limit of the MS operated in nominal conditions is barely enough to detect C₂ and C₃ compounds. In order to improve dynamic range and the

sensitivity of the MS we performed a second series of experiments, as described in Table 17, with an increased pressure. By shortening the sampling capillary length the pressure in the ionization chamber of the MS increases from 10^{-6} mbar (low pressure experiments, LP) up to 10^{-4} mbar (high pressure experiments, HP). The effect of pressure increase is illustrated on Figure 71.

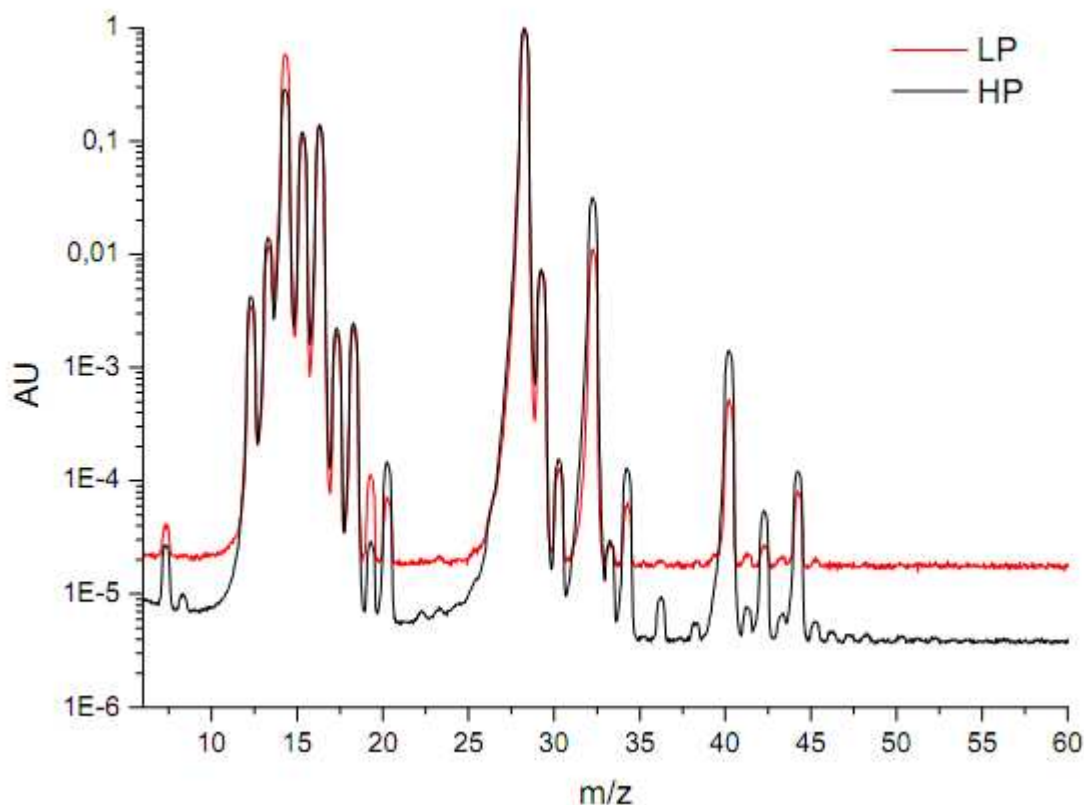


Figure 71: Comparison of the initial mass spectra (scan analog , photon flux off) for a similar 10 sccm experiment. Red curve is the spectrum with a low pressure in the MS and red spectrum is acquired with a high pressure in the MS

As visible in this figure, the baseline efficiently decreases from 2×10^{-5} down to 4×10^{-6} , which enables to detect low concentration products, previously non detectable. However, the increase of the pressure in the MS ionization chamber also has some unwanted effects. Figure 72 illustrates the effect of pressure on the cracking pattern of nitrogen (looking at the ratio between I_{14} and I_{28}).

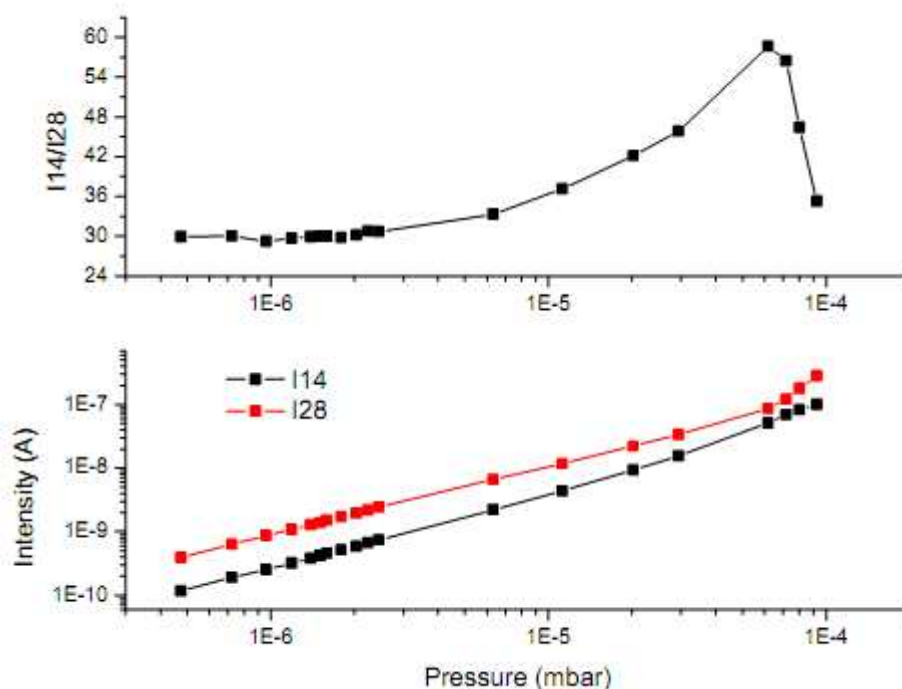


Figure 72: Evolution with the pressure of the cracking pattern of nitrogen (I14/I28 ratio, up) and of I14 and 28 (bottom). Intensities are recorded with a pure nitrogen flux in the MS.

The ratio between the two peaks is supposed to be independent of the pressure since cracking patterns are defined by the direct and the dissociative ionization pathways of the reaction between molecular nitrogen and electrons at 70 eV in the ionization chamber. As visible on Figure 72, although the ratio is constant for pressure in the MS below 6×10^{-6} mbar, a strong nonlinear behavior appears at higher pressures.

The operating instructions of the instrument recommends to work with pressures no larger than 10^{-5} mbar in the ion source with the Secondary Electron Multiplier as a detector, in spite of the possibility to use the filament up to a pressure of 10^{-4} mbar. Mao and Leck 1987 and Tilford 1994 reported that non-linear sensitivities can actually be observed at pressures in the range 10^{-5} – 10^{-4} mbar, possibly due to ion space charge effects. Some variations of cracking patterns of H_2 and H_2O have also been reported at high pressure by Breth et al. 1983. As visible in this figure, an evolution of the cracking pattern of N_2 can also be observed at pressures, below 10^{-5} mbar. We have checked that this effect does not depend on the gas temperature (temperature lowered from room temperature down to about 200 K), and that no

cross-sensitivity is observed by mixing nitrogen with a second gas like argon, helium or hydrogen.

The non-linear effects, detected at high MS pressures on the I_{14}/I_{28} signature, are certainly affecting the cracking patterns of other species and prevent us from any quantitative analysis. Nevertheless, in order to detect products with smaller concentrations in the scan analog MS configuration (see Analytical techniques section), high pressure condition in the mass spectrometer were used for the rest of the study (pressure of a few 10^{-5} mbar), as done also by Imanaka and Smith 2007, 2010.

V.3.5 Products identification (MS)

Figure 73 presents the different mass spectra (DISCO on-DISCO off) of experiments performed with gas flows of 0.6, 2, 7, and 10 sccm.

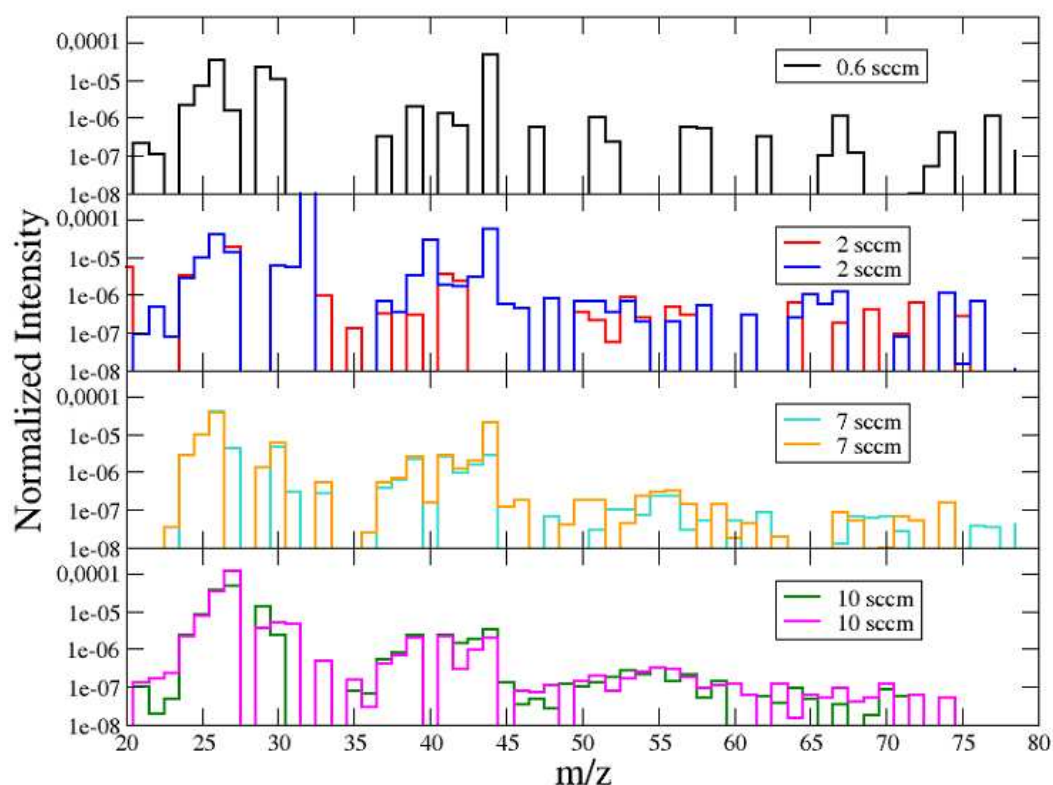


Figure 73: Differential mass spectra in the m/z [20-80] range for different experiments.

As visible on this figure, the repeatability of the experiments is much better for experiments performed with high gas flow (7 and 10 sccm) whereas the detection/identification of species is trickier for low gas flow rate (with exception of the C₂ cluster, around m/z 25, which is seen unambiguously in all spectra). This is probably due to the fact that a low influx induces a low pressure in the MS. As a consequence, the baseline of the signal is much higher (see Figure 71) and the signal-to-noise ratio lower in these conditions. The signal of products is then not strong enough to enhance a significant detection of the species. However, the use of higher gas flow rate (and thus higher pressure in the MS) allows the clear detection of C₃ and C₄ clusters and their quantification relatively to nitrogen. The C₂ are around 10^{-5} , C₃ at 10^{-6} and C₄ slightly higher than 10^{-7} times the concentration of N₂. This decrease of relative concentrations with the number of "heavy" (N or C) atoms is in agreement with both predictions (Dobrijevic and Dutour 2006) and observation (See Chapter III and Gautier et al. 2011).

V.4 Discussion

Figure 74 presents a comparison of several mass spectra of interest for the study of Titan's atmosphere in the m/z [20-60] range corresponding to C₂, C₃ and C₄ compounds. In addition to the APSIS spectrum, are presented:

- The neutral mass spectrum obtained with the PAMPRE plasma (Carrasco et al. 2012)
- The neutral mass spectrum from another synchrotron radiation experiment performed with photons of 60 nm wavelengths (Imanaka and Smith 2010)
- A measurement of Titan's atmosphere neutral mass spectrum obtained by the Ion and Neutral Mass Spectrometer (INMS) instrument onboard Cassini (Waite et al. 2007)

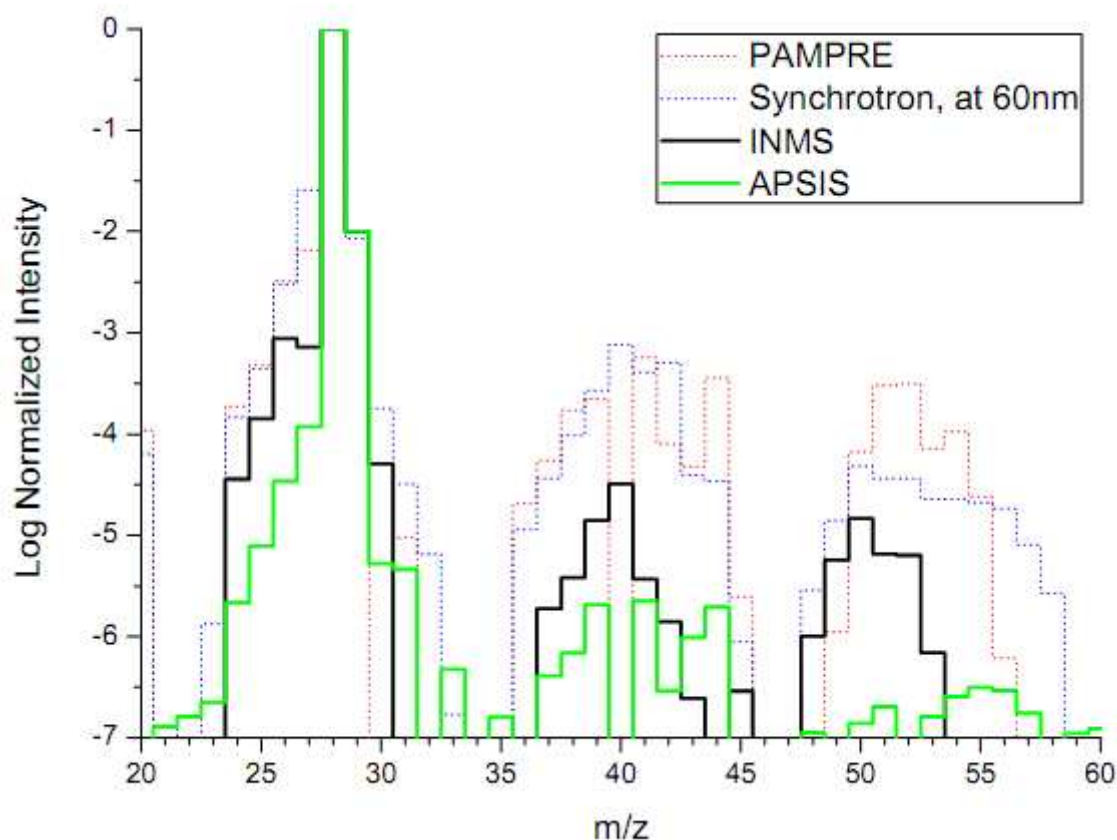


Figure 74: Comparison of the MS for different experiments. PAMPRE (red dot); Synchrotron irradiation at 60 nm (Imanaka and Smith 2007,2010; blue dots); Cassini-INMS instrument spectrum (black curve); and APSIS spectrum (green curve)

In the experimental simulations, the peaks at m/z 40 and 44 are often disturbed by a contribution of argon and carbon dioxide respectively due to residual air signature in the system. The productions at these masses should therefore not be further considered.

Even if the shapes of the clusters are relatively similar, the mixing ratio of PAMPRE and 60 nm synchrotron irradiation experiment are one order of magnitude higher than the spectrum recorder in Titan's atmosphere, and two orders higher than in the APSIS experiment.

For the first two cases, the difference could probably be linked to the higher energy deposition of these experiments. In the case of APSIS, even if the photon influx is higher than in Titan's atmosphere (Peng et al. 2013), the intensity of the products relatively to nitrogen is still lower than in INMS spectrum. This might be due to the residence time in the APSIS setup (a few

minutes) much lower than the 10^7 - 10^8 s residence time in Titan's atmosphere (Lebonnois et al. 2001).

Looking the relative concentrations among the products (i.e. the ratio between one product and another), some other discrepancies are visible. For the ratio between m/z 26 and m/z 27 peaks (that can be roughly seen as the ratio between HCN and C_2H_2), both Imanaka and Smith and PAMPRE plasma experiments present a significant increase of HCN relatively to C_2H_2 . These results are in opposition with the observation made with INMS that show a higher ratio for C_2H_2 , which is also observed in the APSIS experiment.

Other nitrogen-bearing species, CH_3CN m/z 41, and C_2N_2 m/z 52, are detected in Titan and in the APSIS and PAMPRE reactors, but not in the synchrotron experiment of Imanaka & Smith.

CH_3CN and C_2N_2 are both produced by reactions involving atomic nitrogen as a reactant:



and



respectively.

Nitrogen atoms are also efficiently adsorbed on the reactor walls. Therefore, we can suspect in the case of Imanaka & Smith that a lower pressure decreases the bimolecular reaction rate to benefit atomic nitrogen adsorption on the walls (M. Smith, personal communication).

V.5 Conclusion

We have seen in this chapter that an experiment conducted with Synchrotron irradiation is a complementary tool to plasma discharges in order to study the chemistry occurring in the atmosphere of Titan.

The comparison of the results obtained with APSIS and PAMPRE shows that the main products observed in both cases are similar emphasizing that even if the energy sources are

different, the chemistry occurring in the reactors are quite similar. The difference on the ratio of HCN and C₂H₂ also point out that the role of nitrogen chemistry in the case of plasma experiment is possibly over estimated. As a conclusion, in spite of lower photochemical production efficiency, the APSIS reactor seems to simulate Titan's neutral composition rather realistically.

Unfortunately, the slow timescales and the lower photochemical production efficiency of the APSIS reactor make that it is not yet possible to produce tholins in this setup, that might be done in the future by increasing the residence time in the reactor. Tholins produced in such reactor would be of high interest to study and to be compared with tholins produced in a plasma experiment.

General conclusion

The first part of this thesis was dedicated to the study of the gas phase in both the PAMPRE and Bochum experimental setup. The study of the stationary gas phase composition obtained with various initial methane concentrations from 1% to 10%, shows the enrichment of the gas phase – number of species detected and global quantity – with the input of methane.

Ammonia and methanimine are detected in the gas phase, in agreement with the detection by INMS in Titan's ionosphere. The production of such highly polymerizable species may be a first step toward tholins production. Two main opposite effects on aerosol production and growth can then be inferred. The first one is the organic growth process by co-polymerization of imine species. The second one is the inhibiting effect due to atomic hydrogen on the aerosol production. This effect can be related to recent observations showing an efficient fixation of atomic hydrogen on laboratory aerosols made at the expense of the aerosol organic growth itself. This process could be in competition with the aerosol organic growth process.

In the gas phase, a large amount of nitriles in the trapped gas mixture has been found, as high as four times the amount of hydrocarbons for a gas mixture with low methane concentration. The main product detected is hydrogen cyanide which has also been detected in large amounts in Titan's atmosphere. I have also detected heavier nitriles such as ethanenitrile, propanenitrile and propenenitrile. These heavier nitriles, also detected in Titan's atmosphere, are assumed to be the major compounds in the reactive medium. An increase in the ratio between nitriles and hydrocarbons with the decrease of methane concentration in the reactor is also observed

Globally, the composition of the gas phase in my experiments is consistent with Titan's atmospheric composition. This tends to demonstrate that laboratory experiments, at least those allowing nitrogen dissociation, can be used complementarily to observational data in order to predict both the presence and possible concentrations of compounds which are not yet detected. On a larger scale, I have detected more than thirty compounds in the gas phase, which, for some of them, had never been detected in experimental simulations before but

were expected since they had been observed in Titan atmosphere. Heteroaromatic compounds have also been detected, supporting the hypothesis of PANH pathways for the growth of Titan's aerosols.

Unfortunately, the nitrile gas chemistry is still mostly unknown, and nitriles are often underrepresented in Titan atmospheric models, even though we know, both from observations and from computational models, that they could be present in large amounts on Titan.

In addition to the detection of molecules, I have been able to relatively quantify some of the unsaturated mono-nitriles present in the gas phase. The multipass FTIR setup on Bochum reactor allowed me to get an absolute quantification of both HCN and NH₃ in the reactor. On the experiments performed using a cold trap, and by doing relative quantification I can also propose **a power-law model for the concentration of radically saturated mono-nitriles, which is (with HCN normalized to 100%)** $[C_xH_{2x-1}N] = 100x^{-5}$ where x is the number of carbon atoms in the molecule. With this law, it is possible to estimate the concentration of heavy nitriles due to chemical production (no transport) knowing the concentration of the lighter nitriles.

The second part of my thesis is dedicated to the analysis of tholins. The chemical analyses provide a new insight on the exact composition of tholins and unveil the high complexity of this material, implying a statistical approach for the treatment of tholins mass spectra obtained with a high resolution mass spectrometer.

In addition to tholins analyses, a residue of neutral gases polymerization was also analyzed. This provided some information on the reactive pathways to tholins formation, emphasizing differences between a material produced by polymerization of neutral gases and a material (tholins) produced in the reactive plasma by processes including ionized and/or heterogeneous chemistry. The predominant molecules detected in tholins contain more nitrogen than the one detected in residue. We can assume that the main difference between both materials is the ion chemistry, involved in tholins formation but not in residue formation. This could mean that **this ion chemistry enforces nitrogen incorporation into tholins, compared to neutral chemistry that leads to molecules with lower N/C ratio.**

Tholins spectra display polymeric structures which are confirmed by the identification of several polymer families in the material. This **enhances the idea that tholins are co-polymer like materials**, probably not linear co-polymer but hyper branched co-polymer (Klee 2005). Nevertheless, **at high masses ($m/z > 300$), this material can be assimilated to an average ideal $(CH_{1.5}N_{0.5})_n$ polymer** as shown by the convergence of all the polymer families.

I also analyzed the infrared absorption properties of tholins. This work provides for the first time the wavenumber dependence of the linear absorption coefficient ε , from the far-IR (100 cm^{-1}) to the mid-IR (4000 cm^{-1}) range. I also show the way in which **the percentage of methane in the experiment directly impacts the spectrum of tholins in the mid-IR**. This influence is maximum on the amine bands at 3330 cm^{-1} and 3200 cm^{-1} , and also visible on the 2900 cm^{-1} pattern due to aliphatic methyl, and in the 2200 cm^{-1} - 2400 cm^{-1} and 1300 cm^{-1} - 1650 cm^{-1} ranges.

The tholins spectra were then compared with data derived from Cassini CIRS and VIMS observations. The 2900 cm^{-1} pattern is in relatively good agreement with the Cassini-VIMS spectra obtained in Titan atmosphere and possibly attributed to aerosols. The high intensity of these bands in PAMPRE tholins spectra supports the hypothesis that aerosols are the main contributors to the 2900 cm^{-1} ($3.4\text{ }\mu\text{m}$) absorption pattern in Titan's atmosphere. Comparing tholins spectrum with spectra obtained with CIRS in the far-IR frequency range, the two spectra are in good agreement with many absorption bands, especially at 1450 cm^{-1} , 1380 cm^{-1} , 515 cm^{-1} and 325 cm^{-1} , reinforcing the detection of these bands from CIRS. These comparison between laboratory tholins spectra and actual observations of Titan's atmospheric aerosols shows that, if not perfect, **the tholins produced in PAMPRE are good analogs of Titan's aerosols** and that their study can bring clues to understand the formation and properties of aerosols in Titan's atmosphere.

The last part of my thesis is dedicated to experiments performed with APSIS, a new photochemical reactor, used with Synchrotron light as energy source. For these experiments, we used a nitrogen-methane gas flow irradiated by a continuous 60-350 nm VUV beam provided by the DISCO line at SOLEIL Synchrotron radiation facility. The neutral photochemical products were monitored by mass spectrometry, showing a time-scale of about 15 min, and a measurable production of species with two up to four (probably five) heavy

GENERAL CONCLUSION

atoms. The C₂ hydrocarbons are by far the major products, but nitrogen bearing species such as HCN, CH₃CN and C₂N₂ were also detected, in agreement with Cassini's INMS observations at Titan. Results are compared with those obtained by plasma experiment and with the in-situ measurements of the INMS mass spectrometer instrument onboard Cassini probing the neutral content of Titan upper atmosphere. In spite of lower photochemical production efficiency and different environmental conditions, the APSIS reactor seems to simulate Titan's neutral composition rather well. Nevertheless, with the objective to form solid particles with this setup, its production efficiency should be improved in the future by increasing the residence time of the gas in the reactor.

The main conclusions of this thesis can be summarized as in Table 20.

Table 20: Main results of this thesis

	Gas Phase	Solid Phase
Major products	N-Bearing molecules (Main gas product = HCN)	N-Bearing molecules
Products diversity	Wide (HCN <1% of the total carbon amount)	Wide (~15.000 species detected)
Quantification	HCN ~ 90 ppm NH ₃ ~15 ppm	Linear absorption coefficient (ε) => study of the variation of the IR spectra when %CH ₄ increases: <ul style="list-style-type: none"> - Amine bands decrease - Aliphatic carbon increase
Comparison to Cassini	Nitriles quantification power law:	relative IR spectra in agreement: VIMS: 2900 cm ⁻¹ (aliphatic

GENERAL CONCLUSION

	$[C_xH_{2x-1}N]=[HCN].x^{-5}$	carbon)
		CIRS: 1480 – 1350 (aliphatic carbon)
		515 and 325 cm^{-1} (unidentified)
Detection limits	Heavier detected compounds: m/z ~130	Lighter detected compounds: m/z ~60
Initiation processes	<ul style="list-style-type: none"> - Ionic chemistry increases Nitrogen incorporation - Gas-Solid transition probably occurring at a few tens of amu (m/z ~100) 	

The working perspective following my thesis could be focused on three main aspects:

First the detection and characterization of heavy gases (5 – 10 carbon or nitrogen atoms) in the experiments. Indeed, these gases are still poorly constrained but are probably the first step for aerosols construction. Also their study would help to locate the exact transition between the gas phase and the solid phase. Indeed one striking point when looking at the data presented in this thesis, is that no gaseous compounds are detected above m/z ~150, whereas the compounds detected in the solid phase start roughly at m/z 60-70. **The gas-solid transition could then be located around m/z 100, much lower than the several hundreds of amu often admitted in the literature.**

The second investigation should be on identification of a few key molecules in tholins. Indeed high resolution mass spectrometry provides the formula of the compounds but not their structure. The identification of a few molecules has been done on the residue using comparison between orbitrap measurements and Gas Chromatographic ones. The same study on tholins is currently done in collaboration with ICSN and should provide an unambiguous detection of nitrogen-bearing molecules predominant in tholins composition.

GENERAL CONCLUSION

This brings me to the last point, which is the study of the nitrogen pathways on Titan's aerosols formation. Unfortunately the structural basis of Titan's aerosols remains unknown because no instrument onboard Cassini provides precise chemical information on the aerosol composition. The only ACP instrument of the Huygens probe provides qualitative analysis of the global chemical content of the aerosols in Titan's atmosphere. It used pyrolysis to analyze the refractory nucleus of aerosols during its descent through Titan's atmosphere. The major pyrolysis products were HCN and NH₃ showing that Titan's aerosols are in fact very nitrogen-rich, which excludes the previously commonly suggested theory that these aerosols are derived from polycyclic aromatic hydrocarbons (PAHs). PAMPRE tholins structure studied in Chapter IV of this thesis confirms an important contribution of nitrogen in the aerosols composition as in Titan's aerosols; and its central role in the unsaturated component of tholins.

Nevertheless, a few studies on Titan's atmosphere and on pure methane and CH₄-N₂ plasmas emphasize a chemical growth carried by hydrocarbons (through ionic or neutral processes) which could even been scavenged in the presence of nitrogen.

Those two hydrocarbon and nitrogenous pathways are not exclusive and possibly both participate to the chemical blocks constitutive of Titan's aerosols. Nevertheless, it would be hazardous to reduce organic aerosol formation in the Solar System to the only PAH theory just because the nitrogen chemistry is far from being understood. It has to be pointed out that all the studies performed in this thesis confirms **the importance of N-bearing compounds for the production of tholins**. Efforts on this original PANH chemistry should be given in the future and could impact larger scales than the specific Titan's aerosols, especially knowing that these molecules including nitrogen are interesting in astrobiology as well since they are known for their reactivity and as precursor of amino acids.

List of publications related to this thesis

Peer-reviewed publications:

1. **Gautier, T.**, Carrasco, N., Buch, A., Szopa, C., Sciamma-O'Brien, E., Cernogora, G., *Nitrile gas chemistry in Titan's atmosphere*, Icarus 213 (2011) 625-635.
2. **Gautier, T.**, Carrasco, N., Mahjoub, A., Vinatier, S., Giuliani, A., Szopa, C., Anderson, C. M., Correia, J.-J., Dumas, P., Cernogora, G., *Mid- and far-infrared absorption spectroscopy of Titan's aerosols analogues*, Icarus 221 (2012) 320-327.
3. Carrasco, N., **Gautier, T.**, Es-sebbar, E.-t., Pernot, P., Cernogora, G., *Volatile products controlling Titan's tholins production*, Icarus 219 (2012) 230-240.
4. Mahjoub, A., Carrasco, N., Dahoo, P. R., **Gautier, T.**, Szopa, C., Cernogora, G., *Influence of methane concentration on the optical indices of Titan's aerosols analogues*, Icarus 221 (2012) 670-677.
5. Peng, Z., **Gautier, T.**, Carrasco, N., Pernot, P., Giuliani, A., Mahjoub, A., Correia, J. J., Buch, A., Bénilan, Y., Szopa, C., Cernogora, G., *Titan's atmosphere simulation experiment using continuum UV-VUV synchrotron radiation*, Journal of Geophysical Research: Planets (2013)
6. Hadamcik, E., Renard, J.-B., Mahjoub, A., **Gautier, T.**, Carrasco, N., Cernogora, G., Szopa, C., *Optical properties of analogs of Titan's aerosols produced by dusty plasma*. Earth, Planets and Space, accepted
7. **Gautier, T.**, Carrasco, N., Schmitz Afonso, I., Touboul, D., Szopa, C., Buch, A., Pernot, P., *Nitrogen incorporation in Titan's tholins inferred from statistical approach on high resolution orbitrap mass spectrometry*, submitted to *Geochimica et Cosmochimica acta*(2013)
8. Mahjoub, A., Carrasco, N., Dahoo P.R., Fleury, B., **Gautier, T.**, Cernogora, G., *Effect of temperature on optical indices of organic materials produced by N₂-CH₄ RF plasma*. Submitted to *Plasma Process and Polymers*
9. **Gautier T.**, Stefanovic I., Carrasco N., Sikimic B., Cernogora G. and Winter J., *Methane conversion in N₂-CH₄ RF discharge*. Submitted to *Plasma Process and Polymers*

Other publications:

10. **Gautier, T.**, Z. Peng, A. Giuliani, N. Carrasco, G. Cernogora, A. Mahjoub, J.-J. Correia, C. Szopa, P. Pernot, A. Buch and Y. Benilan (2013). *Photochemistry simulation of planetary atmosphere using synchrotron radiation at soleil. Application to Titan's atmosphere*. EAS Publications Series, 58, pp 199-203.
11. **Gautier, T.**, N. Carrasco, A. Mahjoub, I. Stefanovic, C. Szopa, G. Cernogora, E. Hadamcik and J. Winter. *Use of the linear absorption coefficient for absolute comparison of plasma films in the mid-IR range*. *Problems of Atomic Science and Technology* 83(1) (2013) 168-170.

Table of figures

Table 1: Comparaison des différents montages expérimentaux utilisés pour cette thèse	8
Figure 1: Quantification relative des mono-nitriles saturés. Les points de couleurs correspondent aux données expérimentales, les diamants et triangles vides aux observations d'INMS, et les triangles et diamants plein aux sortie de modèle photochimique de l'atmosphère de Titan.....	10
Figure 2: Représentation schématique des différentes reconstructions des spectres de masse. Une bonne concordance correspond à un cercle petit et sombre (voir le corps de la thèse pour de plus amples explications).	12
Figure 3: Comparaison des spectres IR de tholins produits avec différents pourcentage de méthane	13
Figure 4: Comparaison des spectres de tholins (noir) et des observations de l'atmosphère de Titan par CIRS entre 50 et 1500 cm^{-1}	13
Table 2: Principaux résultats de cette thèse.....	14
Figure 5: Composite mass spectra for neutrals (top) and ions (bottom) based on Cassini INMS data (black line) acquired during 17 flybys of Titan ~1000 km. Products signaled above the neutral spectrum are the one used for the mass deconvolution (red dots). From Waite et al. 2007.....	4
Figure 6: Masse/charge spectrum of negatively charged ions taken at 1015 km during flyby with the CAPS instrument (black line), and model outputs for different altitudes (color lines). From Lavvas et al. 2013	5
Figure 7: Proposed main step of aerosols formation in Titan's high atmosphere. From Waite et al. 2007	6
Figure 8: Observation of the 3.4 μm feature in Titan's (black) and Saturn's (red) atmospheres. The blue dashed line represent the CH_4 band at 3.3 μm modeled for 1.6% of CH_4 . From Bellucci et al. 09.....	7
Figure 9: Titan's aerosols spectrum (15°S, ~80 km) in the far-IR. From Vinatier et al. 2010, Anderson & Samuelson 2011, Anderson, private communication.	8

TABLE OF FIGURES

Figure 10: Mass spectrum of the gas resulting from pyrolysis of Titan's aerosols sample at 600°C. From Israel et al. 2005.	8
Figure 11: Titan's atmosphere temperature profile determined by HASI onboard Huygens. From Fulchignoni et al. 2005	10
Figure 12: CH ₄ mixing ratio in the low atmosphere from GC-MS measurements. From Niemann et al. 2005	10
Figure 13: Comparison of IR spectra produced by plasma discharge in CH ₄ /N ₂ 90/10 gas mixture at different pressures. From Imanaka et al. 2004. The main bonding absorption area are reported on the spectra.....	13
Figure 14: PAMPRE experimental setup and diagnoses.....	18
Figure 15: Emission spectrum obtained from 475 to 828 nm for a 95:5 N ₂ /CH ₄ plasma discharge with 5% Ar as actinometer.....	22
Figure 16: Sketch of FTIR setup on the PAMPRE reactor, seen from above.....	23
Figure 17: Scheme of the Bochum plasma reactor, seen from above	24
Figure 18: Energy spectra of APSIS and solar spectrum at the top of Titan's atmosphere. From Peng et al. 2013	27
Figure 19: Scheme of the APSIS reactor	28
Figure 20: Scheme of principle of the orbitrap electrodes. The two electrodes are the cylindrical part in the center of the chamber and the one surrounding the chamber. Scheme from ThermoScientific LTQ-Orbitrap documentation.....	33
Figure 21: Picture of tholins produced in the PAMPRE experiment with different methane concentration in percentage of CH ₄ in N ₂ . (Credits: Pascal Pernot).....	35
Figure 22: Residue polymerization when the cold trap is warmed up from liquid nitrogen temperature to the room temperature	36
Table 3: Advantages and disadvantages of the diagnoses used for this thesis.....	36
Table 4: Comparison of the experimental setup used for this thesis.....	38
Figure 23: Black: Blank mass spectrum of the mass spectrometer only (no connection to PAMPRE). Red: Initial mass spectrum (plasma off) obtained with a N ₂ -CH ₄ gas mixture with 5% of methane.....	41
Figure 24: Mass spectrum of a CH ₄ -N ₂ 10-90% gas mixture plasma off (black) and on (red).....	42
Figure 25: Evolution of H _β and Ar (811.5 nm) lines intensities with the percentage of methane in nitrogen.	43

TABLE OF FIGURES

Figure 26: Evolution of atomic hydrogen density with % CH ₄	44
Figure 27: (Top) Hydrogen production (corresponding to the difference between the stationary and the initial intensities of the m/z=2 peak) according to the initial methane percentage. (Bottom) according to the methane consumption (difference between stationary and initial intensities of the peak at m/z=15).....	45
Figure 28: Evolution of significant peaks detected, according to the initial methane amount. Reported uncertainties are 2 σ calculated on four repetitions of each spectrum and two experiments per methane condition.....	47
Figure 29: Differential mass spectra (stationary state - initial spectrum) for initial gas mixtures of 1% (black), 5% (blue) and 1°% (red) of methane in the initial gas mixture.....	48
Figure 30: Ratio I ₁₇ /I ₁₈ as a function of %CH ₄ , plasma on (red) and plasma off (black)	50
Figure 31: Evolution of the ratio between the increases of m/z 44 and m/z 29 when the plasma is ON. The stable value of about 2 for CH ₄ [0] concentration larger than 2% is in agreement with a co-evolution of fragments intensities for propane. However, the larger value of this ratio for 1% initial methane concentration indicated the additional contribution of methanimine at m/z 29.....	52
Figure 32: Evolution of the total gas pressure in the cold trap after warming up to room temperature (red dots) and of the carbon gas to solid conversion yield (blue triangles, adapted from Sciamma-O'Brien et al. 2010) as a function of CH ₄ concentration.	56
Figure 33: Chromatogram of the cold trap content for an experiment performed with 1% of CH ₄	57
Figure 34: Chromatogram of the cold trap content for an experiment performed with 4% of CH ₄	57
Figure 35: Chromatogram of the cold trap content for an experiment performed with 10% of CH ₄	58
Table 5: List of gaseous compounds detected in our experiment, in Titan's atmosphere and in other laboratory experiments. a: Cui et al., 2009; Robertson et al., 2009; Vuitton et al., 2007 ; b : Bernard et al., 2003; c : Ramírez et al., 2001; Ramírez et al., 2005; d : Tran et al., 2005..	59
Figure 36: Experimental (up) and theoretical (down) spectra of tetrazolo[1,5-b]pyridazine. The topological scheme of this compound is given in the upper spectrum	62

TABLE OF FIGURES

Table 6: Evolution of ρ , the ratio of nitrogen bearing compounds versus hydrocarbon compounds detected in our experiment as a function of methane concentration of the gas mixture injected in the plasma reactor	63
Table 7: Calculated ionization cross section of the nitriles. The calculation is performed using the formula proposed in Fitch and Sauter (1983).....	69
Figure 37: Relative concentration of the nitriles as a function of carbon in the molecules. The red, green and blue dots represent the experimental data from this work, for experiments with 1%, 4% and 10% of methane in the reactor, respectively. The blue line is the empirical power law model ($y=ax^b$) associated to these experimental data. The dot-dashed line represents the model value plus 30% ($a'=a+30\%$; $b'=b-30\%$) while the dashed line is the model value minus 30% ($a''=a-30\%$; $b''=b+30\%$). The empty black diamonds and triangles are observational data (Vuitton et al. 2007 and reference herein), at 1100 and 300km from Titan's ground, respectively. The full diamonds and triangles are data from computer modeling (Lavvas et al. 2008) at 1100 and 300 km from Titan's ground, respectively.....	70
Figure 38: Methane (I_{15}/I_{28} and I_{16}/I_{28}) consumption when triggering on the plasma seen by MID MS. The dashed line is the instant time of plasma ignition.....	75
Figure 39: Time dependence of the MS signal normalized to m/Z 28 for different species. The vertical dashed line represent the instant when plasma is triggered on.	76
Figure 40: Measurement (green dots) and exponential fit (red dashed curve) of the decrease of methane peak when plasma is triggered on. Time is set to 0 for the plasma ignition.....	77
Figure 41: Neutral Mass spectrum of a N ₂ -CH ₄ 90-10 plasma in the Bochum reactor, plasma off (blue) and on (green)	78
Figure 42: Bargraph relative mass spectrum (I/I_{blank}) of a 10% methane experiment	79
Table 8: List of the main peaks detected in the relative mass spectrum and their possible attribution. Possible attribution is not exhaustive but corresponds to the main products expected according to the analysis of the gas phase in PAMPRE both by MS and cryogenic trapping plus GC-MS.	81
Figure 43: in-situ Infrared spectrum of a 90/10 N ₂ /CH ₄ experiment. The reference spectrum is taken with gases in the reactor before plasma ignition. Species consumed appear in negative and products in positive compared to the A=0 line.....	82
Figure 44: Reference spectrum of CH ₄ in gas phase in the 1000-5000 cm ⁻¹ wavenumber range measured at room temperature (from the GEISA database)	83

TABLE OF FIGURES

Figure 45: Close up of Fig.29 in the 600 - 1600 cm^{-1} wavenumber range.....	84
Figure 46: Close up of Fig.29 in the 1600 - 2600 cm^{-1} wavenumber range.....	85
Figure 47: Close up of Fig.29 in the 2600 - 3600 cm^{-1} wavenumber range.....	85
Table 9: Calculation of absolute concentration for HCN and NH_3	87
Table 10: Measured (from FTIR) and inferred (from MS + calculation) concentrations of HCN, CH_3CN and $\text{CH}_3\text{CH}_2\text{CN}$	87
Figure 48: Tholins 5% mass spectrum acquired with LCT-Premier ESI-TOF mass spectrometer. Close up shows the inter-clusters spacing of 13.5u and 74u in the 750-1350 mass range	93
Figure 49: Orbitrap mass spectra in positive ion mode of tholins samples produced with 1%, 2%, 5% and 10% of methane. Spectra at 2% and 10% are adapted from Pernot et al. 2010..	96
Figure 50: Close up of Fig. 5 on the peaks around m/z 127 for each tholins sample.....	98
Figure 51: Van Krevelen representation of tholins 1%, tholins 2%, tholins 5% and tholins 10% samples. Convergence areas are emphasized by red circles.	99
Figure 52: 3D Van Krevelen diagram of tholins 5%. Colors represent families identified within the HCN/CH_2 monomers basis (cf. part 5)	100
Figure 53: Van Krevelen diagram of tholins 5% analyzed in positive (green dots) and negative (red dots) ionization modes.	101
Figure 54: Orbitrap mass spectra of tholins 5% (up) and residue 5% (down)	102
Figure 55: Close up of Figure 54 on the 120-130 m/z range. Textbox indicate formula attribution for the predominant present in the detected clusters.	103
Table 11: Family representation for different bases.....	105
Table 12: Schematic representation of bases. The radii of the dots represent the size of the distribution (i.e. number of families needed to describe the polymer). The colors of the dots are linked to the eccentricity of the distribution: the darkest dots are, the most centered on 0 the distribution is.....	106
Figure 56: Chromatogram of direct analysis of residue (4%) dissolved in Cl_2CH_2 in the 2-20 min retention time range. Identified peaks are labelled.	109
Figure 57: Chromatogram of direct analysis of residue (4%) dissolved in Cl_2CH_2 in the 20-40 min retention time range. Identified peaks are labeled.	110
Table 13: List of molecules detected using direct injection and their formula	111
Table 14: List of detected molecules in residue derivatized	112

TABLE OF FIGURES

Figure 58: Comparative ATR spectra of tholins produced in PAMPRE (red) and in Bochum reactor (blue). Both spectra were normalized.	117
Figure 59: Gaussian deconvolution of aliphatic carbon bands of tholins produced in PAMPRE with 10% of methane.....	118
Figure 60: Gaussian deconvolution of aliphatic carbon bands of tholins produced in Bochum reactor with 10% of methane.	118
Table 15: Ratios between CH ₃ and CH ₂ bands in IR spectra of tholins produced in PAMPRE and Bochum reactor	119
Figure 61: Reconstructed experimental spectrum of tholins produced in PAMPRE with 5% of methane before calibration of the sample thickness.....	122
Table 16: Experimental conditions and thickness of the different studied samples	123
Figure 62: Evolution of ε from the far- to the mid-Infrared for tholins produced in PAMPRE with 5% of methane. Average spectrum is given by the red curve. Pink envelopes indicate this standard deviation (1σ) of the spectra, representing the variation of the spectrum from one measure to another on the same sample. Possible attributions are given for major bands of the spectrum. n-X and c-X mean that the functional group X is attached to respectively an aliphatic or an aromatic skeleton.....	124
Figure 63: Absorption spectra of tholins in the mid-Infrared with different initial CH ₄ concentrations in the gas mixture (1% in blue, 2% in green, 5% in red and 10% in cyan). ..	126
Figure 64 : Absorbance spectrum from far-IR to mid-IR of PAMPRE tholins made with 5% of CH ₄ (black curve) compared to Quirico et al. 2008 tholins spectra (extracted from Khare et al. 1984 tholins, blue), Cassini-CIRS observations (red line, from Anderson and Samuelson 2011 and Vinatier et al. 2011) and Cassini-VIMS spectra (red dots, from Kim et al. 2011). ..	129
Figure 65: Close up of Fig. 57 on the 2900 cm ⁻¹ pattern. Black line represents our tholins 5% spectrum. Red dots are the spectrum derived from observations with Cassini-VIMS attributed to Titan's aerosols (extracted from Kim et al. 2011). The blue line represent tholins spectra reconstituted from Khare et al. 1984 data (from Quirico et al. 2008).....	130
Figure 66: Infrared spectra of toluene (red), 2-methylpyridine (blue) and 3-methylpyridine (green) extracted from the NIST database.	131
Figure 67: Close up of Fig.57 in the far-IR range. Black line represents our tholins 5% spectrum. Titan's aerosols spectra derived from observations with Cassini CIRS (Anderson	

TABLE OF FIGURES

and Samuelson 2011; Vinatier et al. 2011) are plotted in red. The blue line represents tholins spectra reconstituted from Khare et al. 1984 data (from Quirico et al. 2008).....	132
Table 17: List of experiments performed on APSIS	136
Figure 68: Evolution of I_{15}/I_{28} (methane/nitrogen) and I_{26}/I_{28} (acetylene/nitrogen) ratios in an experiment performed with 0.6 sccm total gas flow. The dashed line represent the starting time of the photo-irradiation	139
Table 18: ΔCH_4 and their standard deviation calculated for several experimental conditions	140
Figure 69: Temporal evolution of $\log(I_{ss}-I_t)$ for m/z 26, 27, 38, 39, 41 and 52. Experiment performed at 10 sccm.	141
Table 19: Production time scales	142
Figure 70: GC-MS of the content of the cold trap after an experiment with 7sccm gas flow	143
Figure 71: Comparison of the initial mass spectra (scan analog , photon flux off) for a similar 10 sccm experiment. Red curve is the spectrum with a low pressure in the MS and red spectrum is acquired with a high pressure in the MS.....	144
Figure 72: Evolution with the pressure of the cracking pattern of nitrogen (I_{14}/I_{28} ratio, up) and of I_{14} and 28 (bottom). Intensities are recorded with a pure nitrogen flux in the MS....	145
Figure 73: Differential mass spectra in the m/z [20-80] range for different experiments.....	146
Figure 74: Comparison of the MS for different experiments. PAMPRE (red dot); Synchrotron irradiation at 60 nm (Imanaka and Smith 2007,2010; blue dots); Cassini-INMS instrument spectrum (black curve); and APSIS spectrum (green curve)	148
Table 20: Main results of this thesis.....	154

TABLE OF FIGURES

References

- Alcouffe, G., Production d'équivalent d'aérosols de Titan par plasma Radio-Fréquence. UVSQ, 2010.
- Alcouffe, G., Cavarroc, M., Cernogora, G., Ouni, F., Jolly, A., Boufendi, L., Szopa, C., Capacitively coupled plasma used to simulate Titan's atmospheric chemistry, *Plasma Sources Science and Technology* 19 (2010) 015008.
- Anderson, C. M., Samuelson, R. E., Titan's aerosol and stratospheric ice opacities between 18 and 500 [μm]: Vertical and spectral characteristics from Cassini CIRS, *Icarus* In Press, Corrected Proof (2011) In press.
- Balucani, N., Bergeat, A., Cartechini, L., Volpi, G. G., Casavecchia, P., Skouteris, D., Rosi, M., Combined Crossed Molecular Beam and Theoretical Studies of the $N(^2D) + CH_4$ Reaction and Implications for Atmospheric Models of Titan†, *The Journal of Physical Chemistry A* 113 (2009) 11138-11152.
- Balucani, N., Cartechini, L., Alagia, M., Casavecchia, P., Volpi, G. G., Observation of Nitrogen-Bearing Organic Molecules from Reactions of Nitrogen Atoms with Hydrocarbons: A Crossed Beam Study of $N(^2D) +$ Ethylene, *The Journal of Physical Chemistry A* 104 (2000) 5655-5659.
- Balucani, N., Leonori, F., Petrucci, R., Stazi, M., Skouteris, D., Rosi, M., Casavecchia, P., Formation of nitriles and imines in the atmosphere of Titan: combined crossed-beam and theoretical studies on the reaction dynamics of excited nitrogen atoms $N(^2D)$ with ethane, *Faraday Discussion* 147 (2010).
- Bar-Nun, A., Dimitrov, V., Tomasko, M., Titan's aerosols: Comparison between our model and DISR findings, *Planetary and Space Science* 56 (2008) 708-714.
- Bellucci, A., Sicarusdy, B., Drossart, P., Rannou, P., Nicholson, P. D., Hedman, M., Baines, K. H., Burrati, B., Titan solar occultation observed by Cassini/VIMS: Gas absorption and constraints on aerosol composition, *Icarus* 201 (2009) 198-216.
- Bernard, J.-M., Coll, P., Coustenis, A., Raulin, F., Experimental simulation of Titan's atmosphere: Detection of ammonia and ethylene oxide, *Planetary and Space Science* 51 (2003) 1003-1011.

REFERENCES

- Bernard, J. M., Quirico, E., Brissaud, O., Montagnac, G., Reynard, B., McMillan, P., Coll, P., Nguyen, M. J., Raulin, F., Schmitt, B., Reflectance spectra and chemical structure of Titan's tholins: Application to the analysis of Cassini–Huygens observations, *Icarus* 185 (2006) 301-307.
- Berndt, J., Kovačević, E., Stefanović, I., Stepanović, O., Hong, S. H., Boufendi, L., Winter, J., Some Aspects of Reactive Complex Plasmas, *CoPP* 49 (2009) 107-133.
- Bhat, N. V., Upadhyay, D. J., Adhesion Aspects of Plasma Polymerized Acetonitrile and Acrylonitrile on Polypropylene Surface, *Plasmas and Polymers* 8 (2003) 99-118.
- Bouchoule, A., *Dusty Plasmas: Physics, Chemistry, and Technological Impact in Plasma Processing*, Wiley, 1999.
- Boufendi, L., Bouchoule, A., Particle nucleation and growth in a low-pressure argon-silane discharge, *Plasma Sources Sci. Technol.* 3 (1994) 262.
- Breth, A., Dobrozemsky, R., Schwarzsinger, G., Some basic problems in the deconvolution of gas—analytic mass spectra, *International journal of Mass Spectrometry and Ion Physics* 48 (1983) 3-6.
- Brown, R. H., Baines, K. H., Bellucci, G., Bibring, J. P., Buratti, B. J., Capaccioni, F., Cerroni, P., Clark, R. N., Coradini, A., Cruikshank, D. P., Drossart, P., Formisano, V., Jaumann, R., Langevin, Y., Matson, D. L., McCord, T. B., Mennella, V., Miller, E., Nelson, R. M., Nicholson, P. D., Scurry, B., Sotin, C., The Cassini Visual and Infrared Mapping Spectrometer (VIMS) Investigation, in: C. Russell, (Ed.), *The Cassini-Huygens Mission*. Springer Netherlands, 2004, pp. 111-168.
- Buch, A., Sternberg, R., Szopa, C., Freissinet, C., Garnier, C., Bekri, E. J., Rodier, C., Navarro-González, R., Raulin, F., Cabane, M., Stambouli, M., Glavin, D. P., Mahaffy, P. R., Development of a gas chromatography compatible Sample Processing System (SPS) for the in-situ analysis of refractory organic matter in martian soil: preliminary results, *Advances in Space Research* 43 (2009) 143-151.
- Butterfield, M. T., Yu, T., Lin, M. C., Kinetics of CN reactions with allene, butadiene, propylene and acrylonitrile, *Chemical Physics* 169 (1993) 129-134.
- Cabane, M., Rannou, P., Chassefière, E., Israel, G., Fractal aggregates in Titan's atmosphere, *Planetary and Space Science* 41 (1993) 257-267.

REFERENCES

- Cable, M. L., Hörst, S. M., Hodyss, R., Beauchamp, P. M., Smith, M. A., Willis, P. A., Titan Tholins: Simulating Titan Organic Chemistry in the Cassini-Huygens Era, *Chemical Reviews* 112 (2011) 1882-1909.
- Callahan, M. P., Smith, K. E., Cleaves, H. J., Ruzicka, J., Stern, J. C., Glavin, D. P., House, C. H., Dworkin, J. P., Carbonaceous meteorites contain a wide range of extraterrestrial nucleobases, *Proceedings of the National Academy of Sciences Early Edition* (2011).
- Carey, F., Sundberg, R. J., *Advanced Organic Chemistry*, 5th ed., Springer, 2007.
- Carrasco, N., Gautier, T., Es-sebbar, E.-t., Pernot, P., Cernogora, G., Volatile products *controlling Titan's tholins production*, *Icarus* 219 (2012) 230-240.
- Carrasco, N., Schmitz-Afonso, I., Bonnet, J.-Y., Quirico, E., Thissen, R., Dutuit, O., Bagag, A., Laprévotte, O., Buch, A., Giulani, A., Adandé, G., Ouni, F., Hadamcik, E., Szopa, C., Cernogora, G., Characterization of Titan's Tholins: Solubility, Morphology and Molecular Structure Revisited, *Journal of Physical Chemistry A* 113 (2009) 11195-11203.
- Carty, D., Page, V. L., Sims, I. R., Smith, I. W. M., Low temperature rate coefficients for the reactions of CN and C₂H radicals with allene and methyl acetylene, *Chemical Physics Letters* 344 (2001) 310-316.
- Chan, C. M., Ko, T. M., Hiraoka, H., Polymer surface modification by plasmas and photons, *SurSR* 24 (1996) 1-54.
- Coates, A. J., Cray, F. J., Lewis, G. R., Young, D. T., Waite, J. H., Sittler, E. C., Discovery of heavy negative ions in Titan's ionosphere, *GeoRL* 34 (2007) L22103.
- Coll, P., Coscia, D., Smith, D., Gazeau, M.-C., Ramirez, S. I., Cernogora, G., Israel, G., Raulin, F., Experimental laboratory simulation of Titan's atmosphere: aerosols and gas phase, *Planet. Space Sci.* 47 (1999) 1331.
- Coll, P., Navarro-González, R., Szopa, C., Poch, O., Ramírez, S. I., Coscia, D., Raulin, F., Cabane, M., Buch, A., Israël, G., Can laboratory tholins mimic the chemistry producing Titan's aerosols? A review in light of ACP experimental results, *Planetary and Space Science* 77 (2013) 91-103.
- Comas i Sola, J., Observaciones des Satellites principaux de Jupiter et de Titan, *Astron. Nachr.* 179 (1908) 289-290.

REFERENCES

- Cottin, H., Bachir, S., Raulin, F., Gazeau, M.-C., Photodegradation of hexamethylenetetramine by VUV and its relevance for CN and HCN extended sources in comets, *Advances in Space Research* 30 (2002) 1481-1488.
- Coustenis, A., Bézard, B., Gautier, D., Marten, A., Samuelson, R., Titan's atmosphere from voyager infrared observations: III. Vertical distributions of hydrocarbons and nitriles near Titan's North Pole, *Icarus* 89 (1991) 152-167.
- Coustenis, A., Lellouch, E., SIlcarusdy, B., Roe, H., Earth-Based Perspective and Pre-Cassini-Huygens Knowledge of Titan, in: R. Brown, J.-P. Lebreton, J. H. Waite, (Eds.), *Titan from Cassini-Huygens*. Springer Netherlands, 2010, pp. 9-34.
- Cui, J., Yelle, R. V., Vuitton, V., Waite, J. H., Kasprzak, W. T., Gell, D. A., Niemann, H. B., Müller-Wodarg, I. C. F., Borggren, N., Fletcher, G. G., Patrick, E. L., Raaen, E., Magee, B. A., Analysis of Titan's neutral upper atmosphere from Cassini Ion Neutral Mass Spectrometer measurements, *Icarus* 200 (2009) 581-615.
- de Petris, G., Cartoni, A., Angelini, G., Ursini, O., Bottoni, A., Calvaresi, M., The N_3^+ Reactivity in Ionized Gases Containing Sulfur, Nitrogen, and Carbon Oxides, *ChemPhysChem* 7 (2006) 2105-2114.
- De Vanssay E, G. M. C. G. J. C., Raulin, F., Experimental simulation of Titan's organic chemistry at low temperature, *Planet. Space Sci.* 43 (1995) 25.
- Derenne, S., Coelho, C., Anquetil, C., Szopa, C., Rahman, A. S., McMillan, P. F., Corà, F., Pickard, C. J., Quirico, E., Bonhomme, C., New insights into the structure and chemistry of Titan's tholins via ^{13}C and ^{15}N solid state nuclear magnetic resonance spectroscopy, *Icarus* 221 (2012) 844-853.
- Deschenaux, C., Affolter, A., Magni, D., Ch, H., Fayet, P., Investigations of CH_4 , C_2H_2 and C_2H_4 dusty RF plasmas by means of FTIR absorption spectroscopy and mass spectrometry, *Journal of Physics D: Applied Physics* 32 (1999) 1876.
- Dobrijevic, M., Dutour, I., A random graphs model for the study of chemical complexity in planetary atmospheres, *Planetary and Space Science* 54 (2006) 287-295.
- Dumas, P., Polack, F., Lagarde, B., Chubar, O., Giorgetta, J. L., Lefrançois, S., Synchrotron infrared microscopy at the French Synchrotron Facility SOLEIL, *Infrared Physics & Technology* 49 (2006) 152-160.
- Esposito, L., Barth, C., Colwell, J., Lawrence, G., McClintock, W., Stewart, A. I., Uwe Keller, H., Korth, A., Lauche, H., Festou, M., Lane, A., Hansen, C., Maki, J., West,

REFERENCES

- R., Jahn, H., Reulke, R., Warlich, K., Shemansky, D., Yung, Y., The Cassini Ultraviolet Imaging Spectrograph Investigation, in: C. Russell, (Ed.), The Cassini-Huygens Mission. Springer Netherlands, 2004, pp. 299-361.
- Fitch, W. L., Sauter, A. D., Calculation of relative electron impact total ionization cross sections for organic molecules, *Analytical Chemistry* 55 (1983) 832-835.
- Flasar, F. M., Achterberg, R. K., Conrath, B. J., Gierasch, P. J., Kunde, V. G., Nixon, C. A., Bjoraker, G. L., Jennings, D. E., Romani, P. N., Simon-Miller, A. A., Bézard, B., Coustenis, A., Irwin, P. G. J., Teanby, N. A., Brasunas, J., Pearl, J. C., Segura, M. E., Carlson, R. C., Mamoutkine, A., Schinder, P. J., Barucci, A., Courtin, R., Fouchet, T., Gautier, D., Lellouch, E., Marten, A., Prangé, R., Vinatier, S., Strobel, D. F., Calcutt, S. B., Read, P. L., Taylor, F. W., Bowles, N., Samuelson, R. E., Orton, G. S., Spilker, L. J., Owen, T. C., Spencer, J. R., Showalter, M. R., Ferrari, C., Abbas, M. M., Raulin, F., Edgington, S., Ade, P., Wishnow, E. H., Titan's Atmospheric Temperatures, Winds, and Composition, *Science* 308 (2005) 975-978.
- Fleury, B., Carrasco, N., Gautier, T., Mahjoub, A., He, J., Szopa, C., Hadamcik, E., Buch, A., Cernogora, G., Influence of CO on the N₂-CH₄ Titan atmospheric reactivity, (In preparation).
- Freissinet, C., Buch, A., Sternberg, R., Szopa, C., Geffroy-Rodier, C., Jelinek, C., Stambouli, M., Search for evidence of life in space: Analysis of enantiomeric organic molecules by N,N-dimethylformamide dimethylacetal derivative dependant Gas Chromatography–Mass Spectrometry, *Journal of Chromatography A* 1217 (2010) 731-740.
- Fujii, T., Kareev, M., Diagnostic Studies of a CH₄/H₂ Microwave Plasma by Mass Spectrometry: *Ionic and Neutral Species*, *The Journal of Physical Chemistry A* 105 (2001) 4923-4927.
- Fujii, T., Norihisa, A., Analysis of N-containing Hydrocarbon Species Produced by a CH₄/N₂ Microwave Discharge: Simulation of Titan's Atmosphere, *The Astrophysical Journal* 519 (1999) 858.
- Fujiwara, H., Spectroscopic ellipsometry: principles and applications, Marusen, Tokyo, 2007.
- Fulchignoni, M., Ferri, F., Angrilli, F., Ball, A. J., Bar-Nun, A., Barucci, M. A., Bettanini, C., Bianchini, G., Borucki, W., Colombatti, G., Coradini, M., Coustenis, A., Debei, S., Falkner, P., Fanti, G., Flamini, E., Gaborit, V., Grard, R., Hamelin, M., Harri, A. M.,

REFERENCES

- Hathi, B., Jernej, I., Leese, M. R., Lehto, A., Lion Stoppato, P. F., Lopez-Moreno, J. J., Makinen, T., McDonnell, J. A. M., McKay, C. P., Molina-Cuberos, G., Neubauer, F. M., Pirronello, V., Rodrigo, R., Saggin, B., Schwingenschuh, K., Seiff, A., Simoes, F., Svedhem, H., Tokano, T., Towner, M. C., Trautner, R., Withers, P., Zarnecki, J. C., In situ measurements of the physical characteristics of Titan's environment, *Nature* 438 (2005) 785-791.
- Gautier, T., Carrasco, N., Buch, A., Szopa, C., Sciamma-O'Brien, E., Cernogora, G., Nitrile gas chemistry in Titan's *atmosphere*, *Icarus* 213 (2011) 625-635.
- Gautier, T., Carrasco, N., Mahjoub, A., Vinatier, S., Giuliani, A., Szopa, C., Anderson, C. M., Correia, J.-J., Dumas, P., Cernogora, G., Mid- and far-infrared absorption *spectroscopy of Titan's aerosols analogues*, *Icarus* 221 (2012) 320-327.
- Gautier, T., Carrasco, N., Schmitz-Afonso, I., Touboul, D., Szopa, C., Buch, A., Pernot, P., *Polymerization pathways toward Titan's aerosol analogues inferred from high resolution mass spectrometry*, *Geochimica et Cosmochimica acta* submitted (2013a).
- Gautier, T., Peng, Z., Giuliani, A., Carrasco, N., Cernogora, G., Mahjoub, A., Correia, J.-J., Szopa, C., Pernot, P., Buch, A., Benilan, Y., Photochemistry simulation of planetary atmosphere using synchrotron radiation at soleil. *Application to Titan's atmosphere*, European Astronomical Society Publications Series 58 (2013b) 199-203.
- Gautier, T., Carrasco, N., Mahjoub, A., Stefanovic, C., Szopa, G., Cernogora, E., Hadamcik and J. Winter. Use of the linear absorption coefficient for absolute comparison of plasma films in the mid-IR range. *Problems of Atomic Science and Technology* 83 (1) (2013c) 168-170.
- Gicquel, A., Chenevier, M., Hassouni, K., Tserepi, A., Dubus, M., Validation of actinometry for estimating relative hydrogen atom densities and electron energy evolution in plasma assisted diamond deposition reactors, *JAP* 83 (1998) 7504-7521.
- Gillett, F. C., Further observations of the 8-13 micron spectrum of Titan, *Astrophys. J.* 201 (1975).
- Giuliani, A., Jamme, F., Rouam, V., Wien, F., Giorgetta, J.-L., Lagarde, B., Chubar, O., Bac, S., Yao, I., Rey, S., Herbeaux, C., Marlats, J.-L., Zerbib, D., Polack, F., Refregiers, M., DISCO: a low-energy multipurpose beamline at synchrotron SOLEIL, *Journal of Synchrotron Radiation* 16 (2009) 835-841.

REFERENCES

- Giuliani, A., Yao, I., Lagarde, B., Rey, S., Duval, J.-P., Rommeluere, P., Jamme, F., Rouam, V., Wein, F., De Oliveira, C., Ros, M., Lestrade, A., Desjardins, K., Giorgetta, J.-L., Laprevote, O., Herbaux, C., Refregiers, M., A differential pumping system to deliver windowless VUV photons at atmospheric pressure, *Journal of Synchrotron Radiation* 18 (2011) 546-549.
- Godde, C., Berndt, J., Kovacevic, E., Stefanovic, I., Winter, J., Boufendi, L., Controlled Sampling of Nanoparticles in Reactive Plasmas, *Plasma Science, IEEE Transactions on* 39 (2011) 2766-2767.
- Hadamcik, E., Renard, J.-B., Alcouffe, G., Levasseur-Regourd, A. C., Szopa, C., Laboratory light-scattering measurements with Titan's aerosols analogues produced by a dusty plasma, *Planetary and Space Science* 57 (2009) 1631-1641.
- Hanel, R., Conrath, B., Flasar, F. M., Kunde, V. G., Maguire, W., Pearl, J., Pirraglia, J., Samuelson, R. E., Herath, L., Allison, M., Cruikshank, D. P., Gautier, D., Gierasch, P., Horn, L., Koppany, R., Ponnamperna, C., Infrared Observations of the Saturnian System from Voyager 1, *Science* 212 (1981) 192-200.
- He, C., Lin, G., Smith, M. A., NMR identification of hexamethylenetetramine and its precursor in Titan tholins: Implications for Titan prebiotic chemistry, *Icarus* 220 (2012a) 627-634.
- He, C., Lin, G., Upton, K. T., Imanaka, H., Smith, M. A., Structural Investigation of Titan Tholins by Solution-State ^1H , ^{13}C , and ^{15}N NMR: One-Dimensional and Decoupling Experiments, *The Journal of Physical Chemistry A* 116 (2012b) 4760-4767.
- Hébrard, E., Dobrijevic, M., Bénilan, Y., Raulin, F., Photochemical kinetics uncertainties in modeling Titan's atmosphere: A review, *Journal of Photochemistry and Photobiology C: Photochemistry Reviews* 7 (2006) 211-230.
- Hébrard, E., Dobrijevic, M., Bénilan, Y., Raulin, F., Photochemical kinetics uncertainties in modeling Titan's atmosphere: First consequences, *Planetary and Space Science* 55 (2007) 1470-1489.
- Hoobler, R. J., Leone, S. R., Rate Coefficients for reactions of ethynyl radical (C_2H) with HCN and CH_3CN : Implications for the formation of complex nitriles on Titan, *Journal of Geophysical research* 102 (1997) 28717-28723.
- Hörst, S. M., Yelle, R. V., Buch, A., Carrasco, N., Cernogora, G., Dutuit, O., Quirico, E., Sciamma-O'Brien, E., Smith, M. A., Somogyi, Á., Szopa, C., Thissen, R., Vuitton, V.,

REFERENCES

- Formation of Amino Acids and Nucleotide Bases in a Titan Atmosphere Simulation Experiment, *Astrobiology* 12 (2012) 809-817.
- Horvath, G., Krcma, F., Polachova, L., Klohnova, K., Mason, N. J., Zahoran, M., Matejcik, S., Organic chemistry of NH₃ and HCN induced by an atmospheric abnormal glow discharge in N₂-CH₄ mixtures, *The European Physical Journal - Applied Physics* 53 (2011).
- Hudson, R. L., Moore, M. H., Reactions of nitriles in ices relevant to Titan, comets, and the interstellar medium: formation of cyanate ion, ketenimines and isonitriles, *Icarus* 172 (2004) 466-478.
- Imanaka, H., Cruikshank, D. P., Khare, B. N., McKay, C. P., Optical constants of Titan tholins at mid-infrared wavelengths (2.5–25 μm) and the possible chemical nature of Titan's haze particles, *Icarus* 218 (2012) 247-261.
- Imanaka, H., Khare, B. N., Elsila, J. E., Bakes, E. L. O., McKay, C. P., Cruikshank, D. P., Sugita, S., Matsui, T., Zare, R. N., Laboratory experiments of Titan tholin formed in cold plasma at various pressures: implications for nitrogen-containing polycyclic aromatic compounds in Titan haze, *Icarus* 168 (2004) 344-366.
- Imanaka, H., Smith, M. A., Role of photoionization in the formation of complex organic molecules in Titan's upper atmosphere, *Geophys. Res. Lett.* 34 (2007) L02204.
- Imanaka, H., Smith, M. A., Formation of nitrogenated organic aerosols in the Titan upper atmosphere, *Proceedings of the National Academy of Sciences* 107 (2010) 15.
- Israel, G., Szopa, C., Raulin, F., Cabane, M., Niemann, H. B., Atreya, S. K., Bauer, S. J., Brun, J. F., Chassefiere, E., Coll, P., Conde, E., Coscia, D., Hauchecorne, A., Millian, P., Nguyen, M. J., Owen, T., Riedler, W., Samuelson, R. E., Siguier, J. M., Steller, M., Sternberg, R., Vidal-Madjar, C., Complex organic matter in Titan's atmospheric aerosols from in situ pyrolysis and analysis, *Nature* 438 (2005) 796-799.
- Jacquinet-Husson, N., Crepeau, L., Armante, R., Boutammine, C., Chédin, A., Scott, N. A., Crevoisier, C., Capelle, V., Boone, C., Poulet-Crovisier, N., Barbe, A., Campargue, A., Chris Benner, D., Benilan, Y., Bézard, B., Boudon, V., Brown, L. R., Coudert, L. H., Coustenis, A., Dana, V., Devi, V. M., Fally, S., Fayt, A., Flaud, J. M., Goldman, A., Herman, M., Harris, G. J., Jacquemart, D., Jolly, A., Kleiner, I., Kleinböhl, A., Kwabia-Tchana, F., Lavrentieva, N., Lacome, N., Xu, L.-H., Lyulin, O. M., Mandin, J. Y., Maki, A., Mikhailenko, S., Miller, C. E., Mishina, T., Moazzen-Ahmadi, N.,

REFERENCES

- Müller, H. S. P., Nikitin, A., Orphal, J., Perevalov, V., Perrin, A., Petkie, D. T., Predoi-Cross, A., Rinsland, C. P., Remedios, J. J., Rotger, M., Smith, M. A. H., Sung, K., Tashkun, S., Tennyson, J., Toth, R. A., Vandaele, A. C., Vander Auwera, J., The 2009 edition of the GEISA spectroscopic database, *JQSRT* 112 (2011) 2395-2445.
- Jampala, S. N., Sarmadi, M., Manolache, S., Denes, F. S., Surface functionalization by RF plasma deposition of ethylene diamine, acrylonitrile, and acetonitrile, *Journal of Applied Polymer Science* 107 (2008) 1686-1695.
- Jeans, J., *The dynamical theory of gases*, 3rd Edition ed., Cambridge at the University Press, 1931.
- Kareev, M., Sablier, M., Fujii, T., *Diagnosis of a CH₄/N₂ Microwave Discharge: Ionic and Neutral Species*, *The Journal of Physical Chemistry A* 104 (2000) 7218-7223.
- Khare, B. N., Bakes, E. L. O., Imanaka, H., McKay, C. P., Cruikshank, D. P., Arakawa, E. T., Analysis of the Time-Dependent Chemical Evolution of Titan Haze Tholin, *Icarus* 160 (2002) 172-182.
- Khare, B. N., Sagan, C., Arakawa, E. T., Suits, F., Callcott, T. A., Williams, M. W., Optical constants of organic tholins produced in a simulated Titanian atmosphere: From soft x-ray to microwave frequencies, *Icarus* 60 (1984) 127-137.
- Khare, B. N., Sagan, C., Ogino, H., Nagy, B., Er, C., Schram, K. H., Arakawa, E. T., Amino acids derived from Titan Tholins, *Icarus* 68 (1986) 176-184.
- Kim, S. J., Jung, A., Sim, C. K., Courtin, R., Bellucci, A., SIlcarusdy, B., Song, I. O., Minh, Y. C., Retrieval and tentative indentification of the 3 μm spectral feature in Titan's haze, *Planetary and Space Science* 59 (2011) 699-704.
- Klee, J., Review: Mass spectrometry of step-growth polymers, *European Journal of Mass Spectrometry* 11 (2005) 591-610.
- Kovačević, E., Stefanović, I., Berndt, J., Pendleton, Y. J., Winter, J., A Candidate Analog for Carbonaceous Interstellar Dust: Formation by Reactive Plasma Polymerization, *The Astrophysical Journal* 623 (2005) 242.
- Kovacevic, E., Stefanovic, I., Berndt, J., Winter, J., Infrared fingerprints and periodic formation of nanoparticles in Ar/C₂H₂ plasmas, *JAP* 93 (2003) 2924-2930.
- Krasnopolsky, V. A., A photochemical model of Titan's atmosphere and ionosphere, *Icarus* 201 (2009) 226-256.
- Kuiper, G., Titan: A satellite with an atmosphere, *Astrophys. J.* 100 (1944) 378.

REFERENCES

- Kunde, V. G., Aikin, A. C., Hanel, R., Jennings, D. E., Maguire, W., Samuelson, R. E., C₄H₂, HC₃N and C₂N₂ in Titan's atmosphere, *Nature* 292 (1981) 686.
- Lavvas, P., Yelle, R. V., Koskinen, T., Bazin, A., Vuitton, V., Vigren, E., Galand, M., Wellbrock, A., Coates, A. J., Wahlund, J.-E., Crary, F. J., Snowden, D., *Aerosol growth in Titan's ionosphere*, *Proceedings of the National Academy of Sciences* (2013).
- Lavvas, P. P., Coustenis, A., Vardavas, I. M., Coupling photochemistry with haze formation in Titan's atmosphere, Part II: Results and validation with Cassini/Huygens data, *Planetary and Space Science* 56 (2008) 67-99.
- Lebonnois, S., Toubanc, D., Hourdin, F., Rannou, P., Seasonal Variations of Titan's Atmospheric Composition, *Icarus* 152 (2001) 384-406.
- Lefohn, A. E., Mackie, N. M., Fisher, E. R., Comparison of Films Deposited from Pulsed and Continuous Wave Acetonitrile and Acrylonitrile Plasmas, *Plasmas and Polymers* 3 (1998) 197-209.
- Lellouch, E., Coustenis, A., Gautier, D., Raulin, F., Dubouloz, N., Frère, C., Titan's atmosphere and hypothesized ocean: A reanalysis of the Voyager 1 radio-occultation and IRIS 7.7- μ m data, *Icarus* 79 (1989) 328-349.
- Letourneur, B., Coustenis, A., Titan's atmospheric structure from Voyager 2 infrared spectra, *Planetary and Space Science* 41 (1993) 593-602.
- Maguire, W. C., Hanel, R. A., Jennings, D. E., Kunde, V. G., Samuelson, R. E., C₃H₈ and C₃H₄ in Titan's atmosphere, *Nature* 292 (1981) 683-686.
- Mahjoub, A., Carrasco, N., Dahoo, P. R., Gautier, T., Szopa, C., Cernogora, G., Influence of methane concentration on the optical indices of Titan's aerosols analogues, *Icarus* 221 (2012) 670-677.
- Majumdar, A., Behnke, J. F., Hippler, H., Matyash, K., Schneider, R., Chemical reactions studies in CH₄/Ar and C₂H₂/N₂ mixtures of a dielectric barrier discharge, *J. Chem. Phys.* 109 (2005) 9371.
- Makarov, A., Electrostatic Axially Harmonic Orbital Trapping: A High-Performance Technique of Mass Analysis, *Analytical Chemistry* 72 (2000) 1156-1162.
- Makarov, A., Denisov, E., Kholomeev, A., Balschun, W., Lange, O., Strupat, K., Horning, S., Performance Evaluation of a Hybrid Linear Ion Trap/Orbitrap Mass Spectrometer, *Analytical Chemistry* 78 (2006) 2113-2120.

REFERENCES

- Mao, F. M., Leck, J. H., The quadrupole mass spectrometer in practical operation, *Vacuum* 37 (1987) 669-675.
- Meierhenrich, U., Thiemann, W. H. P., Rosenbauer, H., Pyrolytic methylation assisted enantioseparation of chiral hydroxycarboxylic acids, *Journal of Analytical and Applied Pyrolysis* 60 (2001) 13-26.
- Monks, P. S., Romani, P. N., Nesbitt, F. L., Scanlon, M., Stief, L. J., The kinetics of the formation of Nitrile compounds in the atmospheres of Titan and Neptune, *Journal of Geophysical research* 98 (1993) 17115-17122.
- Mutsukura, N., Deposition of Diamondlike Carbon Film and Mass Spectrometry Measurement in CH₄/N₂ RF Plasma, *Plasma Chemistry and Plasma Processing* 21 (2001) 265-277.
- Neish, C. D., Somogyi, Á., Lunine, J. I., Smith, M. A., Low temperature hydrolysis of laboratory tholins in ammonia-water solutions: Implications for prebiotic chemistry on Titan, *Icarus* 201 (2009) 412-421.
- Neish, C. D., Somogyi, Á., Smith, M. A., Titan's Primordial Soup: Formation of Amino Acids via Low-Temperature Hydrolysis of Tholins, *Astrobiology* 10 (2010) 337-347.
- NIST Mass Spec Data Center, S. E. S., director,, Electron-Impact Cross Sections for Ionization and Excitation, National Institute of Standards and Technology Database,, 2010a.
- NIST Mass Spec Data Center, S. E. S., director,, Infrared Spectra, 2010b.
- O'Brien, D. P., Lorenz, R. D., Lunine, J. I., Numerical calculations of the longevity of impact oases on Titan, *Icarus* 173 (2005) 243-253.
- Olsen, J. V., de Godoy, L. M. F., Li, G., Macek, B., Mortensen, P., Pesch, R., Makarov, A., Lange, O., Horning, S., Mann, M., Parts per Million Mass Accuracy on an Orbitrap Mass Spectrometer via Lock Mass Injection into a C-trap, *Molecular & Cellular Proteomics* 4 (2005) 2010-2021.
- Peng, Z., Gautier, T., Carrasco, N., Pernot, P., Giuliani, A., Mahjoub, A., Correia, J. J., Buch, A., Bénilan, Y., Szopa, C., Cernogora, G., Titan's atmosphere simulation experiment using continuum UV-VUV synchrotron radiation, *Journal of Geophysical Research: Planets* 118 (2013) 778-788.
- Pernot, P., Carrasco, N., Thissen, R., Schmitz-Afonso, I., Tholinomics—Chemical Analysis of Nitrogen-Rich Polymers, *Analytical Chemistry* 82 (2010) 1371-1380.

REFERENCES

- Pintassilgo, C. D., Loureiro, J., Kinetic study of a N_2 - CH_4 afterglow plasma for production of *N-containing hydrocarbon species of Titan's atmosphere*, *Advances in Space Research* 46 (2010) 657-671.
- Pintassilgo, C. D., Loureiro, J., Cernogora, G., Touzeau, M., Methane decomposition and active nitrogen in a N_2 - CH_4 glow discharge at low pressures, *Plasma Sources Science and Technology* 8 (1999) 463.
- Plessis, S., Carrasco, N., Pernot, P., Knowledge-based probabilistic representations of branching ratios in chemical networks: The case of dissociative recombinations, *The Journal of Chemical Physics* 133 (2010) 134110-134121.
- Quirico, E., Montagnac, G., Lees, V., McMillan, P. F., Szopa, C., Cernogora, G., Rouzaud, J.-N., Simon, P., Bernard, J.-M., Coll, P., Fray, N., Minard, R. D., Raulin, F., Reynard, B., Schmitt, B., New experimental constraints on the composition and structure of tholins, *Icarus* 198 (2008) 218-231.
- Ramírez, S. I., Coll, P., Buch, A., Brassé, C., Poch, O., Raulin, F., The fate of aerosols on the surface of Titan, *Faraday Discussion* 147 (2010).
- Ramírez, S. I., Navarro-González, R., Coll, P., Raulin, F., Possible contribution of different energy sources to the production of organics in Titan's atmosphere, *Advances in Space Research* 27 (2001) 261-270.
- Ramírez, S. I., Navarro-González, R., Coll, P., Raulin, F., Organic chemistry induced by corona discharges in Titan's troposphere: Laboratory simulations, *Advances in Space Research* 36 (2005) 274-280.
- Rannou, P., Cabane, M., Chassefiere, E., Botet, R., McKay, C. P., Courtin, R., Titan's Geometric Albedo: Role of the Fractal Structure of the Aerosols, *Icarus* 118 (1995) 355-372.
- Rannou, P., Cours, T., Le Mouélic, S., Rodriguez, S., Sotin, C., Drossart, P., Brown, R., Titan haze distribution and optical properties retrieved from recent observations, *Icarus* 208 (2010) 850-867.
- Rannou, P., McKay, C. P., Lorenz, R. D., A model of Titan's haze of fractal aerosols constrained by multiple observations, *Planetary and Space Science* 51 (2003) 963-976.
- Robertson, I. P., Cravens, T. E., Waite, J. H., Yelle, R. V., Vuitton, V., Coates, A. J., Wahlund, J. E., Agren, K., Mandt, K., Magee, B., Richard, M. S., Fattig, E., Structure

REFERENCES

- of Titan's ionosphere: Model comparisons with Cassini data, *Planetary and Space Science* 57 (2009) 1834-1846.
- Rodil, S. E., Ferrari, A. C., Robertson, J., Milne, W. I., Raman and infrared modes of hydrogenated amorphous carbon nitride, *JAP* 89 (2001) 5425-5430.
- Ruiz-Bermejo, M., Menor-Salván, C., de la Fuente, J. L., Mateo-Martí, E., Osuna-Esteban, S., Martín-Gago, J. Á., Veintemillas-Verdaguer, S., CH₄/N₂/H₂-spark hydrophobic tholins: A systematic approach to the characterisation of tholins. Part II, *Icarus* 204 (2009) 672-680.
- Ruiz-Bermejo, M., Menor-Salván, C., Mateo-Martí, E., Osuna-Esteban, S., Martín-Gago, J. Á., Veintemillas-Verdaguer, S., CH₄/N₂/H₂ spark hydrophilic tholins: A systematic approach to the characterization of tholins, *Icarus* 198 (2008) 232-241.
- Sagan, C., The solar system beyond Mars: An exobiological survey, *SSRv* 11 (1971) 827-866.
- Sato, K., Misawa, K., Kobayashi, Y., Matsui, M., Tsunashima, S., Kurosaki, Y., Takayanagi, T., Measurements of Thermal Rate Constants for the Reactions of N(²D, ²P) with C₂H₄ and C₂D₄ between 225 and 292 K, *The Journal of Physical Chemistry A* 103 (1999) 8650-8656.
- Sciamma-O'Brien, E., Carrasco, N., Szopa, C., Buch, A., Cernogora, G., Titan's atmosphere: an optimal gas mixture for aerosol production?, *Icarus* 209 (2010) 704-714.
- Sciamma-O'Brien, E., Dahoo, P. R., Hadamcik, E., Carrasco, N., Quirico, E., Szopa, C., Cernogora, G., Optical constants from 370 nm to 900 nm of Titan tholins produced in a low pressure RF plasma discharge, *Icarus* 218 (2012) 356-363.
- Scigelova, M., Makarov, A., Orbitrap Mass Analyzer – Overview and Applications in Proteomics, *PROTEOMICS* 6 (2006) 16-21.
- Seki, K., Yagi, M., He, M., Halpern, J. B., Okabe, H., Reaction rates of the CN radical with diacetylene and dicyanoacetylene, *Chemical Physics Letters* 258 (1996) 657-662.
- Sekine, Y., Imanaka, H., Matsui, T., Khare, B. N., Bakes, E. L. O., McKay, C. P., Sugita, S., The role of organic haze in Titan's atmospheric chemistry: I. Laboratory investigation on heterogeneous reaction of atomic hydrogen with Titan tholin, *Icarus* 194 (2008a) 186-200.
- Sekine, Y., Lebonnois, S., Imanaka, H., Matsui, T., Bakes, E. L. O., McKay, C. P., Khare, B. N., Sugita, S., The role of organic haze in Titan's atmospheric chemistry: II. Effect of

REFERENCES

- heterogeneous reaction to the hydrogen budget and chemical composition of the atmosphere, *Icarus* 194 (2008b) 201-211.
- Sims, I. R., Queffelec, J. L., Travers, D., Rowe, B. R., Herbert, L. B., J.Karthäuser, Smith, I. W. M., Rate constants for the reactions of CN with hydrocarbons at low and ultra-low temperatures, *Chemical Physics Letters* 211 (1993).
- Somogyi, A., Oh, C.-H., Smith, M. A., Lunine, J. I., Organic Environments on Saturn's Moon, Titan: Simulating Chemical Reactions and Analyzing Products by FT-ICR and Ion-Trap Mass Spectrometry, *Journal of the American Society for Mass Spectrometry* 16 (2005) 850-859.
- Somogyi, Á., Smith, M. A., Vuitton, V., Thissen, R., Komáromi, I., Chemical ionization in the atmosphere? A model study on negatively charged “exotic” ions generated from Titan's tholins by ultrahigh resolution MS and MS/MS, *International Journal of Mass Spectrometry* 316–318 (2012) 157-163.
- Stefanović, I., Kovačević, E., Berndt, J., Pendleton, Y., Winter, J., Hydrocarbon nanoparticles as a diffuse ISM analogue: morphology and infrared absorption in the 2000–500 cm^{-1} region, *PPCF* 47 (2005) A179.
- Strobel, D. F., Shemansky, D. E., EUV emission from Titan's upper atmosphere: Voyager 1 encounter, *Journal of Geophysical Research: Space Physics* 87 (1982) 1361-1368.
- Szopa, C., Cernogora, G., Boufendi, L., Correia, J. J., Coll, P., PAMPRE: A dusty plasma experiment for Titan's tholins production and study, *Planetary and Space Science* 54 (2006) 394-404.
- Takayanagi, T., Kurosaki, Y., Sato, K., Tsunashima, S., Ab Initio Molecular Orbital Calculations for the $\text{N}(^2\text{D}) + \text{Ethylene}$ Reaction, *The Journal of Physical Chemistry A* 102 (1998) 10391-10398.
- Teanby, N. A., Irwin, P. G. J., de Kok, R., Nixon, C. A., Mapping Titan's HCN in the far infra-red: implications for photochemistry, *Faraday Discussions* 147 (2010) 51-64.
- Teanby, N. A., Irwin, P. G. J., de Kok, R., Vinatier, S., Bézard, B., Nixon, C. A., Flasar, F. M., Calcutt, S. B., Bowles, N. E., Fletcher, L., Howett, C., Taylor, F. W., Vertical profiles of HCN, HC_3N , and C_2H_2 in Titan's atmosphere derived from Cassini/CIRS data, *Icarus* 186 (2007) 364-384.
- Tilford, C. R., Process monitoring with residual gas analyzers (RGAs): limiting factors, *SuCT* 68–69 (1994) 708-712.

REFERENCES

- Tobie, G., Grasset, O., Lunine, J. I., Mocquet, A., Sotin, C., Titan's internal structure inferred from a coupled thermal-orbital model, *Icarus* 175 (2005) 496-502.
- Tomasko, M., West, R., Aerosols in Titan's Atmosphere, in: R. Brown, J.-P. Lebreton, J. H. Waite, (Eds.), *Titan from Cassini-Huygens*. Springer Netherlands, 2010, pp. 297-321.
- Tomasko, M. G., Doose, L., Engel, S., Dafoe, L. E., West, R., Lemmon, M., Karkoschka, E., See, C., A model of Titan's aerosols based on measurements made inside the atmosphere, *Planetary and Space Science* 56 (2008) 669-707.
- Tomasko, M. G., et al., Rain, winds and haze during the Huygens probe's descent to Titan's surface, *Nature* 438 (2005) 765.
- Tomasko, M. G., Smith, P. H., Photometry and polarimetry of Titan: Pioneer 11 observations and their implications for aerosol properties, *Icarus* 51 (1982) 65-95.
- Touvelle, M., Licea, J. L. M., Venugopalan, M., Plasma chemical synthesis. II. Effect of wall surface on the synthesis of ammonia, *Plasma Chemistry and Plasma Processing* 7 (1987) 101-108.
- Tran, B. N., Ferris, J. P., Chera, J. J., The photochemical formation of a titan haze analog. Structural analysis by x-ray photoelectron and infrared spectroscopy, *Icarus* 162 (2003) 114-124.
- Tran, B. N., Joseph, J. C., Force, M., Briggs, R. G., Vuitton, V., Ferris, J. P., Photochemical processes on Titan: Irradiation of mixtures of gases that simulate Titan's atmosphere, *Icarus* 177 (2005) 106-115.
- Uyama, H., Matsumoto, O., Synthesis of ammonia in high-frequency discharges. II. Synthesis of ammonia in a microwave discharge under various conditions, *Plasma Chemistry and Plasma Processing* 9 (1989) 421-432.
- Vinatier, S., Bézard, B., de Kok, R., Anderson, C. M., Samuelson, R. E., Nixon, C. A., Mamoutkine, A., Carlson, R. C., Jennings, D. E., Guandique, E. A., Bjoraker, G. L., Michael Flasar, F., Kunde, V. G., Analysis of Cassini/CIRS limb spectra of Titan acquired during the nominal mission II: Aerosol extinction profiles in the 600-1420 cm^{-1} spectral range, *Icarus* 210 (2010) 852-866.
- Vinatier, S., Rannou, P., Anderson, C. M., de Kok, R., Samuelson, R. E., Optical constants of Titan's stratospheric aerosols in the 70-1500 cm^{-1} spectral range constrained from Cassini/CIRS observations, *Icarus* 219 (2012) 5-12.

REFERENCES

- Vinogradoff, V., Duvernay, F., Danger, G., Theulé, P., Chiavassa, T., New insight into the formation of hexamethylenetetramine (HMT) in interstellar and cometary ice analogs, *A&A* 530 (2011) A128.
- Vuitton, V., Lavvas, P., Yelle, R. V., Galand, M., Wellbrock, A., Lewis, G. R., Coates, A. J., Wahlund, J. E., Negative ion chemistry in Titan's upper atmosphere, *Planetary and Space Science* 57 (2009) 1558-1572.
- Vuitton, V., Yelle, R. V., McEwan, M. J., Ion Chemistry and N-containing molecules in Titan's upper atmosphere, *Icarus* 191 (2007) 722-742.
- Waite, J. H., Niemann, H., Yelle, R. V., Kasprzak, W. T., Cravens, T. E., Luhmann, J. G., McNutt, R. L., Ip, W.-H., Gell, D., De La Haye, V., Müller-Wordag, I., Magee, B., Borggren, N., Ledvina, S., Fletcher, G., Walter, E., Miller, R., Scherer, S., Thorpe, R., Xu, J., Block, B., Arnett, K., Ion Neutral Mass Spectrometer Results from the First Flyby of Titan, *Science* 308 (2005) 982-986.
- Waite, J. H., Young, D. T., Cravens, T. E., Coates, A. J., Crary, F. J., Magee, B., Westlake, J., The Process of Tholin Formation in Titan's Upper Atmosphere, *Science* 316 (2007) 870-875.
- Waite, J. H., Young, D. T., Westlake, J., Lunine, J. I., McKay, C. P., Lewis, W. S., High-Altitude production of Titan's Aerosols, in: R. Brown, J.-P. Lebreton, J. H. Waite, (Eds.), *Titan from Cassini-Huygens*. Springer Netherlands, 2010, pp. 201-214.
- Wellbrock, A., Coates, A.J., Jones, G.H., Arridge, C.S., Lewis, G., Sittler, E.C., Young, D.T, Density trends of negative ions at Titan, Abstract P21F-1898 presented at 2012 Fall Meeting, AGU, San Francisco, Calif., 3-7 Dec.
- Wilson, E. H., Atreya, S. K., Chemical sources of haze formation in Titan's atmosphere, *Planetary and Space Science* 51 (2003) 1017-1033.
- Yang, D. L., Yu, T., Wang, N. S., Lin, M. C., Temperature dependence of cyanogen radical reactions with selected alkanes: CN reactivities towards primary, secondary and tertiary C-H bonds, *Chemical Physics* 160 (1992) 307-315.
- Yasuda, H., Plasma for Modification of Polymers, *Journal of Macromolecular Science: Part A - Chemistry* 10 (1976) 383-420.
- Yelle, R. V., Vuitton, V., Lavvas, P., Klippenstein, S. J., Smith, M. A., Horst, S. M., Cui, J., Formation of NH_3 and CH_2NH in Titan's upper atmosphere, *Faraday Discussions* 147 (2010) 31-49.

REFERENCES

- Young, D. T., Berthelier, J. J., Blanc, M., Burch, J. L., Coates, A. J., Goldstein, R., Grande, M., Hill, T. W., Johnson, R. E., Kelha, V., McComas, D. J., Sittler, E. C., Svenes, K. R., Szegő, K., Tanskanen, P., Ahola, K., Anderson, D., Bakshi, S., Baragiola, R. A., Barraclough, B. L., Black, R. K., Bolton, S., Booker, T., Bowman, R., Casey, P., Crary, F. J., Delapp, D., Dirks, G., Eaker, N., Funsten, H., Furman, J. D., Gosling, J. T., Hannula, H., Holmlund, C., Huomo, H., Illiano, J. M., Jensen, P., Johnson, M. A., Linder, D. R., Luntama, T., Maurice, S., McCabe, K. P., Mursula, K., Narheim, B. T., Nordholt, J. E., Preece, A., Rudzki, J., Ruitberg, A., Smith, K., Szalai, S., Thomsen, M. F., Viherkanto, K., Vilppola, J., Vollmer, T., Wahl, T. E., Wüest, M., Ylikorpi, T., Zinsmeyer, C., Cassini Plasma Spectrometer Investigation, *SSRv* 114 (2004) 1-112.
- Yu, Q., Ye, M., Lu, L., Chen, J., Wang, F., A study of the polymerization mechanism of acetonitrile in glow discharge, *Chinese Journal of Polymer Science* 6 (1988).
- Yung, Y. L., An Update of Nitrile Photochemistry on Titan, *Icarus* 72 (1987) 468-472.
- Zabarnick, S., Kinetics of $CN(X^2S^+)$ Radical reactions with HCN, BrCN and CH_3CN , *Chemical Physics* 134 (1989) 185-191.